PARTIAL OXIDATION OF ETHANOL OVER VANADIUM IRON ANTIMONATE CATALYSTS

By

Boni kaKhuzwayo Mehlomakulu

MSc (Chemistry) University of Natal

Thesis Presented for the Degree of

DOCTOR OF PHILOSOPHY

In the Department of Chemical Engineering

UNIVERSITY OF CAPE TOWN

08 June 2003

ACKNOWLEDGEMENTS

I would like to thank the following people, without whose help this work would never have been achieved.

- Prof. Eric van Steen who, as my supervisor, gave willing help and for his most helpful discussions.
- Dr Jean-Marc Millet for a fruitful collaboration involving the preparation and characterisation of $V_xFe_{1-x}O_4$ catalysts performed under his supervision at the CNRS laboratories in France.
- Sasol Technology R&D for financial support and the National Research Foundation for travelling grants.
- The Creator for the opportunity and raw materials.
- A big thanks to my Catalysis Research Unit colleagues for the pleasant environment and friendship.

Finally, I would like to express my special thanks to my family for all their support and love.

SYNOPSIS

$VSbO_4$ and $FeSbO_4$ are proven catalysts for the amm(oxidation) of propane/propylene. These catalysts systems have been shown to possess over-oxidation limiting characteristics. Ethanol oxidation is carried out in two-staged processes industrially, mainly because of the challenges presented by over-oxidation of the intermediates to carbon oxides. Hence, these catalysts systems were chosen for the systematic investigation of ethanol oxidation to acetaldehyde and preferable to acetic acid and ethyl acetate. Combining the two catalysts systems ($VSbO_4$ and $FeSbO_4$) brings about fascinating catalytic characteristics, since both catalysts crystallize in a tetragonal rutile structure. However, $VSbO_4$ has a defective structure with the composition of $V^{4+}_{0.64}V^{3+}_{0.28}Sb^{5+}_{0.92}\Diamond_{0.16}O_4$ arising from the fact that $VSbO_4$ contains both V^{3+} and V^{4+}, and the presence of V^{4+} is balanced by the formation of vacancies within the structure. $FeSbO_4$, on the other hand does not possess such a structure. Therefore, sequential substitution of V by Fe in $VSbO_4$ should lead to a continuous solid solution from $VSbO_4$ through to $FeSbO_4$, and concurrently affect the V^{3+}/ V^{4+} ratio and cationic vacancies content. The mutual effect should generate data of great catalytic consequence in development of these catalytic systems. $VSbO_4$, $FeSbO_4$ and $V_xFe_{1-x}SbO_4$, $0<x<1$ catalysts were prepared and characterized comprehensively to establish the catalysts characteristics evolution as a function of V/(Fe+V) ratio. Structural changes such as 1) surface area, 2) crystalline phase(s), 3) metal surface composition, 4) acidity, 5) electrical conductivity and 6) variation of V^{3+} / V^{4+} were observed.

A decrease in surface area was observed with increasing V/(Fe+V) ratio in $V_xFe_{1-x}SbO_4$ catalysts. High calcination temperature was found to cause a decrease in surface area attributed to sintering of the catalysts. All prepared catalysts were found to crystallize in a single phase rutile structure. However, a decrease in cell parameter *c* was observed with increasing V/(Fe+V) ratio, attributed to the introduction of vacancies within the structure as the V/(Fe+V) ratio increases. Lewis and Brønsted acidity, electrical conductivity, V^{4+} / V^{3+} ratio and the vacancies content of these catalysts also increased with increasing V/(Fe+V) ratio.

Partial oxidation of ethanol to acetaldehyde, acetic acid and ethyl acetate was used to evaluate the catalytic behavior of the prepared $VSbO_4$, $FeSbO_4$ and $V_xFe_{1-x}SbO_4$, $0<x<1$ catalysts. Oxidation reactions were carried out in a U-type pyrex reactor using air as an oxidant. In addition, advantages of these complex catalyst systems were demonstrated systematically by sequentially increasing the number of components in the catalysts. Starting with single metal oxides (V_2O_5, Fe_2O_4 and Sb_2O_4), and building on to binary oxides ($VSbO_4$ and $FeSbO_4$), then to ternary oxides ($V_xFe_{1-x}SbO_4$, $0<x<1$) catalyst systems. The effectiveness in the oxidation of ethanol, evaluated in terms of ethanol conversion and selectivity to partial oxidation products (acetaldehyde, acetic acid and ethyl acetate), was used to compare these hierarchal classes of catalysts. Single metal oxides at 300°C showed the following trend in catalytic activity upon the oxidation of ethanol: $V_2O_5 > Fe_2O_3 >> Sb_2O_4$. An opposite trend for the selectivity to partial oxidation products was observed: $V_2O_5 > Fe_2O_3 << Sb_2O_4$. Binary oxides ($VSbO_4$ and $FeSbO_4$), exhibited enhanced activity and selectivity compared to the respective single metal oxides. Comparing the two binary oxides, higher activity was observed over $VSbO_4$ compared to $FeSbO_4$, while the selectivity to partial oxidation products was equivalent. A notable enhancement of activity was observed upon the oxidation of ethanol over ternary catalysts ($V_xFe_{1-x}SbO_4$, $0<x<1$) in comparison to compositional binary systems ($VSbO_4$ and $FeSbO_4$). Similar to binary systems, V-rich ternary catalysts showed superiority in terms of activity in comparison to Fe-rich ternary catalysts, while the selectivity was more or less the same.

The kinetics of partial oxidation of ethanol over metal oxides can be described as a first order with respect to ethanol and zero order with respect to oxygen. On these bases, the rate constants for formation of acetaldehyde for each catalyst in the $V_xFe_{1-x}SbO_4$ series were determined. Correlations of the rate constant with different species making up the catalysts (V^{3+}, V^{4+}, ions and vacancies content) showed that V^{3+} ions are the active species at low V/(Fe+V) ratios. At the point where V^{4+} ions start to form and V^{3+} ions content remains the same, the activity can be correlated to the content of the vacancies. Mössbauer and the substitution of Fe^{3+} by Ga^{3+} or Al^{3+} showed that the Fe^{3+}/Fe^{2+} redox couple does not take part in the oxidation of ethanol.

Reaction parameters (space-time, ethanol/oxygen ratio, reaction temperature and inlet water partial pressure) were investigated in an effort to elucidate the oxidation of ethanol

reaction pathway. A parallel-consecutive mechanism was established. Acetaldehyde and diethyl ether are the primary products of the oxidation of ethanol. Acetic acid and ethyl acetate form from acetaldehyde in arguably parallel reactions. Carbon oxides are formed from all the oxidation reaction intermediates as shown below.

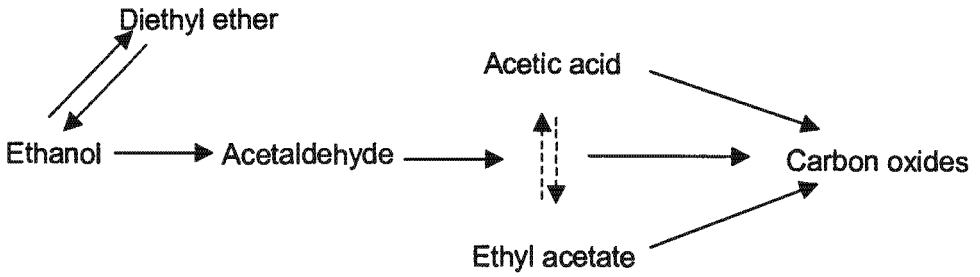

IR and TPD studies on pellets that had been exposed to ethanol and acetaldehyde further confirmed the proposed reaction sequence. Ethoxy species were observed primarily on the surface of the catalyst followed by adsorbed acetaldehyde, acetate species and, eventually, carbonate species as the temperature was progressively increased.

The influence of co-feeding water was investigated systematically at different space-times to establish the effect of water partial pressure at different stages of the ethanol reaction pathway. It was established that the effect of inlet water partial pressure on the oxidation of ethanol is largely affected by other conditions applied (e.g. space-time and temperature). Generally, an increase in partial oxidation products, a decrease in total oxidation products and a decrease in the overall activity were observed with increasing inlet water partial pressure.

TABLE OF CONTENTS

LIST OF FIGURES

LIST OF TABLES

LIST OF PUBLICATIONS

Poster presentations:

"Partial Oxidation of (C_2, n-C_3-C_4) Alcohols to Carboxylic Acid and Esters over Group VI Metal Oxides (CrO_3, MoO_3 and WO_3)"Fifteenth Indian Natiaonal Symposium on Catalysis and Second Conference of the Indo-Pacific Catalysis Association, National Chemical Laboratory, Pune, India, 23-25 January 2001.

"Mechanistic Insights into the Oxidation of (C_2-C_4) Alcohols over Group VI Metal Oxides (CrO_3, MoO_3 and WO_3)". 4th World Congress on Oxidation Catalysis, Berlin/Potsdam, Germany, 16-21September, 2001.

Oral presentations:

"Vanadium and Iron Antimonates as Catalysts for Ethanol Oxidation". Conference of the South African Catalysis Society, Pilanesburg, South Africa, November, 2001.

Papers:

"Mechanistic Insights into the Oxidation of (C_2-C_4) Alcohols over Group VI Metal Oxides (CrO_3, MoO_3 and WO_3)". 4th World Congress on Oxidation Catalysis Book of Extended Abstracts, Volume I, Berlin/Potsdam, Germany, 16-21 September, 2001, pp 395

"Active Sites Characterization in Mixed Vanadium and Iron Antimonates Oxide Catalysts for Propane Ammoxidation". Journal of Catalysis, **205** (2002), 97-106

"Vanadium and Iron Antimonates as Catalysts for Ethanol Oxidation", *in preparation.*

"The Effect of Inlet Water Partial Pressure on the Oxidation of Ethanol at Varying Space-Times over $V_xFe_{1-x}SbO_4$ Catalyst", *in preparation.*

NOMENCLATURE

A_i	pre-exponential factor for component i, mmol/(g_{cat} · min · $bar^{-(m+n)}$)
B	width of a diffraction line radius (degrees 2θ)
d	diameter, mm
E_{ai}	activation energy to form product i, kJ/mol
f_i	response factor for product i
F	volumetric flow, ml (NTP)/min
k_i	rate constant for formation for product i, mmol/(g_{cat}· min · $bar^{-0.5}$)
m	mass, g
$\dot{n}$	molar flow, mol/min
P_i	partial pressure of component i, bar
r_i	rate of formation of product i, mmol/(g_{cat}· min)
R	universal gas constant, 8.314 J/(mol · K)
S	selectivity, C-%
T	absolute temperature, K
x	mol fraction
X	Conversion, reported in mol-%
Y	yield, C-%

Greek Letters

β	X-ray diffraction broadening
λ	radiation wavelength in X-ray diffraction, Å
θ	fraction of catalyst sites on catalyst surface

Sub-and Superscripts

m	order of reaction with respect to oxygen
n	order of reaction with respect to alcohol

List of Abbreviations

WHSV	weight hourly space velocity, $g_{alcohol}/(g_{catalyst}\ h)$
TAP	temporal analysis of product
TPR	temperature programmed reduction
XRD	X-ray diffraction

INTRODUCTION AND LITERATURE REVIEW

1 INTRODUCTION AND LITERATURE REVIEW

Partial oxidation processes range from large-scale production of commodities to the synthesis of minute amounts of pharmaceuticals and fine chemicals. Selective catalytic oxidation is the basis of the modern petrochemical industry, and constitutes the largest category of catalytic organic reactions. Most monomers used in manufacturing artificial fibers and plastics are obtained via catalytic oxidation processes. Products worth an estimated US$ 20-40 billion have been produced (Delmon and Ruiz, 1987). The total production of the top 50 industrial chemicals in the U.S. was 616 billion pounds of which catalytic organic chemicals production was 147 billion pounds. Of these organic chemicals, about half were produced by an oxidation step, including those produced by heterogeneous oxidation, homogeneous oxidation, oxy-chlorination and dehydrogenation (Figure 1-1).

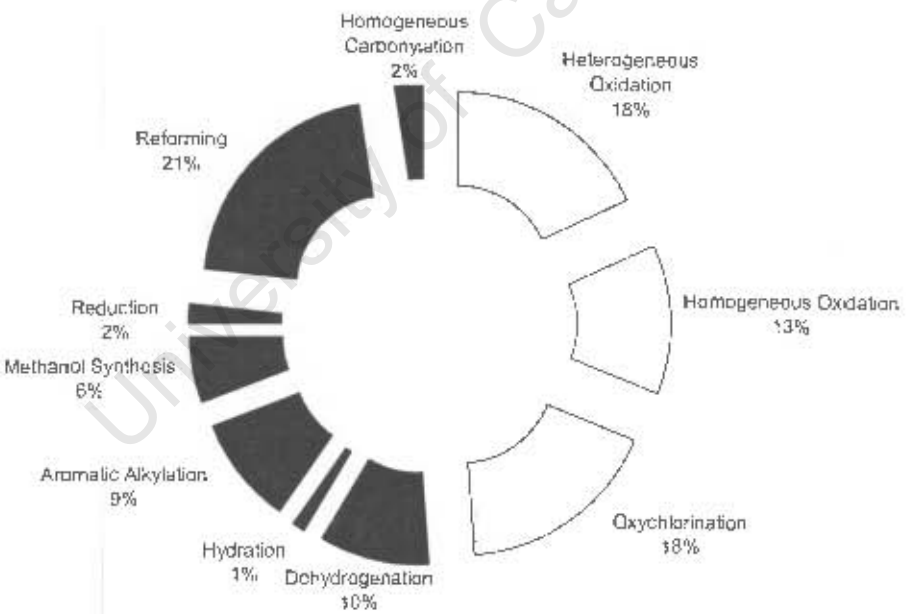

Figure 1-1: Catalytic production of major organic chemicals in the United States in 1991 (adapted from Desikan, 1991)

The market value of oxidation catalysts produced for commerce in the U.S. was US$ 105 million exceeded only by that of polymerization catalysts.

Ethyl alcohol (ethanol) is one of the largest-volume organic chemicals used in a variety of industrial and consumer products. Its principal use is that of a chemical intermediate, to produce other chemicals. Millions of tons each year go into the making of acetaldehyde, acetic acid, ethyl acetate, ethyl chloride, ethylene dibromide, and diethyl ether. The production of acetaldehyde from ethanol has been one of the most spectacular advances in the use of ethanol. In 1962 and 1963, 50% of U.S. consumption of ethanol was used in acetaldehyde manufacture. However, the high ethanol price in Japan, Western Europe and the U.S. decreased the use of ethanol as a feedstock for the production of carboxylic compounds (Hayes, 1970).

In South Africa, 500 000 tons per annum of ethanol (91%) are produced as a side product from the Fischer-Tropsch (oil from coal) process at Sasol (Haddeland, 1976). Table 1-1 gives an overview of the distribution of oxygenates produced in the high temperature Fischer-Tropsch synthesis (Schulze, 1974).

Table 1-1: Distribution of the acidic (27%) and non-acidic (73%) oxygenated compounds from the Synthol reactor (Schulze, 1974)

Main non-acid chemicals	**Mass (%)**	**Acids**	**Mass (%)**
Methanol	1.5	Acetic acid	70.0
Aldehydes C_2-C_4	4.0	Propionic acid	16.0
Acetone	10.5	Butyric acid	9
Ethanol	55.5	Valeric acid and higher	5
Methyl ethyl ketone	3.0		
Methyl-propyl ketone	1.0		
i- Propanol	3.0		
n-Propanol	14.0		
i- Butanol	1.0		
n-Butanol	4.0		
2-Butanol	0.5		
C_5 and higher alcohols	2.0		

Of the oxygenates that form from high temperature Fischer-Tropsch process, ethanol is produced in largest quantity. For decades, Brazil served as a good export market for

Sasol's ethanol blend. Brazil has had the most successful use of ethanol in automobile, owing to the almost complete lack of domestic petroleum reserves. In Brazil about 3.5 million automobiles are running on a 97% ethanol, 3% gasoline blend (the gasoline is not added for its fuel value, but rather to render the ethanol unfit to drink). The other 8 million use a 22% ethanol, 78% gasoline blend. Ethanol has 71% of the caloric value of 2,2,4-trimethylpentane when the fuels are compared on the basis of equal volumes (Raje and Davis, 1996).

During the past few years, however, the Brazil market for Sasol ethanol blend became uncertain due to abundant supply of ethanol from biomass within Brazil. Consequently, research efforts at Sasol were channelled towards adding value to the abundant ethanol. Sasol continued to explore alternative markets for the ethanol and meanwhile introduced the ethanol blend to the domestic petrol pool (Fraser, 1999).

Recently, selective oxidation of ethanol to value-added chemicals has gained increasing technological interest in connection with the utilization of biomass as a chemical source (Kannan *et al.*, 1997). The feedstock advantage South Africa has rendered partial oxidation of ethanol as potentially the better alternative leading to valuable products such as acetaldehyde, acetic acid and ethyl acetate.

1.1 PRODUCTS DERIVED FROM ETHANOL PARTIAL OXIDATION

Acetaldehyde can be produced by dehydrogenation or oxidative dehydrogenation of ethanol (Hayes, 1970). Approximately 95% of the acetaldehyde produced is used internally by the manufacturers as an intermediate leading to other organic chemicals. Table 1-2 shows the end-use pattern, in weight-% consumption, for American producers in 1970.

Table 1-2: Acetaldehyde derived products (adapted from Hayes, 1970)

PRODUCT	% CONSUMPTION
Acetic acid	47
n-Butyl alcohol	29
Acetic anhydride	12
2-Ethylhexanol and other aldol products	7
Pentaerythritol	3.6
Pyridines, chloral, etc	1.4

Acetic acid is the largest single product manufactured from acetaldehyde. The three main uses for acetic acid are in the production of vinyl acetate, monochloroacetic acid and various acetate esters (Hayes, 1970). The market for vinyl acetate has the greatest influence on acetic acid and, consequently, on acetaldehyde production. Acetic anhydride, which is used to make cellulose acetate, is related closely to the fortunes of the textile industry. The third acid which can be derived from acetaldehyde, peroxyacetic acid, is made only in relatively small quantities, to date it is used primarily in the manufacture of epoxides, but it does have potential in other areas such as bleaching. It is expected that peroxyacetic acid will assume greater importance in the immediate future.

Products made by aldol condensation have become important outlets for acetaldehyde. The two major products derived from acetaldehyde via the aldol route are 1-butanol and 2-ethylhexanol. Butanol is used mainly in butyl acetate, a solvent for nitrocellulose lacquers (Rudd, 1981). At some point butyl acetate was the most important lacquer solvent in the medium-boiling range. On the other hand, the consumption of 2-ethylhexanol almost doubled in the 1970s (Rudd, 1981). It is used to make dioctyl phthalate, the largest volume plasticizer for polyvinyl chloride resin. 2-Ethylhexanol has received increasing competition from the oxo alcohols, but lower acetaldehyde costs should allow it to retain its position in the market. Other products, which are produced in small quantities from aldol condensation, are 1,3-butylene glycol (1,3-butanediol), crotonaldehyde, crotonic acid, and butyric acid.

Pentaerythritol, which is made by the condensation of acetaldehyde with formaldehyde, is the next largest consumer of acetaldehyde. As the principal end use of pentaerythritol is in alkyd resin field (Hayes, 1970), it competes directly with glycerol, hence future expansion in this area depends to a large extent on the relative costs of the two polyols.

Chloral, synthetic pyridines, and ethyl acetate require a considerable volume of acetaldehyde (Hayes, 1970). DDT (made from chloral) became a large volume item in the 1945s, but has been eliminated from the market due to environmental regulations. The production of synthetic pyridines made from paraldehyde and ammonia is of growing importance. 5-Ethyl-2-methylpyridine is an intermediate in the manufacture of 2-methyl-5-vinylpyridine, nicotinic acid, and pharmaceuticals. Ethyl acetates have been made for a number of years in Canada and Germany directly from acetaldehyde by the Tishchenko condensation (Houben-Weyl, 1933). Ethyl acetate is used mainly as a solvent and in the paint industry. Acrylonitrile is made commercially in Germany from acetaldehyde cyanohydrin derived from the reaction of acetaldehyde and hydrocyanic acid (Miller, 1968). The economic viability was wiped out by the development of the process to manufacture acrylonitrile from propylene, ammonia, and oxygen that offered distinct economic advantages.

Acetaldehyde has a number of minor industrial uses, such as the condensation with phenol or urea to form thermosetting resins, the reaction with aliphatic and aromatic amines yielding Schiff bases, which are used as accelerators and antioxidants in the rubber industry. Acetaldehyde has also been used as a denaturant for ethyl alcohol, as a preservative for fruit and fish, for hardening gelatin, glue and casein products, and for the prevention of mould growth in leather. Current consumption of these purposes, however, is very small. Butadiene was made by the reaction of ethyl alcohol and acetaldehyde in times of rubber shortage (Hayes, 1970).

Despite the decrease in the use of ethanol as a feedstock for the production of high value oxygenates in the 1960s due to the high price of ethanol (Hayes, 1970), it is still a notable option where ethanol is available in abundance.

1.2 EVOLUTION OF THE OXIDATION OF ALCOHOL PROCESSES

1.2.1 Pioneering studies on the oxidation of alcohols

Production of acetaldehyde from ethanol was first observed by Scheele in 1774 by the action of manganese dioxide and sulphuric acid on ethanol. However, comprehensive earliest references to the oxidation of alcohols are to be found among the studies of Sir Humphrey Davy in 1817 who observed that a platinum spiral when slightly heated and introduced into a mixture of air and a combustible gas (ethanol) becomes incandescent and that this phenomenon is accompanied by a slow combustion of the gas. Edmond Davy in 1822 made the further discovery that platinum black possessed the power to ignite ethanol. Strecker in 1855 and later Grimaux in 1886 discovered that ethanol could be oxidised to acetaldehydes and even to acetic acid by the action of platinum black. Subsequently, in 1893 Kuhlmann observed that vapours of ethanol when mixed with air could be oxidised to acetic acid by passing them through a hot tube containing spongy platinum. Following this discovery, the action of platinum in various forms was made the subject of further investigations (Orloff, 1909). Industrial processes developed to date however are based on copper or silver metals and not platinum.

1.2.2 Industrial ethanol oxidation processes

Ethanol can be converted into acetaldehyde by either dehydrogenation or air oxidation. In both reactions the aldehyde selectivity can only reach 90-95% if the conversion per pass is limited to 30-50% (Hayes, 1970). The dehydrogenation of ethanol is an endothermic reaction, which requires a significant heat input at a temperature of 260-300°C. The reactor and associated heating system have proven to be complex, which is possible the main reason for the lack of references concerning early commercialisation of this route (Hayes, 1970). The main advantage of this process however is the co-production of H_2, which positively affects the economics of the process. A 33 000 tonnes per year acetaldehyde from dehydrogenation of fermented ethanol from sugar cane molasses plant was started up in Indonesia in 1995 (Barteau, 1996).

In contrast, ethanol oxidation is an exothermic reaction, which can be operated under adiabatic conditions when steam is used as a diluent. The oxidation of ethanol over a copper or silver catalyst in the form of wire gauzes or bulk crystals at 300-500°C and atmospheric pressure was widely practised commercially in the 1960s (Hayes, 1970). Steam is generally used as a diluent for ethanol in order to limit the temperature rise across the catalytic reactor. The conversion of ethanol is limited to about 40% in order to attain an acetaldehyde selectivity of about 95% (Hayes, 1970). In 1994 only about 13% of the acetaldehyde production capacity in Western Europe was based on the ethanol partial oxidation route. The last plant in the USA for the partial oxidation of ethanol was shut down in 1983. In Japan, acetaldehyde is exclusively produced by direct oxidation of ethylene Wacker-Hoechst processes. The driving force behind the observed shifts in economic viability of different commercial processes lies in the prices of different feedstocks (Lorenzetti, 2002). Recent developments in the production of ethanol derived from biomass fermentation in countries like Brazil might result in the shift of commercial processes back to ethanol oxidation processes (Barteau, 1996).

Downstream processes for the further oxidation of acetaldehyde to either acetic acid or ethyl acetate also impacts on the production of acetaldehyde. For many years synthetic acetic acid was mainly manufactured from acetaldehyde. At the beginning of World War I, commercial oxidation processes were operated by Hoechst, Wacker and Shawinigan. In 1979, 62% of the acetic acid came from acetaldehyde. Competitive feedstock caused this percentage to decrease to 28% by 1995 under pressure from methanol carbonylation, which then accounted for 55% of the production and was continuing to grow (Lorenzetti, 2002). The direct oxidation of ethanol to acetic acid or ethyl acetate in one step would be a highly desirable method of operation. A number of processes have been patented for the direct oxidation of ethanol to acetic acid (Walter, 1904 and 1905a and b). However, the difficulties of ensuring partial oxidation of the intermediately formed acetaldehyde to acetic acid without at the same time causing complete oxidation to carbon oxides have largely prevented the development of any commercial processes for the direct oxidation of ethanol directly to either acetic acid or ethyl acetate.

Another important product observed upon ethanol oxidation is ethyl acetate. In 1991, the worldwide production capacity for ethyl acetate was more than 700 000 tonnes per year, with about 300 000, 160 000 and 120 000 tonnes per year in Western Europe, Japan,

and the USA, respectively (Lorenzetti, 2002). Of the possible synthetic routes from ethanol to ethyl acetate, only two have been developed into industrial processes. In places where inexpensive ethanol is available, it is esterified with acetic acid using an acidic catalyst; a yield of 99% is obtainable. The Tishchenko reaction with acetaldehyde is the favoured process in countries where acetaldehyde is present in sufficient quantities as in Japan and Germany. The conversion of acetaldehyde into ethyl acetate known as a Tishchenko reaction was first reported in a German patent by Houben-Weyl (1933). The reaction is homogenously catalysed by an Al ethylate solution in an ethanol / ethyl acetate mixture, with zinc and chloride ions as promoters. The reaction is carried out at the temperature between 0 and 5°C and atmospheric pressure. 96% selectivity is obtainable at conversion of 95%, with acetadol being the main by-product.

1.3 MECHANISM OF ALCOHOL OXIDATION

The oxidation of alcohols over mixed metal oxides follows a parallel-consecutive pathway (Golodets, 1983). Reaction pathways have been interpreted as a consequence of bond strengths within the ethanol molecule (Cong *et al.*, 1997; Benziger, 1991), bond strengths in the solid surface (Rethwisch and Dumesic, 1986), geometry and coordination environment of the surface metal cations (Zhang *et al.*, 1995; Ono *et al.*, 1989; Kim and Barteau, 1989), and acidity and basicity of adsorption sites (Matsumara *et al.*, 1987; McKenze *et al.*, 1992).

Alcohols have been found to adsorb to various metal oxide surfaces by heterolytic dissociation of the O-H bond, with the proton going to a surface lattice oxygen and the remaining alkoxide fragment adsorbed to the surface cation (Figure 1-2; Idriss and Seebauer, 2000a).

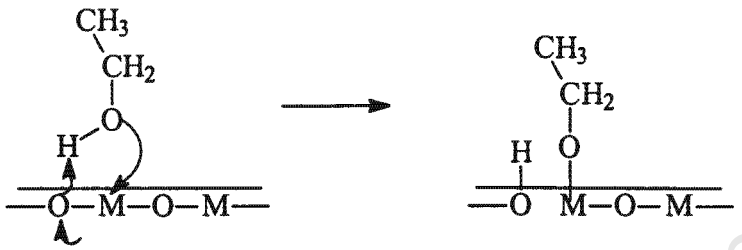

Figure 1-2: The heterolytic dissociation of O-H bond (adapted from Idriss and Seebauer, 2000a)

Yee *et al.* (2000a) used IR spectroscopy to investigate the adsorbtion of ethanol on the surfaces of CeO_2 and Pt/CeO_2. The study confirmed the dissociation of the O-H bond to form adsorbed ethoxy species attached to Ce^{4+} of CeO_2. Interestingly, the bond energy of the O-H bond (471.0 kJ mol^{-1}) is much greater than that of the C-O bond (338.7 kJ mol^{-1}) of an ethanol molecule (Sanderson, 1976). In this O-H proximity, one would assume that the adsorption of ethanol would involve cleaving the C-O bond since it possesses the lowest bond energy to overcome. Yet the majority of surface studies involving the adsorption of alcohols have shown that dissociation of the O-H bond predominates to produce surface alkoxide species (Kim and Barteau, 1990). Ethanol adsorption on oxide surfaces proceeds by heterolytic dissociative cleavage of the O-H bond and not the C-O bond as expected from the bond energy consideration. The stability of the resulting ions on the surfaces determines the observed cleavage pattern. The proton from O-H cleavage can be stabilised easily by the oxide, hence the observed ease of the ionisation of an O-H bond when compared to the C-O bond. Yee *et al.*, (2000a) however, attributed the observed cleavage to the phenomenon called the proximity effect; bonds tend to break when they are in relatively close proximity to the surface.

The adsorption of primary alcohols on ionic surfaces like those of metal oxides is believed to involve dipole-induced dipole bonds, as shown in Figure 1-3 (Yee *et al.*, 2000a).

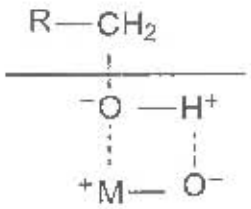

Figure 1-3: Adsorption of primary alcohol and formation of alkoxy species on a metal oxide (adapted from Yee et al., 2000a)

Further investigations in the oxidation of ethanol over CeO_2 have shown that there will be different types of ethoxy species depending on the exposed surface (Madhavaram and Idriss, 2001). The CeO_2 (111) surface contains terminating O^{2-}, while Ce^{4+} cations are in the second layer. The authors suggest that it is highly unlikely that a non-defective (111) surface can accommodate ethoxy species in a bidentate mode due to $O^{2-}_{(lattice)}$–$O_{(ethoxy)}$ electronic repulsion. However, it may accommodate ethoxy species in a monodentate mode if the spacing between two surface oxygen anions is large enough to allow electronic interactions between $O_{(ethoxy\ species)}$ and Ce^{4+} cations in the second layer (Figure 1-4). This structural effect resulted in the monodentate ethoxy ethoxy species being observed on (111) and bidentate species on (310). Different ethoxy species had earlier been reported upon the adsorption of ethanol on CeO_2 surfaces by Tu *et al.* (1994a and b).

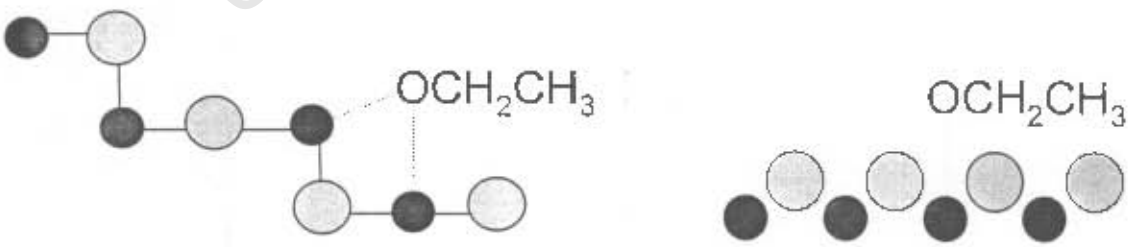

Figure 1-4 Schematic depiction of ethoxy adsorption on the a) CeO_2 (310), b) CeO_2 (111) surfaces. The grey circles represent the oxygen anions (ionic radius: 1.32Å), the black circles represent the Ce^{4+} cations (0.92Å), (adapted from Yee et al., 2000a)

Adsorbed methoxy species (monodentate, bidentate and tridentate) species have also been spectroscopically detected upon adsorption of methanol on various oxide surfaces, CeO_2 (Kiennemann *et al.*, 1991), ZnO (Diagne *et al.*, 1989), Al_2O_3 (Burch *et al.*, 1989) and MgO (Rajesh and Ozkan, 1993).

The amount of adsorbed ethoxy (ethoxy species) does not necessarily correlate with catalytic activity instead it correlates to the number of metal cations that are co-coordinative unsaturated. Furthermore, it can be correlated to the electronic charge distribution around the oxygen anions that tend to abstract the H^+ proton (Idriss and Seebauer, 2000b). The formed ethoxy can undergo dehydrogenation with subsequent electron donation (hydride transfer) to the active metal cation (due to antibonding character between H^+ and O^{2-}) yielding acetaldehyde, the primary product of ethanol oxidation (Figure 1-5).

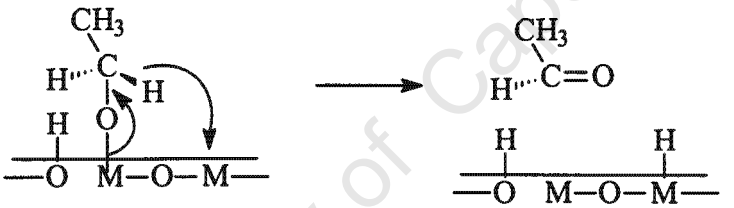

Figure 1-5: Dehydrogenation of ethoxy (adapted from Idriss and Seebauer, 2000b)

From Figure 1-5 above, it is clear that the surfaces that promote oxidative dehydrogenation reactions must contain easily reducible and re-oxidisable cations. The residual hydrogen from ethanol adsorption generally desorbs as H_2O originating from the recombination of adsorbed OH and M-H, desorption of which leaves an O vacancy and a partially reduced metal, which in the presence of gas phase O_2 is re-oxidised. In addition, two adsorbed OH species can combine to make one molecule of H_2O, one oxygen vacancy and one restored oxygen site.

Subsequently, the acetaldehyde may react along different pathways to form products like acetic acid, ethyl acetate, carbon oxides, acetone, crotonaldehyde and other polymerisation products. The adsorbed aldehyde undergoes further oxidation by lattice

oxygen resulting in the formation of acetate species provided the surface contains oxygen of sufficient mobility.

One important product from the further reaction of acetaldehyde over metal oxides is ethyl acetate, which can be formed via the Tishchenko reaction (Idriss and Seebauer, 2000b). Reported first by Ai (1983), Tishchenko reaction was observed over surfaces of U oxides and SnO_2-based catalysts, and later by Idriss *et al.*, (1991a) over Cu/Zn/Al catalyst systems. The reaction requires H transfer from one adsorbed acetaldehyde, which in turn becomes oxidised, to another adsorbed acetaldehyde, which then becomes reduced to an alkoxide. This process may form a complex in a transition state that requires participation of the surface oxygen (Figure 1-6).

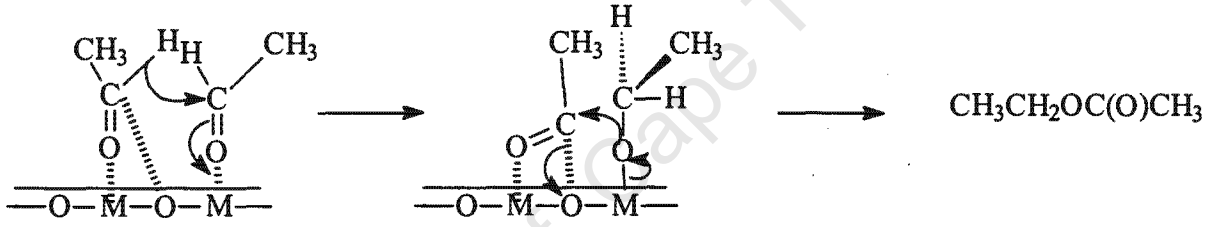

Figure 1-6: The formation of acetate species from adsorbed ethoxy species (adapted from Idriss and Seebauer, 2000b)

This results in a weakly bound acetate species in proximity of an ethoxy species, most likely in an unstable configuration. Both species react together yielding an ethyl acetate molecule and liberating surface oxygen. Basic oxides are found to be more active for this reaction (Idriss and Seebauer, 2000b).

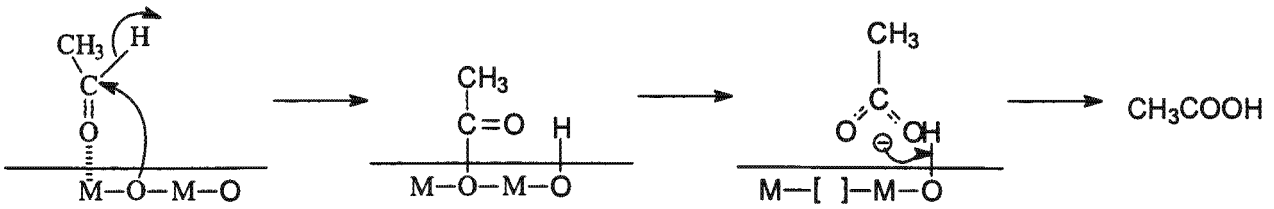

Figure 1-7: The formation of carbonate species from adsorbed acetaldehyde species (adapted from Andrushkevish, 1997)

In the presence of mobile oxygen species, the acetate species will react to form carbonate species that lead to the formation of acetic acid in the presence of surface hydroxyl species (Figure 1-7) or carbon oxides in the absence of any neighbouring species. In the latter, the carbonate species are further broken down by these mobile surface oxygen species to carbon oxides.

Idriss and Seebauer (2000a) as well as Grootedorst *et al.* (1994) showed that acetone is also formed in ethanol oxidation over CeO_2, TiO_2 and Fe oxides when surface acetate species are present. The reaction is thought to proceed via ketonization of two neighbouring acetates as follows:

$$2CH_3COO(a) \rightarrow CH_3C(O)CH_3 + CO_2 + O(s)$$

Figure 1-8: The formation of acetone from adsorbed ethoxy species (adapted from Idriss and Seebauer, 2000b)

O(s) in Figure 1-8 denotes oxygen incorporated into the surface. The authors identified two requirements for this reaction to occur. First, the surface must be able to donate its oxygen to adsorbed acetaldehyde. This requirement substantiates the lack of acetone formation over SiO_2, which has a very strong Si-O bond accompanied by a relatively low electronic polarisability. Second, one surface cation must be able to accommodate two acetate molecules (unsaturated coordination), otherwise the reaction will not proceed (Idriss and Seebauer, 2000a; b).

In some instances, coupling and bimolecular hydrogen hydrogenation reaction can occur to produce higher hydrocarbons as follows:

- Carbon-carbon bond formation from aldehydes is possible through aldolisation reactions. In particular, the β-aldolisation of two acetaldehyde molecules, with subsequent dehydration producing crotonaldehyde. Such reactions on the surface would require Lewis acid or basic sites to bind the two molecules and abstract an α-hydrogen. Crotonaldehyde formation has been observed on surfaces CeO_2 (Doca and Segal, 1985), TiO_2 (Doca and Segal, 1986), Al_2O_3 and β-UO_3 (Kanoun et al.,1991) among the other surfaces, upon the adsorption of acetaldehyde.

$$CH_3CH{=}CHCHO_{(ads)} + CH_3CHO_{(ads)} \longrightarrow CH_3CH{=}CHCH{=}CHCHO_{(ads)} + H_2O$$

Figure 1-9: The formation of crotonaldehyde and polymerization products from adsorbed ethoxy species (adapted from Idriss and Seebauer, 2000b)

- Abstraction of a hydrogen atom from acetaldehyde can yield an adsorbed acetyl species, $CH_3C{=}O_{(ads)}$; Acetyl species have previously been observed from acetaldehyde Pd/CeO_2 (Ono *et al.*, 1989). Further reaction of an acetyl with an adsorbed methyl group can result in the production of acetone (Doca and Segal, 1985).

- Two adsorbed aldehyde molecules may donate their oxygen to a reduced surface and couple together, forming a symmetric olefin molecule. This reaction has been observed on reduced oxides, such as UO_2 (Ono et al., 1989), H_2-reduced TiO_2 and Fe_3O_4 (Iwasawa *et al.*, 1978), and CeO_2 (Doca and Segal, 1985).

- Benzene is thought to form from the crotonaldehyde further reacting with adsorbed acetaldehyde (via the same β-aldolisation reaction) giving 2,4-hexadienal (Figure 1-9). This bulky molecule diffuses slowly in the pores and is thus subjected to further attack by active sites of the catalyst. In case of noble metal promoted metal oxides e.g. Pt/CeO_2 or Pd/CeO_2, it may come in contact with Pt and suffer a C-H bond

dissociation of the methyl group which after intramolecular cyclisation followed by H_2O elimination may give benzene. Benzene has been observed in considerable amounts in noble metal promoted metal oxides.

Figure 1-10 sums up possible reactions of the molecular adsorption of ethanol (Step 1), this is fast and it involves the dissociation of adsorbed ethanol, the rate-determining step. The ethoxy species that formed undergo dehydrogenation (Step 2) to form adsorbed acetaldehyde species.

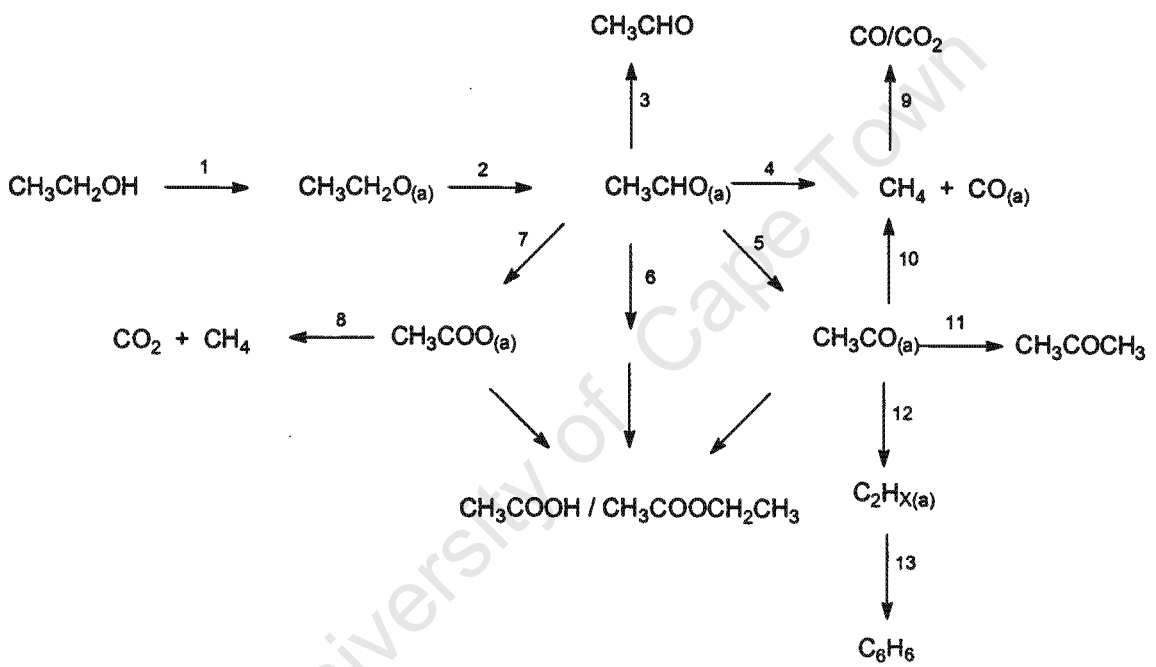

Figure 1-10: Schematic diagram of stoichiometric reactions (reactions 1–13) involved in the conversions ethanol to different oxidation products (adapted from Yee et al., 1999)

The reaction of the acetaldehyde controls the selectivity of the reaction. As depicted in Figure 1-10, there could be several competing reactions from this intermediate depending on the catalyst employed and the reaction conditions (Steps 3-7). The formation of the acetyl species (Step 5) could lead to different products such as acetic acid, ethyl acetate, acetone and combustion products.

The formation of ethylene from ethanol takes place by an independent pathway involving formation of acetyl species and irreversible C-O bond scission (Step 12). Benzene could be formed from polymerisation of the adsorbed ethylene species (Step 13).

Catalyst characteristics leading to different product spectra are explained in more detail in 1.6.1.

1.4 FACTORS AFFECTING ACTIVITY AND SELECTIVITY IN PARTIAL OXIDATION

Controlling selectivity is one of the central problems in catalytic hydrocarbon oxidation (Sokolovskii, 1990; Oyama, 1996; Haber, 1996). The problem arises naturally because reactants undergoing reaction can be oxidised to various extents, the final result depends on many opposing factors, the main factors being the following:

- The hydrocarbon-oxygen mixture can usually react along many different pathways in the network of competing parallel and consecutive reactions (see Figure 1-10).
- The C-H bonds in the initial reactant are usually stronger than those in the intermediate products, which makes oxidation reactions intermediates prone to rapid further oxidation.
- In hydrocarbon oxidation processes, thermodynamics favour the ultimate formation of carbon dioxide and water. Therefore, all products of partial oxidation are derived by kinetic control of the reaction.

The catalyst must, therefore, strictly control the relative rates, accelerating the series of consecutive elementary steps leading to the desired products and hindering those, in which unwanted by-products are formed. The following mostly inter-related factors have been identified as factors affecting the selectivity in oxidation catalysis (Grasselli, 2001).

1.4.1 Electrophillic versus nucleophillic oxygen

In studies on oxidative catalysis, great attention is placed on the state of oxygen on the metal oxide catalyst surface. Owing to the fact that oxygen does not only take part in the oxidation reactions as a reactant, but is also a component of the catalyst. The oxidation catalysts are usually mixed oxides which operate according to the redox process

suggested by Mars and van Krevelen (1954). According to this mechanism the substrate is oxidised by the solid and not directly by molecular oxygen of the gaseous phase. The role of dioxygen is to regenerate or to maintain the oxidised state of the catalyst. The oxygen atoms introduced into the substrate stems from the lattice. This mechanism involves the presence of two types of distinct active species: an active cationic species which oxidises the substrate and another species active for dioxygen reduction.

It has been shown that there are two types of oxygen, viz. electrophillic and nucleophillic oxygen, which are responsible for total and partial oxidation respectively (Bielanski and Haber, 1992). Electrophillic oxygen comprise of electron deficient adsorbed species such as superoxide O_2^-, peroxide O_2^{2-}, and oxide O^-, whereas nucleophilic oxygen includes saturated species such as terminal oxygen groups M=O or μ-oxo bridging groups M-O-M, both with the oxygen atom in a nominal O^{2-} state. For partial oxidation the higher binding energy is desirable as it restrict the over-oxidation.

A relatively inert oxygen molecule is activated by interaction with the surface of oxide catalyst as in Figure 1-11. The activation process involves co-ordination, electron transfer, dissociation and incorporation into the oxide lattice. Depending on the rate ratios of these steps, a certain amount of various activated states of oxygen will exist on the catalyst surface (Bielanski and Haber,1991).

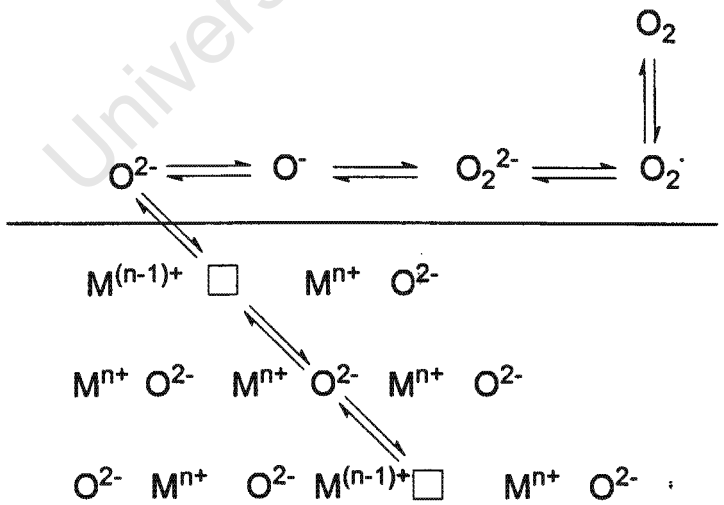

Figure 1-11: Oxygen equilibria at the surface of an oxide (adapted from Haber, 1996)

The concentration of highly reactive surface species on the catalyst surface is determined by the ratio of the rate of primary activation of oxygen to the rate of incorporation into the lattice. The faster the primary activation of oxygen and the slower its subsequent incorporation into the lattice is, the larger the amount of electrophilic oxygen that will form on the catalyst surface.

When the temperature increases, the equilibrium shifts in the direction of higher dissociation pressure of the oxide and the surface becomes populated with electrophillic oxygen species. When used as catalysts in oxidation of hydrocarbons, such oxides may show high selectivity to partial oxidation products at low temperature, when the surface coverage with electrophillic oxygen forms is low. On raising the temperature the selectivity to partial oxidation products rapidly decreases, whereas the conversion in total oxidation increases (Haber, 1988).

The presence of electrophillic oxygen (O_2^-, O_2^{2-} and O^-) at the surface of oxides has been observed by electron spin resonance spectroscopy at sub-ambient temperatures. At catalytic reaction conditions the charge on the oxygen species has been determined by electrical capacitance methods which involves a deduction from total surface space charge measurement. Surface potential measurements performed by Libre *et al.* (1983) and Barbaux *et al.* (1987) at catalytic conditions in an effort to correlate the presence of a specific species on the catalyst surface with the catalytic behaviour of that particular catalyst. It was found that whenever electrophillic oxygen species O_2^-, O_2^{2-} and O^- were present at the surface, total oxidation was observed in the catalytic hydrocarbon oxidation over metal oxide. However, when the nucleophillic O^{2-} species were present on the surface only selective oxidation products were formed.

Little is known about the electrophillic oxygen species population of the surface in transition metal oxides. Transition metal oxides are non-stoichiometric compounds. Their composition depends on the equilibrium between the lattice and the gas phase composition. Variations in oxygen pressure may change the stoichiometry of the oxide. This can be accommodated by the crystal lattice by generation of point defects or by alteration of the mode of linkage between the oxide coordination polyhedra. The latter results in the formation of extended defects (crystallographic shear). The relationship of defects to selectivity is generally not well understood (Oyama, 1996).

Due to the generation of point defects within the structure, a series of equilibria is established between oxygen species on the surface, lattice oxygen from the bulk and gas phase oxygen. Oxides that accommodate the change of stoichiometry by formation of shear structures show a different behaviour, because there are no vacancies formed on extraction of nucleophillic oxygen ion from the oxide. Instead a shear plane is formed or an existing one grows (Haber, 1982). Only nucleophilic oxygen species remain exposed at the surface. On raising the temperature the activity increases with growing mobility of oxygen, but the selectivity to partial oxidation products remain very high because of the absence of electrophillic oxygen. Studies concerning the surface oxygen state in association with crystallographic shear planes have been limited (De Rossi *et al.* 1982). Crystallographic shear planes have been suggested to assist bulk oxygen movement between the sites (O'Keefe, 1973; Anderson, 1970; Grasselli, 1986). Crystallographic shear planes are prevalent in the Mo, W, V, Nb and Ti oxide systems, but in industrial Mo-Te-O and Sn-Sb-O system they are not observed (Gai *et al.*, 1987).

Different studies of oxidation reactions have revealed that combustion is favoured at high oxygen coverage in most transition metals. Hence, oxidation selectivity can further be controlled by manipulating the oxygen coverage (Madix and Roberts, 1994; Bol and Friend, 1995).

1.4.2 Metal-oxygen bond strength

Golodets (1983) and Boreskov *et al.* (1968) investigated the thermochemical characteristics of metal oxides, namely the energy of oxygen binding with the metal of the oxide catalyst. It was proposed that the weaker the oxygen binding with the catalyst surface is, the more efficient complete oxidation is achieved with that particular catalyst. The authors established that for oxidation reactions over metal oxides that can be described with first order rate equation (i.e. first order with respect to the alcohol and zero order with respect to oxygen), the catalytic activity should decrease (Ea should increase) with increasing metal oxygen bond energy since cleavage of M-O bonds is the slow step. In view of the fact that in the formation of deep oxidation products more M-O bonds are broken than in partial oxidation, selectivity towards partial oxidation products increases with Qs

oxides at 300°C to be: Co_3O_4 > CuO > Mn_2O_3 > V_2O_5 ~ NiO > Fe_2O_3 > Cr_2O_3 > TiO_2 > MoO_3. The selectivity to formaldehyde in the oxidation of methanol over metal oxides at 300°C for both studies decreases in the order MoO_3 ~ TiO_2 > V_2O_5 > NiO > Cr_2O_3 > Mn_2O_3 > Fe_2O > CuO > Co_3O_4.

Recently there has been a notable increase in studies concerning the oxidation of ethanol over single metal oxides (Zhang *et al.*, 1995; Yee *et al.* 1999 and 2000a and b; Idriss and Seebauer, 2000a and 2000b). The increased interest in studies concerning the oxidation of ethanol is brought about the increase in biomass in countries like Brazil and Indonesia (Barteau, 1996). Though not as comprehensive as the methanol studies, the isolated studies on ethanol oxidation over single metal oxides have shown that the reaction follows the same pathway as methanol oxidation. Yee *et al.* (1999) demonstrated that that both methanol and ethanol adsorb dissociatively over single metal oxides CeO_2, TiO_2 and Al_2O_3. Idriss and Seebauer (2000a, 2000b) investigated a range of single metal oxides (SiO_2, TiO_2, Fe_2O_3, Fe_3O_4 and CaO) to establish mechanisms of ethanol oxidation over these single metal oxides. The authors found that in all cases ethanol tends to dehydrogenate to acetaldehyde, which for some oxides in turn reacts further to acetone and / or ethyl acetate.

1.5.2 Mixed metal oxides

Schuits and Gates (1983) argued for the need for complex catalyst systems for oxidation catalysts. The authors reviewed different industrial processes and came to a conclusion that it is necessary for the catalysts, especially oxidation catalysts, to be complex, assimilating in them multi-functionality needed to perform a combination of feats. The benefits associated with multifunctional catalysts has been demonstrated by many researcher in the hydrocarbon oxidation studies. Fattore (1975) conducted propylene oxidation over single metal oxides Fe_2O_3 and Sb_2O_4 independently. It was found that Fe_2O_3 was very active but unselective towards partial oxidation products, while the Sb_2O_4 was selective but showed very poor activity. When mixed the resulting catalyst showed overall improved activity and selectivity compared to the individual oxides. Thus the mixed Fe-Sb oxides catalysts combine the advantages of both oxides, i.e., the activity of Fe_2O_3 and the selectivity properties of Sb_2O_4.

colour of the oxide. The oxides with low values of Qs are deeply coloured (e.g. CuO, MnO_2, and Cr_2O_3), the oxides with moderate values of Qs are coloured less intensively (e.g. V_2O_5), and oxides with high Qs are only slightly coloured (e.g. MoO_3, WO_3 and TiO_2). This could be used as a first criterion to select catalyst for an oxidation reaction.

Trifiró *et al.* (1968, 1970 and 1971) studied the importance of the character of the metal-oxygen bond using infrared spectroscopy. A covalent metal-oxygen double bond was observed in a great majority of selective catalysts. Interestingly the covalent double bond was systematically absent from total oxidation catalyst. On the basis of these investigations it was suggested that this covalent metal-oxygen double bond of surface lattice oxygen must be directly involved in selective oxidation of olefins.

1.4.3 Acid-base properties of oxide catalysts

Bielański and Harber (1991) proposed that the acid-base interaction of reactants with the catalyst might affect the process in two ways. 1) As a result of acid-base reaction between the reactant and the catalyst, the active species may be generated which then more easily undergoes the redox process. 2) If strong acid-base interaction with the catalyst exists, strong chemisorption of reactants may take place. This concept was earlier demonstrated by Grzybowska-Swierkosz (1997), showing that the presence of Lewis acid sites of significant strength on the catalyst surface might be detrimental in the oxidation of hydrocarbon molecules with π-electron systems. Such molecules formed stable surface π-complexes with Lewis acid sites and become strongly adsorbed at the surface of the catalyst. Prolonged space-time increases the probability of total oxidation. The phenomenon was further demonstrated in the oxidation of o-xylene to phthalic anhydride on V_2O_5/TiO_2 catalysts, for which the complete coverage of TiO_2 surface by a monolayer of VO_X to block the acids sites considerably improved the selectivity to phthalic anhydride.

In primary alcohol systems, Golodets (1983) suggested that during methanol partial oxidation over a range of single metal oxides that salt-like species are formed during the formation of an alcoholate (alkoxy) species, which will remain on the surface depending on the acid-base properties of the surface. A strong interaction will result in prolonged space time and further attack of the hydrocarbon molecule by active oxygen species,

The authors attempted to correlate the rate of reaction in the oxidation of methanol over simple metal oxides and selectivity to partial oxidation products to the metal oxygen bond strength (Qs) (Figure 1-12). They observed opposite changes in the rate of oxidation of methanol and selectivity towards partial oxidation products with increasing metal oxygen bond strength. However, significant deviations were evident from both correlations suggesting that the oxygen-metal bond strength is not the sole factor determining the activity and selectivity over metal oxides. This can clearly be seen in Figure 1-12b where a rather poor correlation is observed.

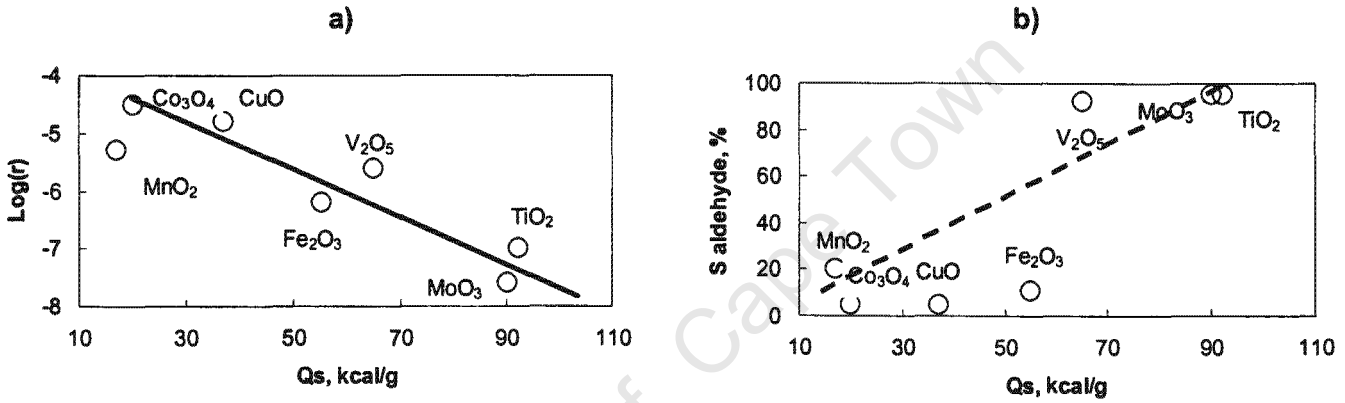

Figure 1-12: The correlation of the metal bond energy Qs with a) rate of methanol oxidation b) selectivity to formaldehyde (Adapted from Golodet, 1983)

Reducibility has often been used as a measure of the metal oxygen bond strength of an oxide. The hypothesis that the higher the reducibility, the higher the conversion and the lower the selectivity to partial oxidation products would be was first proposed by Sachtler and De Boer (1965). In the study of the oxidation of propylene, the authors correlated the differences in selectivity among different catalysts to the reducibility of the catalysts. However, marked differences in the catalytic activity for samples with very similar reducibility were observed. The differences were attributed to different active site densities in these catalysts.

Other characteristics have been used to establish metal oxygen bond energies of metal oxides. Since the metal-oxygen bond energy affects the band structure of the metal oxides, it should be expected that there might be a correlation with the width of the band gap (Golodets, 1969). This correlation should result in a relationship between Qs and the

(Schuit and Gates, 1983). The authors employed a model based on a grid of oxygen atoms to explain selectivity in propylene oxidation on copper oxide. They concluded that oxygen atoms must be distributed over the surface of the catalyst so as to limit the number of oxygen atoms at an active site. The authors postulated that the optimum number of oxygen atoms at an active site should be the number necessary to stoichiometrically obtain the desired product. The number of oxygen atoms could be controlled by isolating the site in various manners such as operating at an intermediate oxidation state, selecting metal oxides with an intrinsic limited grouping of oxygen atoms, or modifying the surface of an oxide with a reagent.

Okuhara and Mosono (1993) demonstrated by $^{18}O_2$ labelling of $(VO)_2P_2O_7$ that the oxidation of *n*-butane involves only catalytic sites near the surface that do not exchange oxygen with the bulk. On the same catalyst system for n-butane oxidation, Cavani and Trifiró (1997) postulated that vanadium sites on the surface are separated by phosphate groups imposing that all oxygen ions necessary for oxidation of the n-butane be in the close neighbourhood of the adsorption site. This limits the over-oxidation of n-butane hence the excellent selectivity obtained over V-P-O catalysts.

1.5 CATALYSTS FOR PARTIAL OXIDATION OF ALCOHOLS

Of the aliphatic alcohols' oxidation catalysis, the partial oxidation of methanol to formaldehyde, formic acid and methyl formate has received comprehensive coverage in literature over the years. In this section, partial oxidation of methanol over single metal oxides is discussed. In addition, some mixed metal oxides are reviewed with special attention given to vanadium antimonates and iron antimonates as proven catalysts for the amm(oxidation) of propane/propylene.

1.5.1 Single metal oxides

Single metal oxides have been studied to establish trends in activity and selectivity upon the oxidation of methanol (Boreskov, 1968, Golodets, 1983; Busca, 1987; Forzatti, 1987, 1989;). Boreskov (1968) has shown that the catalytic activity in the oxidation of methanol over single metal oxides using excess air at 300°C decreases in the order: $CuO > Mn_2O_3 > V_2O_5 > Cr_2O_3 > TiO_2 > MoO_3$. Golodets (1983) studied a wider range of single metal oxides and demonstrated an order of activity for methanol oxidation over single metal

resulting in the formation of total oxidation products. Consequently, the acid–base properties of the catalyst will influence the selectivity to the desired products to a great extent.

1.4.4 Exposed crystal face

There has been a lot of debate in literature surrounding the effect of surface structure in selectivity for partial oxidation reactions. There are two main opposing views: Volta *et al.* (1979, 1980, 1981, 1984; Volta and Portefaix, 1985) suggests that the effect of structure is substantial and can lead to large differences in selectivity depending on exposed crystal face. This conclusion was reached following elaborate studies of the oxidation of propylene over MoO_3. They observed that (100) side face was responsible for the formation of acrolein and the basal (010) phase was responsible for the formation of CO_X. On the other hand, Oyama (1988) acknowledges that there is an effect of exposed crystal phase, but that the selectivity differences are not so extreme.

In related studies, the assignment of selective phases was contested by Bruckman *et al.* (1987), whose study involving oxidation of allyl halides and allyl oxalate over MoO_3 presented a conclusion it is the phase (010) that is responsible for acrolein production. Further studies supported the structure sensitivity over MoO_3, and the sites responsible for selective oxidation were assigned to the low-coordinated molybdenum centres present on the edges of the crystallites (Desikan, 1991). The exposed crystal phase sensitivity has also been observed on the $(VO)_2P_2O_7$ for n-butane oxidation by (Cavani and Trifiró, 1995; Volta *et al.*, 1993) where the basal (100) plane was selective for producing of maleic anhydride while the side faces (021) and (001) were responsible for production of CO_X.

1.4.5 Site isolation

Callahan and Grasselli (1963) developed a concept of site-isolation theory, which requires that the active oxygen species is present in isolated regions on the catalysts surface, in order to obtain high selectivity to the desired product. According to this hypothesis, active sites must be isolated and metal-oxygen bond needs to be of appropriate strength for a useful redox system. The hypotheses led to the development and commercialisation of catalysts for the production of acrylonitrile and acrylic acid

Mixed metal oxides are used extensively in the oxidation of alcohols to different value added products (Golodets, 1990; Vedrine *et al.* 1997). The most important example in the oxidation of alcohols is the use of iron-molybdate oxide catalyst in industrial oxidation of methanol to formaldehyde (Meharg and Adkins, 1933). The oxidation of methanol over iron-molybdate is carried out at lower temperatures (350-400°C) compared to 550-600°C used when the alternative silver catalyst is employed. Pure MoO_3 exhibits high selectivity (>99%) under these conditions, but poor activity. Fe_2O_3 on the other hand is very active, but not selective towards the desired formaldehyde. The addition of Fe_2O_3 to MoO_3 causes an increase in activity, which is proportional to the iron content, up to a ratio of Mo:Fe = 1.5, without a notable effect on the selectivity to formaldehyde.

On ethanol oxidation, Castillo *et al.* (1994) investigated the effect of the addition of α-Sb_2O_4 to $FeMoO_3$, SnO_2 and MoO_3 oxides. The addition of α-Sb_2O_4 to these oxides did not seem to affect the ethanol conversion, however, the selectivity to acetaldehyde increased remarkably. The authors proposed that spill-over oxygen was formed on α-Sb_2O_4 that prevented the reduction of the oxides, thus maintaining the high selectivity. Elsewhere, it has been proposed that the spill-over oxygen transforms the non selective sites on the oxide surface into selective ones (Zhou *et al.*, 1991).

In general, the selectivity of complex systems Me_I-Me_{II}-O is determined by the nature of the more electronegative Me_{II} ion with Me_{II} e.g. Mo^{6+}, W^{6+}, V^{5+} and Ti^{4+}, over these metal oxides the selectivity is high, which is associated with the high selectivity of these higher oxides. When Me_{II} = Co^{3+}, the selectivity is low, which corresponds to low selectivity of Co_3O_4 (Golodets, 1983). The activity on the other hand is controlled by the less electronegative Me_I ion, with Me_I belonging to the class of Fe^{3+}, Co^{3+} and Mn^{3+}.

In catalytic oxidation studies, there is an ongoing search for better catalysts systems to replace old technologies. Two types of mixed oxide catalysts systems have been studied extensively for the amm(oxidation) of propane/propylene and are in consideration for commercialisation:

1) The Bi-V-Mo with scheelite-structure (Guttmann *et al.*, 1988; Andersson *et al.*, 1994).
2) The V-antimonates with rutile-structure (Sureh *et al.*, 1988; Nilsson *et al.*, 1996; Cavani *et al.*, 2000)

Consideration of the data in the patents (Guttmann *et al.*, 1988 and Sureh *et al.*, 1988) the latter catalyst system (V-antimonates) is most promising for industrial use. In the following vanadium and iron antimonates are comprehensively discussed. Extrapolations to more complex vanadium antimonates are also briefly reviewed.

1.5.2.1 Vanadium Antimonate

Vanadium antimony ($VSbO_4$) is a catalyst system with two-redox couples, Sb^{3+}/Sb^{5+} and $V^{3+}/V^{4+}/V^{5+}$ and an intriguing cation deficient rutile structure with the composition $V_{0.92}Sb_{0.92}O_4$ when prepared in air (Schuer and Klemm, 1973). Many researchers in the oxidation by metal oxides have emphasized that understanding of this basic mixed oxides would be key to the development of more complex and more efficient mixed metal oxides of the rutile V-Sb structure, e.g. with Mo, W or Al-modification (Nilsson *et al.*, 1996).

The non-stoichiometric structure of $VSbO_4$ has stimulated a lot of debate in the literature concerning the presence of different vanadium species and which of the species of the complex system are responsible for the activity in these catalysts (Young, 1993).

Recently, it was shown that V^{3+} has an effect on the enhancement of the activation of an alkane molecule (Cavani *et al.*, 2000). However, most of the studies on these catalysts attribute this role to the V^{4+} or V^{5+} centres (e.g. Grzybowska-Swierkosz, 1997).

1.5.2.1.1 Evolution of synthesis methods

The $VSbO_4$ phase was reported for the first time by Vernon and Milligan (1951), produced by a reaction between stoichiometric amounts of Sb_2O_3 and V_2O_5 at 750°C in air. The phase was identified as a tetragonal rutile-type structure that seemingly consisted of Sb^{3+} and V^{5+}. Roth and Waring (1968) confirmed the rutile structure. Schuer and Klemm (1973) measured the magnetic susceptibility of the compound and were able to exclude the presence of V^{5+} and Sb^{3+}, since these have no magnetic moment. The authors then suggested two possible compositions, either $V^{3+}Sb^{5+}O_4$ or $V^{4+}Sb^{4+}O_4$.

Birchall and Sleight (1976) heated equi-molar mixture of Sb_2O_3 and V_2O_5 in evacuated and closed gold tube at 700-800°C. The product contained Sb_2O_4 and a tetragonal rutile-

type phase. When this mixture was heated at 900°C, it resulted in an orthorhombic rutile-related phase with the composition $V_{1.05}Sb_{0.9}O_4$. Mössbauer spectroscopy measurement clearly showed that the antimony was penta-valent. Preparation in air at 800°C resulted in a tetragonal phase with the composition $V_{0.92}Sb_{0.92}O_4$. The authors suggested that the rutile-type phase could be divided into two continues series. The sample prepared in air belonged to the series $V_{1-x}Sb_{1-x}O_4$ ($0< x < 0.1$), and the material prepared in sealed gold tube belonging to the $V_{1+y}Sb_{1-y}O_4$ ($0< y < 0.1$) series.

Berry and Brett (1983) reacted equi-molar amounts of Sb_2O_3 and V_2O_5 in four different atmospheres. Under flowing oxygen-free nitrogen at 750°C, sublimation of Sb_2O_3 and formation of a single rutile-type phase occurred. The rutile-type phase was identical to that obtained by Birchall and Sleight (1976) in a sealed gold tube, but they indexed the phase as being tetragonal and as belonging to the series $VSb_{1-y}O_{4-3/2y}$ ($0 < y < 0.1$). Under similar conditions, except that the oxygen was not removed from the commercial nitrogen, a biphasic products was obtained consisting of a tetragonal rutile-phase and α-Sb_2O_4. The authors suggested that the rutile-type phase belonged to the series $VSb_{1-y}O_{4-2y}$ ($0 < y < 0.1$). The unit cell parameters of the rutile-type phase were within experimental limits of those obtained from oxygen-free nitrogen. Catalyst samples that were heat-treated in evacuated sealed tubes gave a biphasic product consisting of the same rutile-type phase and α-Sb_2O_4. In air the resulting catalyst was a rutile-type phase belonging to the series $V_{1-y}Sb_{1-y}O_4$ ($0 < x < 0.1$).

Hansen *et al.* (1993) confirmed the composition $V_{0.92}Sb_{0.92}O_4$ in a TGA experiment at 800°C in air and by EXD analyses. Young (1993) refinement and bond valence sums confirmed the presence of V^{3+}, V^{4+} and Sb^{5+} within the structure. The most favourable locations for the vacancies were calculated by the bond-valence sums for oxygen to be $OSb_2\Diamond$ (vacancy denoted by $\Diamond$).

Common synthesis methods include solid-state reaction, redox reaction in solution, sol gel and co-precipitation. Brief descriptions of these methods from literature are presented.

1) **Solid-state reaction (Cavani *et al.*, 2000)**: Samples were prepared by mechanical mixing and grinding of commercial V_2O_5 and Sb_2O_3 oxides. The

resulting mixture was calcined at 400°C for 6 hours and then at 600°C for 3 hours.

2) **Redox reaction in solution (Guttmann *et al.*, 1988; Glaesser *et al.*, 1988):** aqueous slurry containing Sb_2O_3 and NH_4VO_3 was refluxed in for 18 hours. The solvent was then evaporated and the resulting slurry dried at 100°C before calcination at 350°C for 4 hours and 500°C for further 6 hours under air. After the heat treatment the samples were ground and calcined further at 600°C for 2 hours.

3) **Sol gel (Toft *et al.*, 1988):** To an aqueous solution containing V_2O_5, a 30% aqueous solution of H_2O_2 was added in three aliquots to form the monoperoxo-vanadium ion. Stirred for 2 hours forming a sol or for about 16 hours to form a gel. Sb_2O_3 was then added to the sol or gel of vanadium and refluxed with stirring for 3 hours. Solvent was evaporated, and then dried at 110°C. Calcination was done at 350°C for 4 hours and 500°C for 6 hours under air, then at 600°C for 2 hours.

4) **Co-precipitation (Pal and Gupta, 1975):** Sb^{5+} -hydroxide is prepared by adding $SbCl_5$ into an aqueous solution of 10% H_2O_2 maintained at about 0°C. The filtered solid is then dried at 110°C. An aqueous solution of V^{4+} was prepared by reduction of V_2O_5 with a slight excess of oxalic acid at about 100°C and then the Sb^{5+}-oxide is added. The slurry was maintained under stirring and reflux for 3 hours, solvent was removed. Dried at 110°C and then calcined at 350°C for 4 hours and 500°C for 6 hours under air, at 600°C for 2 hours.

1.5.2.1.2 Influence of Calcination Temperature

A number of researchers on this catalyst system have shown that the calcinations temperature is of great importance. The chemical analysis of the mixed V-Sb hydroxide obtained after solvent evaporation indicates that all the vanadium was present in the V^{4+} state and about half the antimony was present as Sb^{3+} the remaining being Sb^{5+} for a V:Sb ratio of 1.0. Calcination in air at 500°C of the catalyst resulted in Sb_2O_3, α-Sb_2O_4 and $VSbO_4$ rutile phase as was also observed by Centi *et al.* (1994). Increasing the

calcinations temperature resulted in the decrease in the Sb_2O_3, α-Sb_2O_4 and remaining V^{5+} species. Heat treatment temperature of at least 780°C was shown to be necessary for the formation of pure $VSbO_4$ (Berry *et al.*, 1983; Birchall and Sleight, 1976). Centi and Parathoner (1995) also confirmed that monophasic $V_{1.05}Sb_{0.95}O_4$ [$V^{3+}_{0.95}$ $V^{4+}_{0.1}Sb^{5+}_{0.95}O_4$] forms by calcinations at about 900°C under anaerobic conditions. $V_{0.92}Sb_{0.92}O_4$ [$V^{3+}_{0.28}$ $V^{4+}_{0.64}Sb^{5+}_{0.92}O_4$] is formed by calcinations at about 750°C under aerobic conditions.

Post catalysts treatments to further refine the catalyst for maximum performance have also been reported. Lynch *et al.* (1997) demonstrated that treatment with alcohol post calcination improves the selectivity to the desired product possible by eliminating the formation of unselective side phases.

1.5.2.1.3 Structure of vanadium antimonate

Vanadium antimonate, $VSbO_4$, crystallizes in a rutile structure (Vernon and Milligan, 1951; Irigoyen et al., 2001) (Figure 1-13).

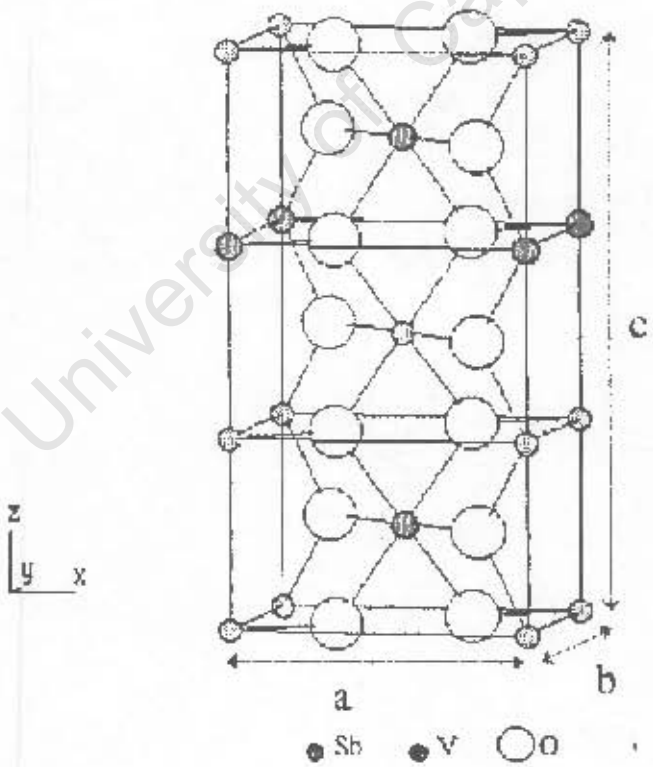

Figure 1-13: Crystal structure of vanadium antimonate tetragonal tri-rutile structure of vanadium antimonates (Irigoyen et al., 2001)

The rutile structure is formed by infinite chains of metal oxygen octahedral with shared edges and corners. Each metal center bounds to six oxygen atoms (O) while each oxygen bounds to three metal atoms (Me). The metal–metal distances in the resulting structure of coordination 6:3 are always relatively long and there is no effective O-O or Me-Me interactions. Additionally, open channels parallel to *z-axis* are formed in the crystal. The lattice parameters for $VSbO_4$ are: a = 4.636 Å b = 4.636 Å, and c = 9.144 Å (= 3 x 3.048 Å) (Berry *et al.* 1996).

1.5.2.2 Iron Antimonates

The properties of $FeSbO_4$ have mainly been studied using propylene or propane oxidation as a test reaction (Boreskov *et al.* 1968; Sala and Trifiro, 1976; Aso *et al.*, 1980; van Steen *et al.*, 1997 and Bowker *et al.*, 1996). Similarly, to the $VSbO_4$ system, the $FeSbO_4$ also crystallises in the tetragonal rutile structure (Boreskov *et al.*, 1968). However, compared to the $VSbO_4$, the $FeSbO_4$ has been shown to be less active in the amm(oxidation) of propane/propylene (Centi *et al.*, 1987).

1.5.2.2.1 Evolution of synthesis methods

Iron antimonates have been known since the end of nineteen's century (Hussak and Prior, 1897). The crystallographic structure of iron antimony was first uncovered by Mason and Vitaliano (1955) during the investigation of various antimony oxides and antimonates. They suggested the ideal formula to be $FeSbO_4$, rather than $Fe_2Sb_2O_7$, $Fe_2Sb_2O_6$ or $Fe_3Sb_3O_{12}$. However, it was Wells (1975) who fully established a random distribution of the cations over the oxygen octahedral with the following cell diameter a = b = 4.6351 Å, and c = 3.0734 Å. Similarly to the $VSbO_4$ in Figure 1-13, the tri-rutile structure with three unit cells stacked on top of each other is observed (Berry et al., 1987).

Common syntheses of iron antimonates are precipitation from slurry, solid state reaction and impregnation as described below:

1) **Precipitation (Allen *et al.*, 1991)**: The ferric nitrate ($Fe(NO_3)_3.9H_2O$) was heated to 60°C until all the ferric nitrate dissolve in its own water of crystallisation. Antimony oxide (Sb_2O_3) was added to the ferric nitrate solution and stirred. The mixture was then heated to 80°C until no further brown fumes evolved, the

resulting solution was then neutralised using NH_4OH, filtered and dried at 110°C for 24 hours. Calcined in air for 20 hours at 500°C and for 2 hours at 900°C.

2) **Solid-state reaction (Straguzzi *et al.*, 1987):** Sb_2O_3 is added to Fe_2O_3, and then calcined in helium for 16hours at 750°C.

3) **Impregnation (Straguzzi *et al.* 1987):** Impregnation of antimony oxide with iron was achieved by heating iron nitrate hydrate to form a solution. Impregnation of iron oxide with antimony was achieved by using a solution of Sb_2O_3 in tartaric acid and distilled water neutralised with aqueous ammonia. The required solution was then added to the iron or antimony oxide, the amount to be impregnated determined by the pore volume of the parent oxide. Alternatively, Yamazoe *et al.* (1980) used measured amounts of antimonic acid solution to impregnate onto iron oxide and calcined at 800°C for 2 hours.

1.5.2.2.2 Influence of Calcination Temperature

The effects of different preparation methods for $FeSbO_4$, including the effect of calcinations temperature have been intensively investigated by Stragussi *et al.* (1987), Burresci *et al.* (1982) and Carbucicchio *et al.* (1985). Generally, the heat treatment (calcination) results in a lower surface area than the uncalcined sample, and gives a more ordered structure. High temperatures are necessary for the completion of the solid-state reaction between Fe_2O_3 and Sb_2O_3. As demonstrated by Burresci *et al.* (1982), $FeSbO_4$ catalysts with the Fe:Sb ratio of 1 calcined below 550°C were contaminated by Sb_2O_3, Sb_2O_4, α-Fe_2O_3. Above 550°C, Sb_2O_3 phase disappeared, as the calcinations temperature is increased further Sb_2O_4 and α-Fe_2O_3 phases progressively decrease and at about 850°C only $FeSbO_4$ phase was observed.

1.5.2.2.3 Influence of Iron to Antimony ratio

Investigations into the partial oxidation catalysis by $FeSbO_4$ catalyst system have shown that excess antimony is beneficial in terms of catalytic activity and selectivity. The reasons given in literature for the observed effect are wide-ranging and mostly speculative. The nature of the active site and the structural changes caused by excess antimony are not well understood.

Boreskov *et al.* (1968) and Shchukin *et al.* (1970) suggest that the increased selectivity when excess antimony is present is due to the complete reaction of Fe_2O_3 to $FeSbO_4$, given that Fe_2O_3 is responsible for total oxidation reactions. However, this explanation is only valid for a Sb to Fe ratio up to 1.0 and cannot explain a further increase of the selectivity for iron antimony with Sb to Fe ratios larger than 1.0, where no Fe_2O_3 is present.

Sala and Trifiró (1976), in the investigation of the oxidation of 1-butene over iron antimonate observed the increase in selectivity with increasing Sb:Fe ratio. They ascribed the increase in selectivity to the formation of $FeSb_2O_6$ ($Fe^{2+}Sb_2^{5+}O_6$) a trirutile with the following structure:

Fe^{2+}-Sb^{5+}-Sb^{5+}-Fe^{2+}-Sb^{5+}-Sb^{5+}-Fe^{2+},

The above ordering, they postulated, gives higher selectivity than the normal 1:1 ratio of Sb:Fe which possesses the following atom order:

Fe-Sb-Fe-Sb

The authors ascribed the activity of iron antimonate to Sb^{5+} ions. The role of Fe^{3+} as they postulate was to catalyse the re-oxidation of the antimony ions, which are reduced during the interaction with the olefin. The assignment of activity centres was supported by others in the field (Grasselli, 1997, Millet *et al.*, 1995). However, in the study by Bowker *et al.* (1996) demonstrated that iron-rich catalysts were more active than antimony-rich catalyst showing that Fe^{3+} may possess some activity in these catalysts. This observation stimulates questions about the earlier conclusions concerning the active sites of the iron antimonates.

A more comprehensive study of the influence of the Sb:Fe ratio in the catalytic oxidation of propane was reported by Aso *et al.* (1980). The antimony content was varied between 0% (pure Fe_2O_3) and 100% (pure Sb_2O_4). In the antimony rich region, the phases of $FeSbO_4$ and Sb_2O_4 were detected by X-Ray diffraction analysis. The influence of the antimony content on the activity and selectivity to partial oxidation product (acrolein) was monitored. Pure Fe_2O_3 is a highly active catalyst, but promotes total combustion. While

Fe_2O_4 is very selective towards acrolein, the activity is very low. The selectivity to acrolein increases sharply at an antimony content of 50% ($FeSbO_4$), while a maximum specific rate for the formation of acrolein is reached at an antimony content of about 60%. The authors proposed that acrolein and CO_2 are formed by different kinds of surface oxygen. $FeSbO_4$ contains both types of surface oxygen species, the presence of excess Sb_2O_4 forms a particular surface structure on top of the $FeSbO_4$ phase and hence suppressing the deep oxidation. It is suggested that $FeSb_2O_6$ might be formed, however it could not be detected by X-ray diffraction analysis, because of similar crystal structure with $FeSbO_4$.

1.5.3 Complex vanadium and Iron antimonates

Other rutile-based systems have been reported in literature for propane ammoxidation, including Sn/V/Sb/O (Albonetti *et al.*, 1998); Cr/Sb/O (Ballarini *et al.*, 2001a, b); Ga/Sb/O (Sokolovskii *et al.*, 1995) and V/Nb/Sb/O (Mimura *et al.*, 1999). Various additives to the $VSbO_4$ have been investigated in the quest to obtain higher selectivity to partial oxidation products. Al and group VI transition metals have also been shown to enter in the active phase structure (Guttmann *et al.* 1988; Nilsson *et al.* 1996; Shishido *et al.*, 2001). It is speculated that they contribute to the further isolation of the active vanadium site in the catalyst, thus improving the selectivity towards acrylonitrile (Andersson *et al.*, 1994). Group VI transition metals, Cr, Mo and W were shown to be effective promoters, and are believed to work by providing active sites for the consecutive transformation of propylene to acrylonitrile leading to more selective catalysts (Guttmann *et al.* 1988; Shishido *et al.*, 2001).

Shishido *et al.* (2001) studied the oxidation of propane over Mo-V-Sb catalysts and found that the conversion of propane over Mo-V-Sb mixed oxides were lower compared to those obtained over V-Sb catalyst. They also observed a marked increase in the selectivity to acrylonitrile, which decreased with increasing Mo loading, due to the increased formation of ethylene and CO_X. When vanadium was absent from the catalyst the rate of ammoxidation and oxidation of propane was very low, confirming that the $VSbO_4$ phase is the active phase for the activation of propane.

More recently titanium has been studied as substituent to vanadium (Nilsson *et al.*, 1996). It was shown that titanium decreases the activity of the catalysts but increases

the selectivity to acrylonitrile. Such effect was explained by isolation of the vanadium centres in the active phase, which resulted in less number of V-O-V moieties. These have been identified as centres responsible for degradation of propane and propylene. The authors proposed that the activity could be correlated with the content of V^{3+} in the unit cell of the active phase whereas the selectivity to acrylonitrile could be correlated to the V^{4+}/V^{3+} ratio.

Ballarini *et al.* (2002) investigated the use of $CrSbO_4$ catalysts in the ammoxidation of propane, and later extended the study to rutile $CrVSbO_4$ systems Ballarini *et al.* (2002). The addition of vanadium to the $CrSbO_4$ increases the catalyst activity considerable. However, the selectivity to acrylonitrile decreases (Ballarini *et al.*, 2002).

1.5.3.1 Synthesis

Shishido *et al.* (2001) prepared the modified V-antimonate (Mo-V-Sb) using the slurry method. Sb_2O_3 was dispersed in oxalic acid aqueous solution, in which hot aqueous solution of NH_4VO_3 and $(NH_4)_3Mo_7O_{24}.4H_2O$ was added. The mixture was heated under reflux conditions at 90°C for 24 hours and water was evaporated at 90°C. The resulting mixture was dried at 100°C for 15 hours, and calcined at 350°C for 4 hours and then at 600°C for 6 hours in air.

Nilsson *et al.* (1996) prepared the Al-V-Sb catalysts employing the solid-state reaction method. The regions, in which a mixed phase is formed, were investigated under air at atmospheric pressure. The required amounts of $Al(OH)_3$, Sb_2O_3 and V_2O_5 were ground together and heated up to a maximum temperature of 680°C for 4 days.

Al-W-V-Sb has prepared using a slurry method (Nilsson *et al.*, 1996). The necessary amounts of $Al(OH)_3$, Sb_2O_3, V_2O_5 and $(NH_4)_6W_{12}(OH)_2O_{38}$ were reacted together according to the method described by Guttmann *et al.*(1988) and Glaesser *et al.*(1988 and 1989), and calcined as described above. In these catalysts, Al^{3+} is believed to replace V^{3+}, and two W^{4+} ions replace one Sb^{5+}

Ballarini *et al.*, (2001a, b, 2002) prepared the $CrSbO_4$ and $CrVSbO_4$ catalysts employing the co-precipitation technique, developed for the preparation of rutile SnO_2-based systems claimed by Rhodia (Blanchard *et al.*, 1997). The preparation involves the

dissolution of $Cr(NO_3)_3.6H_2O$, $VO(acac)_2$ and $SbCl_5$ in absolute ethanol, followed by dropping the solution into a buffered aqueous solution maintained at pH 7. A precipitate is obtained, which is separated from the supernatant liquid by centrifugation and filtration. The solid is then dried at 120°C, and calcined in air at 700°C for 6 hours, with a heating rate of 1°/min.

1.6 KINETICS OF ALCOHOL OXIDATION

The addition of oxygen to a hydrocarbon is nearly always thermodynamically favoured. When selective oxidation is aimed at, the reaction has to be kinetically controlled because the most stable situation is the complete combustion into water and carbon dioxide.

In general, the oxidation of alcohols over oxides obeys the first order rate equation:

$$r = k\,[\text{ethanol}]^n \bullet [O_2]^m \qquad (1\text{-}1)$$

Where n=1 and m tends to zero at and above 20% oxygen composition (Idriss and Seebauer, 2000a). The authors investigated the oxidation of ethanol over a range of single metal oxides (SiO_2, TiO_2, Fe_2O_3, Fe_3O_4 and CaO) and computed Arrhenius parameters as shown in Table 1-3. Also includes in the table is the data from Yee et al. (1999) which preceded Idriss and Seebauer (2000a) study. In this study, Yee *et al.* (1999) demonstrated that the doping of the metal oxide with a noble metal (Pt and Pd) substantially decreases the apparent activation energy and the pre-exponential factor.

Isolated studies by Zhang *et al.* (1995) on the oxidation of ethanol over single metal oxides are also presented in Table 1-3 for comparison purposes.

Table 1-3: Arrhenius parameters for ethanol oxidation over single metal oxides

Oxide	Ea (kJ/mol)	A (ml/g s)	References
Fe_3O_4	48.6	$1.2x10^4$	Idriss and Seebauer (2000a)
Fe_2O_3	59.6	$9.6x10^4$	Idriss and Seebauer (2000a)
TiO_2	76.9	$6.5x10^5$	Idriss and Seebauer (2000a)
CaO	61	$1.2x10^5$	Idriss and Seebauer (2000a)
SiO_2	104.8	$1x10^3$	Idriss and Seebauer (2000a)
CeO_2	75.4	$3.8x10^9$	Yee et al. (1999)
Pd/CeO_2	40	$4.7x10^5$	Yee et al. (1999)
CuO	50.6	$3.1x10^5$	Yee et al. (1999)
MoO_3	129		Zhang *et al.* (1995)

Idriss and Seebauer (2000a) confirmed the first order rate behaviour with respect to ethanol by the variation of conversion with flow rate at constant oxygen concentration. Acetaldehyde was formed as a major product. The authors proposed a relationship between the pre-exponential factor, activation energy, polarisability and the rate constant.

1.6.1 Elementary reactions

The reaction kinetics of the conversion of ethanol over metal oxides at temperature of 200-350°C has previously been reported by Gursahani *et al.* (2001). However, the study was performed under anaerobic conditions. Other studies of the kinetics of ethanol oxidation have been reported by Cong *et al.* (1997) and Rajumon *et al.* (1998) and were performed using Pt single crystal. Direct comparison to Gursahani *et al.* (2001) study cannot be made since temperatures, pressures and site geometries were different in these studies. However, surface chemistry comparisons can be made. Partial ethanol decomposition to form acetaldehyde is similar in all the studies. In addition, decomposition of acetaldehyde to C_XH_Y (C-O cleavage) as reported in Pt studies supports that proposed by Gursahani *et al.* (2001). The reaction pathway over a metal,

such as Pt, is expected to be quite different from the pathway over a (mixed) metal oxide under earobic conditions, which is the topic of this study. Golodets(1983) has shown that the primary and major product of the conversion of ethanol over metal oxides is acetaldehyde formed via the following stoichiometric reaction:

$$C_2H_5OH + ½\ O_2 \rightarrow CH_3CHO + H_2O \qquad (1\text{-}2)$$

The reaction of adsorbed acetaldehyde controls the product selectivity in the oxidation of ethanol. The prevailing conditions when the ethoxy species are formed determine the product selectivity spectrum. There can be many competing reactions of adsorbed acetaldehyde species resulting in different reaction products, the desired partial oxidation products shown below:

$$2CH_3CHO \rightarrow CH_3COOCH_2CH_3 \qquad (1\text{-}3)$$

$$2CH_3CHO + O_2 \rightarrow 2CH_3COOH \qquad (1\text{-}4)$$

These products can in turn react further to form combustion products and different undesired products. Partially reduced surfaces of V_2O_5, TiO_2, MoO_3, WO_3 and SnO_2 contain V^{4+}, Ti^{3+}, Mo^{5+}, W^{5+}, and Sn^{2+} ions associated with amphoteric oxides. These oxides easily form salt-like species and decompose them as acetaldehyde and secondary partial oxidation products. The catalysts Fe_2O_3 and ZnO in their partially reduced forms are characterised by basic properties which should give rise to strong salt-like species, the rates of desorption of these species should be low and this will decrease the rate of formation of acetaldehyde and consequently secondary partial oxidation products. The oxides of Ni, Co, Cu and Mn also show low selectivity to acetaldehyde, in this case the rate of acetaldehyde is fast however, that of the formation of total oxidation products from acetaldehyde is also fast leading to carbon oxides. The characteristic that renders the latter group metal oxides unselective is the low metal oxygen bond strength (Golodets, 1993).

1.6.2 Influence of reaction parameters

Oxidation reactions are not only dependent on the properties of the catalyst, but also on the conditions under which the reaction is carried out, i.e. temperature, contact time, diffusion parameters, efficiency of heat transport, pressure, etc. Extensive investigations on the effect of process variables on the oxidation of methanol over the vanadium titania catalyst were performed by Busca *et al.* (1987). The authors investigated the effect of temperature, pressure and space-time in the oxidation of methanol over metal oxides.

1.6.2.1 Influence of reaction temperature

The mechanism of a catalytic reaction on a given catalyst can change significantly with temperature. All oxidation processes are strongly exothermic and the temperature control is crucial. At moderate temperatures that are typical of industrial catalysis, mechanisms of alternating surface reduction-re-oxidation involving lattice oxygen (O^{2-} species) predominate. In accordance with earlier discussion on different oxygen species, the dominating intermediate under these conditions is O^{2-}, catalytic properties should depend on its bond energy, Qs. Sokolovskii (1990) explains that when the complete oxidation occurs through oxidised carbonate-carboxylate intermediates, the stepwise and concerted mechanisms reflect two paths of decomposition of surface species, under the action of molecular oxygen and thermal decomposition. The transition of one mechanism into another is determined by the thermal stability of surface species, which, in turn, depends on the heat of binding of oxygen abstracted from the catalyst during the course of decomposition of these species. The lower the heat of oxygen binding, the lower the temperature of the mutual transition of the mechanisms. The increase in temperature should therefore lead to the increase in electrophillic oxygen species which are responsible for over-oxidation products (carbon oxides).

1.6.2.2 Influence of reactants partial pressure

Muggli and Falconer (1998) proposed that the sites to which ethanol weakly adsorbs preferentially produce acetaldehyde, and the sites that form strong bonds with ethanol preferentially produce CO_2. Increasing the gas phase ethanol concentration should increase the amount of weakly bound ethanol species and therefore increases the rate of acetaldehyde production. Additionally, higher ethanol concentration should displace the adsorbed acetaldehyde into the gas phase faster. These observations are in agreement with the first order rate relationship proposed by Golodets (1983) and Idriss and Seebauer (2000a).

1.6.2.3 Influence of co-feeding water

The effect of mixing water with reactants in partial oxidation reactions was first reported by Trillat at the beginning of the 20th century (1902, 1903). Uhl and Cooper (1949) patented the idea in 1949, which concerned the overall increase in partial oxidation products when water is added to the reagents. There were many different some

opposing accounts for the observed effects. Valitov and Lakiza (1975) reported that the addition of water reduces the rate of dehydration of sec-butyl alcohol during its oxidative dehydrogenation over silver catalyst. Kurina and Morozov (1976) suggested that water prevents the decomposition of formaldehyde in the oxidation of methanol to formaldehyde. Sperber (1969) suggested that the observed effect was due to improved heat removal caused by the increased thermal capacity of the mixture thus decreasing reactor temperature in industrial processes. Recently, Medeiros *et al.* (2000) and Gonzalves *et al.* (2000) argued that there are two different types of oxygen species involved in dehydrogenation and total oxidation. The added water will interact preferential with one or other of these oxygen sites, thus affecting selectivity. The study used very low feed concentrations of ethanol to counter the argument by Sperber (1969).

Medeiros *et al.* (2000) argued that the addition of water decreases the formation of bridging carboxylate species by adsorbing to the sites decreasing the number of 2 free neighbouring sites that are needed for the formation of bidentate intermediates. The authors investigated the effect of adding water during the oxidation of ethanol over SnO_2 supported MoO_3. A 20% increase in the selectivity of acetic acid was observed. However, this increase in acetic acid appears to be accompanied by an increase in CO_X.

$^{18}O_2$ experiments in the presence and absence of water indicated a strong interaction between water and the catalyst surface, whereby water exchanged oxygen with the surface of the catalyst. Konishi *et al.* (1982) showed that water can act as a nucleophillic reactant by increasing the hydroxyl species on the catalyst surface or it can directly act as an oxidising reactant as shown by Yokoyama *et al.* (1995) for the reaction of benzaldehyde to benzoic acid over zirconium oxide. The agreeable conclusion from most of the researchers in this field is that the presence of water improves selectivity during oxidation of alcohols by suppressing the formation of carbon oxides.

1.7 RESEARCH OBJECTIVES

About 285 000 tons of ethanol are produced annually from the Sasol Fischer-Tropsch (hydrocarbons from coal) process in South Africa. The main objective of this thesis was to investigate the catalysis of the oxidation of ethanol over metal oxide to partial oxidation products (acetaldehyde, acetic acid, and ethyl acetate). A systematic catalysis study into the oxidation of ethanol was necessary in the South African context for the following reasons:

- South Africa has a feedstock advantage with more than 285 000 tons of ethanol produced from the Sasol Fischer-Tropsch process every year.
- During the time this study was proposed, Sasol was running out of storage facilities for the ethanol due to the shrinking Brazillian market owing to abundant supply of ethanol from biomass within Brazil. There was an urgent need for academic understanding of the ethanol oxidation catalysis technologies for a possible economical-viable, value-adding process.
- There are established processes for the oxidation of ethanol to acetaldehyde, however, direct oxidation to acetic acid or ethyl acetate has not been achieved industrially. The challenges associated with the direct oxidation of ethanol to acetic acid have not been fully understood. Over-oxidation has been quoted as one of the main reasons two-stage processes are adapted industrially.

To the best of our knowledge, there has not been a study on the oxidation of ethanol over $VSbO_4$ and $FeSbO_4$ catalysts (and modifications thereof). $VSbO_4$ and $FeSbO_4$ are well researched and proven catalysts for the amm(oxidation) of propane/propylene. Their ability to limit overoxidation is a desirable characteristic that can bring insight into understanding the mechanism of ethanol partial oxidation. Modification of these catalyst systems by sequential substituting V for Fe in $FeSbO_4$ or Fe for V in $VSbO_4$ was identified as a domain within these classes of catalysts that has not been explored.

The breakdown of the thesis objectives into research projects

1) To synthesise and characterise vanadium iron antimonate catalysts ($VSbO_4$, $FeSbO_4$ and $V_xFe_{1-x}SbO_4$, 0>x>1):

    a. To establish the formation of a solid solution as V/(V+Fe) ratio changes in $V_xFe_{1-x}SbO_4$, 0>x>1; given that $FeSbO_4$ crystallises with the same tetragonal rutile structure as $VSbO_4$.

    b. To investigate the effect of V/(V+Fe) ratio on the defective structure of $VSbO_4$ given that $FeSbO_4$ is stoichiometric and non-defective.

    c. To investigate the change in important $VSbO_4$ and $FeSbO_4$ characteristics such as the surface area, Lewis and Brønsted acidity, surface metal composition, electrical conductivity, V^{3+} / V^4 and vacancies content as a function of V/(V+Fe) ratio.

2) To investigate the effect of complexity of the catalyst in the partial oxidation of ethanol: i.e. single metal oxides (V_2O_5, Fe_2O_4 and Sb_2O_4), versus binary oxides ($VSbO_4$ and $FeSbO_4$), versus ternary oxides ($V_xFe_{1-x}SbO_4$, 0<x<1 catalysts).

3) To investigate the effect of V/(V+Fe) ratio of the ternary oxides ($V_xFe_{1-x}SbO_4$, 0<x<1) catalysts in the partial oxidation of ethanol. And more importantly identify active sites in these catalysts for the oxidation of ethanol.

4) To establish a reaction pathway for the oxidation of ethanol over vanadium iron antimonates by investigating the influence of reaction conditions (reaction temperature, ethanol/oxygen ratio, space-time and co-feeding water at different space-times) on the conversion of ethanol and selectivity to products.

EXPERIMENTAL

2 EXPERIMENTAL

2.1 CATALYSTS

Vanadium pentoxide, iron oxide, antimony oxide, vanadium antimonate, iron antimonate, vanadium iron antimonates and vanadium (aluminium or gallium) antimonates were used as catalysts for the ethanol oxidation.

2.1.1 Single metal oxides

The single metal oxides used for this study were obtained from commercial suppliers and were not treated further before use.

Table 2-1: Single metal oxides used for the study of ethanol oxidation

Metal Oxide	Purity (%)	Supplier	Batch number
Fe_2O_3	99.9	Strem	26-2750
Sb_2O_3	99.9	Strem	97-0380
V_2O_5	99.5	Strem	93-2321

2.1.2 Binary, ternary and quaternary mixed metal oxides

2.1.2.1 Iron antimonates and (iron-rich) vanadium iron antimonates

Iron rich compounds ($V_xFe_{1-x}SbO_4$, $x < 0.5$) were prepared according to a procedure described for the synthesis of iron antimonate by Bowker *et al.* (1996).

Preparation of iron antimonate ($FeSbO_4$)

To make 10g of $FeSbO_4$, 16.7g $Fe(NO_3)_3 \cdot 9H_2O$ (Saarchem, 98%) was heated to 80°C, 12.1g Sb_2O_3 (Strem, 99.9%) was then added under stirring. The solution was neutralized using an aqueous ammonia solution (Saarchem, 25% NH_3). The solvent was evaporated

from the resulting slurry and dried at 110°C for 24 hours. The solid obtained after drying was calcined in air at 500°C for 20 hours and 900°C for 2 hours.

Preparation of iron-rich vanadium iron antimonates

To make 10g of for example $V_{0.2}Fe_{0.8}SbO_4$, 13.4g $Fe(NO_3)_3 \cdot 9H_2O$ (Saarchem, 98%) was heated to 80°C, 12.1g Sb_2O_3 (Strem, 99.9%) and 1.0g NH_4VO_3 (Saarchem, 99%) were then added under stirring. The solution was neutralized using an aqueous ammonia solution (Saarchem, 25% NH_3). The solvent was evaporated from the resulting slurry and dried at 110°C for 24 hours. The solid obtained after drying was calcined in air at 500°C for 20 hours and 900°C for 2 hours.

2.1.2.2 Vanadium antimonate and (vanadium-rich) vanadium iron antimonates

Vanadium rich compounds ($V_xFe_{1-x}SbO_4$, $x > 0.4$) were prepared according to a procedure described for the synthesis of vanadium antimonate by Nilsson *et al.* (1994).

Preparation of vanadium antimonate ($VSbO_4$)

To make 10g of $VSbO_4$, 4.9g NH_4VO_3 was stirred in 150ml distilled water at 80°C then 12.3g Sb_2O_3 was added. The resulting slurry was then stirred under reflux at 110°C for 18 hours. The solvent was then evaporated and the resulting mixture was dried at 110°C for 24 hours. The solid obtained after drying was calcined in air at 200°C for 3 hours and 700°C for further 2 hours.

Preparation of vanadium-rich vanadium iron antimonates

To make 10g of for example $V_{0.7}Fe_{0.3}SbO_4$, 6.9g NH_4VO_3 and 10.2g $Fe(NO_3)_3 \cdot 9H_2O$ were stirred in 150ml distilled water at 80°C. 12.2g Sb_2O_3 was added to the NH_4VO_3 and $Fe(NO_3)_3 \cdot 9H_2O$ solution. The resulting slurry was then stirred under reflux at 110°C for 18 hours. The solvent was then evaporated and the resulting mixture was dried at 110°C for 24 hours. The solid obtained after drying was calcined in air at 200°C for 3 hours and 700°C for further 2 hours.

2.1.2.3 Vanadium aluminium antimonate and vanadium gallium antimonate

A similar procedure was used for the synthesis for $V_{0.7}M_{0.3}SbO_4$, (M = Ga or Al) as for the synthesis of vanadium antimonate (see section 2.1.2.2). The $Fe(NO_3)_3 \cdot 9H_2O$ was replaced with 3.235g $Al(NO_3)_3 \cdot 9H_2O$ (Saarchem, 98%) or 2.1270g $Ga(NO_3)_3 \cdot 9H_2O$ (Saarchem, 98%) to obtain the catalysts $V_{0.7}Al_{0.3}SbO_4$ and $V_{0.7}Ga_{0.3}SbO_4$, respectively.

2.1.2.4 Tungsten and niobium substituted vanadium iron antimonates ($V_{0.8}Fe_{0.3}Sb_{0.9}M_{0.1}O_4$, M = W or Nb)

The procedure for the synthesis of these compounds was similar to that for the synthesis of vanadium antimonate (see section 2.1.2.2). The reagents 1.004g $(NH_4)_6H_2W_{12}O_{40} \cdot XH_2O$ (Strem, 99.9%) or 1.4039g oxalic acid niobium salt (consisting of a mixture of 2:1 and 3:1 molar ratio of oxalic acid to niobium acetate complexes as well as some uncomplexed oxalic acid, having the total molar ratio of oxalic acid: niobium of 2.7) were added to the reagents in section 2.1.2.2 to obtain catalysts $V_{0.8}Fe_{0.2}Sb_{0.9}W_{0.1}O_4$ and $V_{0.8}Fe_{0.2}Sb_{0.9}Nb_{0.1}O_4$, respectively.

2.1.3 Post-synthesis treatment

To investigate the effect of washing, the washing of the catalyst after calcination was achieved by stirring the prepared solid in water at 80°C for 3 hours. Samples that were washed are suffixed with a (W).

2.1.4 Catalyst nomenclature

The catalysts were named according to the theoretical atomic composition of individual catalysts.

Table 2-2: Nomenclature used for prepared catalyst

Nomenclature	Theoretical molar composition, mol				
	V	Fe	Ga or Al	W or Nb	Sb
$VSbO_4$	1				1
$V_{0.9}Fe_{0.1}SbO_4$	0.9	0.1			1
$V_{0.8}Fe_{0.2}SbO_4$	0.8	0.2			1
$V_{0.7}Fe_{0.3}SbO_4$	0.7	0.3			1
$V_{0.7}Fe_{0.3}SbO4(W)$*	0.7	0.3			1
$V_{0.6}Fe_{0.4}SbO_4$	0.6	0.4			1
$V_{0.5}Fe_{0.5}SbO_4$	0.5	0.5			1
$V_{0.4}Fe_{0.6}SbO_4$	0.4	0.6			1
$V_{0.2}Fe_{0.8}SbO_4$	0.2	0.8			1
$V_{0.1}Fe_{0.9}SbO_4$	0.1	0.9			1
$FeSbO_4$		1			1
$V_{0.7}Al_{0.3}SbO_4$	0.7		0.3		1
$V_{0.7}Ga_{0.3}SbO_4$	0.7		0.3		1
$V_{0.8}Fe_{0.2}Sb_{0.9}W_{0.1}O_4$	0.8	0.2		0.1	0.9
$V_{0.8}Fe_{0.2}Sb_{0.9}Nb_{0.1}O$	0.8	0.2		0.1	0.9

*W means that the sample has been post treated by washing (see section 2.2)

2.2 CHARACTERISATION TECHNIQUES

2.2.1 Elemental analysis

The chemical compositions of the prepared solids were determined by atomic absorption using a Varian SpectrAA-30 spectrometer. Samples were prepared by digestion of the solid in hydrofluoric acid followed by dilution with boric acid and water.

2.2.2 BET surface area

The surface area was measured by nitrogen adsorption using a Micromeritics Accelerated Surface Area and Porosimetry (ASAP2000) instrument. The catalysts samples were initially dried *in-situ* at 350°C, nitrogen was then adsorbed stepwise at –196.15°C until ambient pressure was reached.

2.2.3 X-Ray diffraction

The step-scanned X-ray powder diffraction patterns were recorded at room temperature with 0.02°(2θ) steps over the 10-88°(2θ) angular range for 10 seconds counting time per step, using a Siemens D500 diffractometer and filtered CuKα radiation. The data obtained from the powder patterns have been used to calculate the unit cell of the compounds using a method proposed by De Wolff (1968).

2.2.4 Mossbauer spectroscopy

^{57}Fe Mössbauer spectroscopy was performed at 25°C with a time mode spectrometer and a constant acceleration drive. 2 GBq ^{57}Co/Rh was used as radiation source. The hyperfine parameters were determined using computational fitting programme with a precision of about 0.02 mm.s^{-1}. For iron-rich compounds, approximately 50 mg catalyst was mixed with 100 mg Al_2O_3 to avoid high Mössbauer absorption. However, for vanadium rich compounds Al_2O_3 was not used as a diluent; the samples were used as are. The samples were pressed into pellets and mounted in the cell.

2.2.5 *X-ray Photoelectron spectroscopy (XPS)*

XPS measurements were performed using a VG ESCALAB 200 R (Al Kα radiation, 1486.5 eV). Binding energies were corrected relative to the carbon 1S signal at 284.6 eV. For quantitative analysis, the signal intensities of Fe2p, $V2p_{3/2}$, $Sb3d_{3/2}$ and O1s were measured by using integrated areas under the detected peak according to the method of Reilmann *et al.* (1976). The O1s and $Sb3d_{3/2}$ peaks being superimposed, the O1s signal intensity was obtained by subtraction of the calculated $Sb3d_{5/2}$ signal intensity to the total intensity of the peak. Results expressed in terms of elemental ratios, were calculated with an experimental precision around 10%.

2.2.6 *Infrared spectroscopy*

IR spectra were recorded using a Bruker Vector 22 Fourier transform spectrometer. Self-supporting disks were prepared by pressing the calcined samples (about 70 mg). Adsorption experiments were carried out in a quartz infrared cell. The pressed catalyst samples were mounted into the cell and connected to a conventional vacuum line maintained at a base pressure of 5×10^{-5} Torr with a diffusion pump. The samples were heat-treated under vacuum for 1 hour at 220°C to remove any physiosorbed molecules. The background spectra were measured at 25°C. Pyridine was adsorbed at room temperature for about 3 minutes. A spectrum was then taken upon evacuating the cell for 20 to 30 minutes at 25°C. The cell was then sequentially heated and evacuated at 100°C, 150°C, 200°C, 220°C and 250°C for 1 hour, followed by spectra recording. All spectra were recorded at room temperature. The spectra presented in this work were obtained by subtracting the spectrum of the catalyst sample prior to adsorption from that of the sample on which pyridine was adsorbed at 25°C and desorbed for 1 hour at a particular temperature.

2.2.7 *Electrical conductivity*

The electrical conductivity (EC) measurements of the catalysts were carried out in a static cell as previously described by Hermann (1994). 120 mg of the powdered sample was placed between two platinum electrodes under a constant approximately atmospheric pressure ca. 10^5 Pa. The temperature of both electrodes was measured by two soldered thermocouples whose wires were also used as conductors for electrical

measurements when short-circuited. The electrical resistance of the samples was measured, according to the range investigated, with a Kontron multimeter (model DMM 4021) or with a digital teraohm-meter (Guildline Instruments, model 9520).

The samples behaved as bulk conductors and the apparent electrical conductivity σ ($ohm^{-1}.cm^{-1}$) was calculated from the conductance 1/R, and the geometric factor including the thichness t (*ca.* 2.5 mm) and the cross-sectional area S of the circular electrode whose diameter is equal to 1.00 cm.

$$\sigma = \frac{1}{R} \times \frac{t}{S} \qquad (2\text{-}1)$$

The measurements were carried out under programmed temperatures from 22 to 400°C with a heating rate of 5°C min^{-1} under dynamic vacuum.

2.2.8 XANES spectroscopy

V-K edge XANES spectra were collected at the LURE synchrotron facility in Orsay (D44) with a varying energy step of 1 eV/1s in the range 5420-5450, 0.3 eV/2s in the range 5450-5490 and 0.6 eV/1s in the range 5490-5560, with 3 scans per sample. A Si (311) double crystal monochromator was used for energy selection. To compare the different XANES spectra, the absorption background was first carried out using a linear law over the entire range and the spectra were normalized in the middle of the first EXAFS oscillation, at ca. 80 eV above the absorption edge (measurements done by Dr Jean-Marc Millet of the CNRS in France).

2.3 CATALYTIC TESTING

2.3.1 Experimental set-up for partial oxidation of ethanol

The catalyst samples were tested for their activity and selectivity in the partial oxidation of ethanol in a fixed bed reactor. Figure 2-1 shows the flow sheet of the partial oxidation

apparatus. The flow of air and nitrogen was controlled using the mass flow controllers (Unit).

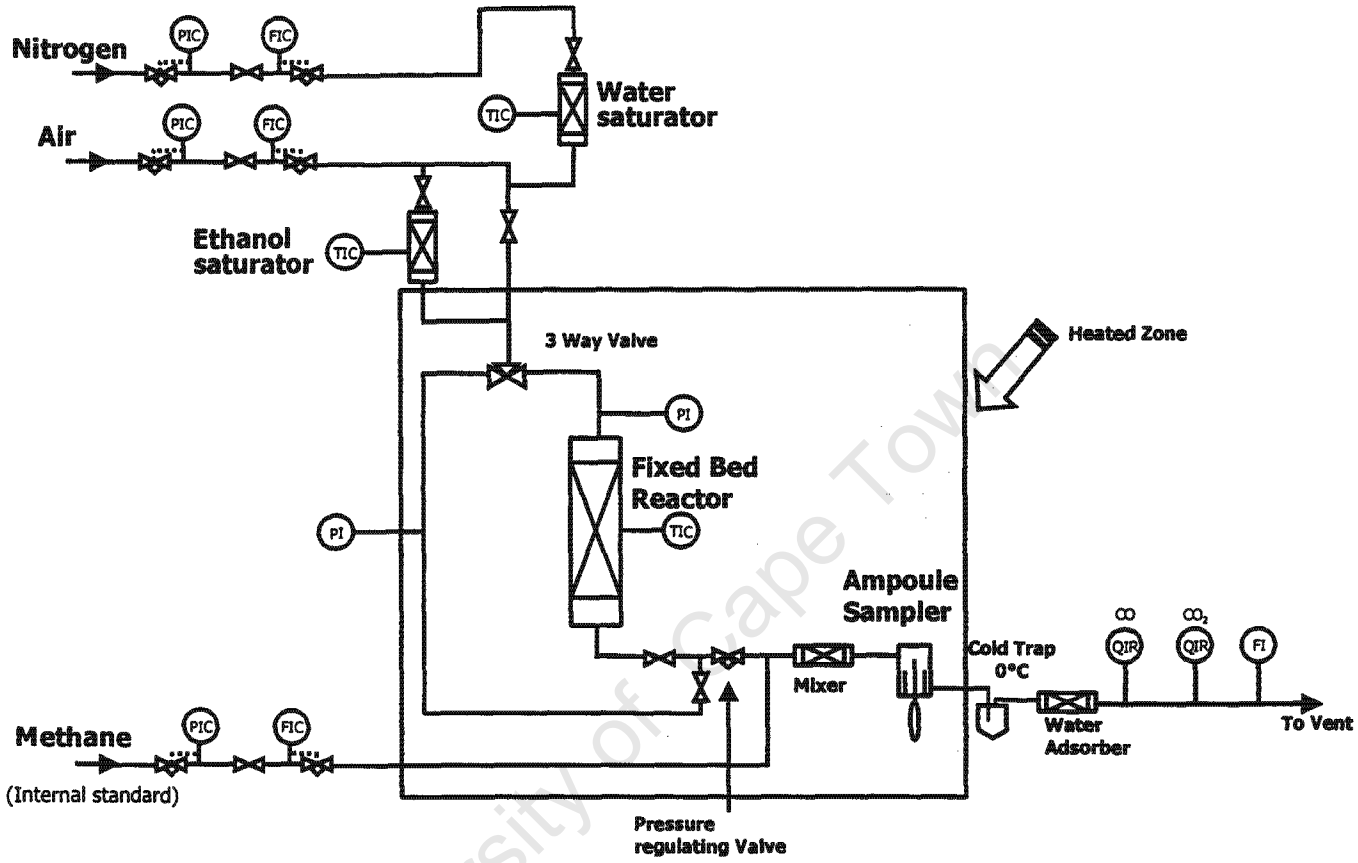

Figure 2-1: Flow sheet of experimental set-up for partial oxidation of alcohols

Ethanol and water (where applicable) were fed by passing a known flow of air through a fixed bed saturator, which contains acid washed chromosorb macroporous ®P (Sigma, 60 –80 mesh, surface area 4 m^2g^{-1}) serving as an adsorbent for the liquid (Figure 2-2). A water bath was used to regulate the temperature inside the saturator. A thermometer was inserted inside the saturator halfway through the chromosorb to monitor the temperature inside the saturator. A required partial pressure of ethanol at the saturator outlet was obtained by setting the saturator temperature at the value determined according to Antoine's Equation ($\ln (P_{vaporasation}) = A - (B/T=C)$. The saturator was maintained at that temperature using hot water bath circulation. A saturator calibration was performed by condensing the vaporised ethanol at the outlets over a period of time to ensure the reliability of the saturation procedure.

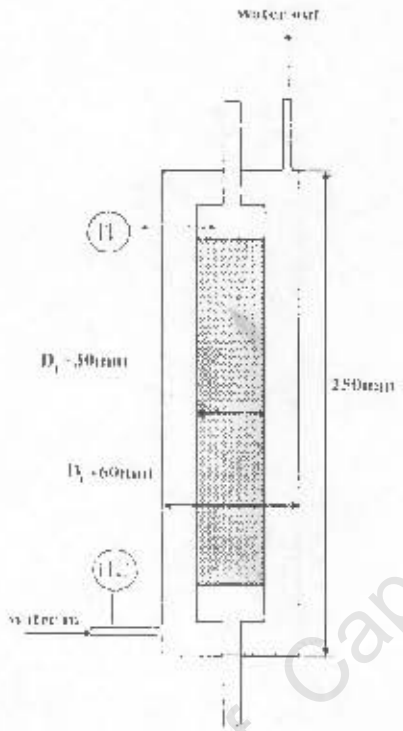

Figure 2 2. Chromosorb filled fixed bed saturator

Partial oxidation of ethanol was carried out in a U-shaped Pyrex reactor (see Figure 2-3) mounted in a convection oven. The pre-heater leg of the reactor was filled with washed sea sand (d_p >500μm), and the other leg with 0.5g of catalyst (d_p<106μm) mixed with 4.0g of silica carbide (d_p >200-450μm) to minimise temperature gradient. To measure the exact temperature inside the catalyst bed a thermocouple was inserted into the thermo-well that cuts through the catalyst bed as shown in Figure 2-3. The catalyst was heated up in air to reaction temperature. The reactants were introduced at the reaction temperature through the preheated leg of the reactor into the catalyst bed. The reaction conditions were kept uniform for all the runs, if not stated otherwise, i.e. WHSV of 2.436 $g_{alcohol}/(g_{catalyst} \cdot h)$, $p_{ethanol}$ = 0.2 bar, p_{O2} = 0.3 bar, balanced by N_2 to a total pressure of 1.7 bar. The reaction temperature was varied between 150 and 350°C.

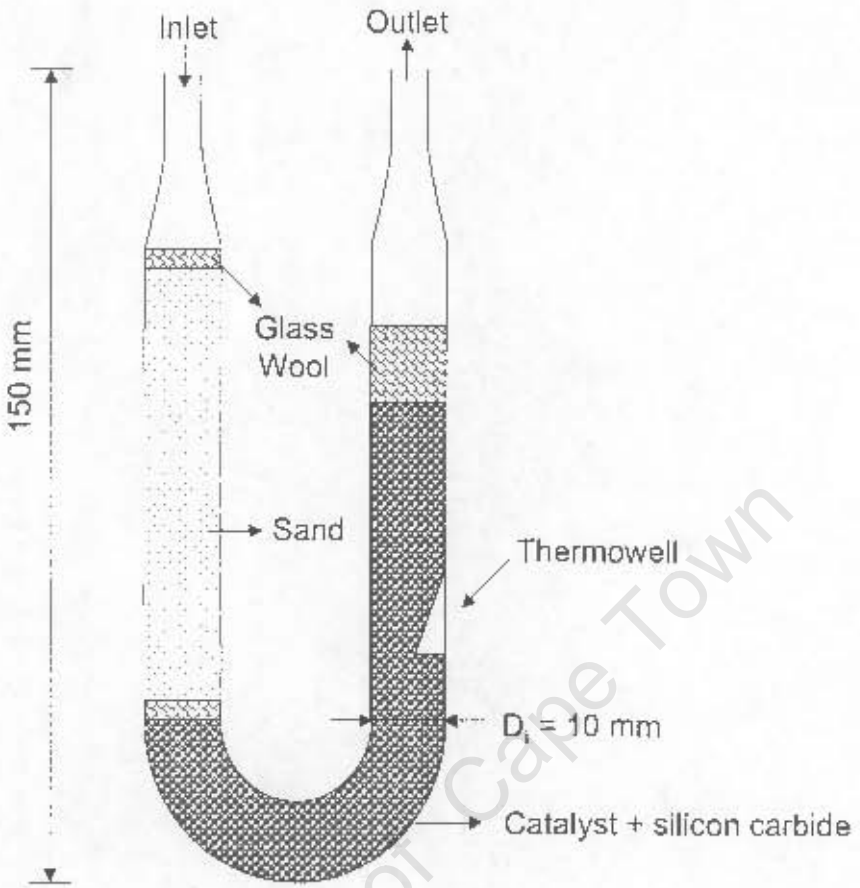

Figure 2-3: Pyrex U-shaped reactor used for catalytic oxidation of alcohols

A constant flow of an internal standard (methane) was added through a mass flow controller (Brooks) to the effluent of the reactor in order to obtain a quantitative momentary evaluation of the mass balance during the experiment.

Samples of the effluent stream were taken using an off line ampoule sampling technique (described in section 2.3.2.1). The complete oxidation products CO and CO_2 were monitored continuously using an on-line IR-analyser. The flow of the dry effluent was determined using a soap bubble meter before venting off.

2.3.2 *Product sampling and analysis*

2.3.2.1 Ampoule Sampling Technique

The off gas samples were taken using the ampoule sampling technique developed by Schulz *et al.* (1984). Samples of the reactor efffluent were collected by inserting a pre-evacuated glass ampoule in the effluent line (Figure 2-4). Breaking the glass ampoule with a fork allowed the gas to flow into the ampoule. The ampoule filled with the sample was then sealed off using a flame. The samples contained in ampoules were analysed by breaking them in a heated ampoule-breaking device and flushing the content into the capillary column of a gas chromatograph.

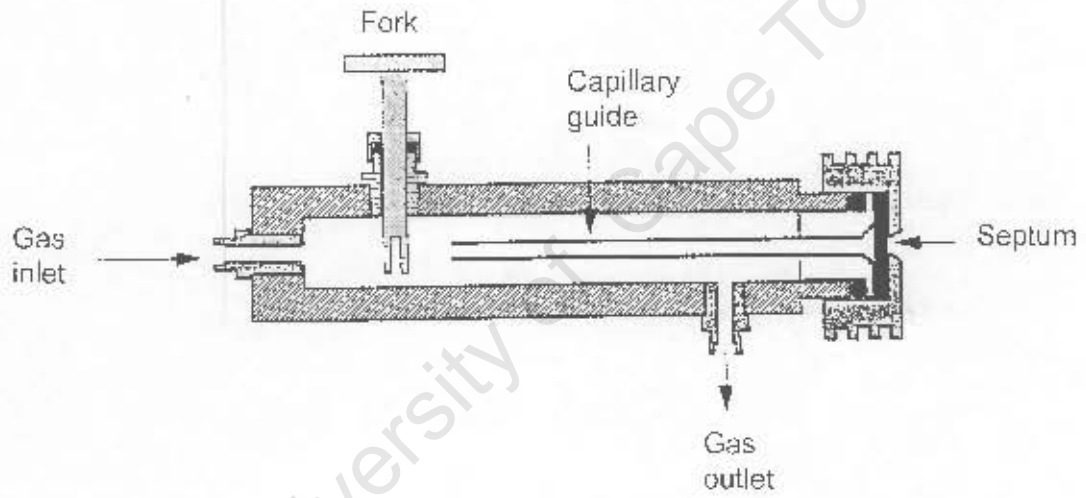

Figure 2-4: Ampoule Sampling System (adapted from Schulz et al., 1984)

2.3.2.2 Gas Chromatography Analysis of Organic Products Compounds

GC analysis of the samples contained in ampoules was carried out using a Varian 3400 gas chromatograph with a modified GC injector port as shown in Figure 2-5. The ampoule to be analysed was carefully placed inside the ampoule breaker cevise using glass wool to cushion the descent into the well. The well was then sealed at the top using a movable plunger. Nitrogen was used to flush the ampoule breaker. Prior to the analysis the 6-way valve was switched, so that the carrier gas, N_2, was flowing through the ampoule breaker. The ampoule was then broken to release the sample by pushing

down the plunger crashing the glass ampoule against the base of the device. The carrier gas (hydrogen) carried the sample to the injector port of the GC into the capillary column. After analysis a nitrogen stream flushed the ampoule breaker. The lines of the ampoule breaker device were heated to 170°C to prevent product condensation. The injector temperature was kept at 150°C.

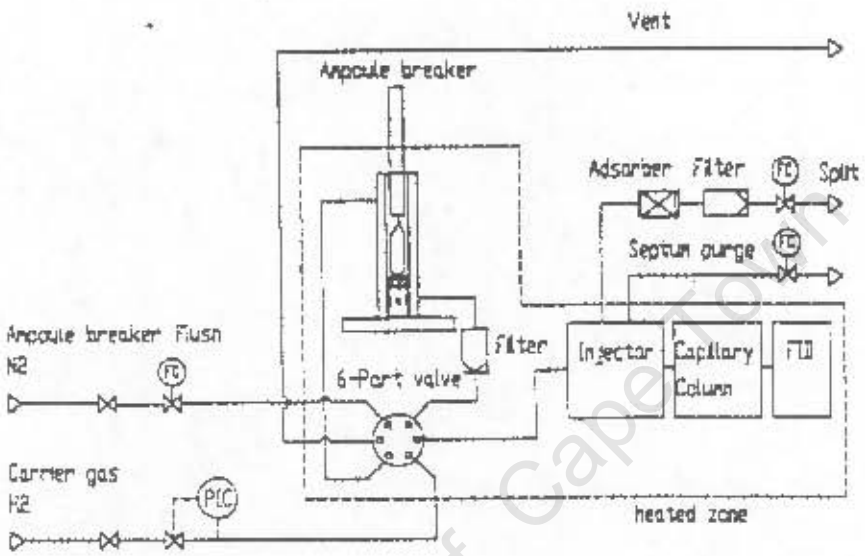

Figure 2-5: Flowsheet for the ampoule breaker device (adapted from Schnobel, 1997)

The GC was equipped with a flame ionisation detector (FID) maintained at 250°C. An OV-101 type capillary column was used to separate organic products under conditions shown in Table 2-3. The organic products compounds were analysed under isothermal conditions (35°C)

Table 2-3: Gas Chromatography operating conditions for the analysis of organic product compounds in ethanol oxidation.

Column	OV-101
Column length (m)	25
Inner diameter (mm)	0.32
Stationery phase	Phenyl dimethyl siloxan
Film thickness (μm)	0.5
Column head pressure (psi)	15
Split ratio	1:100
Gas flows	H_2 (30 ml (NTP) / min)
	Air (300 ml (NTP) / min)
Make-up gas	N_2 (20 ml (NTP) / min)
$T_{injector}$	150°C
$T_{detector}$	250°C
$T_{analysis}$	350°C

An example of a GC traces will be shown in **Appendix I.**

2.3.2.3 CO and CO_2 analysis

Carbon oxides were analysed on-line using a Hartmann and Braun CO/CO_2 IR-analyser. Magnesium perchlorate was used to dry the stream before entering the analyser. The instrument measures the volume percent on dry basis of the carbon oxides in the exit stream of the reactor.

2.3.3 Evaluation of catalytic runs

2.3.3.1 Conversion, Yield and Selectivity

The conversion and yield of the various product compounds were determined based on the amount of carbon in ethanol fed to the reactor. All calculations were done on a carbon basis.

$$X_{ETOH} = 1 - \frac{\dot{n}_{C,ETOH,out}}{\dot{n}_{C,ETOH,in}} \quad (2\text{-}2)$$

$$Yi = \frac{\dot{n}_{C,i,out}}{\dot{n}_{C,i,in}} \quad (2\text{-}3)$$

The molar flows of the organic compounds in the effluent and in the feed were determined using the ratios of the area A_i of the peaks for each component i relative to the area A_{ref} of the peak for the internal standard (methane) from the GC analysis.

$$X_{ETOH} = 1 - \frac{\left(\frac{A_{ETOH}}{A_{ref}}\right)_{out}}{\left(\frac{A_{ETOH}}{A_{ref}}\right)_{in}} \quad (2\text{-}4)$$

$$Yi = \frac{\left(\frac{A_i}{A_{ref}} \cdot f_i\right)_{out}}{\left(\frac{A_{ETOH}}{A_{ref}} \cdot f_{ETOH}\right)_{in}} \quad (2\text{-}5)$$

With f_i being the carbon based response factor for the component i for the flame ionisation detector (FID). The response factor for the alcohols used in the experiments were determined experimentally based on the response of n-heptane, which is defined as 1.0 per carbon atom. Different mixtures of n-heptane and an oxygenate for which the response factor is required were prepared and analysed by Gas Chromatography. The response factors were calculated using the following equation

$$f_i = \frac{A_i}{A_{n-heptane}} \cdot \frac{n_i}{n_{n-heptane}} \cdot f_{n-heptane} \quad (2\text{-}6)$$

The response factors for the reactants and products are summarised in Table 2-4

Table 2-4: Response factors (f_i) for ethanol and ethanol partial oxidation products

Compound	Experimental f_i	Calculated f_i
Ethanol	0.775 ± 0.005	0.75
Acetaldehyde	0.50± 0.01	0.50
Acetic acid	0.33± 0.03	0.5
Ethyl acetate	0.65± 0.02	0.625
Diethyl Ether	0.75± 0.02	0.75

These values compared agreeably to those calculated according to the method proposed by Kaiser (1969), which stipulates that the signal of a CH_3- and of a CH_2- groups equal to 1.0, CH_2-O equal 0.5, while the signal of an aldehyde and acetate groups equal to 0.

The product CO and CO_2 were not detected by the FID and therefore Equation (2-6) could not be applied for those products. The IR photometer measured the concentrations of CO and CO_2 in the effluent in vol-%, which is equivalent with mol-%, x_i. The molar flow of CO and CO_2 in the effluent were calculated using the ideal gas law:

$$\dot{n} = \frac{p \cdot F}{R \cdot T} \cdot x_i \qquad i = CO, CO_2 \tag{2-7}$$

$$Y_i = \frac{\frac{p \cdot F}{R \cdot T} \cdot x_i}{\left(\frac{A_{ETOH}}{A_{ref}} \cdot f_{ETOH} \right)_{in} \cdot \dot{n}_{ref}} \tag{2-8}$$

The flow F was measured using a soap bubble meter and the flow was corrected to standard conditions (T = 25°C, p = 1,013 mbar)

The selectivity for the formation of compound *i* was defined as:

$$S_i = \frac{Y_i}{\sum Y_i} \tag{2-9}$$

This definition was chosen to minimise errors due to inaccuracies in the C-balance.
In order to track the fate of all carbon atoms fed into the reactor during the experimental run, a carbon balance for each run was calculated using Equation (2-8):

$$C-balance = \frac{\sum_i^n \left(\frac{A_i \cdot f_i}{A_{ref}} \right)_{out} + \frac{\frac{p \cdot F}{R \cdot T} \cdot (x_{CO} + x_{CO_2})}{\dot{n}_{ref}}}{\left(\frac{A_{ETOH} \cdot f_{ETOH}}{A_{ref}} \right)_{in}} \tag{2-10}$$

2.3.3.2 Kinetic evaluation

The selective oxidation of ethanol was modelled as a 1st order reaction, i.e.

$$-r_{ETOH} = k \cdot p_{ETOH} \tag{2-11}$$

(Golodets 1983; Zhang *et al.*, 1995; Yee *et al.*, 1999; Idriss and Seebauer 2000a). The change in the partial pressure to expansion can be neglected, since the nitrogen content in the feed gas is high.

$$-r_{ETOH} = k \cdot p_{ETOH,feed} \cdot (1-x) \tag{2-12}$$

The reactor was approximated as a plug flow reactor, and thus the rate constant k is obtained from

$$k = \frac{-\ln(1-x)}{p_{ETOH,feed} \cdot \frac{W}{F}} \tag{2-13}$$

The activity of the catalysts was determined as a function of temperature. The activation energy and pre-exponential factor were obtained by the best fit of the measured conversion as a function of temperature in the range of conversion between 5 to 30 %-

mol. The lower limit is given by the accuracy in the determination of the conversion, whereas the upper limit is given by possible deviation from 1st order kinetics, due to oxygen depletion and product inhibition.

2.3.4 Overview of catalytic experiments

2.3.4.1 Ethanol oxidation over single and mixed metal oxides

The catalytic activity and selectivity of the mixed metal oxides were tested in the selective oxidation of ethanol. The partial oxidation of ethanol was investigated under the following set of reaction conditions: WHSV = 2.436 $g_{ethanol}/(g_{catalyst} \cdot h)$, $p_{ethanol}$ = 0.27 bar, P_{O2} = 0.3 bar, balanced by N_2 to a total pressure of 2.0 bar. The reaction temperature was varied by 10 or 20°C increments between 200 and 350°C.

2.3.4.2 Effect of inlet water partial pressure in ethanol oxidation

In order to elucidate the effect of water in the selective oxidation of ethanol, various space-times were employed for the oxidation of ethanol over $V_{0.7}Fe_{0.3}SbO_4$. In which water was co-fed to the reactor. The space-time was varied by changing the mass of catalyst between 0.0625 and 1.0000g as shown in Table 2-5.

Table 2-5: Catalyst mass used for the effect of inlet water partial pressure experiments

Experiment no	Catalyst mass, g
1	0.0625
2	0.1250
3	0.2500
4	0.5000
5	1.0000

The inlet partial pressure of ethanol was kept constant at 0.27 bar and the inlet partial pressure of oxygen at 0.3 bar. The inlet water partial pressure was varied between 0.0 and 0.27 bar. The total inlet pressure was kept constant at 2 bar, by changing the inlet partial pressure of nitrogen. The reaction temperature was varied between 210 and 270°C. Two saturators were used for these experiments; conditions were varied as shown in Table 2-6. The parameters in Table 2-6 were altered systematically to enable

the study to focus on the effect on one parameter on the oxidation of ethanol, i.e. water partial pressure.

Table 2-6: Conditions used for the investigating the effect of water partial pressure on oxidation of ethanol over $V_{0.7}Fe_{0.3}SbO_4$ catalysts

P_{water}	$V_{air\text{-}ethanol}$, ml	$V_{air\text{-}water}$, ml	$T_{sat\text{-}ethanol}$, °C	$T_{sat\text{-}water}$,°C
0.00	58.1	0.0	49.0	25.0
0.05	36.8	19.9	56.6	55.1
0.10	31.8	23.5	59.2	65.6
0.15	28.9	25.1	61.0	72.3
0.20	26.7	26.1	62.4	77.4
0.25	25.0	26.6	63.6	81.5
0.27	24.4	26.7	64.1	83.0

P_{water} is the partial pressure of water obtained at a set temperature of the water saturator $T_{sat\text{-}water}$. Tsat-ethanol is the temperature of the ethanol saturator, which increases, with the decreasing volume of air through the ethanol saturator ($V_{air\text{-}ethanol}$) to ensure a constant partial pressure of ethanol. The total volume of air passing through the system had to remain constant throughout the series of experiments to ensure a constant partial pressure of oxygen. The volume of air through the water saturator ($V_{air\text{-}water}$) was increased with increasing partial pressure of water

2.3.4.3 The effect of ethanol/oxygen ratio in the oxidation of ethanol over $V_{0.7}Fe_{0.3}SbO_4$ catalysts

The conditions used for this exercise were the following: WHSV of 0.3045 $g_{alcohol}/(g_{catalyst} \cdot h)$, $P_{alcohol}$ = 0.7 - 0.47 bar, P_{O2} = 0.3 bar, balanced by N_2 to a total pressure of 2.0 bar, $T_{Reaction}$ = 210 and 250°C.

Table 2-7: Saturator temperature and the resulting vapour pressure of ethanol for the study of varying ethanol concentrations in the oxidation of ethanol over $V_{0.7}Fe_{0.3}SbO_4$

$T_{Saturator}$, °C	$P_{Ethanol}$, bar
24	0.7
40	0.17
49	0.27
55	0.37
60	0.47

2.3.4.4 The rig shut down procedure

The termination of an experimental test of alcohol oxidation over metal oxides was performed as follows:

- The alcohol feed was switched off (by isolating the saturator, and cooling it down).
- Then the temperature was decreased in 50°C increments under the airflow.
- Once at room temperature, the air supply was shut off.
- The catalyst was then unloaded from the glass reactor

2.3.5 Intermediates and products identification techniques

2.3.5.1 Temperature Programmed Desorption (TPD)

Temperature programmed desorption of ethanol over mixed metal oxides were performed using a U-type quartz reactor coupled to the Leybold Quadropole H200M mass spectrometer (Figure 2-6) to determine qualitatively the products desorbing at different temperatures from the catalyst surface. TPD was performed using a fixed-bed reactor. Prior to reaction, 0.5g catalyst was heated for 2 hours under air at 500°C before being allowed to cool down to room temperature (under flowing air). Once at room temperature, the gas flow was switched to helium to remove the oxidising gas from the system. After about an hour the helium flow was diverted through a saturator containing

ethanol or acetaldehyde for 15 minutes to ensure coverage of the catalyst surface. The catalyst was then purged with helium to remove any weakly adsorbed ethanol from the surface for about 1 hour. The reactor was then heated at the rate of 1°C/min and the output m/z values were obtained with increasing temperature.

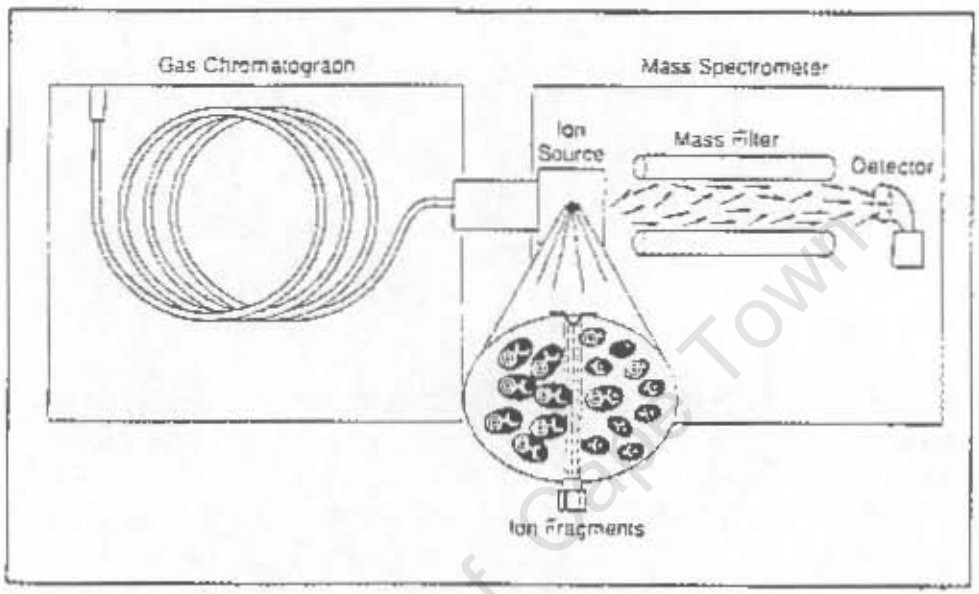

Figure 2-6: Simplified schematic representation of the working of the mass spectrometer (adapted from Hewlett Packard, 1989)

2.3.5.2 Infrared spectroscopy

The tests were performed as outlined in section 2.2.6 above, with ethanol used as a probe molecule instead of pyridine.

RESULTS

3 RESULTS

This chapter details the results obtained from different techniques used to characterize $V_xFe_{1-x}SbO_4$ catalysts (and variations thereof). One important characterisation technique is the catalytic oxidation of ethanol, which was performed over: Single metal oxides (V_2O_5, Fe_2O_3 and Sb_2O_3); Binary metal oxides ($FeSbO_4$ and $VSbO_4$) and Ternary metal oxides ($V_xFe_{1-x}SbO_4$, $0 < x < 1$). Furthermore, the reaction parameters (space-time, ethanol/oxygen ratio, inlet water partial pressure, reaction temperature) were investigated and are used to elucidate a reaction pathway. Intermediates identification using IR, TAP and TPD is also presented.

3.1 CHARACTERISATION $V_XFe_{1-X}SbO_4$ CATALYSTS

The $V_xFe_{1-x}SbO_4$ catalysts were characterised to ascertain structural characteristics of these catalyst, namely; crystalline phase(s) determination using the X-Ray diffraction, surface area determination using the BET surface area method, the actual elemental composition of the catalysts using chemical analysis; the metal surface composition determined using the XPS analysis, the acidity of the solids determined using Infrared spectroscopy and pyridine adsorption, electrical conductivity used to establish whether $V_xFe_{1-x}SbO_4$ catalysts are conductors and which conductor type characteristics these catalysts exhibit; XANES spectroscopy to determine variation of V^{3+} / V^{4+} with increasing vanadium content.

3.1.1 Chemical analysis

Table 3-1 summarises the results obtained from the chemical analysis of synthesised $V_xFe_{1-x}SbO_4$ catalysts ($0 < x < 1$ as described in section 2.1.2) as determined using AAS. On the whole, experimentally determined elemental composition of the $V_xFe_{1-x}SbO_4$ catalysts is well in agreement with the theoretical values. However, a rather high (V+Fe)/Sb ratio is observed for $V_{0.5}Fe_{0.5}SbO_4$ and $V_{0.4}Fe_{0.6}SbO_4$. Theoretically, this ratio should be equal to 1. The observed variation is not systematic (i.e. increasing or decreasing with increasing vanadium content), thus the variation can only be attributed to some experimental inconsistency during catalyst preparation procedures and/or in the elemental analysis.

Table 3-1: Chemical composition of $V_xFe_{1-x}SbO_4$ catalysts series, for $0 < x < 1$

Catalyst	$T_{Calcination}$ °C	Fe wt.-%	V wt.-%	Sb wt.-%	V/(V+Fe) mol/mol	(V+Fe)/Sb mol/mol
$VSbO_4$	700	-	21.5	49.5	1.00	1.04
$V_{0.9}Fe_{0.1}SbO_4$	700	2.2	19.0	48.9	0.90	1.03
$V_{0.8}Fe_{0.2}SbO_4$	700	4.2	16.8	48.9	0.81	1.01
$V_{0.7}Fe_{0.3}SbO_4$	700	6.9	14.3	52.0	0.69	0.95
$V_{0.6}Fe_{0.4}SbO_4$	700	8.9	12.6	50.3	0.61	0.98
$V_{0.5}Fe_{0.5}SbO_4$	900	11.7	12.2	48.9	0.53	1.12
$V_{0.4}Fe_{0.6}SbO_4$	700/900	15.2	8.9	49.5	0.39	1.10
$V_{0.2}Fe_{0.8}SbO_4$	900	18.6	4.2	51.5	0.20	0.98
$V_{0.1}Fe_{0.9}SbO_4$	900	20.8	2.2	51.8	0.10	0.98
$FeSbO_4$	900	22.9	-	50.4	0.00	0.99

Other substituted vanadium antimonates and vanadium iron antimonates were prepared using the same method as the original $V_xFe_{1-x}SbO_4$ catalysts. Table 3-2 shows the elemental composition of these substituted compounds. The elemental composition corresponds well with the theoretical values, as with the vanadium iron antimonates.

Table 3-2: Chemical composition of $V_{0.7}Me_{1(0.3)}SbO_4$, Me_1 = Fe / Al / Ga and $V_{0.8}Fe_{0.2}Me_{2(0.1)}SbO_4$, Me_2 = W / Nb, $T_{Calcination}$ = 700°C

Catalyst	[2]Me_1	V	Sb	[3]Me_2	V/(V+Me_1)	(V+Me_1) (Sb+Me_2)
	wt.-%	wt.-%	wt.-%	wt-%	mol/mol	mol/mol
$V_{0.8}Al_{0.2}SbO_4$	2.6	17.6	53.3		0.78	1.01
$V_{0.8}Ga_{0.2}SbO_4$	5.3	16.4	50.3		0.81	0.96
$V_{0.8}Fe_{0.2}W_{0.1}SbO_4$	4.7	15.9	45.6	7.2	0.79	0.97
$V_{0.8}Fe_{0.2}Nb_{0.1}SbO_4$	5.3	16.9	47.4	2.8	0.78	1.02

[1]Me_1 = Fe / Al / Ga

[2]Me_2 = W / Nb

3.1.2 X-Ray diffraction (XRD)

A tetragonal rutile structure has been reported for both catalyst systems, $FeSbO_4$ (Wyckhoff, 1963; Schnobel, 1997) and $VSbO_4$ (Nilsson *et al.*, 1994). Prepared $V_xFe_{1-x}SbO_4$ catalysts were analysed using the XRD to determine the structure of the solids and to establish changes in the crystallinity as the vanadium content is increased.

XRD-spectra obtained for $V_xFe_{1-x}SbO_4$ catalysts are presented in Figure 3-1. They all correspond to a single well-crystallised rutile type phase. The phase remained pure and undistorted with changing vanadium content of the catalysts.

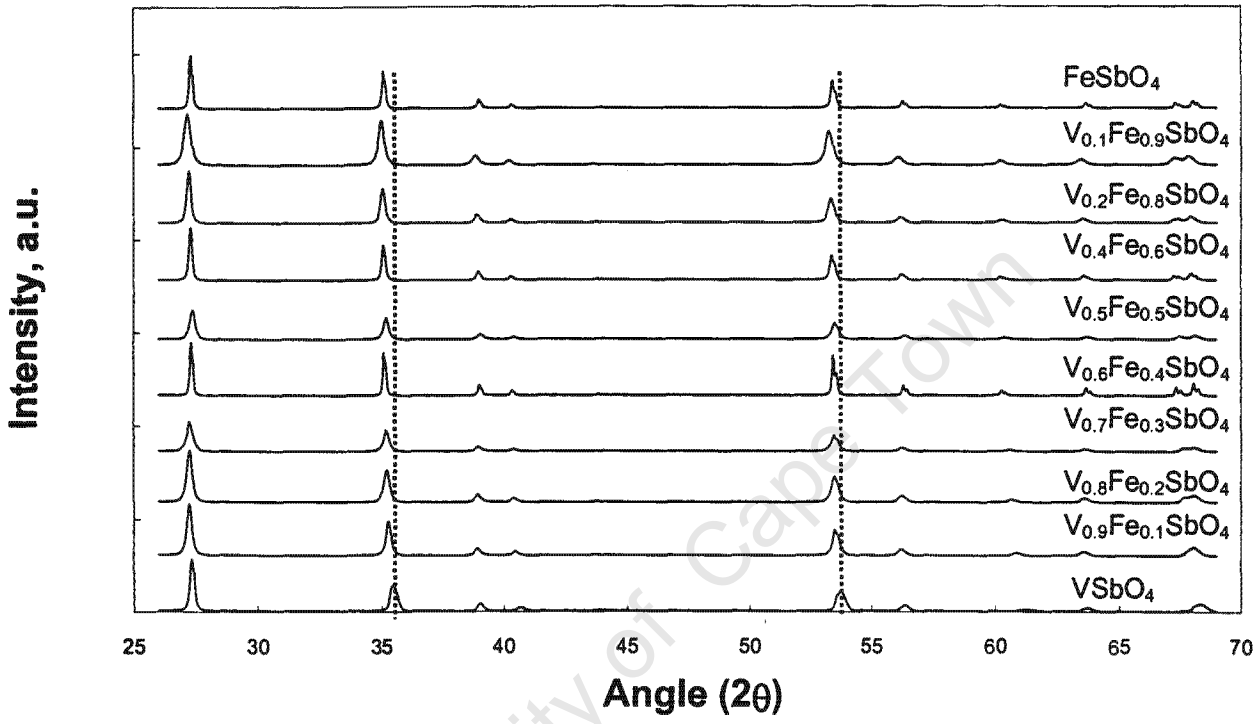

Figure 3-1: X-Ray Diffraction pattern for $V_xFe_{1-x}SbO_4$ catalysts series, for $0 < x < 1$

The observed shifts in the diffraction angle as shown for the diffraction on the (1,0,1) plane (2θ=35.1) and (2,1,1) plane (2θ=53.3) in Figure 3-1 indicate a variation in the cell parameters. Iron and antimony in stoichiometric rutile phase have been shown to be randomly distributed in the cationic sites (Berry *et al.*, 1987). Whereas, vanadium and antimony undergo partial ordering leading to a 32-fold super cell with parameter $2\sqrt{2}a$, $2\sqrt{2}b$ and 4c (Bauer, 1994). However, for practical purposes, a simple tetragonal unit cell has been used to calculate $a = b$ and c parameters.

For the tetragonal $FeSbO_4$ and $VSbO_4$ systems ($a = b$; $\alpha = \beta = \gamma$) the relationship between d-spacing of a (h,k,l) plane and unit cell parameters a and c is given by (Mckie and Mckie 1980):

$$\frac{1}{d_{hkl}^2} = \frac{h^2+k^2}{a^2} + \frac{l^2}{c^2} \qquad (3\text{-}1)$$

The values for *a* and *c* were calculated using the d-spacing of 9 different planes listed in Table 3-3.

Table 3-3: 2θ values corresponding to peaks used to calculate crystal planes

2θ	27.2°	35.1°	38.8°	40.2°	53.3°	56.3°	60.2°	63.4°	67.3°
h,k,l	1,1,0	1,0,1	2,0,0	1,1,1	2,1,1	2,2,0	0,0,2	3,1,0	1,1,2

Table 3-4 and Figure 3-2 show calculated cell parameters of the tetragonal rutile structure as a function of vanadium content in the catalysts. The cell parameter *a* hardly varies with increasing vanadium content. While, cell parameter *c* decreases with increasing vanadium content, this effect is prominent in the region V/(V+Fe) > 0.5).

Table 3-4: Cell parameters a and c of tetragonal rutile structure $V_xFe_{1-x}SbO_4$ catalysts

Catalyst	***a*** **Å**	***c*** **Å**
$VSbO_4$	4.624 ± 0.001	3.0332 ± 0.0008
$V_{0.9}Fe_{0.1}SbO_4$	4.631 ± 0.001	3.046 ± 0.001
$V_{0.8}Fe_{0.2}SbO_4$	4.627 ± 0.001	3.0543 ± 0.0006
$V_{0.7}Fe_{0.3}SbO_4$	4.626 ± 0.001	3.0562 ± 0.0009
$V_{0.6}Fe_{0.4}SbO_4$	4.6280 ± 0.0009	3.0692 ± 0.0005
$V_{0.5}Fe_{0.5}SbO_4$	4.6247 ± 0.0007	3.0697 ± 0.0004
$V_{0.4}Fe_{0.6}SbO_4$	4.6278 ± 0.0007	3.0752 ± 0.0004
$V_{0.2}Fe_{0.8}SbO_4$	4.6328 ± 0.0007	3.0772 ± 0.0004
$V_{0.1}Fe_{0.9}SbO_4$	4.6329 ± 0.0009	3.0737 ± 0.0005
$FeSbO_4$	4.637 ± 0.001	3.0737 ± 0.0007

The calculated *a* and *c* parameters compare well with the parameters $FeSbO_4$ reported by Wyckhoff (1963) for $FeSbO_4$, which are: *a* = 4.623 Å and c = 3.011 Å.

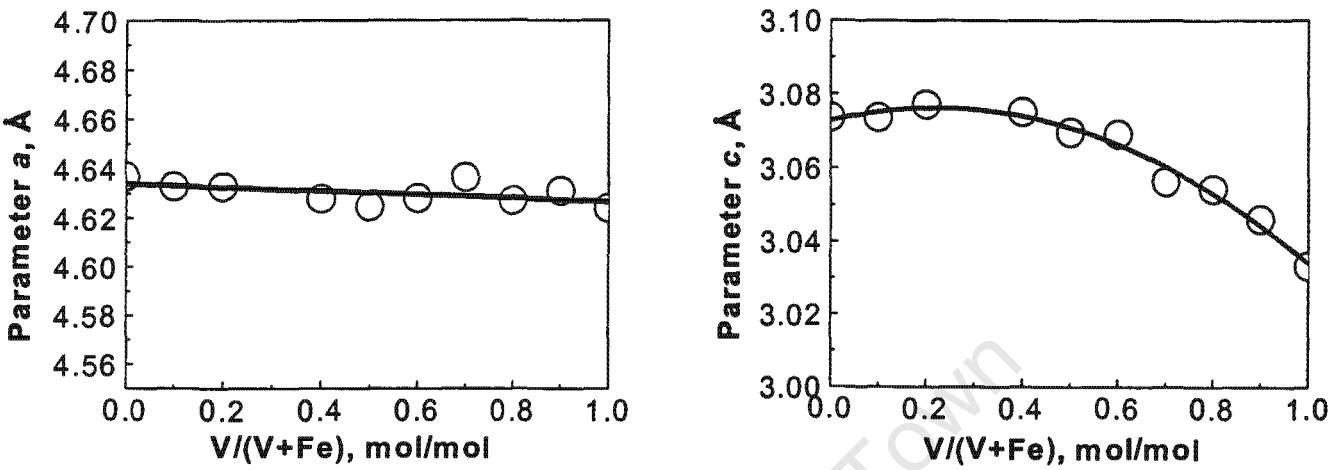

Figure 3-2: Cell parameters a and c as a function of the vanadium content in $V_xFe_{1-x}SbO_4$ catalysts

A study of catalyst washing as a post-preparation catalyst treatment was investigated. It was observed that the catalysts that were washed after preparation (e.g. $V_{0.7}Fe_{0.3}SbO_4$ W) were structurally closely related to the unwashed counterparts (e.g. $V_{0.7}Fe_{0.3}SbO_4$), see Figure 3-3).

Substitution of the iron in $V_{0.7}Fe_{0.3}SbO_4$ catalyst system by other tri-valent ions (i.e. Al^{3+} and Ga^{3+}) does not distort the rutile structure or result in the formation of new phases. Implying that aluminium and gallium adaptations of $V_{0.7}Fe_{0.3}SbO_4$ catalyst crystallise in the same structure as the original $V_{0.7}Fe_{0.3}SbO_4$ catalyst.

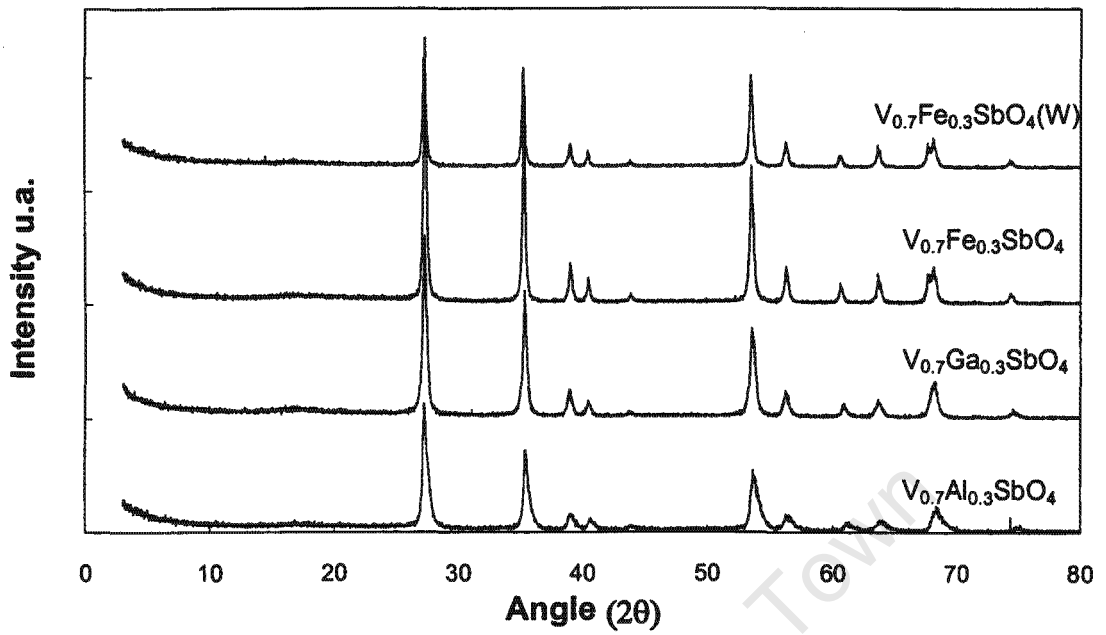

Figure 3-3: X-Ray Diffraction pattern for $V_{0.7}M_{0.3}SbO_4$ catalysts, M =Fe, Al or Ga. Also showing the effect of washing on the crystallinity of $V_{0.7}M_{0.3}SbO_4$ catalysts.

Table 3-5 shows the variation of the cell parameters *a* and *c* for the rutile structure upon introduction of different elements in the structure. The cell parameter *a* remains unchanged after the introduction of the various elements in the rutile vanadium antimonate structure. Upon substitution of iron in the structure with either aluminium or gallium, a slight decrease in the cell parameter *c* is observed. The variation of the cell parameter *c* appears to be correlated to ionic radii of the substituted element, i.e. cell parameter *c* decreases with decreasing ionic radius (see Table 3-5).

Table 3-5: Cell parameters a and c of tetragonal rutile structure of $V_{0.7}M_{0.3}SbO_4$, M =Fe, Al and Ga

Catalyst	*a* Å	*c* Å	$M_{ionic\ radii}$ Å
$V_{0.7}Fe_{0.3}SbO_4$	4.626 ± 0.001	3.0562 ± 0.0009	0.64
$V_{0.7}Ga_{0.3}SbO_4$	4.616 ± 0.003	3.032 ± 0.002	0.62
$V_{0.7}Al_{0.3}SbO_4$	4.610 ± 0.001	3.0268 ± 0.0007	0.51

M = Fe/Al/Ga

In addition to the $V_{0.7}M_{0.3}SbO_4$ (M =Fe, Al or Ga) catalyst series, $V_{0.8}Fe_{0.2}Sb_{0.9}M_{0.1}O_4$, (M = W or Nb) catalysts were prepared. Figure 3-4 presents the XRD spectra for complex $V_{0.8}Fe_{0.2}Sb_{0.9}M_{0.1}O_4$ (M = W or Nb) catalysts.

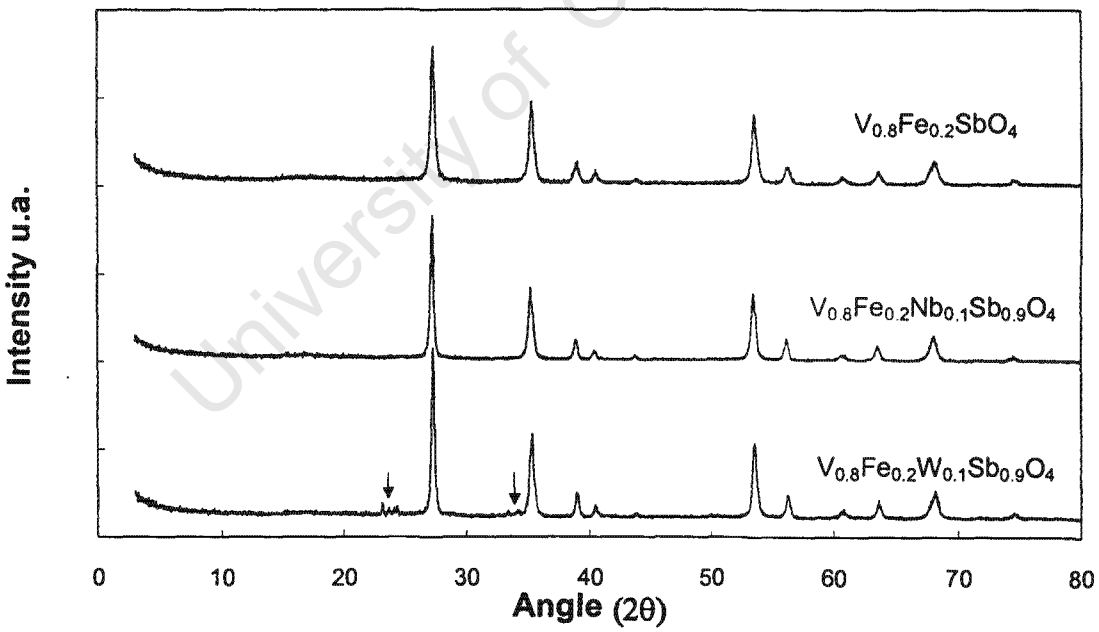

Figure 3-4: X-Ray Diffraction pattern for complex $V_{0.8}Fe_{0.2}Sb_{0.9}M_{0.1}O_4$ catalysts, M = W and Nb. Arrows highlighting additional peaks observed on $V_{0.8}Fe_{0.2}Sb_{0.9}W_{0.1}O_4$

A 10% substitution of niobium for antimony shows that a solid solution is obtained, i.e. a

pure rutile phase is formed. While a 10% tungsten for antimony substitution shows the rutile structure of the parent $V_xFe_{1-x}SbO_4$ catalysts and additional diffraction peaks at 2θ = 22-24° and 34°. These peaks correspond to tungsten oxide. Thus, this synthesis method employed for the substitution of tungsten for antimony in vanadium iron antimonates does not yield the incorporation of tungsten into the rutile structure.

A total substitution of niobium for antimony in $V_{0.8}Fe_{0.2}SbO_4$ resulted in a structure that was completely different from the rutile structure as illustrated in Figure 3-5. Thus, with the synthesis method employed, there appears to be a maximum niobium for antimony substitution composition beyond which the rutile structure starts becomes distorted, or new phase(s) formation. Though the aim of preparing such a catalyst was to obtain a structure of $V_{0.8}Fe_{0.2}NbO_4$ type, no matches were found for such a structure. It would appear that a number of different phases were formed.

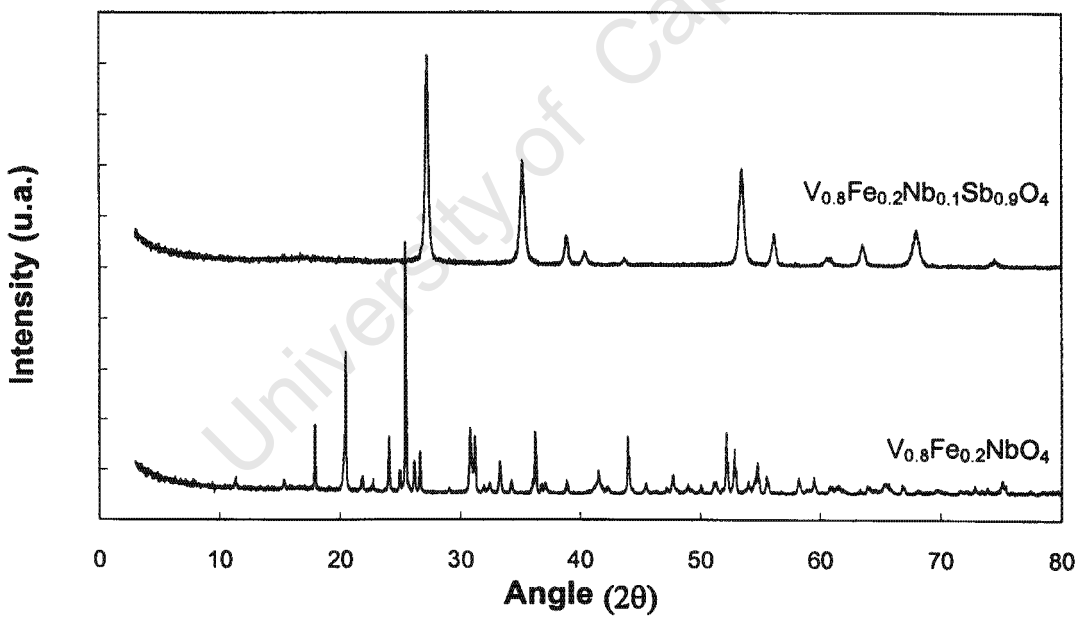

Figure 3-5: X-Ray Diffraction pattern for $V_{0.8}Fe_{0.2}Sb_{0.9}Nb_{0.1}O_4$ and $V_{0.8}Fe_{0.2}NbO_4$ catalysts

3.1.3 Mössbauer spectroscopy

The complexity of the $V_xFe_{1-x}SbO_4$ catalysts requires in-depth understanding of species taking part in the catalytic oxidation of ethanol. If iron (present as Fe^{3+} in the fresh catalyst) is directly participating in the reaction, then it is expected that it would be reduced to Fe^{2+} after the catalytic reaction. Mössbauer spectroscopy was used to verify the valence-state of iron in the compounds. The ^{57}Fe Mössbauer spectra of the samples were fitted with one ferric doublet (Figure 3-6 and Figure 3-7). The calculated parameters corresponded to those published by Kriegsmann *et al.* (1977) for $FeSbO_4$, where Fe is present as Fe^{3+}.

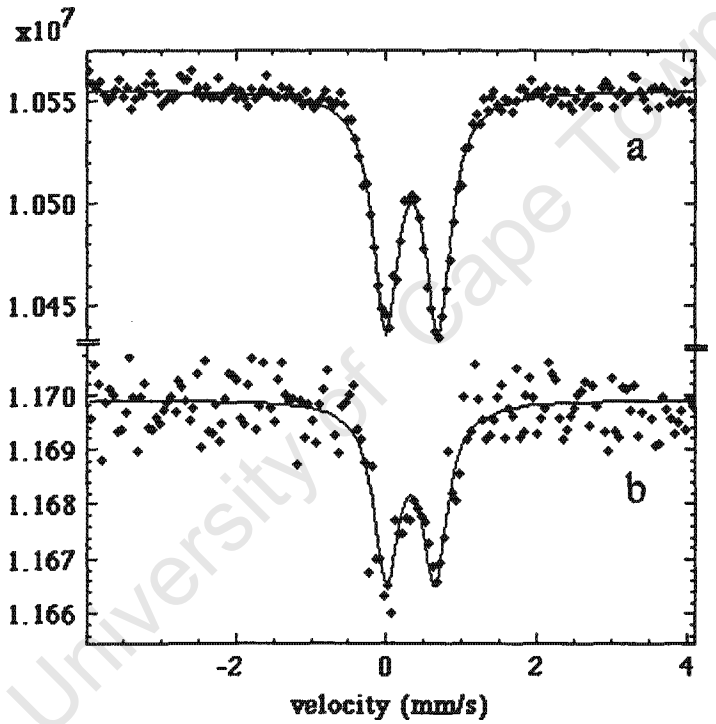

Figure 3-6: Mössbauer spectrum for the compound $V_{0.8}Fe_{0.2}SbO_4$ (Parameters: δ = 0.32 mm/s W = 0.40 mm/s Δ = 0.64 mm/s), a) fresh catalyst, b) after ethanol oxidation. Measured at 25°C with a time mode spectrometer and a constant acceleration drive.

The Mössbauer parameters of the solids after catalytic test (Figure 3-6b and Figure 3-7b) were similar to those obtained for the fresh catalyst (Figure 3-6a and Figure 3-7a). Implying that the chemical environment of iron under catalytic testing conditions did not change for these catalysts. Some scattering is observed after catalytic test that is

attributed to the presence of more than 80% silicon carbide in the catalyst (Silicon carbide is added to the catalyst material during catalytic test to minimize temperature gradient).

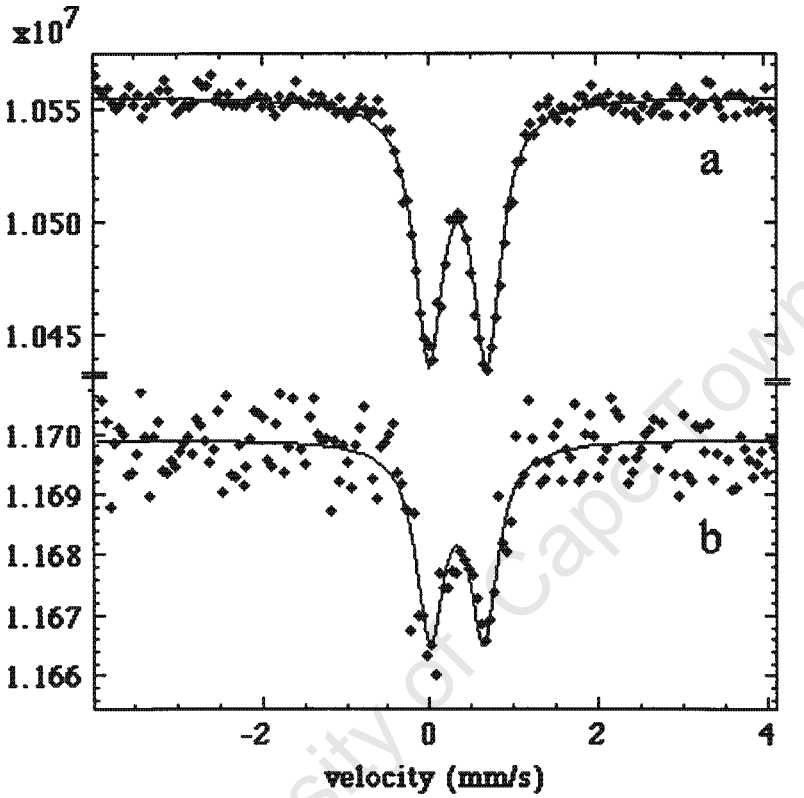

Figure 3-7: Mössbauer spectrum for the compound $V_{0.6}Fe_{0.4}SbO_4$ (Parameters: δ = 0.32 mm/s W = 0.40 mm/s Δ = 0.64 mm/s), a) fresh catalyst, b) after ethanol oxidation. Measured at 25°C with a time mode spectrometer and a constant acceleration drive

From these measurements there is a clear indication that Fe in these complex vanadium catalysts ($V_{0.8}Fe_{0.2}SbO_4$ and $V_{0.6}Fe_{0.4}SbO_4$) remains at Fe^{3+} state and hence thought not to play a role in catalytic oxidation of ethanol.

3.1.4 XANES spectroscopy

$VSbO_4$ catalysts when prepared under air, possess a defective structure with the composition of $V^{4+}_{0.64}V^{3+}_{0.28}Sb^{5+}_{0.92}\square_{0.16}O_4$ (Landa-Canovas *et al.*, 1995). A hypothesis has been put forward that sequential substitution of vanadium by iron should have a direct effect on the V^{3+}/V^{4+} ratio.

The V^{3+}/V^{4+} for the ratios for $V_xFe_{1-x}SbO_4$ catalysts $0 < x < 1$ were determined using XANES (measurements done as part of a collaboration study by Roussel *et al.*, (2002)). The V-K edge spectra of the $V_xFe_{1-x}SbO_4$ catalysts samples along with that of the V^{4+} standard $(VO)_2P_2O_7$ phase were taken as shown in the publication (Roussel *et al.* 2002). For the iron-rich $V_{0.4}Fe_{0.6}SbO_4$ sample a single pre-edge peak at 5470.0 eV was observed whereas for the vanadium-rich $VSbO_4$ and $V_{0.8}Fe_{0.2}SbO_4$ compounds a second peak at 5472.2 eV was observed. These peaks have been attributed to V^{3+} and V^{4+} respectively by comparison with standard phase and literature data. Results of fitting to a model with a weighted superposition of V^{4+} and V^{3+} components showed that the V^{4+}: V^{3+} ratio obtained for $VSbO_4$ (62:38) was close to the theoretical one calculated for the $V^{4+}_{0.64}V^{3+}_{0.28}Sb^{5+}_{0.92}O_{0.16}O_4$ stoichiometry (65:35).

Together with the Mössbauer and elementary analysis results the vacancies were calculated assuming the 4-oxygen tetragonal structure unit cell (see

Table 3-6). It can be seen from the table that iron rich samples contain vanadium as V^{3+}. From V/(V+Fe) = 0.5 vanadium is also incorporated as V^{4+} which results in a charge imbalance. Hence, cationic vacancies are introduced in the structure. It should be noted however that the increase in the number of V^{4+} as the vanadium content increases is not proportional to the cationic vacancies content.

Table 3-6: Calculated formulae for the iron vanadium antimonates

Sample	Fe^{3+}	V^{3+}	V^{4+}	◊	Sb^{5+}	O
$VSbO_4$		0.32	0.61	0.20	0.91	4
$V_{0.9}Fe_{0.1}SbO_4$	0.08	0.32	0.52	0.18	0.92	3.95
$V_{0.8}Fe_{0.2}SbO_4$	0.18	0.33	0.41	0.14	0.92	3.88
$V_{0.7}Fe_{0.3}SbO_4$	0.28	0.30	0.33	0.11	0.94	3.89
$V_{0.6}Fe_{0.4}SbO_4$	0.38	0.33	0.24	0.08	0.95	3.92
$V_{0.5}Fe_{0.5}SbO_4$	0.47	0.39	0.14	0.05	0.94	3.95
$V_{0.4}Fe_{0.6}SbO_4$	0.64	0.41			0.85	4
$V_{0.2}Fe_{0.8}SbO_4$	0.81	0.20			1.01	4
$V_{0.1}Fe_{0.9}SbO_4$	0.90	0.10			0.99	4
$FeSbO_4$	0.99				0.99	4

In the region between V/(V+Fe) = 0.5 to 0.9, there are also oxygen vacancies observed. In the pure binary $VSbO_4$, there are 4 oxygen atoms per unit cell. Whilst in the vanadium rich $V_xFe_{1-x}SbO_4$ catalysts, the number of oxygen atoms per unit cell ranges between 3.88 and 3.95, indicating the presence of oxygen vacancies.

3.1.5 X-ray Photoelectron spectroscopy (XPS)

The (0.01 μm deep) surface composition of the catalysts was determined using XPS on the freshly prepared catalysts. Table 3-7 shows the surface composition determined using XPS in comparison to the bulk composition as determined using chemical analysis. The most striking effect is the observed enrichment of the surface with antimony, prevailing throughout the catalysts series. The effect has also been observed and reported by Ballarini *et al.* (2002) on $CrSbO_4$ systems.

Table 3-7: Surface composition of vanadium iron antimonates as determined using XPS, and the bulk composition as determined by chemical analysis

Sample	Surface V/(V+Fe) mol/mol	Bulk V/(V+Fe) mol/mol	Surface (V+Fe)/Sb mol/mol	Bulk (V+Fe)/Sb mol/mol
$VsbO_4$		1	0.77	1.04
$VsbO_4$[1]		1	0.72	
$V_{0.9}Fe_{0.1}SbO_4$	0.94	0.90	0.91	1.03
$V_{0.8}Fe_{0.2}SbO_4$	0.90	0.81	0.77	1.01
$V_{0.7}Fe_{0.3}SbO_4$	0.70	0.69	0.83	0.95
$V_{0.7}Fe_{0.3}SbO_4W$[2]	0.72		0.58	
$V_{0.7}Fe_{0.3}SbO_4WW$[3]	0.59		0.56	
$V_{0.6}Fe_{0.4}SbO_4$	0.70	0.61	0.67	0.98
$V_{0.5}Fe_{0.5}SbO_4$	0.51	0.53	0.78	1.12
$V_{0.4}Fe_{0.6}SbO_4$	0.48	0.39	0.52	1.10
$V_{0.2}Fe_{0.8}SbO_4$	0.15	0.20	0.67	0.98
$FeSbO_4$			0.78	0.99

[1]Sample after catalyst testing (ethanol oxidation)

[2] $V_{0.7}Fe_{0.3}SbO_4$ washed prior to calcination step

[3]$V_{0.7}Fe_{0.3}SbO_4$ washed prior and after calcination step

In addition, Nilsson *et al.* (1996) observed for $FeSbO_4$ that a rutile crystallites concentration gradients of catalyst components existed, with Sb-richer zones on the outside parts of the crystallites and consequently Fe-rich zones in the inner parts. Comparing the surface composition of $VSbO_4$ before and after ethanol oxidation it can be observed that under the (rather mild 150-300°C) ethanol oxidation conditions the surface V/Sb-ratio remains almost constant. Whereas under harsher propane ammoxidation conditions (450-500°C), further Sb surface enrichment has been observed after reaction (Roussel, *et al.*, 2002).

Washing of the catalysts prior and after heat-treatment (calcinations) leads to a strong increase in the surface antimony content (further Sb enrichment). The molar surface ratios of vanadium to iron of the prepared samples correspond to the bulk composition

throughout the catalysts range. Only the freshly prepared sample $V_{0.7}Fe_{0.3}SbO_4WW$ shows a surface enrichment with iron.

The binding energies for V (517.0 ± 0.1 eV) Sb (540.25 ± 0.10 eV) and Fe (712.0 ± 0.3 eV) remained quite constant throughout the catalyst series and Sb binding energy varied slightly after catalytic test over $VSbO_4$, V (517.05 ± 0.1 eV) Sb (540.50 ± 0.10 eV).

3.1.6 BET surface area

The BET-surface area of the mixed metal oxides is an indication for the crystal size in these materials. Measured BET surface area for $V_xFe_{1-x}SbO_4$ catalysts is shown in Table 3-8

Table 3-8: BET surface area of $V_xFe_{1-x}SbO_4$ catalysts series, where $0 < x < 1$

Catalyst	Tcalcination °C	BET surface area m^2/g
$VSbO_4$	700	4.9
$V_{0.9}Fe_{0.1}SbO_4$	700	11.7
$V_{0.8}Fe_{0.2}SbO_4$	700	14.8
$V_{0.7}Fe_{0.3}SbO_4$	700	16.1
$V_{0.6}Fe_{0.4}SbO_4$	700	21.4
$V_{0.5}Fe_{0.5}SbO_4$	700	16.7
$V_{0.4}Fe_{0.6}SbO_4$	700/900	20.5*/2.7*
$V_{0.2}Fe_{0.8}SbO_4$	900	6.6
$V_{0.1}Fe_{0.9}SbO_4$	900	8.3
$FeSbO_4$	900	16.9

*Catalyst calcined at both 700 and 900°C to substantiate the effect of calcinations temperature.

To clearly illustrate the trends in the BET surface area as V/(V+Fe) increases, BET surface area was plotted as a function of V/(V+Fe) Figure 3-8. BET-surface area generally decreases with increasing vanadium content. The transpiring two distinct categories of high vanadium content and high iron content catalyst is a result of the varying calcination temperature employed (900°C for iron rich samples versus 700°C for

vanadium rich catalysts). This implies that the crystallite size increase with increasing vanadium content. To further demonstrate the effect of preparation temperature on the BET surface area of the catalysts, two samples of the catalyst with V/(V+Fe) = 0.4 were calcined at different temperatures (one at 700°C and the other at 900°C). The difference in the resulting BET surface area of the two samples is clearly evident in Figure 3-8.

The use of high preparation temperatures for the iron rich catalyst is necessitated by a solid-state reaction that takes place only at high temperature (900°C) to produce a pure tetragonal rutile phase $FeSbO_4$ (Allen *et al.*, 1991; van Steen *et al.*, 1997). Hence, for the catalytic tests, the 900°C–calcined sample was used. Due to the different preparation methods that were used in these two groups of catalysts, the solid solution is not expected to form with $V_{0.4}Fe_{0.6}SbO_4$ calcined at 700°C.

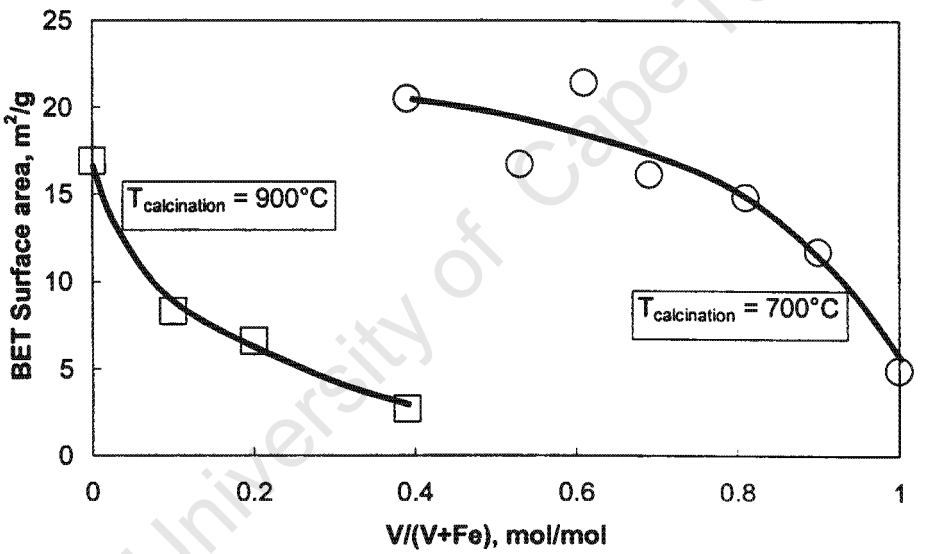

Figure 3-8: BET-surface area as a function of the vanadium content in the $V_xFe_{1-x}SbO_4$ catalysts series, where 0 < x <1

The introduction of Al^{3+} instead of Fe^{3+} into the vanadium antimonate structure leads to a smaller BET-surface area, whereas the introduction of Ga^{3+} leads to a larger surface area (Table 3-9). This is indicative of the formation of larger crystals in Al substituted catalyst and smaller crystals formation in Ga substituted catalysts.

Table 3-9: BET surface of substituted iron vanadium antimonates ($T_{preparation}$ = 700°C), Me_1 = Fe / Al / Ga and Me_2 = W / Nb

Catalyst	BET area m^2/g
$V_{0.7}Fe_{0.3}SbO_4$	16.1/24.0[1]
$V_{0.8}Al_{0.2}SbO_4$	6.1/13.4[1]
$V_{0.8}Ga_{0.2}SbO_4$	25.6
$V_{0.8}Fe_{0.2}W_{0.1}SbO_4$	28
$V_{0.8}Fe_{0.2}Nb_{0.1}SbO_4$	1.3/3.1[1]

[1]Samples washed prior to calcinations

Furthermore, it is observed that washing the catalyst samples prior to calcination yields larger BET surface areas, this in good agreement with the less crystalline structures observed for the washed catalysts compared to the unwashed counterpart. This could mean that washing removes ions on the structure that facilitate crystal growth.

3.1.7 Infrared (IR) Spectroscopy (pyridine adsorption acidity analysis)

The surface acidity of $VSbO_4$ has already been described in literature on the basis of IR studies of ammonia adsorption (Centi *et al.*, 1997). In this study, the acidity of $V_xFe_{1-x}SbO_4$ catalysts was determined using pyridine as a probe molecule in IR studies. Pyridine was chosen as a probe molecule instead of ammonia because Zanthoff *et al.* (1996) earlier reported that NH_3 reacts with the lattice oxygen of $VSbO_4$ oxides to form N_2 and NO_x at temperatures slightly higher than room temperature. While, pyridine is less basic than NH_3 (pKa $\approx$ 5 and 9 respectively), but since it is also a hard base (Tanabe, 1970), it will adsorb on the same acid sites as ammonia. There are thus marked advantages in using pyridine instead of ammonia as a probe molecule.

From the spectrum recorded at 25°C, two bands corresponding to physisorbed pyridine at 1581 and 1438 $cm^{-1}$are observed, decreasing drastically between 25°C and 100°C, (see Figure 3-9). The bands at 1606, 1576, 1488 and 1447 cm^{-1} are typical of pyridine chemisorbed on Lewis sites originating from coordinative unsaturated V surface ions (Boehm and Knözinger, 1983). The presence of a peak at the frequency of 1606 cm^{-1} is

a clear indication of the presence of medium to strong Lewis acid sites. The observed broad peak at (1538 cm^{-1}) is typical of vanadium-based (V-OH) Brønsted acid sites (Centi *et al.*, 1992). Furthermore a band at 1638 cm^{-1} results from the pyridinium cation whose presence confirms the presence Brønsted acid site (Figure 3-9) for the vanadium-rich catalyst and (Figure 3-10) for the iron-rich catalyst.

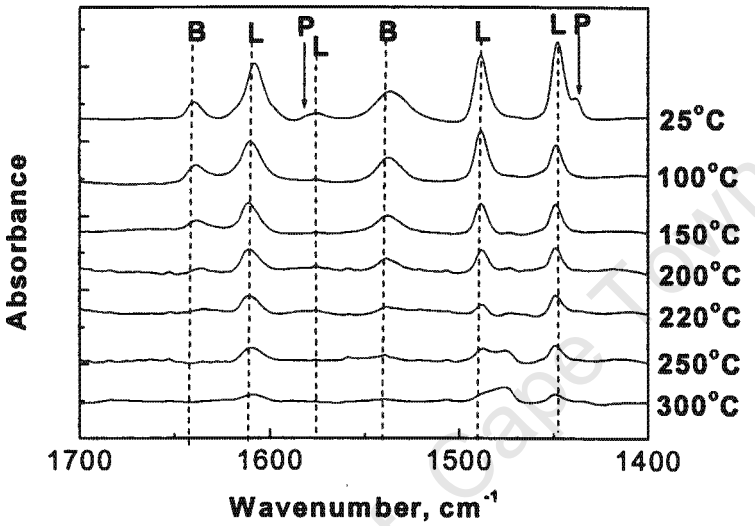

Figure 3-9: Pyridine desorption pattern for a high vanadium content catalyst ($V_{0.7}Fe_{0.3}SbO_4$); $T_{pretreatment}$ = 220°C for 2 hours under vacuum; $T_{adsorption}$ = 25°C; $T_{evacuation}$ = 25°C, 100°C, 150°C, 200°C, 220°C and 250°C for 1 hour; spectra recorded at 25°C. L stands for Lewis, B for Brønsted acid sites, and P stands for physisorbed pyridine

It can be observed that for the iron-rich catalysts (Figure 3-10) a strong decrease in the adsorption bands of adsorbed pyridine at temperatures between 100-150°C. The low temperature desorption of pyridine in Fe-rich catalysts is an indication of weaker acid sites in comparison to V-rich catalysts.

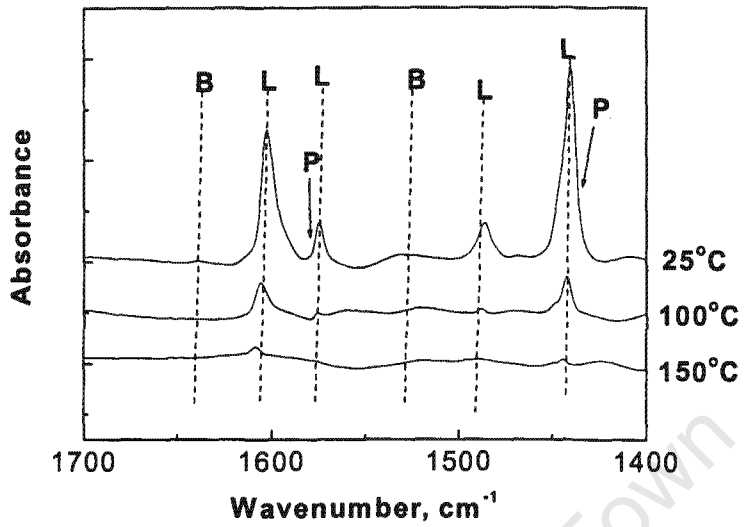

Figure 3-10: Pyridine desorption pattern for a high iron content catalyst ($FeSbO_4$). $T_{pretreatment}$ = 220°C for 2 hours under vacuum, $T_{adsorption}$ = 25°C, $T_{evacuation}$ = 25°C, 100°C, 150°C, for 1 hour, spectra recorded at 25°C. L stands for Lewis, B for Brønsted acid sites, while P stands for physisorbed pyridine

Pyridine desorption patterns for all $V_xFe_{1-x}SbO_4$ catalysts characterised for acidity in this manner are given in Appendix III.

To determine the strength of the acid sites, adsorbed pyridine peaks were integrated using a combination of a Lorentz-Gaussian fit of the data. Figure 3-11 shows a typical peak fitting for one of the IR spectra, Lewis acid peak at 1448 cm^{-1} Figure 3-11a) and Brønsted acid peak at 1537 cm^{-1}Figure 3-11b).

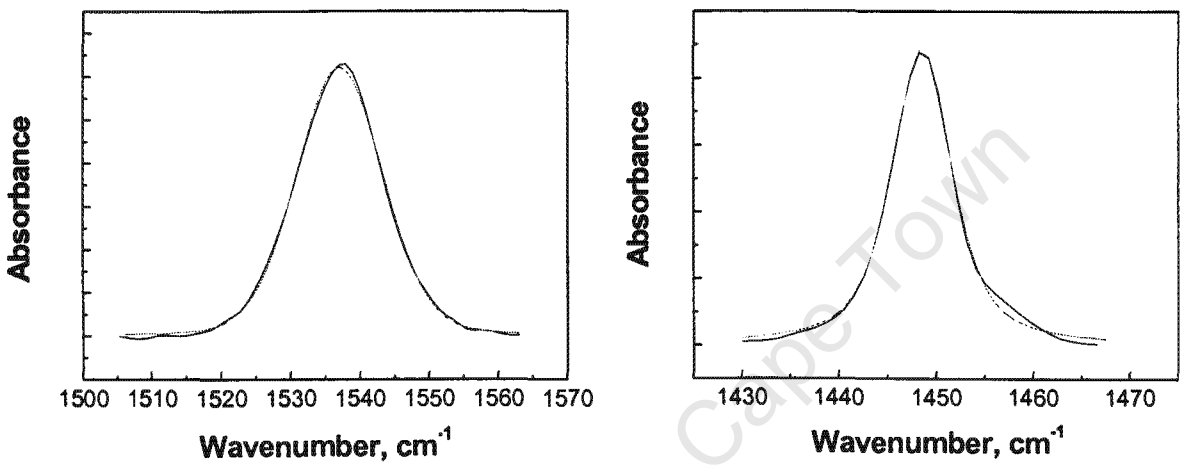

Figure 3-11: An example of fitting curves for the integration of the Lewis acid peak site-adsorbed pyridine (1448 cm^{-1}) and Brønsted acid site-adsorbed pyridine (1537 cm^{-1}) obtained from IR spectrum

The resulting peak intensities were then normalised with respect to the catalysts measured surface area and pellet mass to standardise the measurements.

The fitting was performed for each evacuation temperature and the composite representation of the decrease of the adsorbed pyridine peaks with temperature is presented in Figure 3-12 for catalyst $V_{0.7}Fe_{0.3}SbO_4$.

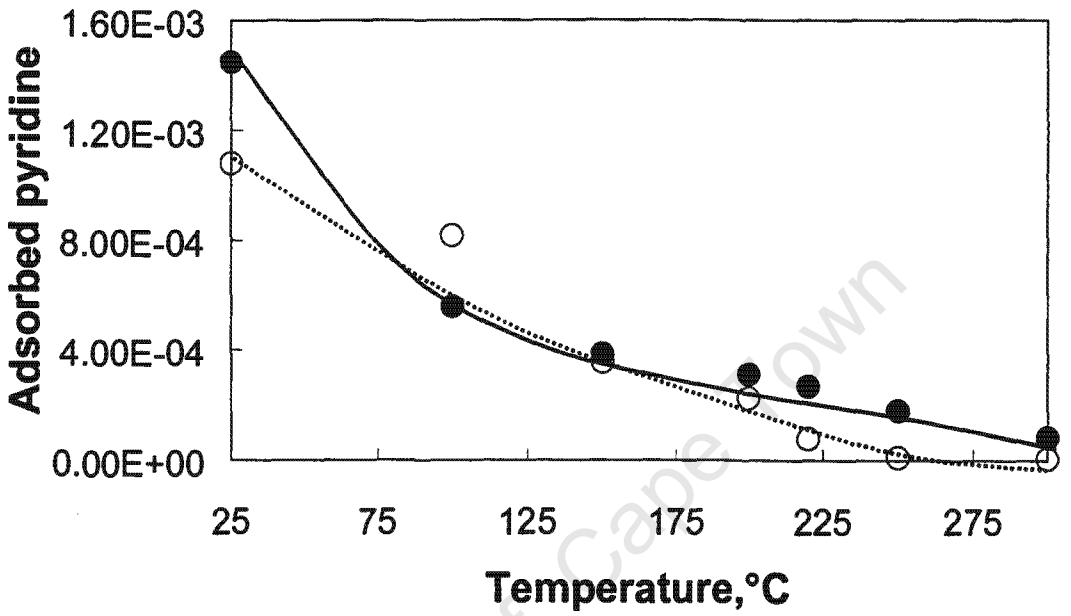

Figure 3-12: The evolution of pyridine adsorbed on the catalyst surface with increasing evacuation temperature for catalyst ($V_{0.7}Fe_{0.3}SbO_4$); $T_{pretreatment}$ = 220°C for 2 hours under vacuum; $T_{adsorption}$ = 25°C; $T_{evacuation}$ = 25°C, 100°C, 150°C, 200°C, 220°C and 250°C for 1 hour; spectra recorded at 25°C

Different $V_xFe_{1-x}SbO_4$ catalysts (Appendix III) were compared for Brønsted and Lewis acidity at the evacuation temperature of 100°C; the results are presented as a function of vanadium content (see Figure 3-13). It is clear from the graph that acidity reaches a maximum at x = 0.5 of $V_xFe_{1-x}SbO_4$ catalysts.

Low vanadium content (high iron content) catalysts exhibit low acidity. While, high vanadium content (low iron content) catalyst exhibit high acidity. Also demonstrated on Figure 3-13 is that parent binary oxides ($FeSbO_4$ and $VSbO_4$) catalysts possess much less acidity than their corresponding ternary $V_xFe_{1-x}SbO_4$ catalyst with low metal content of the other end binary antimonate. For instance, $V_{0.9}Fe_{0.1}SbO_4$ exhibits higher acidity than pure $VSbO_4$ and $V_{0.2}Fe_{0.8}SbO_4$ exhibits higher acidity than pure $FeSbO_4$.

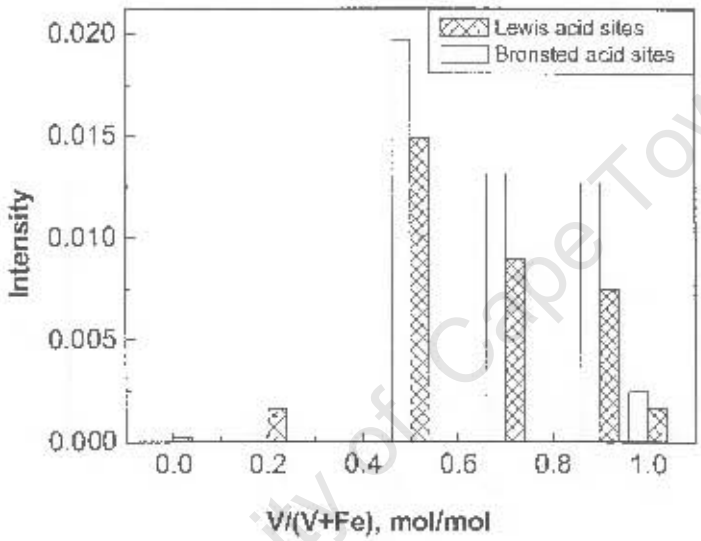

Figure 3-13: Brønsted and Lewis acidity determined after evacuation at 100°C as a function of V/(V+Fe) of the $V_xFe_{1-x}SbO_4$ catalysts.

3.1.8 Electrical conductivity

Electrical conductivity (σ) measurements carried out on oxide-based catalysts can provide information on the nature of surface structure defects, the existence of oxidizing species (ion-adsorbed oxygen species, active surface anion, etc.) and the nature of the oxidising phase involved in catalytic reactions as described by Herrmann (1994). This is a useful tool in oxidation catalysis reactions where redox properties are often observed.

Electrical conductivity behaviour of $V_xFe_{1-x}SbO_4$ catalysts was measured as a function of temperature (Figure 3-14) to determine the activation energy of conduction E_c under air at atmospheric pressure.

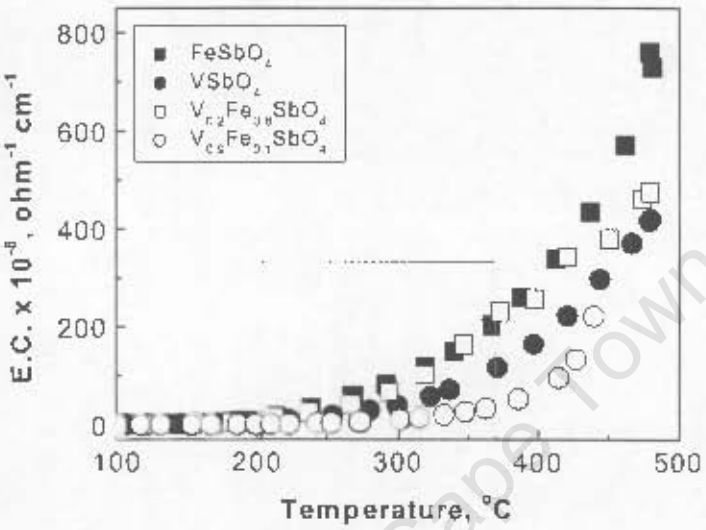

Figure 3-14: Electrical conductivity of selected $V_xFe_{1-x}SbO_4$ catalysts

There appears to be a characteristic temperature for each catalyst where the electrical conduction starts to sharply increase. In Figure 3-14 it can be observed that this temperature is low for iron-rich catalysts, while it is relatively high for vanadium-rich catalyst. Furthermore, it can be observed that this particular temperature is higher for ternary oxides in comparison to corresponding binary oxides.

The semi-log plots [logσ = f(1/T)] obtained are given in Figure 3-15.

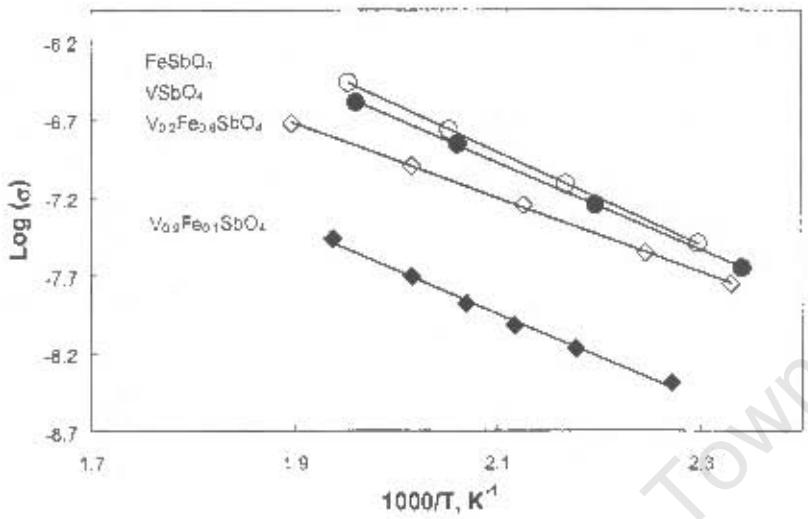

Figure 3-15: Arrhenius plots for the electrical conductivity sigma (ohm^{-1} cm^{-1}) of selected $V_xFe_{1-x}SbO_4$ catalysts under air at atmospheric pressure

The slopes were used to calculate the E_C values shown in Table 3-10. It can be observed that the values for E_C are similar except for $V_{0.9}Fe_{0.1}SbO_4$ that shows a fairly low E_C.

Table 3-10: Activation energy for conduction calculated from the Arrhenius plot for selected $V_xFe_{1-x}SbO_4$ catalysts under air at atmospheric pressure.

Catalyst	E_C (kJ mol)	Intercept (σ_0)	E_C (eV)
$FeSbO_4$	57	$e^{-2.066}$	0.60
$V_{0.2}Fe_{0.8}SbO_4$	54	$e^{-0.275}$	0.56
$V_{0.9}Fe_{0.1}SbO_4$	46	$e^{-0.004}$	0.48
$VSbO_4$	53	$e^{-0.103}$	0.56

It can be seen that the intercept for $V_{0.9}Fe_{0.1}SbO_4$ is larger than the other catalysts characterized in this manner. This could be due to the presence of anionic vacancies within this catalyst structure, which are not present in the other three catalysts according to the XANES characterization in Section 3.1.4.

3.1.9 Temperature programmed reduction

Figure 3-16 displays the reduction profiles obtained using TPR. The reduction of $V_xFe_{1-x}SbO_z$ catalysts begins at about 220°C, with $FeSbO_4$ showing a shoulder at 280°C. It appears that ternary oxides e.g. $V_{0.7}Fe_{0.3}SbO_4$, show a steeper rise in H_2 consumption, i.e. a higher degree of reduction can be obtained at ca. 400°C than the binary oxides ($FeSbO_4$ and $VSbO_4$).

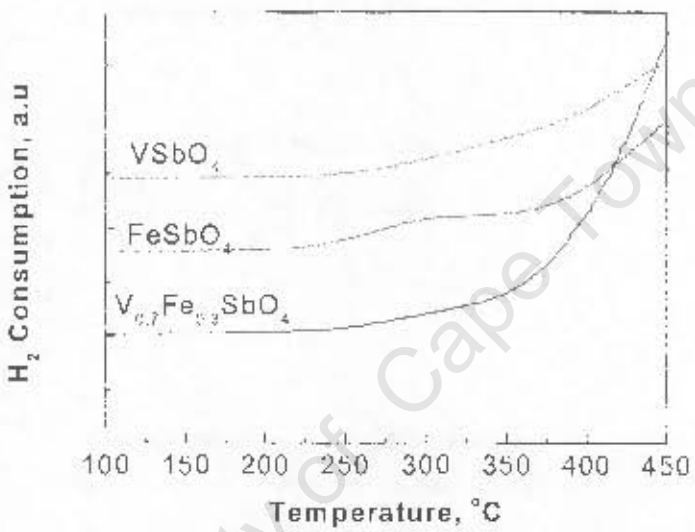

Figure 3-16: Temperature programmed reduction of $V_xFe_{1-x}SbO_4$ catalysts

TPR studies performed on $FeSbO_z$ and $CrFeSbO_z$ catalysts have also shown that complex antimonates are relatively easier to reduce than the corresponding binary oxides (Ballarini *et al.*, 2001).

3.2 ELUCIDATING REACTION PATHWAY IN ETHANOL OXIDATION OVER A VANADIUM IRON ANTIMONY CATALYST

To establish the reaction pathway for selective oxidation of ethanol over a vanadium iron antimonate catalysts ($V_{0.7}Fe_{0.3}SbO_4$), the influence of reaction parameters such as space-time, ethanol to oxygen ratio, inlet water partial pressure and reaction temperature was investigated. Furthermore, the reaction intermediates were investigated using IR, TAP, and TPD.

3.2.1 Effect of space- time on the oxidation of ethanol

Three temperatures were used for the study of the effect of space-time on the oxidation of ethanol, viz. 210, 250 and 270°C. Figure 3-17a shows the conversion of ethanol as a function of space time (τ'). As expected the conversion of ethanol increases with increasing space-time. At space-time of ca. 1 g_{cat} hr/g_{EtOH} and at temperatures higher than 250°C, complete conversion of ethanol is obtained.

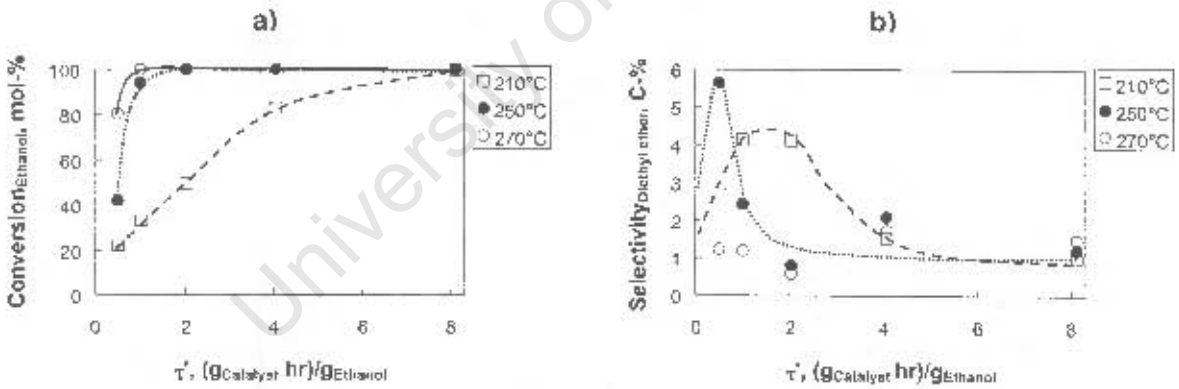

Figure 3-17: a) Conversion of ethanol as a function of space-time; b) selectivity to diethyl ether (non-oxidation reaction product) as function of space-time in the oxidation of ethanol over $V_{0.7}Fe_{0.3}SbO_4$ catalyst at $P_{alcohol}$ = 0.27 bar, P_{water} = 0, P_{O2} = 0.3 bar, balanced by N_2 to a total pressure of 2bar

The oxidation products formed in the oxidation of ethanol have been lumped together and separated from the side product diethyl ether that is not formed by the oxidative

reaction. Figure 3-17b shows the change in the diethyl ether selectivity with an increasing space-time. With increasing space time the diethyl ether selectivity passes a maximum. The maximum diethyl ether selectivity shifts to lower space-time with increasing temperature. With increasing temperature the maximum diethyl ether selectivity seems to increase (this is not observed at 270°C, but this might be ascribed to the range of space-times tested). The formation of diethyl ether is a reversible reaction. Hence, a decrease in diethyl ether selectivity is expected at high ethanol conversion (i.e. high space-time and high temperature).

The diethyl ether selectivity at $\tau'=0$ seems to be unequal zero. Thus, diethyl ether is likely to be a primary product of the reaction of ethanol over $V_{0.7}Fe_{0.3}SbO_4$ catalyst. Overall, the selectivity to diethyl ether observed in the space-time investigation was always less than 6%. Diethyl ether is not an oxidation product. It is formed by the condensation of the ethoxy species with adsorbed ethanol (Forzatti *et al.* 1987). For the reaction to occur the proximity of the ethoxy and adsorbed ethanol species is important. Surface hydroxyl groups are therefore important in this reaction for the acceptance of the OH^- from the ethanol to form water. The observed initial increase in the selectivity to diethyl ether with increasing space-time (Figure 3-17b) might be ascribed to generation of acid sites due to the heterolytic cleavage adsorption of ethanol to form ethoxy species.

The selectivity to oxidation products (acetaldehyde, acetic acid, ethyl acetate and carbon oxides) is presented within the oxidation products excluding the formation of diethyl ether as shown in Figure 3-18. The selectivity to acetaldehyde within the oxidation products fraction is shown in Figure 3-18a, and it decreases with increasing space-time. The extrapolated selectivity for acetaldehyde in the fraction of oxidation products at $\tau'=0$ seems to be 100%. Thus, it can be deduced that acetaldehyde is the sole primary oxidation product, formed parallel to the non-oxidation product diethyl ether. Thus, all other oxidation products are formed from acetaldehyde.

A notable trend in the selectivity of acetaldehyde with increasing temperature and increasing space-time is that the selectivity at 270°C is higher than that observed at 250°C. With increasing temperature the selectivity to acetaldehyde should increase,

reach a maximum and decrease due to secondary product formation. The minimum observed at 250°C was therefore not expected.

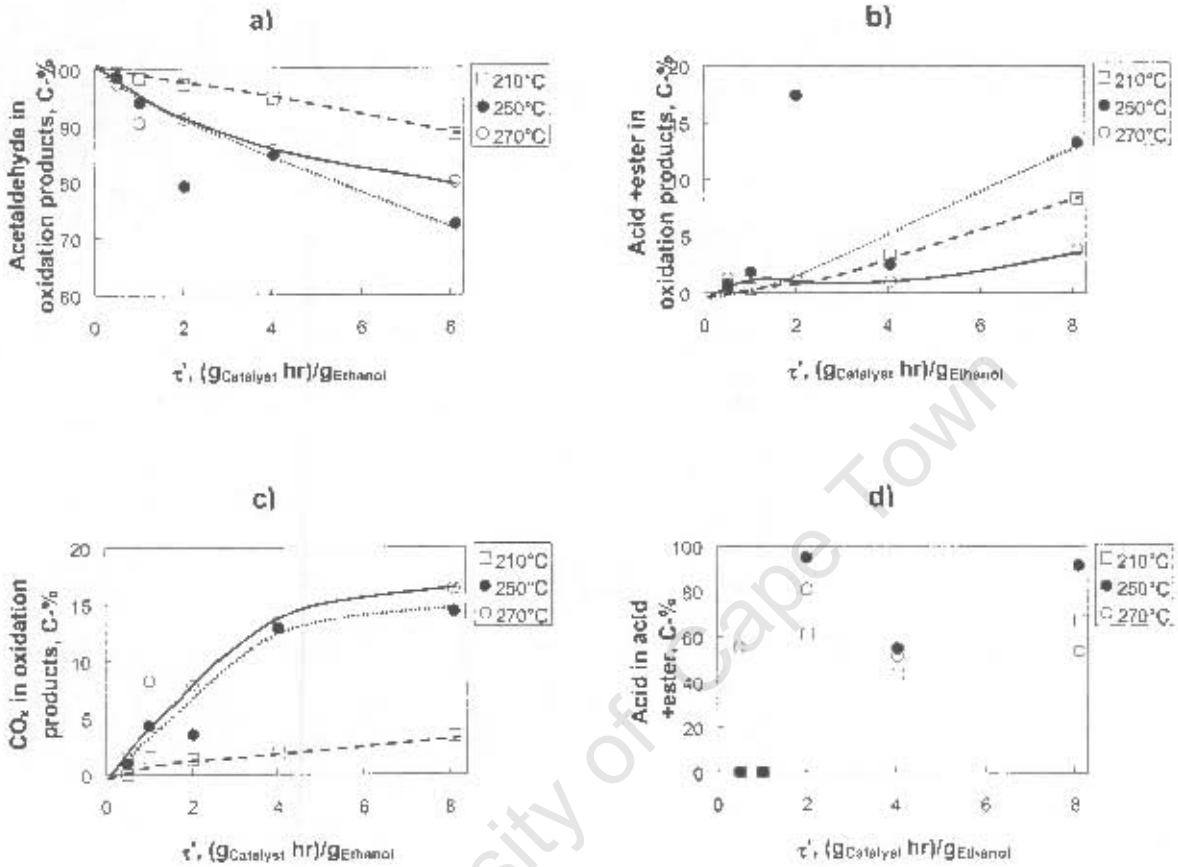

Figure 3-18: Selectivity patterns as the space time is increased in the oxidation of ethanol at 210, 250, 270°C over $V_{0.7}Fe_{0.3}SbO_4$ catalyst. WHSV = 0.31 to 4.87 $g_{alcohol}$ /($g_{catalyst}$ h); $P_{alcohol}$ = 0.27 bar, P_{water} = 0, P_{O2} = 0.3 bar, balanced by N_2 to a total pressure of 2bar

The selectivity to acetic acid and ethyl acetate within the oxidation products fraction is shown in Figure 3-18b. The acetates selectivity increases with increasing space-time. Similarly, the unexpected trend with increasing temperature is observed, with 270°C giving the lowest selectivity towards the acetates. There is large scatter in the acetic acid content within the acetate species observed (see Figure 3-18d). It must be mentioned at this point that there were difficulties associated with the analysis of acetic acid arising

from acetic acid GC outputs (broad, strongly tailing peaks). Hence, the error in analysis of acetic acid versus the error in analysis of ethyl acetate will be large. Nevertheless, based on the results obtained here, it might be speculated that ethyl acetate and acetic acid are formed in parallel (Figure 3-26d might be interpreted as a non-zero / non-100 % acid content).

The selectivity to carbon oxides increases strongly as the space-time is increased at 250°C and 270°C, and only slightly increases at 210°C. The strong increase in the selectivity towards carbon oxides at 250 and 270°C can be associated with different reactions leading to the carbon oxides setting off at elevated temperatures facilitate by the increased mobility of the lattice oxygen. Incomplete oxygen processing from molecular oxygen to lattice oxygen resulting in electrophillic oxygen species has also been cited as a reason for the increase in carbon oxides selectivity with increasing temperature.

The ethanol oxidation can be described with the following parallel-consecutive reaction pathway:

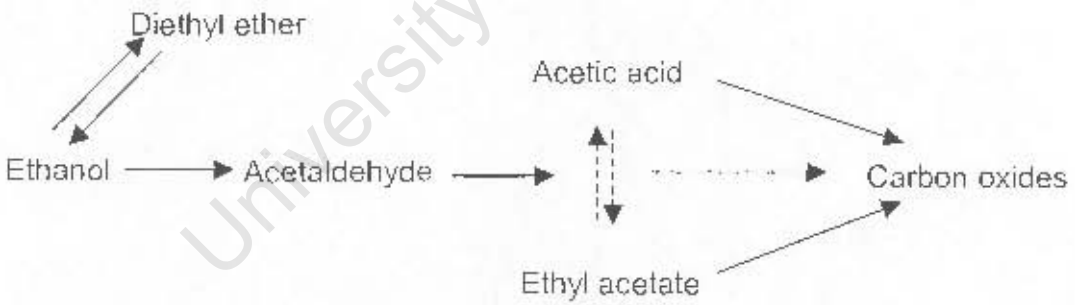

The reaction conditions are very close to equilibrium; hence the reversible reaction from diethyl ether to ethanol is feasible. The authors did not feed diethyl ether into the reactor, so there is exclusive evidence for the formation of CO_x from diethyl ether and acetaldehyde.

3.2.2 *The effect of ethanol to oxygen ratio in the oxidation of ethanol*

To build up the kinetics of the oxidation of ethanol over $V_xFe_{1-x}SbO_4$ catalysts, a study of varying ethanol to oxygen ratios was undertaken.

Presented in Figure 3-19a, the effect of increasing ethanol to oxygen ratio on the conversion of ethanol. Generally, ethanol conversion decreases with increasing ethanol to oxygen ratio. Busca *et al.* (1987) observed similar trends by in the oxidation of methanol over V/TiO_2 catalysts. The authors demonstrated the decrease in the methanol conversion with the increasing methanol to oxygen ratio. And concluded that the decreasing amount of oxygen was responsible for the observed decrease in methanol conversion.

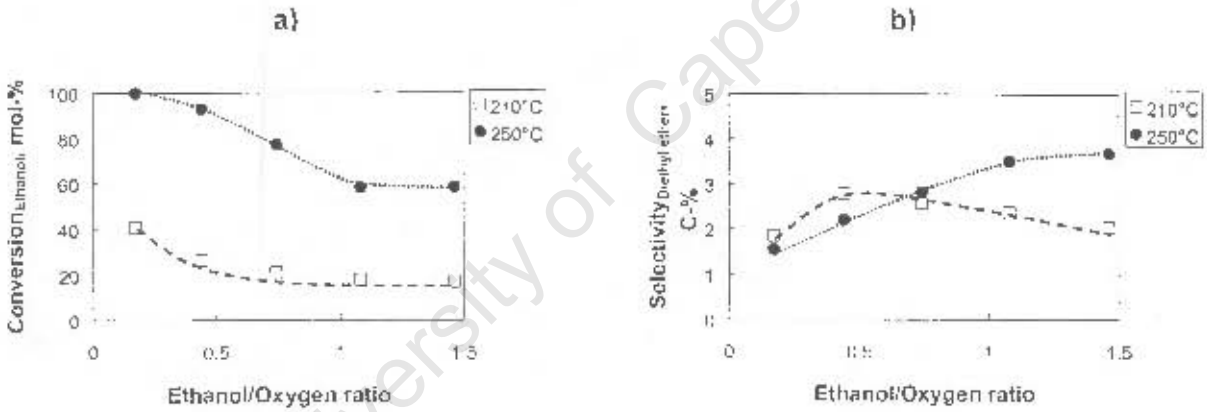

Figure 3-19: The effect of ethanol to oxygen ratio on: a) the conversion of ethanol; b) Selectivity to diethyl ether in the oxidation of ethanol over $V_{0.7}Fe_{0.3}SbO_4$ catalyst. $T_{reaction}$ = 210 and 250°C, Catalyst mass = 0.0625g; $P_{Ethanol}$ = 0.7 to 0.47 bar. P_{O2} = 0.3 bar, balanced by N_2 to a total pressure of 2 bar

Figure 3-19b shows the selectivity to diethyl ether as a function of ethanol to oxygen ratio. The selectivity to diethyl ether goes through a maximum, which shift to higher ethanol to oxygen ratios with increasing temperature. Diethyl ether is an undesirable by-product in the selective oxidation of ethanol, with the observed overall selectivity of less than 4% throughout the investigated ethanol to oxygen ratios.

The effect of the increasing ethanol to oxygen ratio on the oxidation products (acetaldehyde, acetic acid, ethyl acetate and carbon oxides) is shown in Figure 3-20. As the ethanol to oxygen ratio increases the acetaldehyde content in the oxidation products fraction increases slightly (Figure 3-20a). This might be solely attributed to the decrease in the ethanol conversion, which will cause this shift in a typical consecutive-type of reaction pathway.

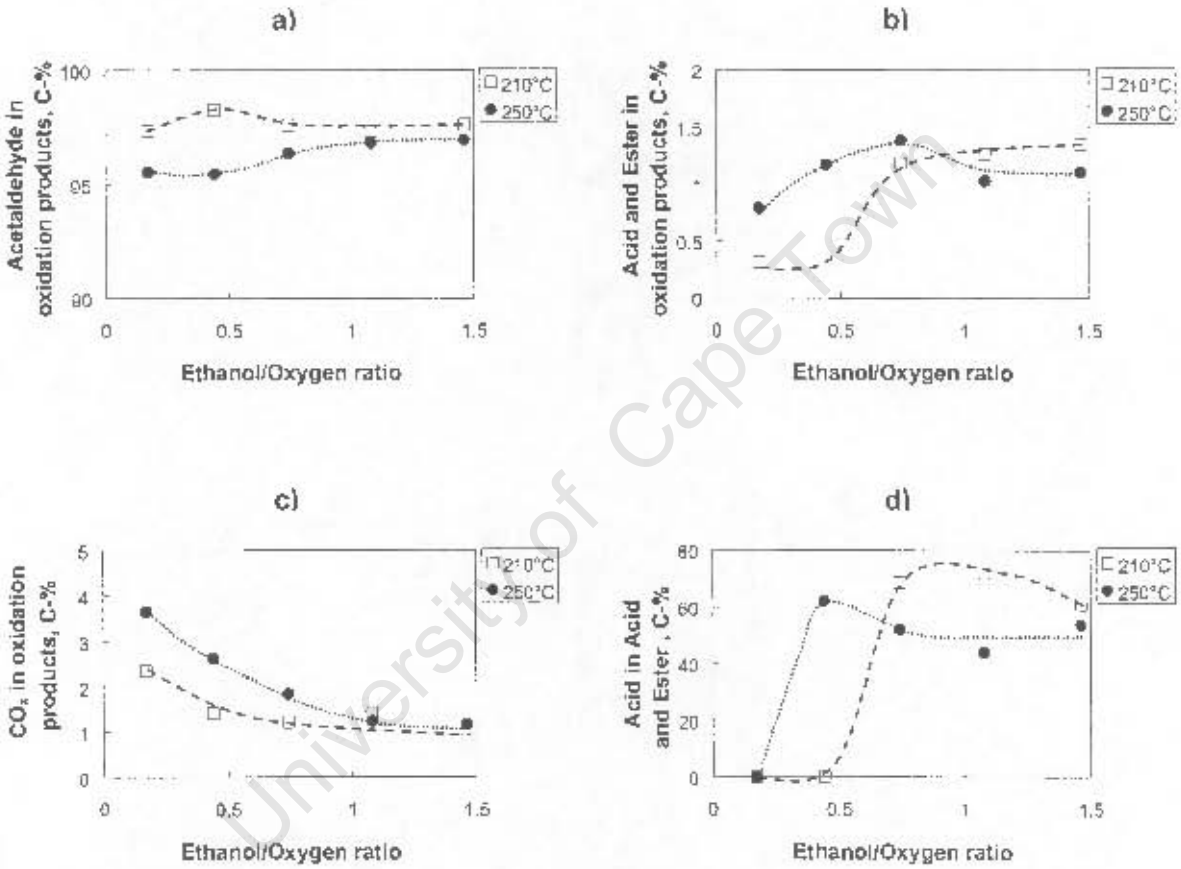

Figure 3-20: The effect of ethanol to oxygen ratio on the: content of acetaldehyde; b) content of acid and ester; c) content of carbon oxides within the oxidation products fraction and d) content of acetic acid in acid and ester fraction in the oxidation of ethanol over $V_{0.7}Fe_{0.3}SbO_4$ catalyst. $T_{reaction}$ = 210 and 250°C, WHSV = 0.31 $g_{ethanol}$ /($g_{catalyst}$ h), $P_{Ethanol}$ = 0.7 to 0.47 bar, P_{O2} = 0.3 bar, balanced by N_2 to a total pressure of 2 bar

The acid and ester content goes through the maximum (Figure 3-20b), which also concurs with the observed decrease in ethanol conversion. The content of the carbon

oxides decreases as expected (Figure 3-20c). The content of acetic acid within the acetic acid +ethyl acetate fraction seems to pass a maximum with increasing ethanol to oxygen ratio (Figure 3-20d).

The observed selectivity trends were comparable to those reported by Busca *et al.* (1987), Forzatti *et al.* (1987) in the oxidation of methanol over V/TiO_2 catalysts. Are the explanations also comparable?

3.2.3 Effect of water partial pressure

Different researchers in the oxidation catalysis field have studied the effect of water in the catalytic oxidation of hydrocarbons widely. Product inhibition was reported by Holstein *et al.* (1996) during a study of methanol oxidation over an iron molybdate catalyst. Suppression of the formation of CO_2 by water blocking the most active sites was proposed by Saleh-Alhamed *et al.* (1995). Medeiros *et al.* (2000) demonstrated that water improves the selectivity to partial oxidation products and decreases the selectivity to carbon oxides. A study to investigate the effect of inlet water partial pressure on the oxidation of ethanol at different space-times would uncover a great deal of information about the effect of water on the primary and consecutive reactions in the ethanol oxidation. Most of the studies quoted above were performed at single, fixed water partial pressure. This study presents an investigation into this effect over a range of water partial pressures and a range of space times on the oxidation of ethanol.

The effect of water partial pressure on the conversion of ethanol at different space times and temperature (210, 250 and 270°C) is shown in Figure 3-21.

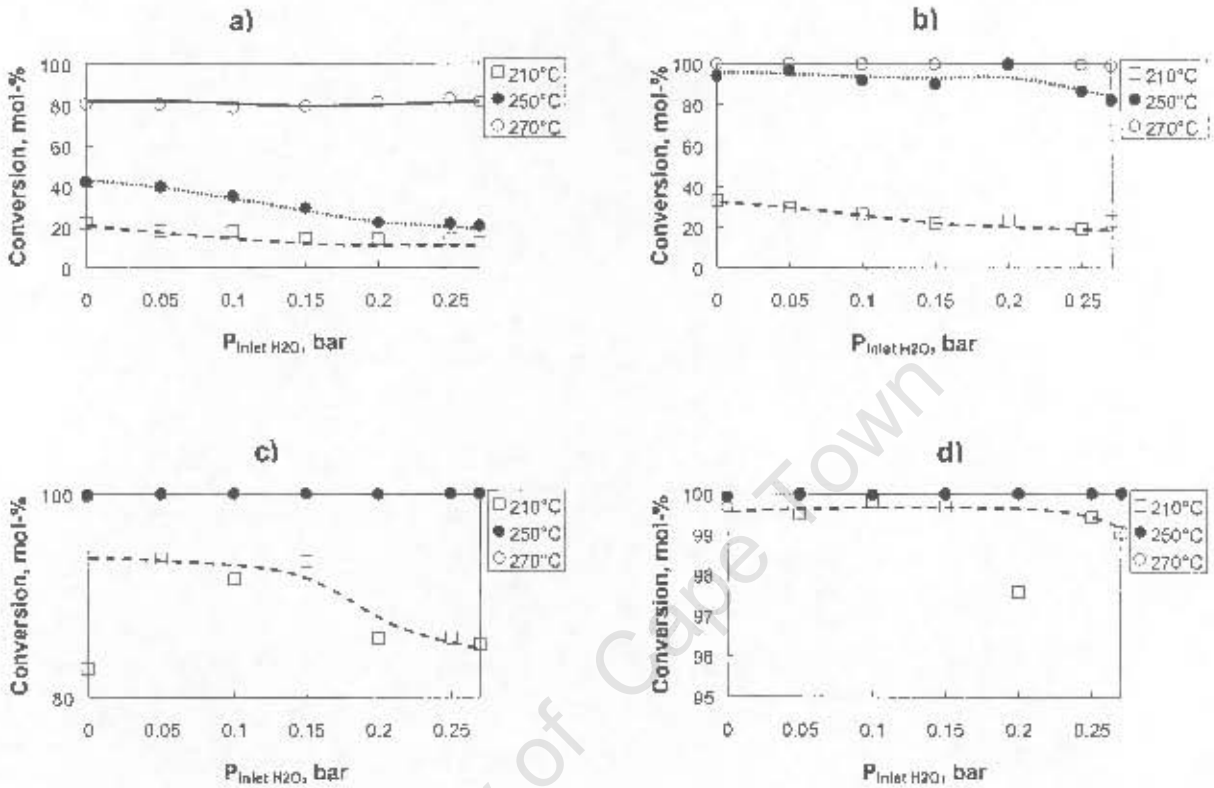

Figure 3-21: The effect of inlet water partial pressure on the conversion of ethanol over $V_{0.7}Fe_{0.3}SbO_4$ catalyst. $T_{reaction}$ = 210, 250, 270°C, varying WHSV: a) = 0.31; b) = 0.6; c) = 2.4; d) = 4.9 $g_{ethanol}/(g_{catalyst}\ h)$, $P_{ethanol}$ = 0.27 bar, P_{water} = 0 to 0.27 bar, P_{O2} = 0.3 bar, balanced by N_2 to a total pressure of 2 bar

At low space-time (Figure 3-21a and b), there is a slight decrease in the conversion of ethanol with increasing water partial pressure indicating a slight inhibition of ethanol oxidation over mixed vanadium iron antimonates. At intermediate (Figure 3-21c) and high space-time (Figure 3-21d), there is a marked decrease in ethanol conversion observed at 210°C with increasing water partial pressure. The observed decrease can be ascribed to the competitive adsorption of water on the active sites of the catalyst.

Figure 3-22 presents the 1st order rate constant for the conversion of ethanol as a function of the partial pressure of water. The rate constant remains rather constant with

increasing water partial pressure. Hence it can be deduced that the reaction is approximately zero order with respect to the water concentration.

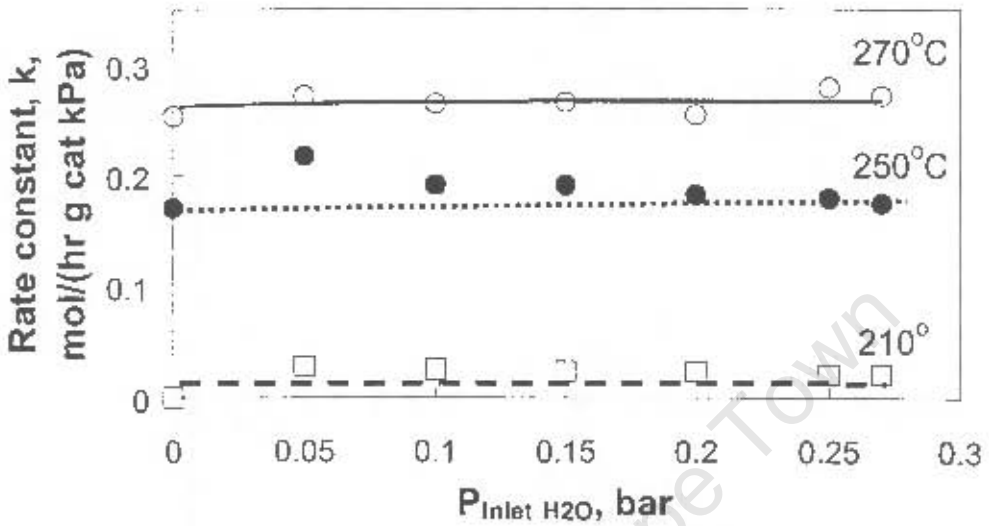

Figure 3-22: The effect of the inlet partial pressure of water on the rate constant for the oxidation of ethanol over $V_{0.7}Fe_{0.3}SbO_4$ catalyst. $T_{reaction}$ =210°C, 250°C and 270°C, WHSV = 0.3045 $g_{ethanol}$ /($g_{catalyst}$ h); $P_{ethanol}$ = 0.27 bar, P_{water} = 0 to 0.27 bar, P_{O2} = 0.3 bar, balanced by N_2 to a total pressure of 2 bar

To effectively display the effect of the water partial pressure, the selectivity of products is shown in 4 different space times. Oxidation products have been separated from diethyl ether, which is a non-oxidative route product. There were other products observed and they were identified as acetaldehyde condensation products (i.e. acetone, crotonaldehyde, etc.). These products formed not more than 3% of the total product spectrum observed.

Presented in Figure 3-23 is the selectivity to diethyl ether as a function of the space-time at 210, 250 and 270°C.

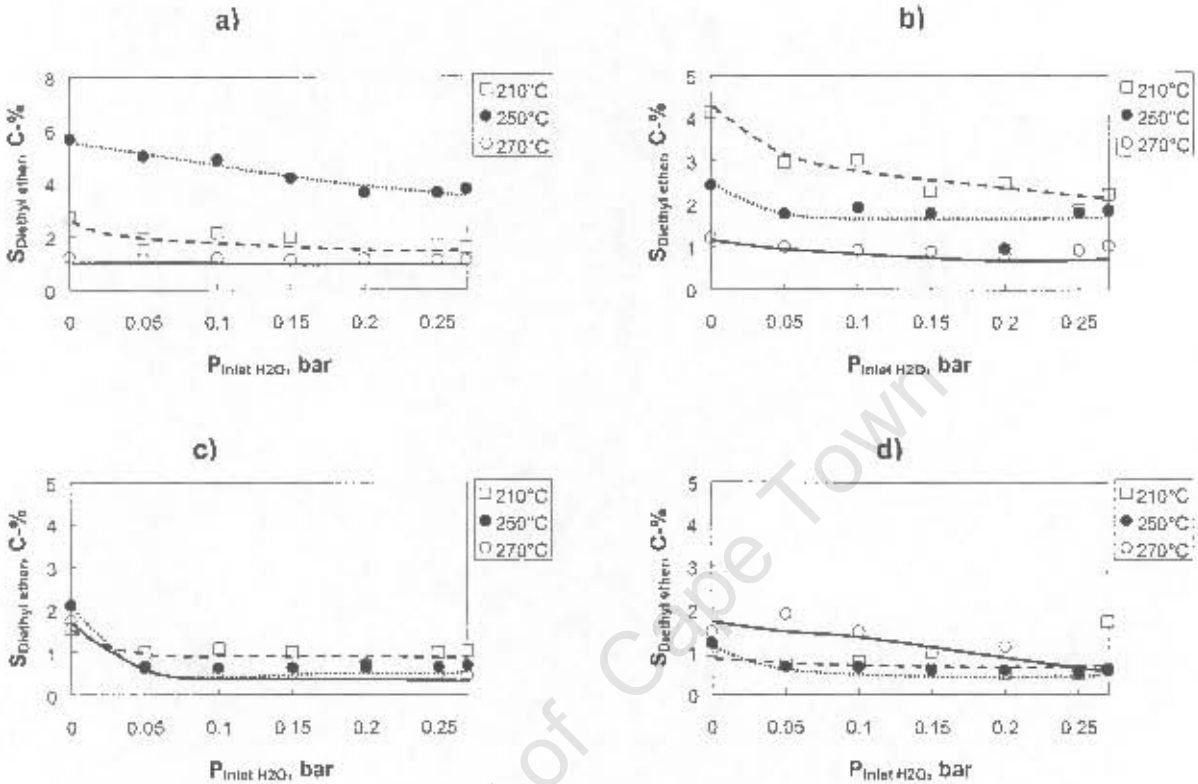

Figure 3-23: Influence of inlet water partial pressure on the selectivity to diethyl ether in the oxidation of ethanol over $V_{0.7}Fe_{0.3}SbO_4$ catalyst. $T_{reaction}$ =270°C, varying WHSV: a) = 0.31; b) = 0.6; c) = 2.4; d) = 4.9 $g_{ethanol}/(g_{catalyst}\ h)$, $P_{ethanol}$ = 0.27 bar, P_{water} = 0 to 0.27 bar, P_{O2} = 0.3 bar, balanced by N_2 to a total pressure of 2 bar

Generally, the selectivity to diethyl ether decreases with increasing inlet water partial pressure. There is no effect observed in the selectivity of diethyl ether at high temperature (270°C) and high space-time (Figure 3-23c and d). This is expected since at these conditions (high conversion) very low selectivity to diethyl ether is observed due to low concentration of ethoxy species.

The content of acetaldehyde within the fraction of oxidation products (i.e. excluding diethyl ether) is hardly affected by the increase in water partial pressure. A notable observation at 250°C, and low space-time (Figure 3-24a and b) is that there is an increase in the selectivity to acetaldehyde with increasing inlet water partial pressure. This can be ascribed to the decrease in the selectivity of the condensation products, such as crotonaldehyde (not shown). At 270°C and high space- time (Figure 3-24 c and d), a strong decrease in the selectivity of acetaldehyde with increasing inlet water partial pressure is observed. This concurs with an increase in the acetic acid and ethyl acetate content in the fraction of oxidation products. Thus, water affects the consecutive conversion of acetaldehyde.

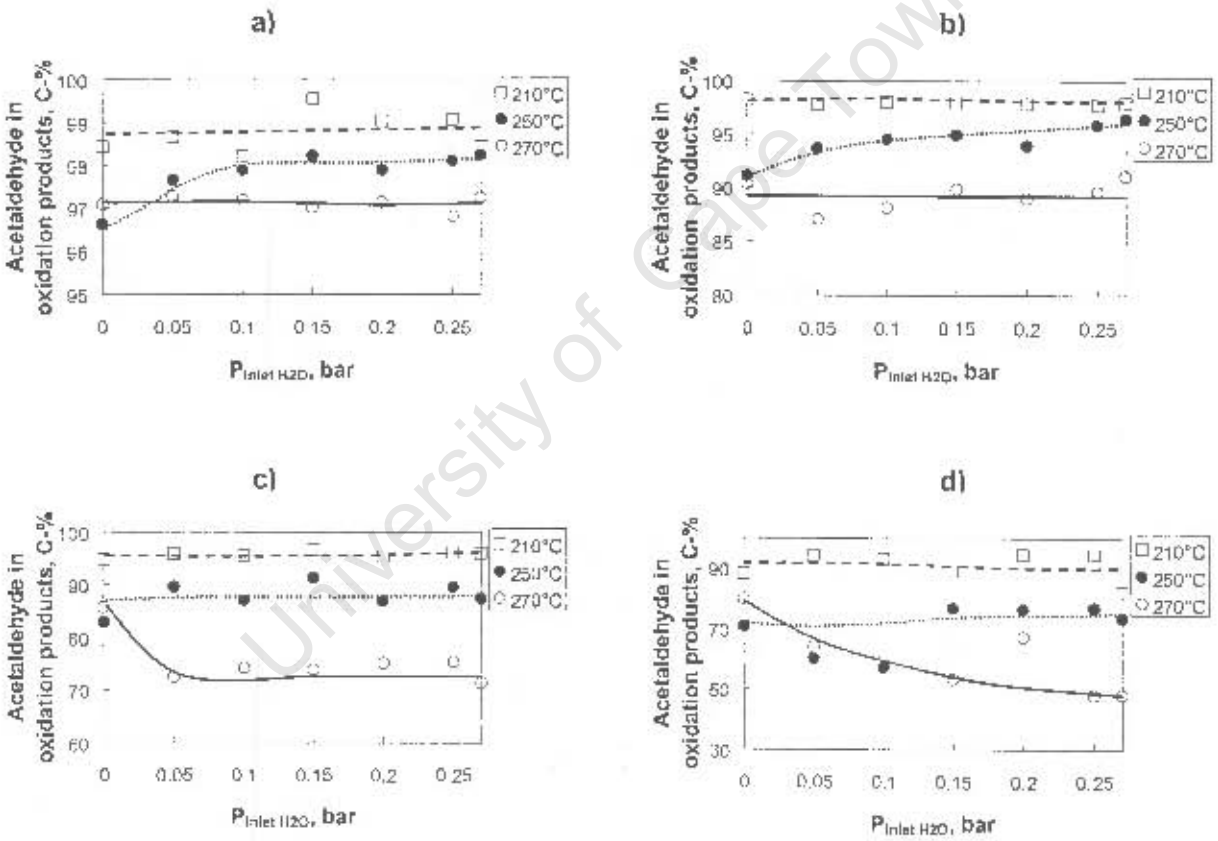

Figure 3-24: Influence of inlet water partial pressure on the aldehyde content in fraction of oxidation products in the oxidation of ethanol over $V_{0.7}Fe_{0.3}SbO_x$ catalyst. $T_{reaction}$ = 250°C, varying WHSV; a) = 0.31; b) = 0.6; c) = 2.4; d) = 4.9 $g_{ethanol}/(g_{catalyst}\ h)$, $P_{ethanol}$ = 0.27 bar, P_{water} = 0 to 0.27 bar, P_{O2} = 0.3 bar, balanced by N_2 to a total pressure of 2 bar

The effect of the water partial pressure on the selectivity to acetic acid and ethyl acetate within the oxidation products fraction is shown in Figure 3-25 and Figure 3-26.

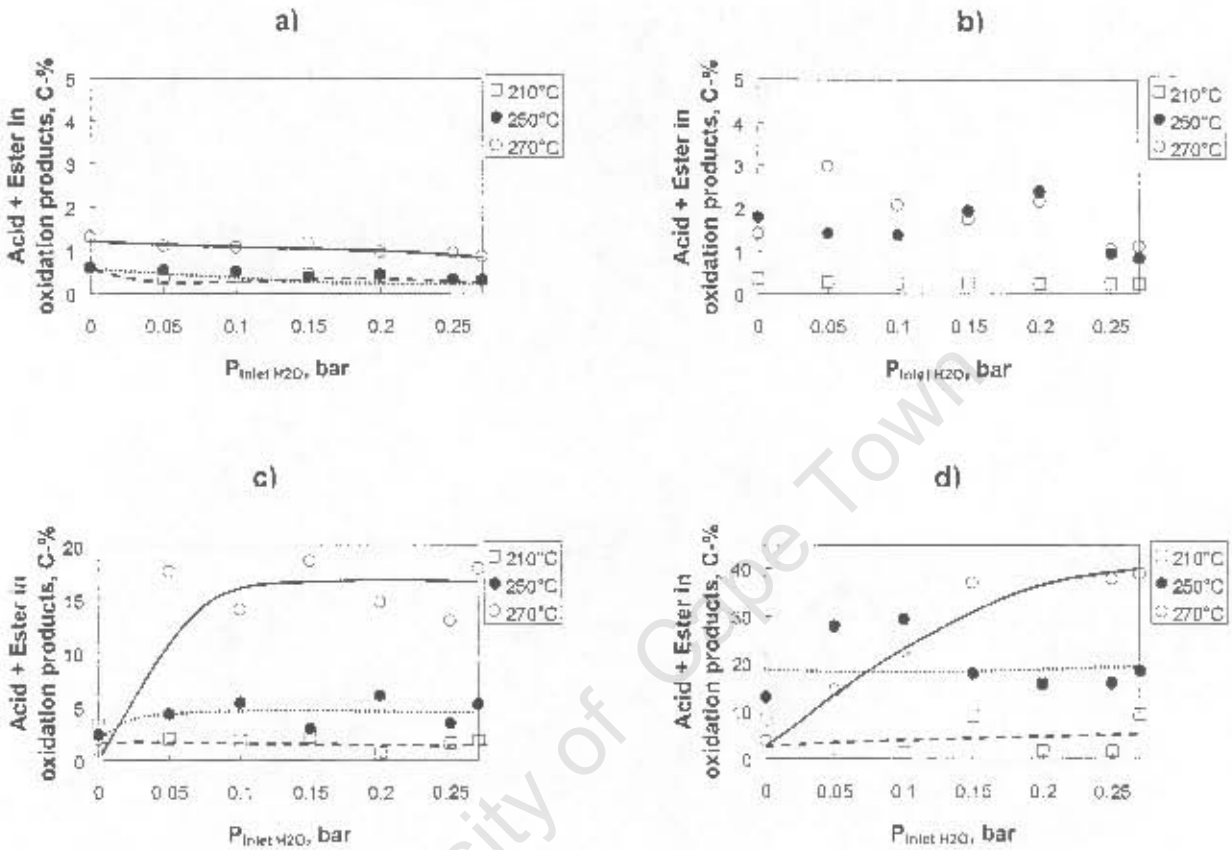

Figure 3-25: Influence of inlet water partial pressure on the acetic acid plus ethyl acetate content in the fraction of oxidation products in the oxidation of ethanol over $V_{0.7}Fe_{0.3}SbO_4$ catalyst. $T_{reaction}$ = 250°C, varying WHSV: a) = 0.31; b) = 0.6; c) = 2.4; d) = 4.9 $g_{ethanol}/(g_{catalyst}\ h)$, $P_{ethanol}$ = 0.27 bar, P_{water} = 0 to 0.27 bar, P_{O2} = 0.3 bar, balanced by N_2 to a total pressure of 2 bar

There is a marginal effect observed throughout the space times investigated. At higher space-times Figure 3-25 c and d, a notable increase in the selectivity of acetic acid plus ethyl ether is observed at 250°C and 270°C. This corresponds to a marked decrease in acetaldehyde observed under these conditions. Thus, water seems to enhance the consecutive conversion of acetaldehyde to ethyl acetate and acetic acid. Within the acetate group, acetic acid content in the fraction of acetic acid and ethyl acetate seems to decrease with increasing inlet water partial pressure (Figure 3-26) at high space-time and high reaction temperature. The effect is not strong at low reaction temperature and

low space-time. That might be ascribed to the low amount of ethyl acetate and acetic acid in the product stream under these conditions, and thus to the larger error associated with the determination of the acetic acid content in the fraction of ethyl acetate and acetic acid.

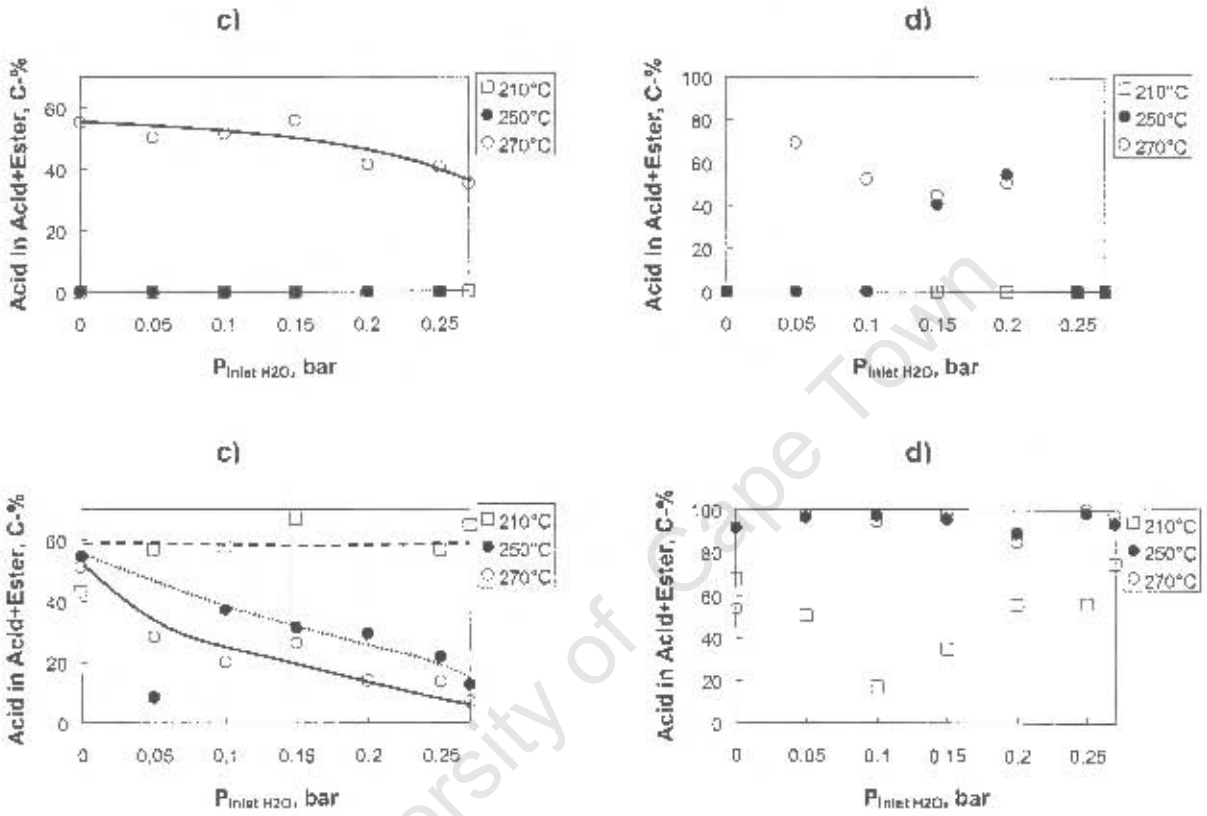

Figure 3-26: Influence of inlet water partial pressure on the acetic acid content in the fraction of acetic acid plus ethyl acetate in the oxidation of ethanol over $V_{0.7}Fe_{0.3}SbO_4$ catalyst. $T_{reaction}$ = 250°C, varying WHSV: a) = 0.31; b) = 0.6; c) = 2.4; d) = 4.9 $g_{ethanol}/(g_{catalyst}$ h), $P_{ethanol}$ = 0.27 bar, P_{water} = 0 to 0.27 bar, P_{O2} = 0.3 bar, balanced by N_2 to a total pressure of 2 bar

Conceptually, water is supposed to increase the concentration of surface hydroxyl groups and thus hydrolysis of the adsorbed species will be enhanced, which will lead to an increase in acetic acid content. Evident from the experimental data in Figure 3-26 is that the content of acetic acid and ethyl acetate decreases with increasing water partial pressure. A plausible explanation is discussed proposing that the formation of acetic

acid requires the hydrogen abstraction as H^+ from the dioxyethylene species (acetate species), this abstraction is depressed by water because of the transformation of O^{2-} to OH^- surface species.

The selectivity towards carbon oxides within the oxidation products is not affected by the increasing inlet water partial pressure at short space-time (Figure 3-27a). However, at high space-time, a decrease in the selectivity to carbon oxides with increasing inlet water partial pressure is observed.

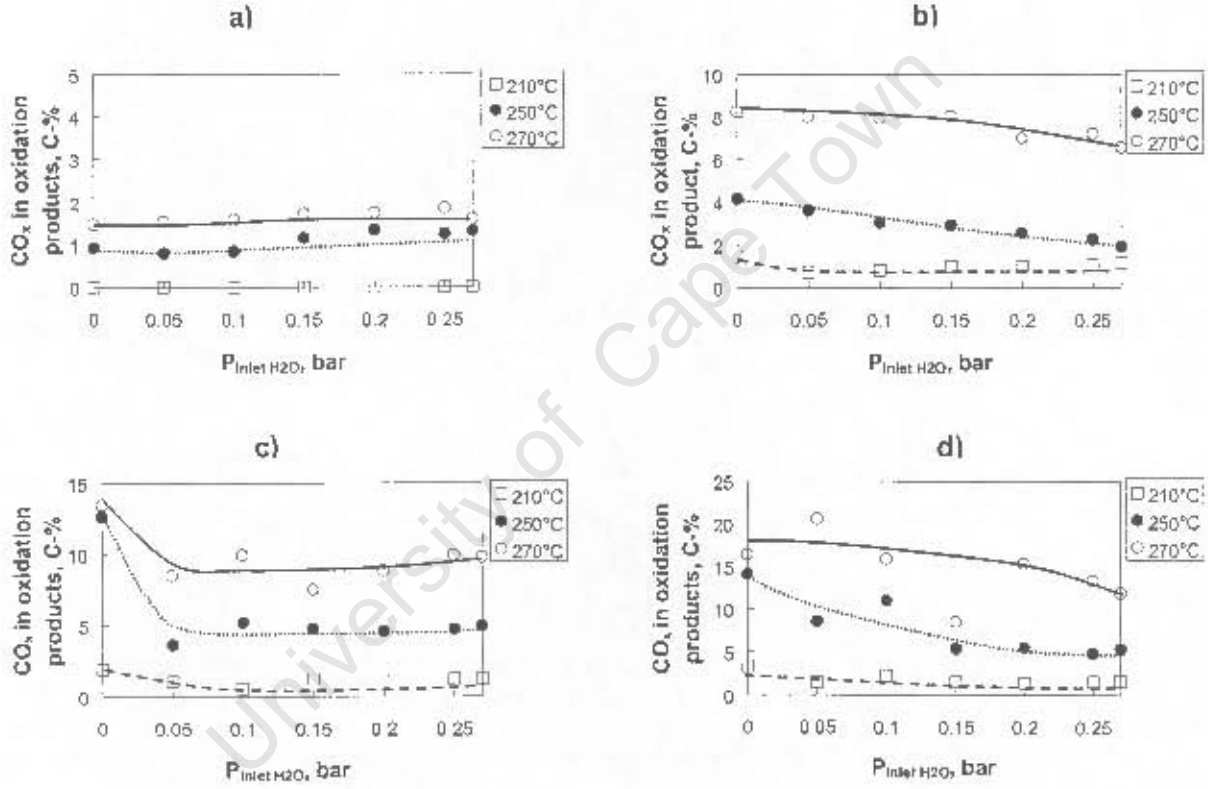

Figure 3-27: Influence of inlet water partial pressure on Carbon oxides content in the fraction of oxidation products in the oxidation of ethanol over $V_{0.7}Fe_{0.3}SbO_4$ catalyst. $T_{reaction}$ = 250°C, varying WHSV: a) = 0.31; b) = 0.6; c) = 2.4; d) = 4.9 $g_{ethanol}/(g_{catalyst}\ h)$, $P_{ethanol}$ = 0.27 bar, P_{water} = 0 to 0.27 bar, P_{O2} = 0.3 bar, balanced by N_2 to a total pressure of 2 bar

The consecutive reaction leading to the formation of CO_x, seems to be inhibited with increasing inlet water partial pressure. Concurrently, the selectivity for acetic acid and

ethyl acetate increases. Thus, water inhibits the further oxidation of a common reaction intermediate.

3.2.4 *The effect of temperature on the oxidation of ethanol*

The effect of temperature in the oxidation of ethanol over $V_{0.7}Fe_{0.3}SbO_4$ was investigated between 150 and 300°C (see Figure 3-28 and Figure 3-29).

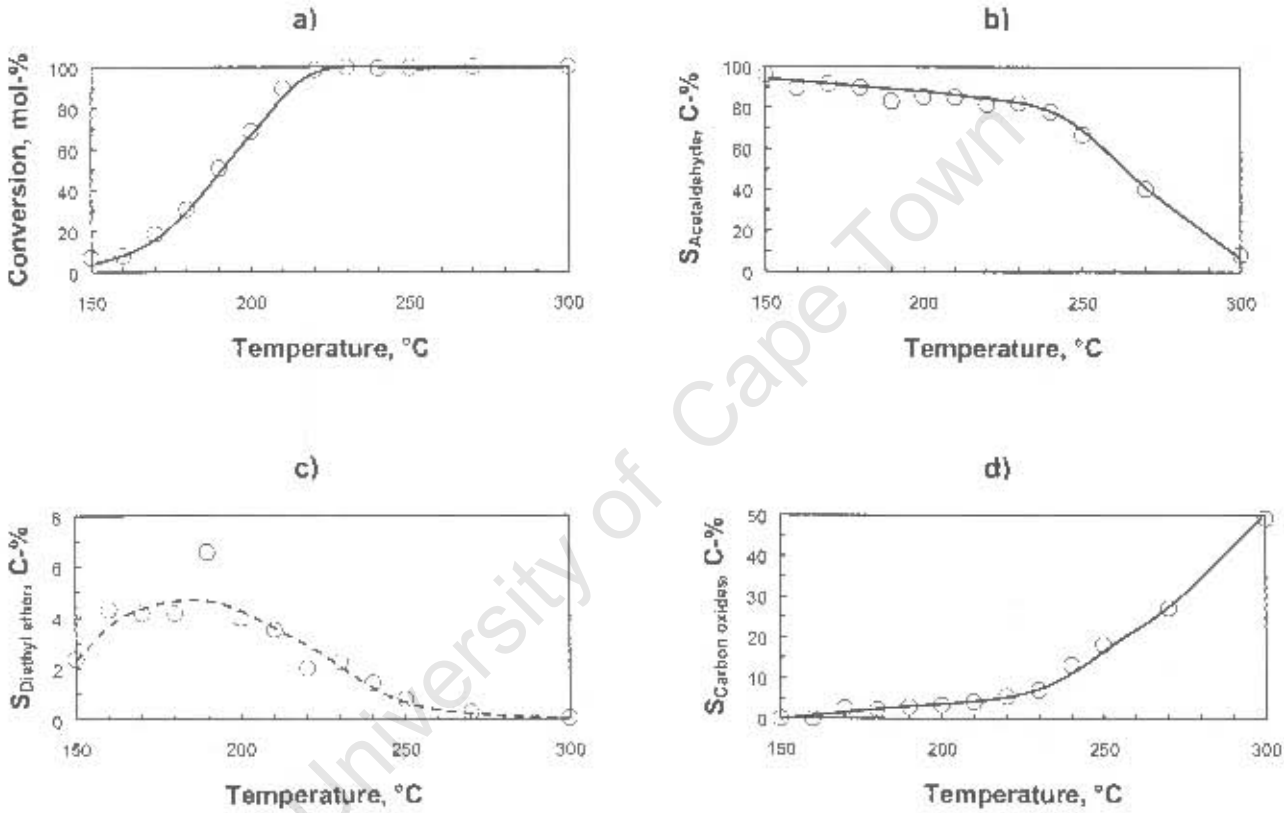

Figure 3-28: a) Conversion of ethanol as a function of temperature over $V_{0.7}Fe_{0.3}SbO_4$ catalyst. Selectivity to b) acetaldehyde, c) diethyl ether and d) carbon oxides as a function of temperature: $T_{reaction}$ = 150-300°C, WHSV = 2.44 $g_{ethanol}/(g_{catalyst}\ h)$; $P_{ethanol}$ = 0.27 bar, P_{O2} = 0.3 bar, balanced by N_2 to a total pressure of 2 bar

Ethanol conversion increases with increasing temperature (Figure 3-28a). Acetaldehyde is a major primary oxidation product in the conversion of ethanol over $V_{0.7}Fe_{0.3}SbO_4$ catalyst. The selectivity to acetaldehyde as shown in Figure 3-28b decreases steadily from 150 to 240°C. From 250°C a sharp decrease in the acetaldehyde selectivity is

observed. Diethyl ether is also a primary product forming at relatively low amount over this catalyst. The selectivity to diethyl ether decreases with increasing temperature Figure 3-28c. Above 210°C, carbon oxides start to form increasing steeply with increasing temperature as shown in Figure 3-28d. Diethyl ether forms competitively with acetaldehyde. The sharp decrease with increasing temperature of the selectivity indicates that the reaction from ethanol to diethyl ether is reversible. The increase in temperature favours the reverse reaction.

Acetic acid and ethyl acetate selectivity increases steadily with increasing temperature in the region of 150-240°C (see Figure 3-29a). A rapid increase is observed between 240 and 270°C. The acetic acid plus ethyl acetate selectivity passes a maximum at about 270°C.

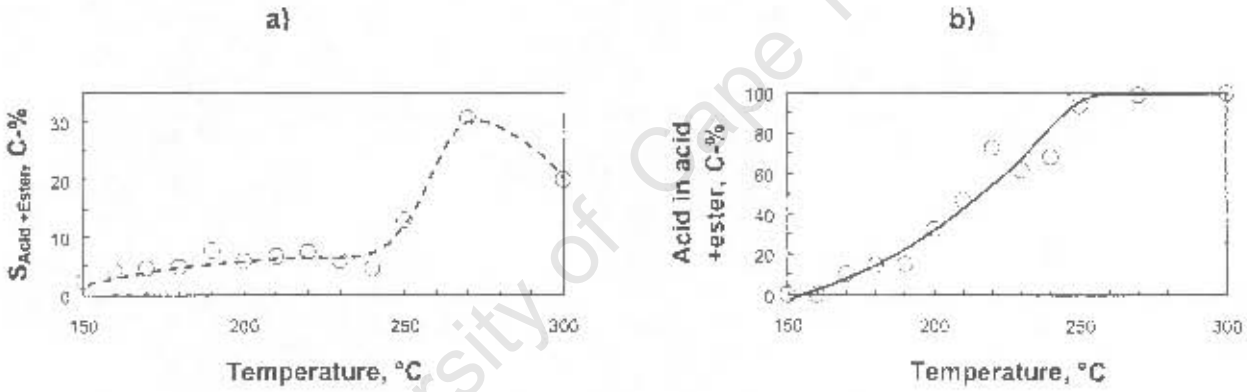

Figure 3-29: Selectivity to a) acetic acid + ethyl acetate, b) acetic acid in the acetic acid + ethyl acetate fraction as a function of temperature in the oxidation of ethanol over $V_{0.7}Fe_{0.3}SbO_4$ catalyst. $T_{reaction}$ = 150-300°C, WHSV = 2.44 $g_{ethanol}/(g_{catalyst}\ h)$; $P_{ethanol}$ = 0.27 bar, P_{O2} = 0.3 bar, balanced by N_2 to a total pressure of 2 bar

Figure 3-29b shows the acetic acid content in the acetic acid and ethyl acetate fraction as a function of reaction temperature. With increasing temperature the acetic acid content in the fraction of acetic acid plus ethyl acetate increases.

3.2.5 Surface characterization by adsorption of ethanol

In heterogeneous catalysis, adsorbed species react with each other or with gas phase molecules to form new products. Before reaction can take place however, gas-phase

reactants must adsorb on the catalytic surface and before the process is complete the newly formed product must desorb. Thus, gaining knowledge of adsorption / desorption processes is an integral part of achieving fundamental understanding of the interactions between the catalyst and organic compounds taking part in the reaction. Subsequently, reaction mechanisms can be elucidated. This section reports on the use of TPD, TAP and IR techniques used to identify products and intermediates formed during ethanol oxidation over $V_xFe_{1-x}SbO_4$ catalysts.

3.2.5.1 Temporal analysis of product (TAP)

TAP experiment by design operates in the millisecond time regime and offers better resolution compared to commonly used non-steady state reactor systems (Gleaves et al. 1989). TAP experiments were performed using ethanol as a probe molecule over $V_{0.7}Fe_{0.3}SbO_4$ catalysts. The mass balance for all the experiments performed using TAP was less than 20%; hence the results obtained in this study could not be used for kinetic analysis. It is speculated that products were formed and were adsorbed very strongly on the catalyst surface, hence the slow desorption observed resulting in products not being detected in the millisecond time range of operation.

3.2.5.2 Temperature programmed desorption (TPD) – products analysis

A TPD study was performed to identify products formed during the ethanol oxidation over $V_{0.7}Fe_{0.3}SbO_4$ catalysts. Figure 3-30 presents a profile of product desorption upon ethanol adsorption (at 25°C) as a function increasing temperature. This study was merely for qualitative analysis, hence the y-axis in the products profile figures are set as arbitrary. Examining desorption profile, ethanol (m/z = 31 and 45); acetaldehyde (m/z = 15, 29, 43 and 44); water (m/z = 17 and 18), ethylene (m/z = 26) are observed, all desorbing at 152°C. Water, however, starts desorbing at 152°C and continues to desorb until 400°C (evident from the broad peaks (m/z= 17 and 18) stretching between 150 and 400°C). This is indicative of water continually desorbing and re-adsorbing on the catalyst surface.

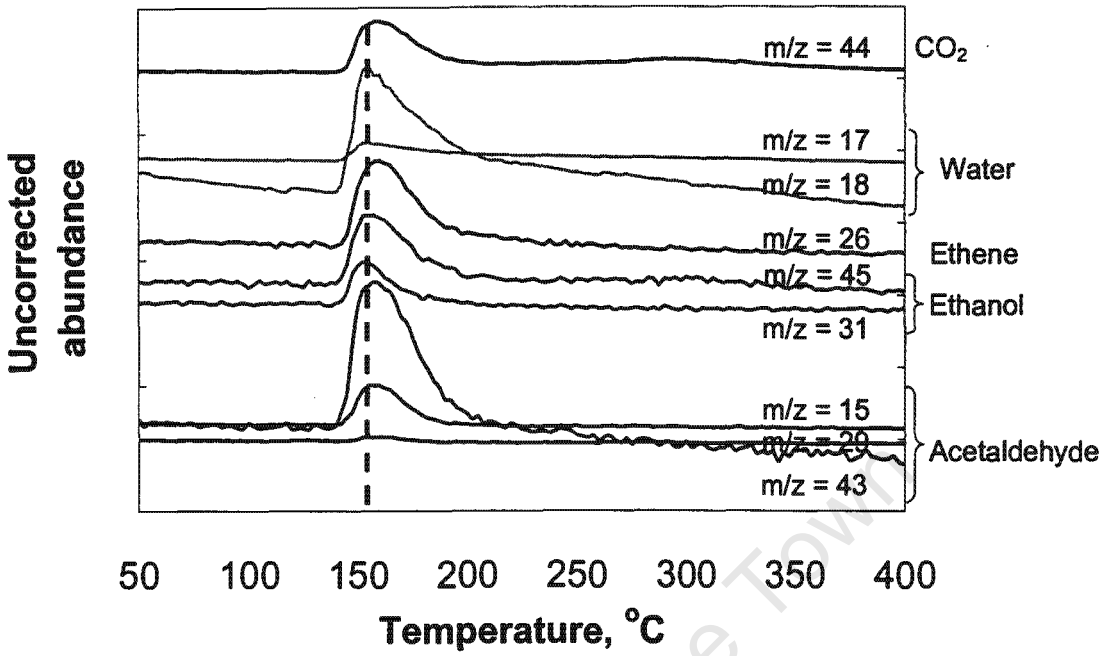

Figure 3-30: Desorption of products with increasing temperature upon ethanol adsorption followed by a TPD analysis over $V_{0.7}Fe_{0.3}SbO_4$ catalyst.

Figure 3-31 presents a profile of products desorption upon acetaldehyde adsorption (at 25°C) and progressively increasing temperature. Once again, water (m/z = 17 and 18) is observed, with the characteristic broad peaks stretching between 100 and 400°C. However, an unexpected outcome was observed. Prominent peaks (m/z = 37, 39 and 68) were observed which matched a fragmentation pattern of furan. This product desorbs between 100°C and 280°C.

It is apparent that the reaction taking place in TPD study is not identical to those during catalytic reaction. The dynamics in the catalytic tests in a fixed-bed reactor are expected to be different from those on the TPD study.

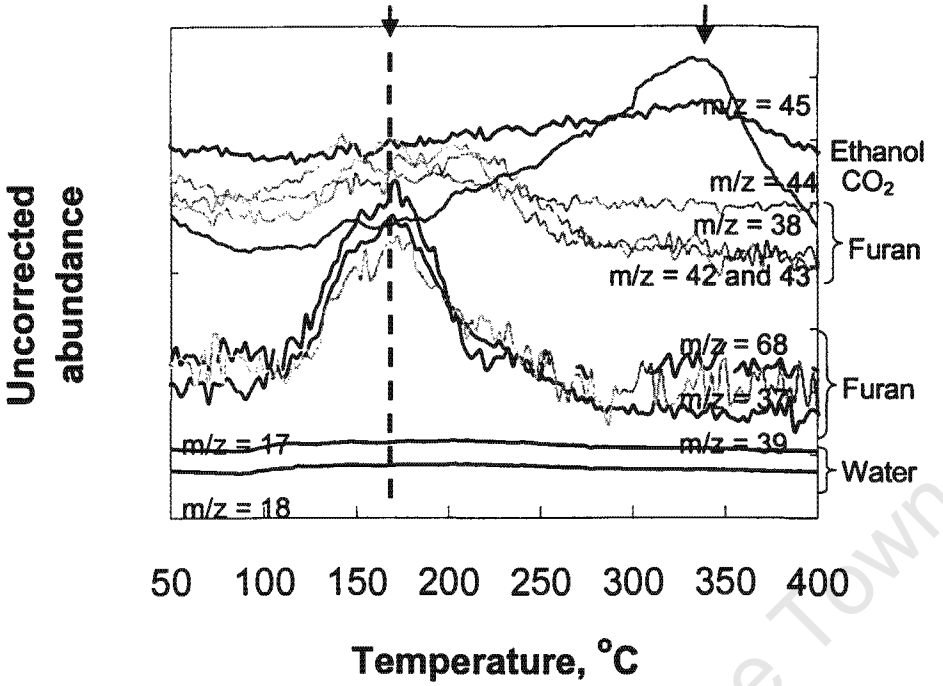

Figure 3-31: Desorption of products with increasing temperature upon acetaldehyde adsorption followed by a TPD analysis over $V_{0.7}Fe_{0.3}SbO_4$ catalyst

Also observed were various peaks stretching over the same temperature range (m/z = 38, 42 and 43). Closer scrutiny of the fragmentation pattern shows that the peaks are characteristic of furan fragmentation. Madhavaram and Idriss (1997) reported the formation of furan upon adsorption of ethanol over β–UO_3. Furan forms directly from crotonaldehyde through the intra-cyclization of the molecule. Carbon-carbon bond formation leading to products such as crotonaldehyde and furan from aldehydes is possible through aldolisation reactions. β-aldolisation of two acetaldehyde molecules with subsequent dehydration produces crotonaldehyde. Crotonaldehyde formation has been observed upon adsorption of ethanol on surfaces of CeO_2 (Idriss *et al.*, 1955), TiO_2 (Idriss *et al.*, 1993), Al_2O_3 and β–UO_3 (Madhavaram and Idriss, 2001).

At about 340°C, desorption due to carbon dioxide (m/z = 44 and 45) was observed. These are the only products observed at this high temperature domain (highlighted by arrows in Figure 3-31).

3.2.5.3 Infrared Spectroscopy

The adsorption of ethanol over $V_{0.7}Fe_{0.3}SbO_4$ at 25°C produced a spectrum with bands at 3672, 3435, 2970, 2906, 2341, 1757, 1474, 1401, 1055 and 980 cm^{-1} (Figure 3-32). The formation of ethoxy species upon the adsorption of ethanol is evidenced by bands at 2906 ($\nu_{as}(CH)$), 1474 ($\delta(CH_2)$) and 1401 cm^{-1} ($\delta_s(CH_3)$).

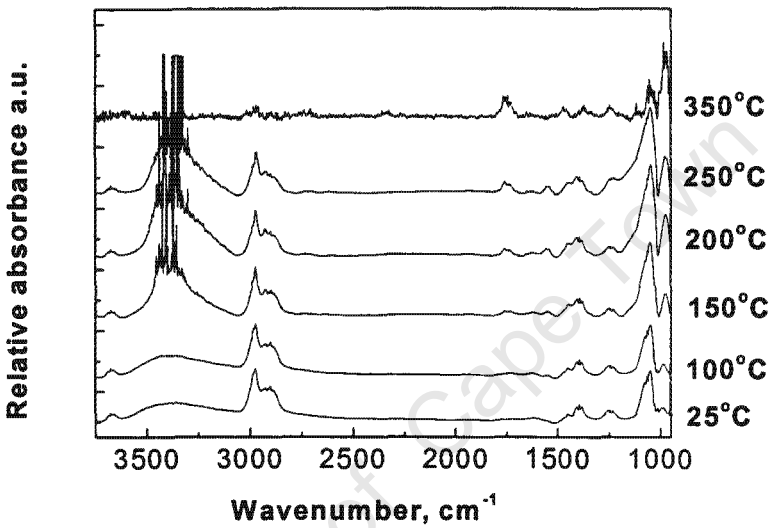

Figure 3-32: FT-IR spectra of $V_{0.7}Fe_{0.3}SbO_4$ after pretreatment at 180°C and adsorption of ethanol at 25°C and progressively increasing temperature

The small band at 1055 cm^{-1} is attributed to bidentate ethoxy species increasing remarkably with increasing temperature. Ethoxy species observed during this investigation over $V_{0.7}Fe_{0.3}SbO_4$ have shifted to higher wavenumbers by 5cm^{-1} compared to those observed over Pt/CeO_2 and Pd/CeO_2 (Yee *et al.*, 1999). The band at 3435 cm^{-1}, assigned to δ(OH) increases strongly with increasing temperature. The increase is most probable due to dissociative adsorption of ethanol over surface Brønsted acid sites (OH), resulting in the generation of OH species on the surface. The observed band at 1750 cm^{-1}, which also increases with temperature, is assigned to η-acetaldehyde (Yee *et al.*, 1999).

A pair of bands at 1553 / 1338 cm^{-1} developing simultaneously at 150°C is attributed to carbonate species. Carbonates of oxide materials (ν(C-O)) have been observed as a pair of peaks by other researchers upon adsorption of ethanol over, α-Cr_2O_3 (1556 / 1340 cm^{-1}), La_2O_3 (1560 / 1340 cm^{-1}), Co_3O_4 (1545 / 1324 cm^{-1}) and $Na_6(Ce(CO_3)_5\ H_2O$ 1560 / 1370 cm^{-1} (Busca and Lorenzelli, 1982; Yee *et al.*, 1999). According to Yee *et al.* (1999) these bands are associated with ν(C=C) and ρ(CH_3) of adsorbed crotonaldehyde species.

Intermediates observed upon the adsorption of ethanol and over $V_{0.7}Fe_{0.3}SbO_4$ catalysts are summarized in Table 3-11.

Table 3-11: Vibrational frequencies and mode assignments obtained from adsorption of ethanol over $V_{0.7}Fe_{0.3}SbO_4$ catalyst, $T_{pretreatment}$ = 180°C, $T_{adsorbption}$ = 25°C, and temperature increased sequentially

Vibrational wavelength (cm^{-1})	Assignment	Vibrational wavelength (cm^{-1})	Assignment
3667 (3670)[1]	$\nu_{as}(H_2O)$	1450 (1474)	$\delta_{as}(CH_3, CH_2)$
3435	ν(O-H)	1430(1420-1429)	ν_s(OCO)
2970 (2960)	ν(CH_3, CH_2)	1377 (1383)	$\delta_s(CH_3, CH_2)$
2929	ν(CH_3, CH_2)	1338 (1341)	ν_{as}(OCO)
2900	ν(CH_3, CH_2)	1254 (1292)	δ(O-H)
1731-1758 (1692)	η-acetaldehyde	(1154)	ν(C=C)
1717 (1711)	ν(C=O)	1127 (1125)	Monodentate ν(C-O)
1661 (1661)	ν(C=O)	1077 (1080)	ν(C-O)
1635 (1637)	ν(C=C)	1067	ν(C-O)
1616	ν_{as}(OCO)	1050 (1057)	Bidentate ν(C-O)
1553 (1553-1578)	ν_{as}(OCO)	980 (1026)	ν(C-O)[1]

Vibrational frequencies in brackets have been adapted from (Yee *et al.*, 1999; and Yee and Idriss, 2000)

[1] (Busca et al., 1987)

Peaks at 1760 and 980 cm^{-1}, which also increase notable with increasing temperature are thought to belong to the acetate species (ν_{as}(OCO) and ν(C-O), respectively). The carbonate and acetate species increase progressively with increasing temperature, while other products increase initially and as the temperature is increased they start to decrease. At high temperature of 350°C only the carbonates and acetate peaks are observed.

To confirm the assignment of products (acetaldehyde, acetates and carbonates) species, acetaldehyde was adsorbed over $V_{0.7}Fe_{0.3}SbO_4$ at 25°C, and the temperature was progressively increased (Figure3-33).

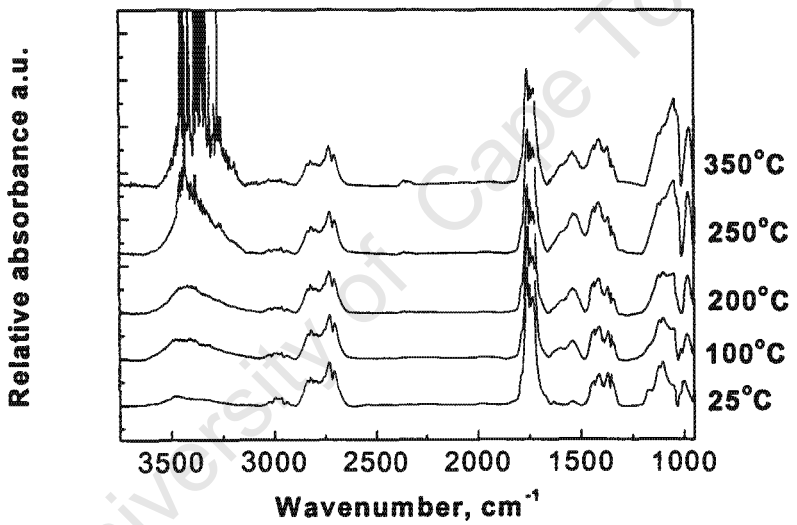

Figure3-33: FT-IR spectra of $V_{0.7}Fe_{0.3}SbO_4$ after pretreatment at 250°C and adsorption of acetaldehyde at 25°C and progressively increasing temperature

Primarily, the η-acetaldehyde peak at 1750 cm^{-1} was more prominent, hence the acetaldehyde species assignment from the ethanol adsorption was confirmed. The carbonate couple that was not clear in the ethanol adsorption study at (1560/1370cm^{-1}) came out clearer with increasing temperature upon acetaldehyde adsorption (Figure3-33). In addition acetate peaks at 1553 (ν_{as}(OCO), 1430 (ν_s(OCO) and 980 ρ(OCO) cm^{-1} were observed. A peak at 1184 cm^{-1} decreasing sharply with increasing

temperature between 25°C and 50°C is also associated with acetaldehyde vibrations. $\delta_s(CH_3, CH_2)$ are observed at 1374 cm^{-1}. Monodentate ν(C-O) and bidentate ν(C-O) vibrations are observed at 1108 and 1060 cm^{-1}, respectively. Additional peaks (1141, 1097 cm^{-1}) are observed at high temperatures (250°C), these can be associated with total oxidation products.

Overall, the following intermediates were observed from the adsorption of ethanol and acetaldehyde over $V_xFe_{1-x}SbO_4$ catalysts.

Table 3-12: Vibrational frequencies and mode assignments obtained from the adsorption of acetaldehyde over $V_{0.7}Fe_{0.3}SbO_4$ catalyst, $T_{pretreatment}$ = 180°C, $T_{adsorption}$ = 25°C, and temperature increased sequentially

Vibrational wavelength (cm^{-1})	Assignment	Vibrational wavelength (cm^{-1})	Assignment
1814	Bridged (C-O)	1450 (1474)	$\delta_{as}(CH_3, CH_2)$
1731-1758 (7000)	η-acetaldehyde	1537	ν_s(OCO)
1717 (1711)	ν(C=O)	1420 (1420-1429)	ν_s(OCO)
1698	ν(C=O)	1370 (1383)	$\delta_s(CH_3, CH_2)$
1684	ν(C=O)	1340 (1341)	ν_{as}(OCO)
1676	ν(C=O)	1184	ν_s(OCO)
1665 (1661)	ν(C=O)	1154	ν_s(OCO)
(1154)	ν(C=C)	1134	ν_s(OCO)
1633 (1637)	ν(C=C)	1127 (1125)	Monodentate ν(C-O)
1618	ν_{as}(OCO)	1094 (1080)	ν(C-O)
1575-1586 (1578)	ν_{as}(OCO)	1061	ν(C-O)
		1044-1053 (1057)	Bidentate ν(C-O)

Fixed bed experiments in section 3.3.3, indicated that there is a marked difference in the reactivity of high acidity versus low acidity $V_xFe_{1-x}SbO_4$ catalysts. Carboxylic acetates formation was only observed over the catalysts that possessed high acidity. Hence it was decided to investigate the effect of the pre-treatment temperature of the catalyst

with the object of altering surface species (acid sites). It was expected that the acetate intermediate leading to the formation of acetic acid would be affected by the pre-treatment temperature as acidity decreases vastly between 180 and 250°C, and acetic acid formation beginning at about 220°C, this temperature corresponds to the complete desorption of pyridine in the IR study of the vanadium-rich catalysts which show high selectivity to acetic acid.

Figure3-34 shows the intermediates formed when acetaldehyde was adsorbed over $V_{0.7}Fe_{0.3}SbO_4$ after pre-treatment at 180°C instead of 250°C (Figure3-33). Except for the lower concentration of the adsorbed species due to the experimental conditions, there is basically no observable change in infrared bands.

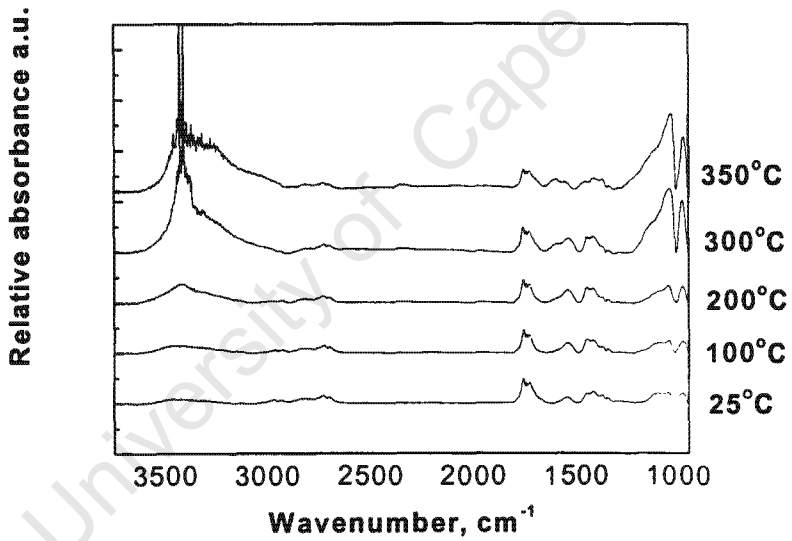

Figure3-34: FT-IR spectra of $V_{0.7}Fe_{0.3}SbO_4$ after pretreatment at 180°C and adsorption of acetaldehyde at 25°C and progressively increasing temperature

Therefore, it can be postulated that the pretreatment temperature does not seem to affect the nature of the species forming on the surface of $V_xFe_{1-x}SbO_4$ catalysts upon the adsorbtion of acetaldehyde.

3.3 CHARACTERISATION OF METAL OXIDES USING THE PARTIAL OXIDATION OF ETHANOL IN A FIXED BED REACTOR

Partial oxidation of ethanol was performed over three different catalyst systems with progressively increasing number of metal ions to demonstrate the advantage of complex catalysts, 1) single metal oxides (V_2O_5, Fe_2O_4 and Sb_2O_3), 2) binary metal oxides ($VSbO_4$ / $FeSbO_4$), and 3) complex ternary metal oxides ($V_xFe_{1-x}SbO_4$ where $0 < x < 1$).

3.3.1 Partial oxidation of ethanol over single metal oxides (V_2O_5, Fe_2O_3 and Sb_2O_3)

To establish some basic understanding of the oxidation of alcohols over metal oxide catalysts, the study of ethanol oxidation over single metal oxides was undertaken. The basis for studying a wide range of simple metal oxides was to establish trends for activity in ethanol oxidation and selectivity towards corresponding partial oxidation products. In this section, only the study of the oxidation of ethanol over V_2O_5, Fe_2O_4 and Sb_2O_3 metal oxides are presented. Studying ethanol oxidation over single metal oxides should bring about fundamental understanding of the mechanisms and reaction pathways involved in the oxidation of primary alcohols over metal oxides. Furthermore, such a study should serve as a basis for corroborating isolated studies on the oxidation of ethanol over simple versus complex metal oxides. Figure 3-35 shows the conversion of ethanol over V_2O_5, Fe_2O_4 and Sb_2O_3 metal oxides.

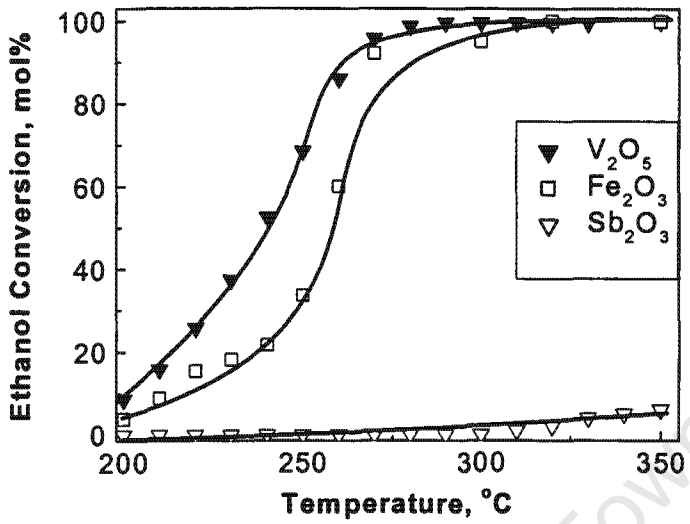

Figure 3-35: Conversion of ethanol over different single metal oxides (V_2O_5, Fe_2O_3 and Sb_2O_4) as a function of reaction temperature. $T_{reaction}$ = 200-350°C, WHSV = 2.44 $g_{ethanol}$ /($g_{catalyst}$ h); $P_{ethanol}$ = 0.27 bar, P_{O2} = 0.3 bar, balanced by N_2 to a total pressure of 2 bar

V_2O_5 exhibits a high activity compared to other metal oxides under the stipulated reaction conditions, while Sb_2O_4 appear to be rather unreactive in the oxidation of ethanol under the stipulated set of reaction conditions. The observed trend in catalytic activity upon the oxidation of ethanol over simple metal oxides at 300°C is as follows: V_2O_5 > Fe_2O_3 >> Sb_2O_4.

Some single metal oxides show a break point, where the conversion suddenly increases sharply. This effect is observed upon the oxidation of ethanol over Fe_2O_3, (CuO, and MoO_3 in Appendix VI). These metal oxides exhibit low activity at moderate temperatures and the activity suddenly increases sharply at a particular characteristic temperature. For reproducibility the temperature was increased and decreased, and in both sequences the observed jump is at about the same temperature for a particular metal oxide. For Fe_2O_3 the break point occurs at ca. 250°C.

Table 3-13 presents the kinetic parameters obtained from the oxidation of ethanol over single metal oxides, given that the reaction can be modelled as a first order reaction.

Table 3-13: Apparent activation energies Ea and pre-exponential factors obtained from the oxidation of ethanol over single metal oxides

Metal Oxide	BET-Surface area m^2/g	Activation energy, Ea (kJ mol^{-1})	Pre-exponential factor, A (mmol g^{-1} sec^{-1})
V_2O_5	1.2661	117	$7 \times 10^{+11}$
Fe_2O_3		117	$1 \times 10^{+18}$
Sb_2O_3	2.	-	-

It has been reported that the main reaction product from the oxidation of ethanol over metal oxides is acetaldehyde (Marek and Hahn, 1930). Minor products that have been observed include diethyl ether, ethyl acetate, acetic acid, acetone and carbon oxides. Yee *et al.* (1999) reported the formation of crotonaldehyde and benzene in addition to the above products as by-products of the oxidation of ethanol over $CeO_2$and $Pd/PtCeO_2$. Figure 3-42 presents products selectivity over single metal oxides (V_2O_5 and Fe_2O_3).

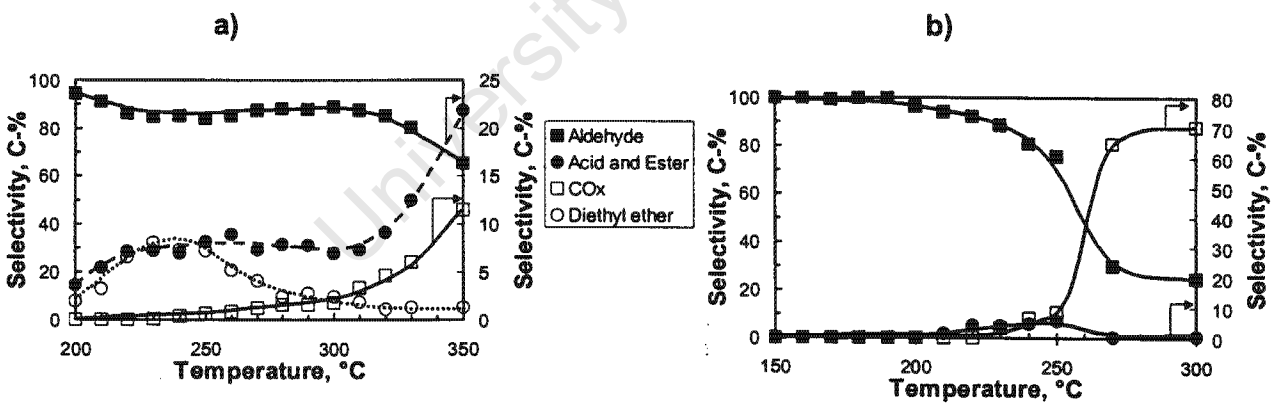

Figure 3-36: Selectivity patterns obtained from ethanol oxidation over single metal oxides a) V_2O_5 and b) Fe_2O_3. $T_{reaction}$ = 200-350°C over V_2O_5 and 150-300°C over Fe_2O_3, WHSV = 2.44 $g_{ethanol}/(g_{catalyst}\ h)$; $P_{ethanol}$ = 0.27 bar, P_{O2} = 0.3 bar, balanced by N_2 to a total pressure of 2 bar

From both experiments, a typical consecutive parallel reaction pathway is observed. Acetaldehyde selectivity is high at low temperature and decreases steadily with increasing temperature. Over V_2O_5 illustrated in Figure 3-36a, the main competing reaction pathway at low reaction temperatures is that leading to the formation of diethyl ether. Selectivity to diethyl ether increases with increasing temperature and reaches a maximum at about 220°C, and then decreases and remains below 2% with further increase in temperature. Vanadia is more acidic than iron oxide (Golodets, 1983), both diethyl ether and ethyl acetate are acid catalysed reactions.

At these low temperatures, ethyl acetate selectivity also increases in the same manner as diethyl ether reaching the maximum at 230°C then decreases. At the temperature range where both diethyl ether and ethyl acetate selectivity is high, acetaldehyde selectivity forms a local minimum and then somewhat increases as the two products selectivity decrease simultaneously (i.e. competing diethyl ether pathway becomes unfavourable with increasing temperature). The decrease in the selectivity of diethyl ether and ethyl acetate is to be expected with increasing temperature, since the formation of diethyl ether requires two neighbouring sites to exist. Typically, adsorption decreases with increasing temperature; therefore, the likelihood for bimolecular reactions decreases with increasing temperature.

Notable though is that as the diethyl ether and ethyl acetate selectivity starts to decrease, the selectivity to acetic acid and carbon oxides starts to increase. This is indicative of both parallel and consecutive mechanism playing a role at this stage of the reaction. Over V_2O_5, the selectivity to acetic acid reaches a maximum at about 340°C then starts to decrease, giving way to complete oxidation products (carbon oxides and water) whose selectivity increases progressively.

Selectivity pattern over Fe_2O_3 metal oxide as illustrated in Figure 3-36b shows a break effect (i.e. sharp decrease in acetaldehyde selectivity a certain temperature (250-270°C)). The break is associated with a sudden increase in ethanol conversion, and always results in a sudden increase in the selectivity to carbon oxides and decrease in acetaldehyde selectivity. Small amounts of acids and esters were observed, and negligible amounts of diethyl ether were also observed.

Over Sb_2O_3, the only product observed throughout the temperature range was acetaldehyde. This is expected since the maximum ethanol conversion achievable over Sb_2O_3 under set reaction conditions was 6%.

3.3.2 *Partial oxidation of ethanol over binary metal oxides ($VSbO_4$ and $FeSbO_4$)*

Vanadium antimonates and iron antimonates are proven catalysts for the ammoxidation of propane (Centi *et al.*, 1992). However, there has not been a reported study on the use of these catalyst systems in the oxidation of ethanol to partial oxidation products such as acetaldehyde, acetic acid and ethyl acetate. The two binary oxides $FeSbO_4$ and $VSbO_4$ were investigated for reactivity in the partial oxidation of ethanol. In comparison to trends established upon the oxidation of ethanol over single metal oxides from which these binary oxides are derived.

The impact of an exercise of this nature is in establishing benefits of complex metal oxides over simple metal oxides. For example, as shown in section 3.3.1 above, Fe_2O_3 is very active but rather unselective towards partial oxidation products at temperature above 250°C. While, Sb_2O_3 is almost inactive and very selective towards partial oxidation products (acetaldehyde). Therefore it is expected that $FeSbO_4$ should incorporate both metal oxides characteristics, resulting in a catalysts that more active than Sb_2O_3 yet more selective to partial oxidation products than Fe_2O_3. Figure 3-37 shows the conversion of ethanol as a function of temperature over $FeSbO_4$ and $VSbO_4$. Single metal oxides (unbulleted lines) are shown on the same graph for direct comparison. It can be observed that $VSbO_4$ is more active as a catalyst for the oxidation of ethanol than $FeSbO_4$. Centi *et al.* (1992) have reported the similar difference in the reactivity of these tetragonal rutile-structured compounds upon the ammoxidation of propylene.

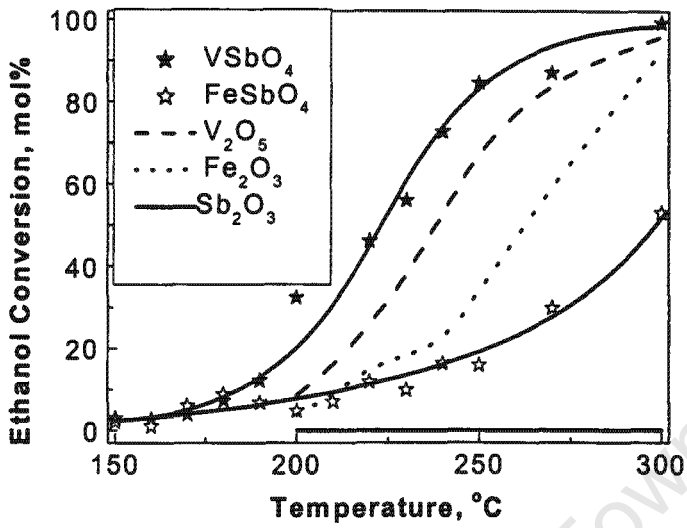

Figure 3-37: Conversion of ethanol as a function of temperature over binary oxides $VSbO_4$ and $FeSbO_4$ catalysts in comparison to single metal oxides (unbulleted lines). $T_{reaction}$ = 150-300°C, WHSV = 2.44 $g_{ethanol}$ /($g_{catalyst}$ h); $P_{ethanol}$ = 0.27 bar, P_{O2} = 0.3 bar, balanced by N_2 to a total pressure of 2 bar

In comparison to single metal, it can be observed that $VSbO_4$ is more reactive than both of the compositional single metal oxides (V_2O_5 and Sb_2O_3). The observed activity is indicative of activity enhancement over $VSbO_4$, which clearly does not correspond to the mean of the activity of the two individual compositional metal oxides (V_2O_5 and Sb_2O_3). While, $FeSbO_4$ catalyst shows activity that is lower than that of Fe_2O_3 but higher than that of Sb_2O_3, i.e. activity lying in-between the compositional metal oxides.

Selectivity to different products upon the oxidation of ethanol over binary oxides ($VSbO_4$ and $FeSbO_4$) is shown in Figure 3-38.

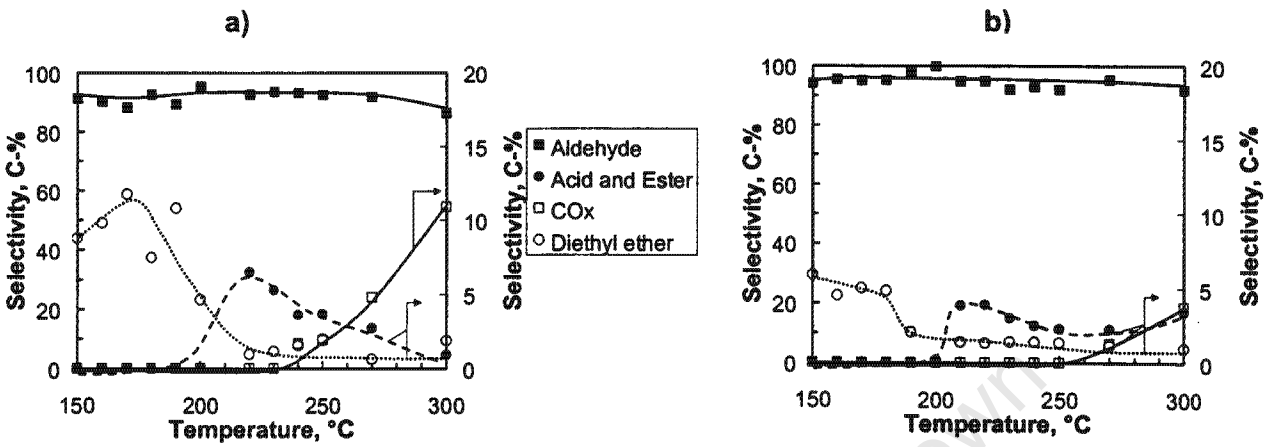

Figure 3-38: Selectivity patterns obtained from ethanol oxidation over binary metal oxides a) $VSbO_4$ and b) $FeSbO_4$ $T_{reaction}$ = 150-300°C, WHSV = 2.44 $g_{ethanol}/(g_{catalyst}\ h)$; $P_{ethanol}$ = 0.27 bar, P_{O2} = 0.3 bar, balanced by N_2 to a total pressure of 2 bar

It can be observed that similar products are formed in both metal oxides, albeit in different quantities. Over $VSbO_4$ (Figure 3-38a), about 93% selectivity to acetaldehyde is observed between 150 and 250°C, after which the selectivity drops to about 85%. The competing reaction at low temperatures is that leading to the formation of diethyl ether. The selectivity to diethyl ether increases between 150 and 170°C and then decreases. From 200°C, selectivity to carboxylic acetates (ethyl acetate and acetic acid) starts to form increasing and forming a maxima of about 8% at 220°C and then decreases. As the selectivity to carboxylic acetates starts to decrease, the selectivity to carbon oxides progressively increases with increasing temperature, reaching 11% at 300°C.

Over $FeSbO_4$ (Figure 3-38b), the selectivity to acetaldehyde is higher (95%) and it does not decrease significantly the temperature range (150 and 300°C). Compared to $VSbO_4$, lower selectivity to all minor products was observed, i.e. diethyl ether, carboxylic acetates and carbon oxides (maxima observed 5, 4 and 4%, respectively).

Comparing the two binary oxides, similar product spectra are observed in the oxidation of ethanol over $VSbO_4$ and $FeSbO_4$. However, it can be seen that consecutive reactions products (i.e. carboxylic acetates and carbon oxides) as well as parallel reactions products (diethyl ether) are more evident in the oxidation of ethanol over $VSbO_4$ compared to $FeSbO_4$.

Comparing the selectivity trends observed over binary metal oxides to trends observed over single metal oxides, generally a higher stability of the primary product (acetaldehyde) throughout the temperature range is observed. Implying that there is an overall selectivity advantage for partial oxidation products over binary oxides compared to single metal oxides. About the same amount of carbon oxides (11%) are formed at 80% ethanol conversion over V_2O_5 and $VSbO_4$. However, a remarkably difference is observed in the selectivity upon the oxidation of ethanol over Fe_2O_3 and $FeSbO_4$. 40% selectivity to carbon oxides at a 50% ethanol conversion over Fe_2O_3 compared to (<5%) selectivity to carbon oxides observed over the binary metal oxide $FeSbO_4$ at the same ethanol conversion level. Clearly demonstrating the feats of multi-component catalysts in comparison to simple metal oxides.

3.3.3 Partial oxidation of ethanol over ternary metal oxides $V_xFe_{1-x}SbO_4$, $0 < x < 1$

There are a number of remarkable aspects about these catalytic systems that render this study a profoundly wealthy exercise. Both $FeSbO_4$ and $VSbO_4$ crystallise in the same structure, tetragonal rutile structure (Shannon and Prewitt, 1969). Hence, sequential substitution of vanadium by iron in $VSbO_4$ (or iron by vanadium in $FeSbO_4$) should lead to a continuous solid solution from $VSbO_4$ through to $FeSbO_4$.

Furthermore, $VSbO_4$ when prepared under air possesses a defective structure with the composition of $V^{4+}_{0.64}V^{3+}_{0.28}Sb^{5+}_{0.92}\square_{0.16}O_4$. The structure arises from the fact that $VSbO_4$ contains both V^{3+} and V^{4+}, and the presence of V^{4+} is balanced by the formation of vacancies (Landa-Canovas *et al.*, 1995). It is therefore hypothesised that the sequential substitution of vanadium by iron should have a direct effect on the V^{3+}/ V^{4+} ratio. In this section, evaluation of $V_xFe_{1-x}SbO_4$ catalysts based on ethanol partial oxidation is presented in comparison to parent binary oxides ($FeSbO_4$ and $VSbO_4$).

Figure 3-39 presents ethanol conversion as a function of temperature over $V_xFe_{1-x}SbO_4$ catalysts. There are two distinct groupings that can be observed from the graph, iron rich catalyst (hollow symbols) and vanadium rich catalyst (full symbols). Also included in the graph for comparison are the two binary oxides $FeSbO_4$ and $VSbO_4$, from which these ternary oxides are derived. In line with the objective to track changes in activity and selectivity as the V/(V+Fe) changes, it was imperative to present the activity over the $V_xFe_{1-x}SbO_4$ catalysts series in one graph and selectivity over this range in a separate graph. The selectivity to observed products has been presented in such a way as to differentiate between oxidation products and non-oxidation product (diethyl ether). This is important in following consecutive reaction from the primary oxidation product (acetaldehyde), and thus the reaction pathway.

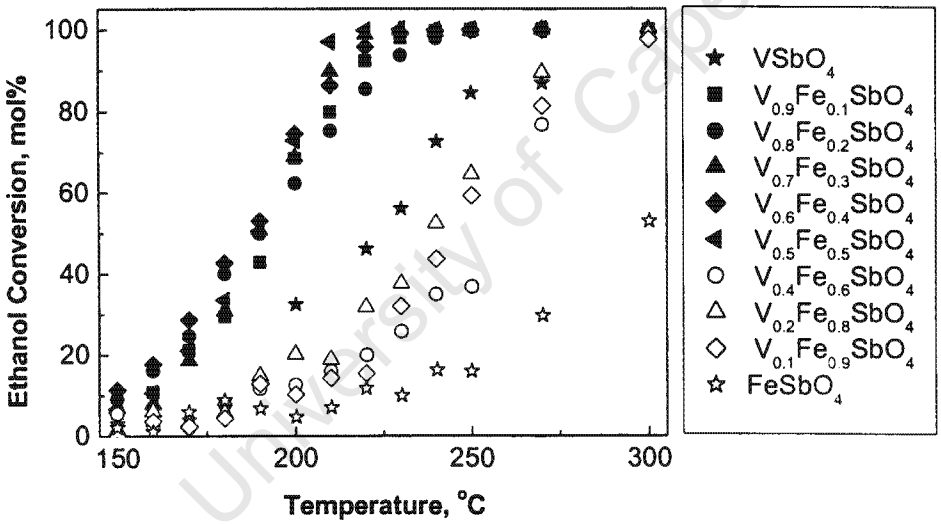

Figure 3-39: Conversion of ethanol as a function of temperature over $V_xFe_{1-x}SbO_4$ catalysts series, where $0 < x < 1$. $T_{reaction}$ = 150-300°C, WHSV = 2.44 $g_{ethanol}/(g_{catalyst}\ h)$; $P_{ethanol}$ = 0.27 bar, P_{O2} = 0.3 bar, balanced by N_2 to a total pressure of 2bar

It can clearly be observed that vanadium rich ternary $V_xFe_{1-x}SbO_4$ catalysts exhibit higher activity than the corresponding binary oxides $VSbO_4$ and $FeSbO_4$. Yet, ternary oxides richer in iron show an activity between that of the binary oxides.

Kinetic parameters were calculated using acetaldehyde formation as the measure of the conversion, since acetaldehyde is a major product at low ethanol conversion. Table 3-14 presents the kinetic parameters obtained upon the oxidation of ethanol over $V_xFe_{1-x}SbO_4$ catalysts.

Table 3-14: Apparent activation energy and pre-exponential factor obtained from the oxidation of ethanol over $V_xFe_{1-x}SbO_4$ catalysts $0 < x < 1$

Metal Oxide	Activation energy, Ea (kJ mol^{-1})	Pre-exponential factor, A (mmol g^{-1} sec^{-1})
$VSbO_4$	84	$9 \times 10^{+5}$
$V_{0.9}Fe_{0.1}SbO_4$	80	$4 \times 10^{+5}$
$V_{0.8}Fe_{0.2}SbO_4$	86	$2 \times 10^{+6}$
$V_{0.7}Fe_{0.3}SbO_4$	87	$2 \times 10^{+6}$
$V_{0.7}Fe_{0.3}SbO_4$ (W)	86	$2 \times 10^{+6}$
$V_{0.6}Fe_{0.4}SbO_4$	80	$3 \times 10^{+5}$
$V_{0.5}Fe_{0.5}SbO_4$	89	$1 \times 10^{+7}$
$V_{0.4}Fe_{0.6}SbO_4$	64	$5 \times 10^{+3}$
$V_{0.2}Fe_{0.8}SbO_4$	75	$5 \times 10^{+4}$
$V_{0.1}Fe_{0.9}SbO_4$	77	$3 \times 10^{+4}$
$FeSbO_4$	60	$8 \times 10^{+1}$

The activation energy is presented as a function of vanadium content in Figure 3-40. The activation energy for the formation of acetaldehyde tends to increase with the increasing vanadium content. This is indicative of development of sites that are more active on the catalyst surface as vanadium is sequentially added to $FeSbO_4$ catalyst.

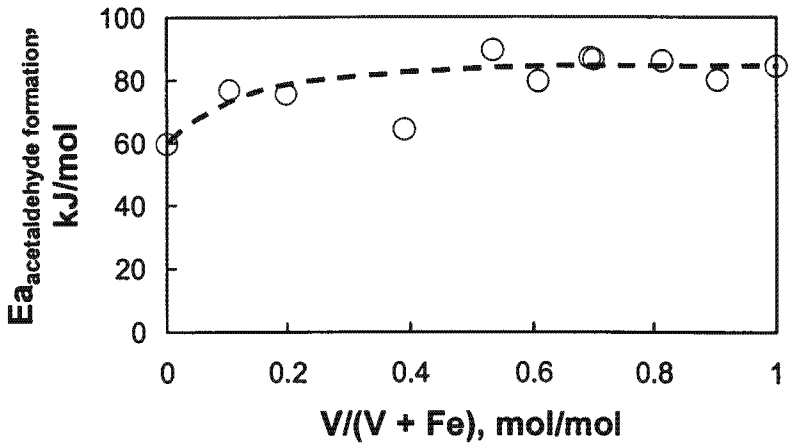

Figure 3-40: Activation energy for the oxidation of ethanol as a function of vanadium content over $V_xFe_{1-x}SbO_4$ catalyst range, where $0 < x < 1$. $T_{reaction}$ = 150-300°C, WHSV = 2.44 $g_{ethanol}/(g_{catalyst}\ h)$; $P_{ethanol}$ = 0.27 bar, P_{O2} = 0.3 bar, balanced by N_2 to a total pressure of 2 bar

The pre-exponential factor also increases with the increasing vanadium content (see Figure 3-41). This observation does not correspond to the measured BET-surface area; this could be due to differences in active site concentration per unit surface area.

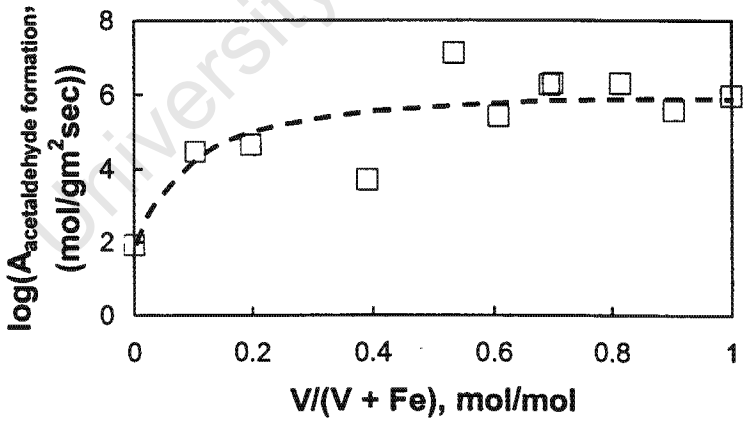

Figure 3-41: Pre-exponential factor energy for the oxidation of ethanol as a function of vanadium content over $V_xFe_{1-x}SbO_4$ catalyst range, where $0 < x < 1$. $T_{reaction}$ = 150-300°C, WHSV = 2.44 $g_{ethanol}/(g_{catalyst}\ h)$; $P_{ethanol}$ = 0.27 bar, P_{O2} = 0.3 bar, balanced by N_2 to a total pressure of 2 bar

Typical product selectivity pattern over vanadium-rich in comparison to iron-rich catalysts is shown Figure 3-42. Diethyl ether selectivity seems to form a maximum at low temperature (200°C) over vanadium-rich catalysts (Figure 3-42a). There is a lot of scattering observed over iron-rich catalyst, however, there is a non-zero selectivity observed at about (200°C). Within the oxidation products fraction, acetaldehyde selectivity generally decreases with increases temperature (Figure 3-42). The difference between the vanadium-rich and iron-rich catalysts is demonstrated above 250°C in the selectivity of acetaldehyde. A marked decrease in the selectivity to acetaldehyde over vanadium–rich catalysts observed. This decrease is associated with rather high selectivity to acetic acid plus ethyl acetate (Figure 3-42c) and carbon oxides (Figure 3-42d) observed over vanadium-rich catalysts.

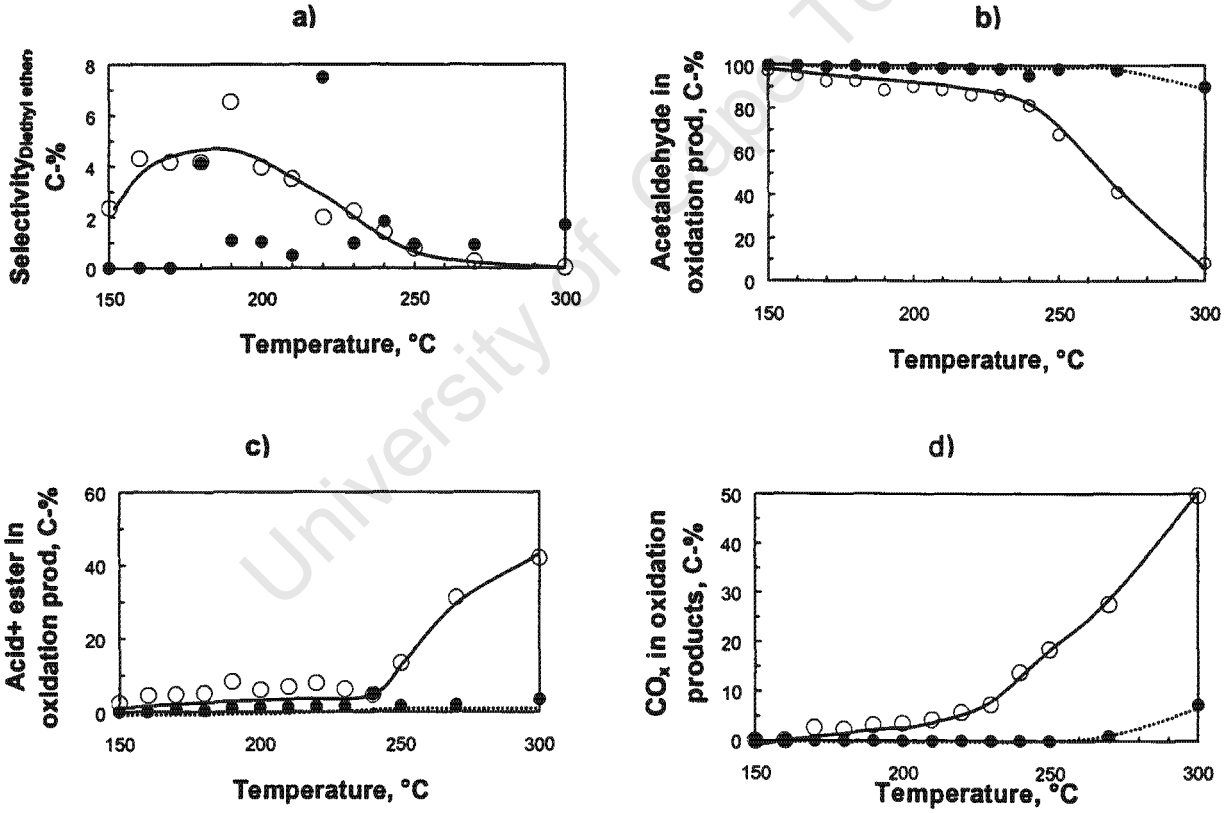

Figure 3-42: Typical product selectivity patterns over V-rich ($V_{0.7}Fe_{0.3}SbO_4$) catalysts (hollow circles) in comparison to Fe-rich ($V_{0.4}Fe_{0.6}SbO_4$) catalyst (full circles). $T_{reaction}$ = 150-300°C, WHSV = 2.44 $g_{ethanol}/(g_{catalyst}\ h)$; $P_{ethanol}$ = 0.27 bar, P_{O2} = 0.3 bar, balanced by N_2 to a total pressure of 2 bar

Evident from the patterns in the graphs above is a typical series-parallel reaction pathway. The primary product is acetaldehyde, diethyl ether is formed by a competing parallel reaction, Acetic acid and ethyl acetate are formed from acetaldehyde, and all intermediates are susceptible to further oxidation to carbon oxides.

3.3.4 *Effect of substituting iron with other tri-valent cations (Ga^{3+} and Al^{3+})*

A study was undertaken to establish the role of Fe^{3+} in the catalytic oxidation of ethanol over $V_{0.7}Fe_{0.3}SbO_4$ catalyst by substituting Fe^{3+} with other tri-valent cations (Al^{3+} and Ga^{3+}). Figure 3-43 presents conversion of ethanol as a function of temperature over $V_{0.7}M_{0.3}SbO_4$ catalysts (M = Fe, Al or Ga).

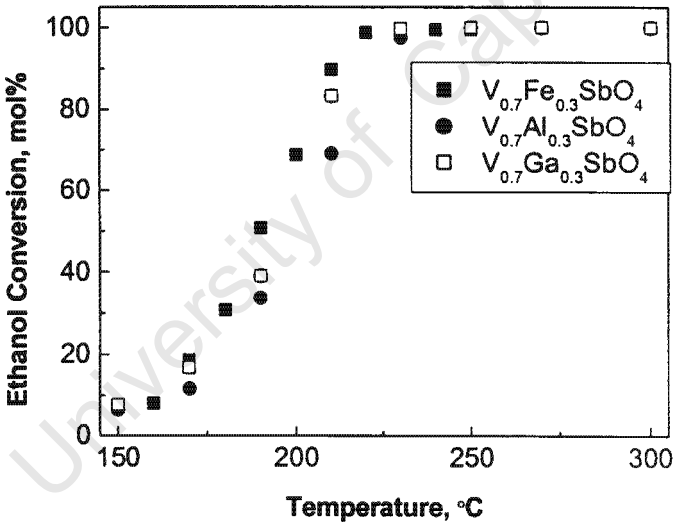

Figure 3-43: The effect of substituting Fe^{3+} with Al^{3+} and Ga^{3+} on the conversion of ethanol over $V_{0.7}M_{0.3}SbO_4$ catalysts M= Fe, Al or Ga. $T_{reaction}$ =150°C- 300°C, WHSV = 2.44 $g_{ethanol}$ /($g_{catalyst}$ h); $P_{ethanol}$ = 0.27 bar, P_{O2} = 0.3 bar, balanced by N_2 to a total pressure of 2 bar

The idea is that if the redox couple Fe^{3+}/Fe^{2+} plays a role in the catalytic oxidation of ethanol over $V_xFe_{1-x}SbO_4$ catalysts ($0 < x < 1$), then substitution by other tri-valent ions

without any redox coupling would results in drastic decrease in activity. Aluminium and gallium have been investigated as additives in the $VSbO_4$ catalyst systems (Nilsson *et al.*, 1996). It has been shown that these ions are incorporated the rutile structure of the $VSbO_4$ systems. It is illustrated in Figure 3-43 that the conversion of ethanol over $V_{0.7}M_{0.3}SbO_4$ catalysts M = Fe, Al or Ga is comparable. This indicates that the redox couple is not playing a catalytic role in the oxidation of ethanol, this corroborates well with the Mössbauer study that shows that Fe^{3+} is not reduced to Fe^{2+} during ethanol oxidation reaction.

Table 3-15 presents the kinetic parameters obtained from the oxidation of ethanol over $V_{0.7}M_{0.3}SbO_4$ catalysts M = Fe, Al or Ga. The parameters obtained confirm that there is essentially no difference in activity of these catalysts in the oxidation of ethanol.

Table 3-15: Activation energies and pre-exponential factors obtained from the oxidation of ethanol over $V_{0.7}M_{0.3}SbO_4$ catalysts M = Fe, Al or Ga

Metal Oxide	**Activation energy, Ea (kJ mol^{-1})**	**Pre-exponential factor, A (mmol g^{-1} sec^{-1})**
$V_{0.7}Fe_{0.3}SbO_4$	102	$2 \times 10^{+11}$
$V_{0.7}Al_{0.3}SbO_4$	100	$4 \times 10^{+10}$
$V_{0.7}Ga_{0.3}SbO_4$	99	$2 \times 10^{+10}$

Figure 3-44 below shows the selectivity to acetaldehyde as a function of temperature upon the oxidation of ethanol over $V_{0.7}M_{0.3}SbO_4$ catalysts M= Fe, Al or Ga.

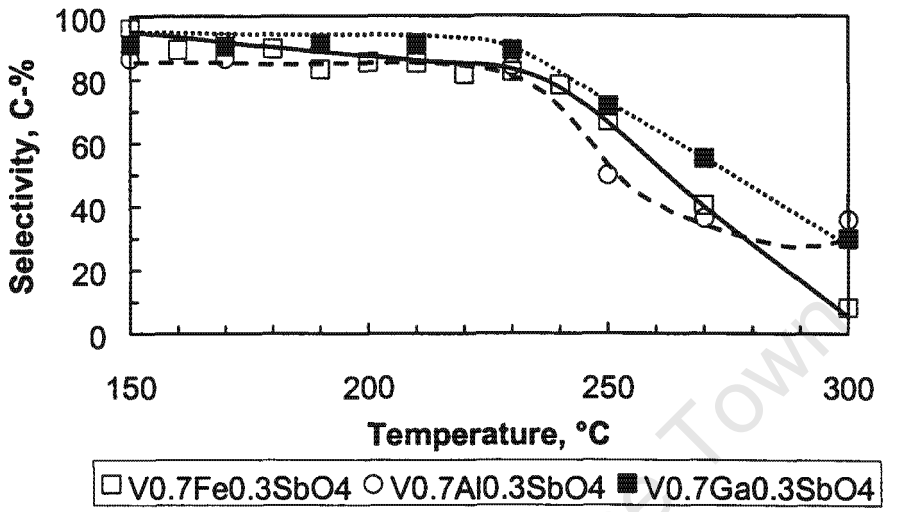

Figure 3-44: The effect of substituting Fe^{3+} with Al^{3+} and Ga^{3+} on the selectivity to acetaldehyde in oxidation of ethanol over $V_{0.7}M_{0.3}SbO_4$ catalysts M= Fe, Al or Ga. $T_{reaction}$ = 150-300°C, WHSV = 2.44 $g_{ethanol}/(g_{catalyst}\ h)$; $P_{ethanol}$ = 0.27 bar, P_{O2} = 0.3 bar, balanced by N_2 to a total pressure of 2 bar

The selectivity to carbon oxides mirrors that of acetaldehyde, and it will not be shown. Carboxylic acetates (acetic acid and ethyl acetate) selectivity also varies slightly with substitution of Fe with either Al or Ga. Overall the selectivity to different products upon the oxidation of ethanol over $V_{0.7}M_{0.3}SbO_4$ catalysts M= Fe, Al or Ga does not seem to vary with the substitution of Fe by either Al or Ga. A slight deviation at high temperatures is observed and that can be caused by the characteristics of the substituting metal ion (e.g. acidity, reducibility etc.).

3.3.5 *Effect of washing (post-catalyst preparation) treatment*

Some of the $V_xFe_{1-x}SbO_4$ catalysts were washed after preparation to test for structural changes that might transpire as a result of the washing. The structural changes are reported in the characterisation section 3.1 above. The catalysts were then tested for ethanol oxidation and compared with the corresponding unwashed catalysts. Figure 3-45 presents ethanol conversion as a function of reaction temperature for washed and unwashed catalysts.

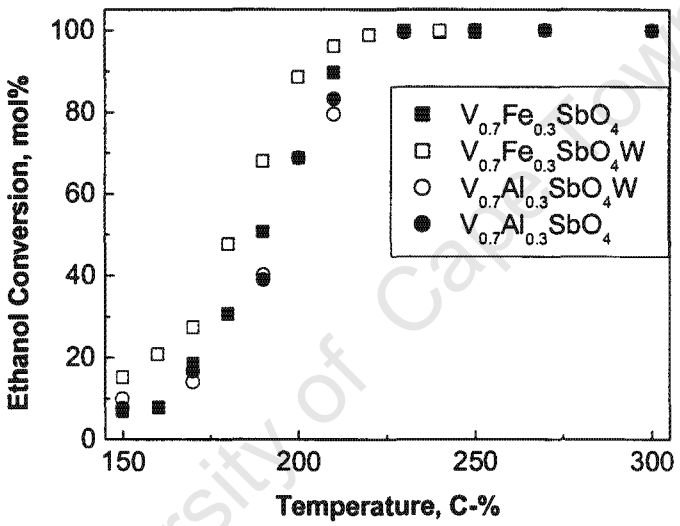

Figure 3-45: Ethanol conversion as a function of temperature over washed and unwashed $V_xFe_{1-x}SbO_4$ catalysts. $T_{reaction}$ = 150°C- 300°C, WHSV = 2.44 $g_{ethanol}/(g_{catalyst}\ h)$; $P_{ethanol}$ = 0.27 bar, P_{O2} = 0.3 bar, balanced by N_2 to a total pressure of 2 bar

Insignificant differences in the conversion of ethanol were observed. The washed $V_{0.7}Fe_{0.3}SbO_4$ catalyst shows slightly higher activity than unwashed $V_{0.7}Fe_{0.3}SbO_4$ catalyst. While there is no differences observed in the activity of washed $V_{0.7}Al_{0.3}SbO_4$ and unwashed $V_{0.7}Al_{0.3}SbO_4$ catalysts.

An interesting aspect about this study is observed in the selectivity patterns exhibited by these post-treated catalysts. While the selectivity to acetaldehyde, diethyl ether and carbon oxides scattered about, the selectivity patterns over the washed and unwashed

catalysts for carboxylic acetate followed a specific pattern. Selectivity to carboxylic acetate (acetic acid and ethyl acetate) is presented in Figure 3-46. There is a significant difference observed between washed and unwashed catalyst samples in the selectivity of acetic acid and ethyl acetate. Washed catalyst samples exhibit higher selectivity towards these products than the corresponding unwashed samples. The selectivity to carbon oxides changes in the reverse manner, with unwashed samples showing higher selectivity towards carbon oxide than washed catalysts.

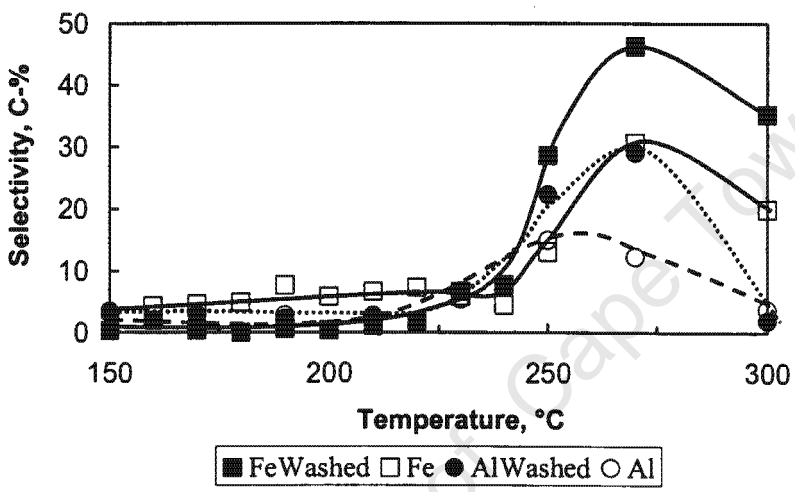

Figure 3-46: Selectivity to acetic acid and ethyl ether as a function of temperature over washed and unwashed $V_xM_{1-x}SbO_4$ catalysts M= Fe or Al. $T_{reaction}$ =150°C- 300°C, WHSV = 2.44 $g_{ethanol}/(g_{catalyst}\ h)$; $P_{ethanol}$ = 0.27 bar, P_{O2} = 0.3 bar, balanced by N_2 to a total pressure of 2 bar

It is interesting to note that only the selectivity to carboxylic acetates (acetic acid and ethyl acetate) that is enhanced by washing. This is indicative of a change in surface species (e.g. acidity) that contribute to the formation of these products during the reaction pathway.

DISCUSSION

4 DISCUSSION

In this section, the comprehensive characterisation study to establish catalyst evolution as a function of V/(V+Fe) ratio is reviewed. The partial oxidation of ethanol as a test reaction to characterise these catalysts in comparison to single metal oxides is also discussed. Furthermore, systematic correlations are demonstrated between catalytic activity in the partial oxidation of ethanol and catalyst structural evolution as a function of V/(V+Fe) ratio. A reaction pathway and mechanism for the oxidation of ethanol over $V_xFe_{1-x}SbO_4$ catalysts is proposed based on results obtained from the study of reaction parameters as well as IR and TPD intermediates identification studies

4.1 CHARACTERISATION OF $V_XFe_{1-X}SbO_4$ CATALYSTS

The surface area measurements obtained in this study are in the same range as those reported previously for $VSbO_4$ (Centi *et al.*, 1997) and $FeSbO_4$ (Bowker *et al.*, 1996). Although the two groups (iron-rich and vanadium-rich) are differentiated by the calcinations temperature, there is generally a notable decrease in surface area with increasing vanadium content.

X-ray diffraction patterns of the prepared $V_xFe_{1-x}SbO_4$ catalysts correspond well to a single well-crystallised rutile phase. The shift observed at 2θ = 35.2° and 54.4° were attributed to the decrease in the cell parameter *c* with increasing vanadium content. The substitution of Fe^{3+} by other ions such as Al^{3+} and Ga^{3+} results in small changes in *c* parameters, while parameter *a* is unaffected.

Another interesting feature in the characterisation of $V_xFe_{1-x}SbO_4$ catalysts was the observed (V+Fe)/Sb ratio as determined by XPS analysis. The results obtained clearly show that this ratio is consistently lower than that expected on the basis of the bulk composition. This surface enrichment has been attributed to the presence of antimony oxide dispersed on the surface of the rutile solid solution, in small enough quantities that it is not detectable by the X-ray diffraction (Bowker *et al.*, 1996). However, this line of reasoning has been questioned in the work of Ballarini *et al.* (2001) on the analogous

$CrSbO_4$ system with varying the Cr/Sb ratio. They found Sb enrichment even at Cr/Sb ratios > 1, for example Cr/Sb ratio = 1.2. Neither FT-IR nor Raman spectroscopy indicated the presence of dispersed antimony oxide, but XPS showed consistent enrichment with Sb.

A different phenomenon has been proposed for $FeSbO_4$ systems that rutile crystallites concentration gradients of catalyst components exist, with Sb-richer zones on the outside parts of the crystallites and consequently Fe-rich zones in the inner parts (Nilsson *et al.*, 1996). The rutile structure is known to be a highly flexible structure, characterised by open channels due to rows of vacant octahedral positions, which terminate at the surface with interstitial sites. It has been proposed that Sb^{5+} ions can be located on the compound surface in correspondence with these interstitial sites, which develop from geminate Sb=O double bonds (or in general of two contiguous Me=O double bonds). This results in Sb-O_x-rich skins in the outer zones of non-stoichiometric rutile crystallites observed previously by Sala and Trifiro (1976). In this study, further enrichment is observed when catalysts are washed before and after calcinations. Hence it can be deduced that washing further enhances these Sb-O_x-rich skins on the surface of the catalysts. Comparing the surface composition of $VSbO_4$ before and after ethanol oxidation shows that under the fairly mild ethanol oxidation conditions, the surface (V+Fe)/Sb-ratio remains almost constant.

The surface acidity of $VSbO_4$ has already been described in literature on the bases of ammonia adsorption (Centi *et al.*, 1997). In this study, the acidity of $V_xFe_{1-x}SbO_4$ catalysts was determined using pyridine as a probe molecule. Pyridine was chosen as a probe molecule instead of ammonia because it is less basic than NH_3 (pKa $\approx$5 and 9 respectively). Zanthoff *et al.* (1996) earlier reported that NH_3 reacts with the lattice oxygen of $VSbO_4$ oxides to form N_2 and NO_x at temperatures slightly higher than room temperature. Pyridine is also a hard base (Tanabe, 1970) thus it will adsorb on the same acid sites as ammonia. From the spectrum recorded at 25°C, two bands corresponding to physisorbed pyridine at 1581 and 1438 cm^{-1} decrease drastically between 25°C and 100°C. The bands at 1606, 1576, 1488 and 1447 cm^{-1} are typical of pyridine chemisorbed on Lewis sites originating from coordinative unsaturated V surface ions (Boehm and Knözinger, 1983). The presence of a peak at the frequency of 1606 cm^{-1} is a clear indication of the presence of medium to strong Lewis acid sites. The observed

broad peak at (1538 cm^{-1}) is typical of vanadium-based (V-OH) Brønsted acid sites (Centi *et al.*, 1996). Furthermore, a band at 1638 cm^{-1} results from the pyridinium cation whose presence confirms the presence of Brønsted acid site.

It is important to note that the protonation of a relatively weak base such as pyridine is an indication of the rather strong Brønsted acid sites. Moreover, the stability of the pyridinium cations even after evacuation at 200°C is a further indication that these sites are fairly strong. A higher concentration of acid sites is observed in ternary oxides than in corresponding binary oxides. Vanadium rich catalysts show a higher concentration of both Lewis and Brønsted acid sites in comparison to iron-rich catalysts.

Electrical conductivity measurements clearly show that $V_xFe_{1-x}SbO_4$ catalysts can be classified as conductors since their conductivity varies exponentially with temperature according to equation 2-3. The activation energies of conduction were found to be similar indicating that at the applied reaction temperatures the mechanisms over the investigated catalysts are similar. A notable observation with regard to electrical conductivity is that the temperature at which the electrical conduction increases rapidly corresponds well with the temperature at which the acid sites on the surface fade away.

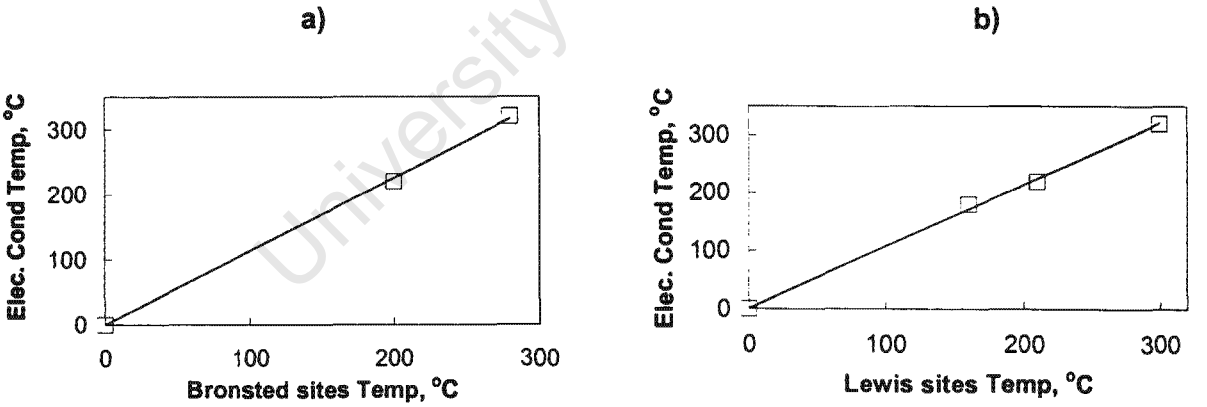

Figure 4-1: The correlation of the temperature at which a rapid increase in electrical conductivity is observed with the temperature at which a) Brønsted and b) Lewis acid sites acid site fade away,

When acid sites vanish, oxygen vacancies are formed leading to a strong increase in electrical conductivity. This is well in agreement with the fact that $V_xFe_{1-x}SbO_4$ compounds are *n*-type semi-conductors. (It must be mentioned that only 4 of the 9

$V_xFe_{1-x}SbO_4$ catalysts prepared were characterised for electrical conductivity as part of the collaboration with the CNRS in France. Hence, the fewer points on the graphs below.)

TPR measurements show that the reducibility of ternary $V_xFe_{1-x}SbO_4$ oxides is remarkably different from that of binary oxides ($VSbO_4$ and $FeSbO_4$) as shown in Figure 3-16. The high H_2 consumption in ternary oxide ($V_{0.7}Fe_{0.3}SbO_4$) indicates a high electron accepting character of the ternary oxides in comparison to binary oxides ($VSbO_4$ and $FeSbO_4$).

The Mössbauer parameters obtained indicate that iron is present as Fe^{3+} in both fresh and used catalysts (Figure 3-6 and Figure 3-7). Therefore, it can be concluded that the Fe^{3+} / Fe^{2+} should not be involved in the redox mechanism of catalytic oxidation of ethanol. These findings corroborates well with the substitution of Fe^{3+} by Ga^{3+} or Al^{3+}, which showed no effect in the activity of these catalysts in the oxidation of ethanol.

Also important was the determination of the actual formulae of the catalysts using chemical analysis and XANES spectroscopy assuming the presence of the rutile structure consisting of four oxygen atoms per formula (as shown in

Table 3-6, Roussel *et al.* (2002)). Using the results from these techniques, the cation-deficient composition of $VSbO_4$ earlier characterised by Landa-Canovas *et al.*, (1995) was confirmed. It is well accepted that for V/Sb ratio = 1, V-species exists in different valence states in this non-stoichiometric rutile structure. However, the nature of the V-species in catalyst systems with V/Sb ratios less than 1 has been in the centre of literature debates.

Nilsson *et al.*, (1994) observed a decrease in the binding energy of V $2p_{3/2}$ with decreasing V/Sb ratio indicating a progressive increase in the relative amount of V ions of lower valence state. This implies that as the V is substituted, V4+ ions are affected in the V^{3+}/V^{4} couple. This study substantiates Nilsson *et al.*, (1994) argument and shows systematically that on Fe/V/Sb catalyst system, iron substitution by vanadium up to V/(V+Fe) = 0.5, V^{4+} ions are affected. The V^{3+} ions are not affected in this range. It is this variation of the V^{4+} that results in the variation of cationic vacancies in the structure. Recently, an interesting discussion was generated regarding the V^{3+}/V^{4+} ratio variation with increasing V/(V+Fe) as reported in Roussel *et al.* (2002). Ballarini *et al.* (2001) studied an analogous Cr/V/Sb catalyst system and concluded that it is V^{3+} of the V^{3+}/V^{4+} couple that is affected primarily.

Further studies using ESR were conducted related to this study and confirmed the decrease of the V^{4+} content when iron substitutes vanadium in the $V_xFe_{1-x}SbO_4$ catalysts (Nguyen *et al.*, in preparation). With the ESR study a differentiation is made between isolated and coupled V^{4+} ions and confirmed the decrease of the total V^{4+} content when iron substitutes vanadium in the $V_xFe_{1-x}SbO_4$ catalysts.

4.2 ELUCIDATION OF THE REACTION PATHWAY

A reaction pathway for selective oxidation of ethanol over $V_{0.7}Fe_{0.3}SbO_4$ catalyst was proposed base on the results obtained from the influence of reaction parameters such as space-time, ethanol to oxygen ratio, inlet water partial pressure and reaction temperature on the oxidation reaction. To supplement that data, intermediates formed on the catalyst surface were investigated using IR, TAP, and TPD.

The effect of space-time on the oxidation of ethanol (Figure 3-17) showed that ethanol conversion increases with increasing space-time; diethyl ether selectivity goes through a maximum at low space-times and is affected by ethanol conversion. Generally, as the ethanol conversion increases the diethyl ether selectivity decreases. Forzatti *et al.* (1987) proposed for methanol oxidation over metal oxides, that the formation of the ether species require the presence of an alkoxy species in close proximity with an alcoholate (adsorbed alcohol species). Thus, with increasing alcohol conversion, there would be less alcoholate species to react with alkoxy species; the proximity of the species would also be affected by the presence of surface OH, acetaldehyde and other species. Because the formation of diethyl ether is a reversible reaction, the decrease in the quantity of alcoholate species drives the reaction to the direction of the reactants, resulting in the continuous decrease in the selectivity to diethyl ether observed. The consumption of the alcoholate and ethoxy species by consecutive oxidation reactions is a major contribution to the decrease in the selectivity of diethyl ether with increasing space-time. Diethyl ether is not an oxidation product; Diethyl ether is suggested to form via the following sequence of reactions on the metal oxide surface:

2 [$M_1^{(n+)}$-O and $M_2^{(m+)}$] + 2 CH_3CH_2OH

↓

2 [$M_1^{(n+1)}$-OH and $M_2^{(m-1)}$-OCH_2CH_3]

Ethanol is a weak acid and loses the hydrogen as H^+. The condensation of the two neighbouring $M_2^{(m-1)}$-OCH_2CH_3 species results in the formation of diethyl ether and water.

↓

$CH_3CH_2OCH_2CH_3$

Acetaldehyde content in the oxidation products decreased with increasing space-time, while the content of acetate species (acetic acid + ethyl acetate) and carbon oxides increased (Figure 3-18). It is evident that the acetate species and carbon oxides are formed from acetaldehyde. There is however a difference in the shape of the curves for acetate species and that for carbon oxides. The rapid increase in carbon oxides content in comparison to a rather flat increase in the content of acetate species as the space-time increases is intriguing. The formation of the carbon oxides from all oxidation intermediates is the reason for the sudden rise of the carbon oxides content. There is also an inhibition effect observed on the carbon oxides content due to oxygen being a limiting reagent. The content of acetic acid in the acetates species fraction seems to indicate that acetic acid and ethyl acetate are formed in parallel. The increase in the acetic acid content at high space-time is merely due to the decrease of alcoholates on the catalysts surface as a result of high conversion. Similar findings and conclusions were drawn by Forzatti *et al.* (1987) and Busca *et al.* (1987) in the study of the effect of space-time on the oxidation of methanol over V/Ti oxide system. Hence, the proposed formation of acetaldehyde, ethyl acetate, acetic acid as shown in Figure 4-2.

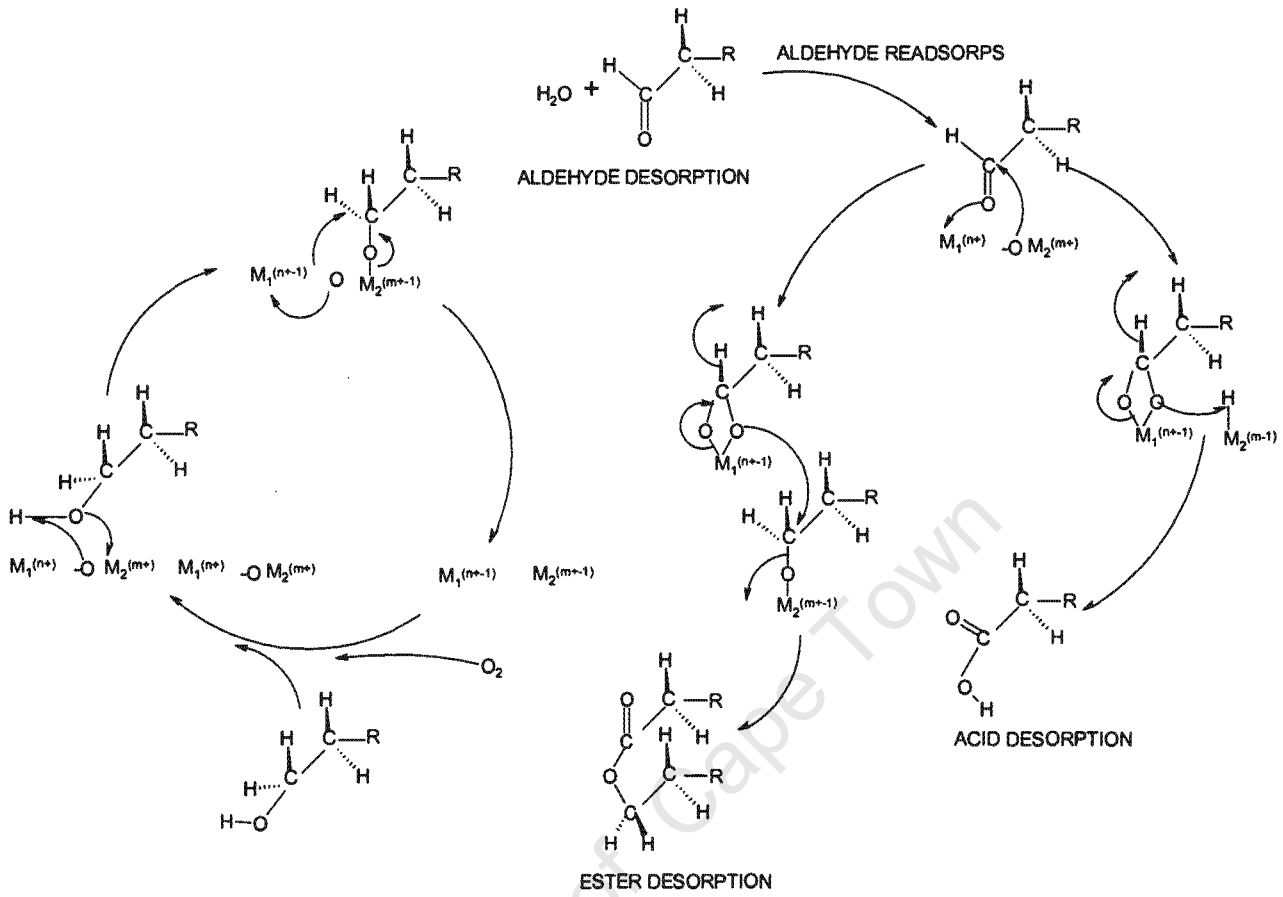

Figure 4-2: Proposed reaction mechanism leading to major oxidative dehydrogenation products in the oxidation of ethanol over metal oxides.

The positive effects of co-feeding water in partial oxidation reactions have been demonstrated by many researchers in the oxidation catalysis field (Saleh-Alhamed *et al.*, 1995; Medeiros *et al.*, 2000). Different (sometimes opposing) accounts for the observed effect have been proposed. Given the range of different reaction conditions applied in oxidation catalysis and the diversity of products that are possible from one oxidation reaction it is not surprising that often, different conclusions are reached. In this study the oxidation of ethanol over $V_{0.7}Fe_{0.3}SbO_4$ catalysts was performed at different space-times. This enabled the investigation of the effect of water partial pressure on the oxidation of ethanol to cover a range of reaction conditions and products formation domains, focusing on each domain and identifying the effect of water partial pressure within that domain.

Generally, a decrease in ethanol conversion was observed with increasing inlet water partial pressure (Figure 3-21). This could result from competitive adsorption of water on active sites resulting in lower activity. For the adsorption of ethanol, there has to be an exposed oxygen site that will act as an acceptor for the hydrogen. Therefore, if most oxygen sites are covered by OH species from water, the adsorption of ethanol is expected to decrease.

Since this study was done over a range of space-time, product selectivity was sometimes affected differently by the inlet water partial pressure depending on the space-time employed. Diethyl ether selectivity generally decreased with increasing inlet water partial pressure (Figure 3-23). The observed decrease can be ascribed to the proximity effect of the ethoxy species and adsorbed ethanol needed for the formation of diethyl ether. With the increasing population of adsorbed water molecules on the surfaces the chances of the two species being in neighbouring sites decrease. Thus, the decrease in the observed selectivity.

A marked increase in the selectivity of acetic acid plus ethyl acetate is observed at high-space time and 270°C; this was compensated by the decrease in acetaldehyde selectivity (Figure 3-25. These conditions presents a unique opportunity in the ethanol oxidation pathway, where the lattice oxygen is labile enough for further oxidation of acetaldehyde to occur, while further attack by oxygen is minimised by the presence of OH species on the surface.

Generally, the selectivity to carbon oxides decreases with inlet water partial pressure (Figure 3-27), thus increasing partial oxidation products selectivity. According to Saleh-Alhamed *et al.* (1995), it is the competitive adsorption that causes the decrease of the carbon oxides selective, due to blockage of the most active sites by water. The oxygen is bound as OH species and is not available for hydrogen abstraction action required in the formation of carbon oxides from organic molecules. Another view is that the addition of water decreases the formation of bridging carboxylate species by adsorbing to the sites decreasing the number of two free neighbouring sites that are needed for the formation of bidentate intermediates responsible for the formation of CO_x (Medeiros *et al.*, 2000).

Increasing temperature in the oxidation of ethanol resulted in an increase in ethanol conversion (Figure 3-28), decrease in acetaldehyde selectivity, and a maximum at lower temperatures in the selectivity to diethyl ether, a maximum at high temperatures in the selectivity of acetic acid + ethyl acetate and an increase in the selectivity of carbon oxides. Mainly due to labile oxygen species and formation of electrophillic oxygen species on the surface.

The results obtained from TPD and IR studies using ethanol as a probe molecule largely supported the fixed bed investigation of reaction parameters. TPD studies showed the formation of acetaldehyde, water, ethylene and carbon dioxide on evacuation of ethanol adsorbed over $V_{0.7}Fe_{0.3}SbO_4$ (Figure 3-30). Typical products from ethanol oxidation over metal oxides in a fixed bed reactor, such as acetic acid, diethyl ether, ethyl acetate, acetone and carbon oxides were not observed. This could have resulted from the short contact time of ethanol with the catalysts pellet, not allowing for consecutive reaction to occur. The reaction mechanism implications of the observed desorption profile are that acetaldehyde (formed by oxidative dehydrogenation) and ethylene (formed by dehydration) are competing primary reaction pathways over $V_xFe_{1-x}SbO_4$ catalysts.

The identification of furan when acetaldehyde was adsorbed indicated the β-aldolisation taking place on the catalyst surface (Figure 3-31).

IR studies showed the presence of ethoxy, acetaldehyde, acetate and carboxylate species (. Small bands associated with the formation of crotonaldehyde (Yee *et al.*, 1999) were also observed. Carboxylate species were observed at elevated temperature, this corroborates well with the need for labile oxygen species for the intermediates to form.

Comparing the TPD and IR results it is clear that the two techniques supplement each other in the elucidation of the reaction mechanism. TAP experiments showed that that ethanol and its products adsorb strongly on the surface and that the continued feeding of air in a fixed-bed reactor plays an important role in desorption of the products.

4.3 CHARACTERISATION OF SINGLE, BINARY AND TERNARY OXIDE USING ETHANOL OXIDATION

The partial oxidation of ethanol used as a test reaction was performed over three different classes of catalysts with increasing complexity.

4.3.1 Partial oxidation of ethanol over single metal oxides (V_2O_5, Fe_2O_3 and Sb_2O_3)

Catalytic activity in these metal oxides increased with increasing temperature in the order order: V_2O_5 > Fe_2O_3 >> Sb_2O_3 at 300°C. Similar order was established by Golodets (1983) during a study on methanol oxidation over a number of metal oxides. Golodets established that the reaction over oxides follows a parallel-consecutive scheme, and that the overall process on the majority of oxides obeys the first order rate equation. Over the region of validity of the rate equation (first order reaction), the catalytic activity should decrease with increasing oxygen-metal bond energy, Qs (Golodets, 1983).

Generally, the selectivity to partial oxidation products decreases with increasing temperature. There are many factors contributing to the observed decrease in the selectivity to partial oxidation products with increasing temperature, Haber (1996) ascribes the change in selectivity to the equilibrium shift in the direction of higher dissociation pressure of the oxide and the surface becoming more and more populated with electrophilic oxygen species.

The increase in temperature results in a different reaction pathway setting in, promoting the formation of CO/CO_2 (Sokolovskii, 1990). The complete oxidation occurs through oxidised carbonate-carboxylate intermediates, reflecting two paths of decomposition of surface species, under the action of molecular oxygen and thermal decomposition. The transition of one mechanism into another is determined by the thermal stability of surface species, which, in turn depends on the heat of binding of oxygen abstracted from the catalyst during the course of decomposition of these species (metal oxygen bond energy). The lower the heat of oxygen binding, the lower the temperature of mutual transition of the mechanisms

Subsequent to the elaboration above, for first order reactions, the selectivity should increase with increasing oxygen-metal bond energy, Qs (Golodets, 1983). Owing to the fact that in the formation of deep oxidation products, a larger number of M-O bonds would have to be broken than in partial oxidation products formation. This explains the predominant formation of acetaldehyde at low temperature where less energy is available to break the M-O bonds. When the temperature is increased, i.e. more energy available to break M-O bonds, the selectivity to acetaldehyde (primary product) decreases and the selectivity to acetic acid, ethyl acetate (secondary products) and CO/CO_2 (total oxidation products) increase.

Golodets (1983) suggests that deviations are observed suggesting that the oxygen-metal bond strength is not a unique factor determining the activity and selectivity over metal oxides. Since the ethoxy complex (from which an aldehyde is formed) is a salt-like compound, desorption or further reaction of this intermediate should depend not only on Qs, but also on the acid base properties of the catalyst.

4.3.2 Partial oxidation of ethanol over binary ($FeSbO_4$ and $VSbO_4$) and ternary $V_xFe_{1-x}SbO_4$ metal oxides

The fascination about the combination of $FeSbO_4$ and $VSbO_4$ catalyst systems is in the similarities (the tetragonal rutile structure) and the differences (the presence of a defective structure with the composition of $V^{4+}_{0.64}V^{3+}_{0.28}Sb^{5+}_{0.92}\Diamond_{0.16}O_4$ for $VSbO_4$ and not for $FeSbO_4$). In this section, the characterisation of binary and ternary $V_xFe_{1-x}SbO_4$ using ethanol oxidation as a test reaction is reviewed.

The difference in activity between vanadium-rich ternary oxides and iron-rich ternary oxides was clearly demonstrated in the ethanol conversion. Iron-rich catalysts showed selectivity characteristics of higher acetaldehyde selectivity, lower selectivity to diethyl ether, acetic acid + ethyl acetate and carbon oxides. The opposite pattern was observed for vanadium-rich catalysts.

To identify active centres for the oxidation of ethanol over $V_xFe_{1-x}SbO_4$ catalysts, the rate of formation of acetaldehyde was modelled as a first order reaction with respect to ethanol and zero order with respect to oxygen. Based on this model the rate constant for

each of the catalysts was obtained. Figure 4-3 shows the rate constant at 210°C normalised with respect to the BET-surface area as a function of the surface V/(V+Fe) ratio as measured by XPS. Provided the addition of Fe to the V-antimonate structure is purely additive, a linear relationship between the normalised rate constant and the V/(V+Fe) ratio can be expected. However, it can clearly be seen that the rate constant increases strongly between V/(V+Fe)= 0 - 0.4, forming a curve above the expected linear relationship (dotted line).

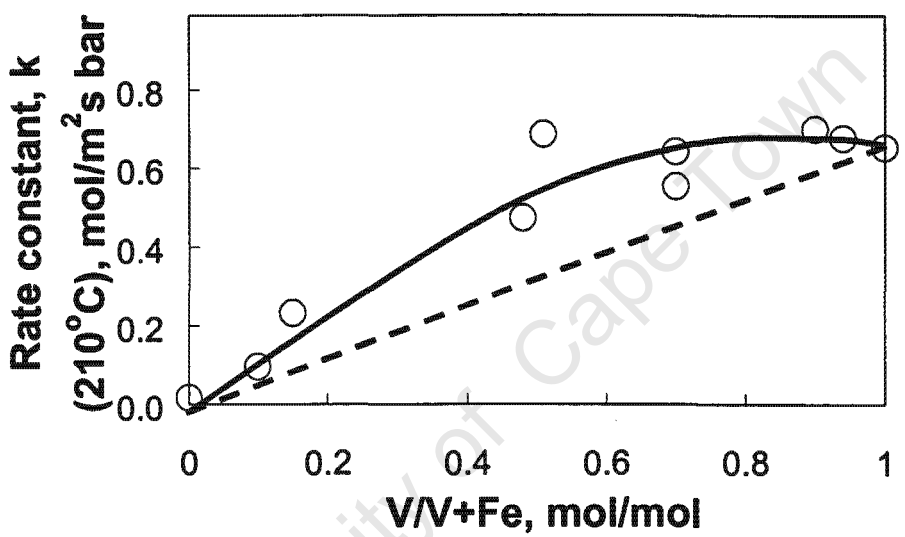

Figure 4-3: First order rate constant for the formation of acetaldehyde in the ethanol oxidation at 210°C over $V_xFe_{1-x}SbO_4$ catalysts 0 < x < 1 normalized with respect to the BET surface area as a function of the vanadium content. WHSV = 2.44 $g_{ethanol}/(g_{catalyst}\ h)$; $P_{ethanol}$ = 0.27 bar, P_{O2} = 0.3 bar, balanced by N_2 to a total pressure of 2bar

Hence it can be concluded that the effect of increasing V/(V+Fe) ratio is not purely additive. There is a clear synergy between the catalysts components observed. To assign active species within these catalyst components, correlation of the various species in the catalysts with the observed catalytic activity were performed (shown in, Figure 4-4, Figure 4-5 and Figure 4-6).

Correlation of the catalytic activity with the V^{3+}-content as shown in Figure 4-4, indicates a direct correlation of the activity to the V^{3+} content up to V/(V+Fe) > 0.5 after which the V^{3+}-content does not vary much (indicated by a circle in Figure 4-4).

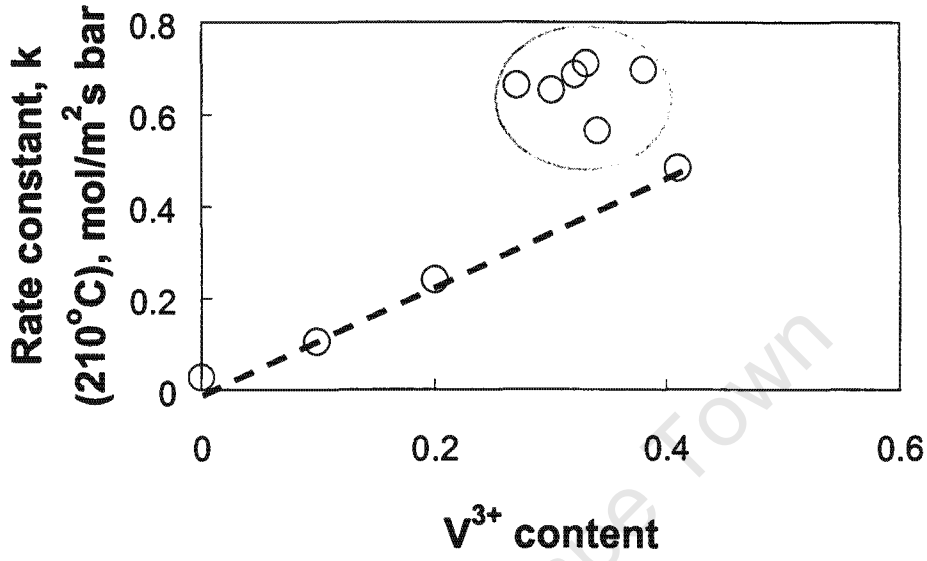

Figure 4-4: First order rate constant for the formation of acetaldehyde in the ethanol oxidation at 210°C over $V_xFe_{1-x}SbO_4$ catalysts 0 < x < 1 normalized with respect to the BET surface area as a function of V^{3+} content WHSV = 2.44 $g_{ethanol}/(g_{catalyst}\ h)$; $P_{ethanol}$ = 0.27 bar, P_{O2} = 0.3 bar, balanced by N_2 to a total pressure of 2bar. The content of V^3 remains rather constant with increasing vanadium content after V/(V+Fe) > 0.5 (Circled region).

Figure 4-5 presents the correlation of the rate constant with the V^{4+}-content.

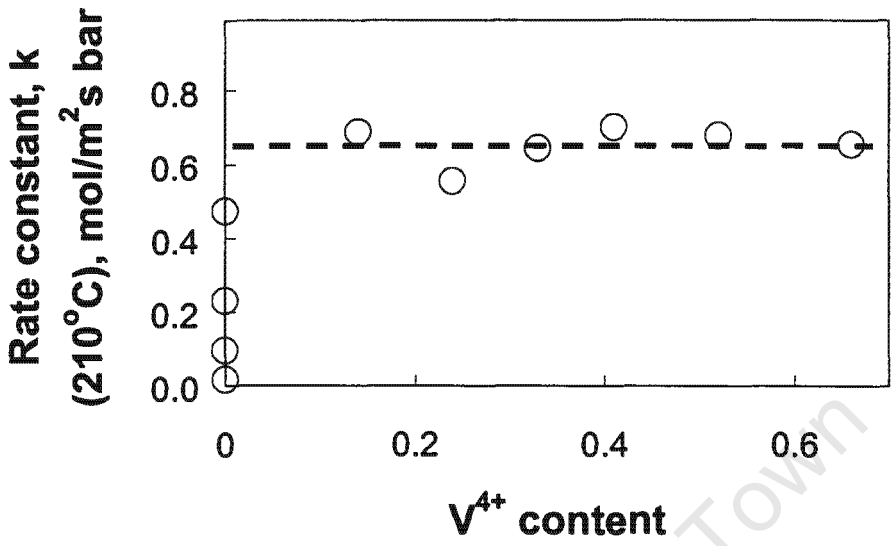

Figure 4-5: First order rate constant for the formation of acetaldehyde in the ethanol oxidation at 210°C over $V_xFe_{(1-x)}SbO_4$ catalysts $0 < x < 1$ normalized with respect to the BET surface area as a function of V^{4+} content. WHSV = 2.44 $g_{ethanol}/(g_{catalyst}\ h)$; $P_{ethanol}$ = 0.27 bar, P_{O2} = 0.3 bar, balanced by N_2 to a total pressure of 2bar

It can clearly be seen that the rate constant does not correlate with V^{4+} content. A strong increase in V^{4+} content is observed for the samples with V/(V+Fe) > 0.5, in which region a marginal increase in the rate constant is observed).

However, there are theoretic considerations that render this kinetic analysis open to further consideration. The determination of V^{4+} and V^{3+} content was done by XANES, which is a bulk technique. The catalytic reaction proceeds on the catalyst surface where this ratio can be different. Since ethanol proceeds in a cyclic reduction and reoxidation of the vanadium sites it is expected that the activity should increase with the redox potential of the active redox couple in the order $V^{2+}/V^{3+} < V^{3+}/V^{4+} < V^{4+}/V^{5+}$. Implying that activity increase should correlate more positively with V^{4+} than with V^{3+}. Furthermore, the binding energies for vanadium species determined for these catalysts were about 517.0 eV, which is closer the binding energy of V^{4+} (VO_2 = 516.3 eV) than to that of V^{3+} (V_2O_3 = 515.7 eV) (Chastain and King, 1995).

Correlation of the catalytic activity with the cationic vacancies content is shown in Figure 4-6. A marginal correlation is observed between the rate constant for the formation of acetaldehyde and the content of the cationic vacancies.

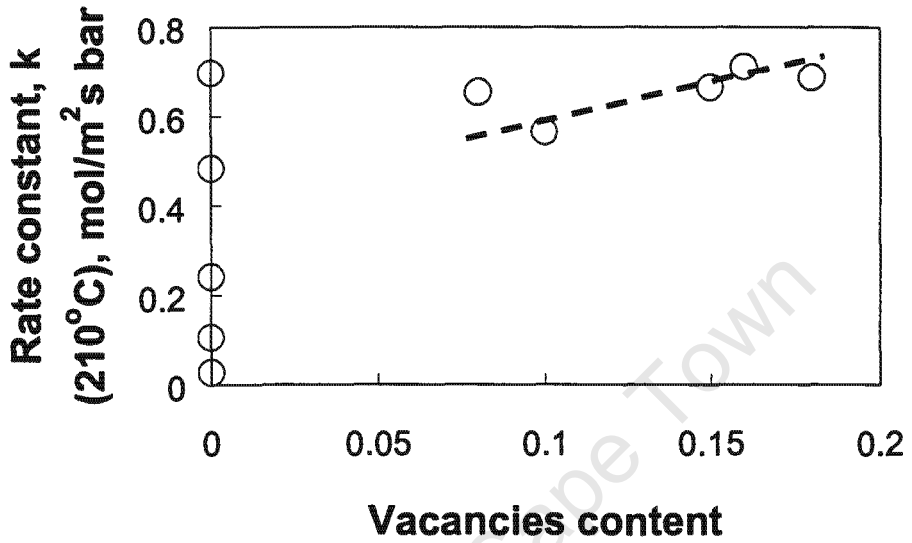

Figure 4-6: First order rate constant for the formation of acetaldehyde in the ethanol oxidation at 210°C over $V_xFe_{(1-x)}SbO_4$ catalysts $0 < x < 1$ normalized with respect to the BET surface area as a function of the cationic vacancies content. WHSV = 2.44 $g_{ethanol}/(g_{catalyst}\ h)$; $P_{ethanol} = 0.27$ bar, $P_{O2} = 0.3$ bar, balanced by N_2 to a total pressure of 2bar

The initial increase in the rate constant correlates strongly with the V^{3+}-content. Hence, it can be concluded, that V^{3+} are the active centres in the ethanol oxidation. Above V/(V+Fe)>0.5 the V^{3+}-content does not vary much, although a slight further increase in the rate constant is observed. This increase was accounted for by the positive correlation of the rate constant at high vanadium content with the amount of vacancies in the structure. The rate constant does not correlate with V^{4+}-content (a strong increase in V^{4+} content is observed for the samples with V/(V+Fe)>0.5, in which region a marginal increase in the rate constant is observed).

A full kinetic analysis shows that the increase in the rate constant at low V/(V+Fe is associated with a variation in the activation energy, implying a change in the reaction mechanism (i.e. a switch from Fe^{3+} being the active centre to V^{3+} being the active centre). The change in the rate constant at high vanadium content is not associated with a change in the activation energy, but with a change in the pre-exponential factor. This implies that the introduction of vacancies might clean up the surface and makes the active site more accessible for reaction.

To compare all the $V_xFe_{1-x}SbO_4$ catalysts, iso-conversion of 50% was used (Figure 4-7 and Figure 4-8 below). The selectivity to diethyl ether over $V_xFe_{1-x}SbO_4$ catalysts at 50% conversion is presented in Figure 4-7.

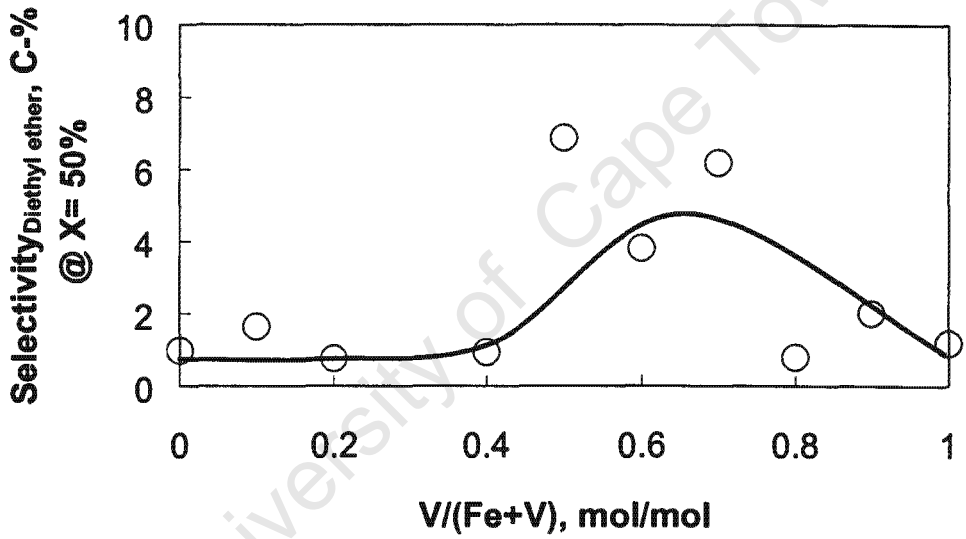

Figure 4-7: Selectivity to diethyl ether as a function of vanadium content at 50% conversion in the oxidation of ethanol over $V_xFe_{1-x}SbO_4$ catalysts, where $0 < x < 1$. WHSV = 2.44 $g_{ethanol}$ /($g_{catalyst}$ h), $P_{ethanol}$ = 0.27 bar, P_{O2} = 0.3 bar, balanced by N_2 to a total pressure of 2 bar

Slight differences are observed between the vanadium-rich and iron-rich catalysts at 50 % ethanol conversion. It would appear that the catalysts rich in vanadium exhibit higher selectivity to diethyl ether in comparison to iron-rich catalysts. The observed trend is attributed to a general higher electron transfer capability of the vanadium-rich ternary oxides. Selectivity of oxidation products within the oxidation products fraction (i.e.

excluding diethyl ether) at 50% ethanol conversion is shown in Figure 4-8 below. Selectivity to acetaldehyde tends to be higher in iron-rich catalysts. While the selectivity to acetic acid plus ethyl acetate and carbon oxides tend to be higher in vanadium-rich catalysts. The acetic acid content in the acetic acid plus ethyl acetate fraction decreases with increasing vanadium content. This implies that over vanadium-rich catalysts, the adsorbed acetate species desorp preferentially as ethyl acetate.

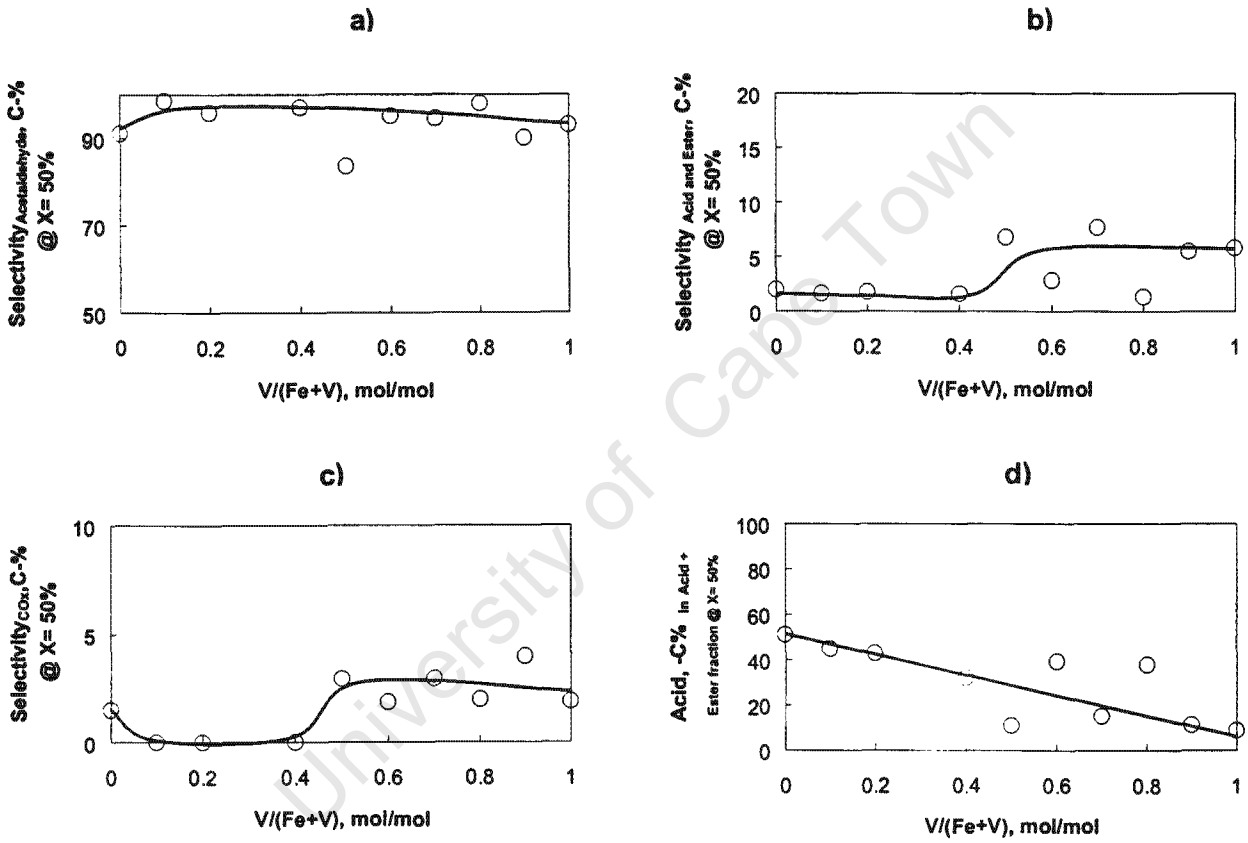

Figure 4-8: Products selectivity within the oxidation products fraction as a function of vanadium content, a) acetaldehyde b) carbon oxide c) acetic acid plus ethyl acetate d) acetic acid content in the acid and ester fraction at 50% conversion in the oxidation of ethanol over $V_xFe_{1-x}SbO_4$ catalysts, where $0 < x < 1$. WHSV = 2.44 $g_{ethanol}/(g_{catalyst}\ h)$; $P_{ethanol}$ = 0.27 bar, P_{O2} = 0.3 bar, balanced by N_2 to a total pressure of 2 bar

Comparing binary oxides and ternary oxides it is important that the high activity is not achieved at the expense of the selectivity to partial oxidation products. Binary oxide $FeSbO_4$ exhibits lower acetaldehyde selectivity compared to ternary $V_xFe_{1-x}SbO_4$

catalysts (where $0 < x < 0.5$), albeit higher ethanol conversion observed over the ternary oxides. The observed trends in selectivity of various products indicate that there must exist some characteristics in the iron–rich catalysts that stabilises the primary product (acetaldehyde) and hinders further reaction to consecutive products. It also should be noted that the acetic acid plus ethyl acetate and carbon oxides were not favoured over the iron-rich catalysts.

This study has demonstrated progressively improved overall catalytic performance observed the more complex the catalyst system became. For example, V- based catalysts showed the following trend in catalytic activity and selectivity to partial oxidation products: single metal oxide: V_2O_5 < binary metal oxide: $VSbO_4$ < ternary metal oxides: $V_xFe_{1-x}SbO_4$, $0.4<x<1$. The enhancement is attributed to site isolation, i.e. the V^{3+} ions (active sites) become more isolated when different 'spectator' ions are added.

CONCLUSIONS

5 CONCLUSIONS

The core objective of this study was to investigate partial oxidation of ethanol over vanadium iron antimonates in order to establish the active sites for this reaction. To achieve that objective, activity over single metal oxides (V_2O_5, Fe_2O_3 and Sb_2O_3) was first established, then binary metal oxides ($VSbO_4$ and $FeSbO_4$) and ultimately ternary ($V_xFe_{1-x}SbO_4$, $0 < x < 1$). The feats associated with vanadium iron antimonate catalyst system were clearly demonstrated by progressive improvement in overall catalytic performance observed, the more complex the catalyst system became. The phenomenon believed to be responsible for the observed effect is the site isolation theory introduced to oxidation catalysis by Callanan and Grasselli (1963).

To assign the active sites for the oxidation of ethanol over complex $V_xFe_{1-x}SbO_4$, $0 < x < 1$ catalysts, the rate constants for formation of acetaldehyde was correlated with species making up the catalysts (V^{3+}, V^{4+} and Sb^{5+}). Fe^{3+}/Fe^{2+} redox couple was shown not to take part in the reaction by substituting Fe^{3+} by Ga^{3+} or Al^{3+} and Mössbauer parameters. The most important outcome seems to be activity dependence on V^{3+} ions and enhancement of activity by the presence of vacancies. It is therefore the conclusion of this study that the V^{3+} ions are the active centres in the ethanol oxidation. In $FeSbO_4$, Fe^{3+} ions are active centres, as the vanadium is substituted for iron, a switch from Fe^{3+} being the active centre to V^{3+} being the active centre is evidenced by the change in the activation energy. It can also be concluded that the introduction of vacancies makes the active site more accessible for the reaction.

Important conclusion can be drawn from the characterization study of $V_xFe_{1-x}SbO_4$, $0 < x < 1$ catalysts:

- BET surface area decreases with increasing V/(V+Fe) ratio.
- A solid solution is formed between $VSbO_4$ and $FeSbO_4$
- Number of Lewis and Brønsted acid sites normalised with respect to surface area increases with increasing V/(V+Fe) ratio.

- Surface Sb enrichment factor was constant throughout the catalyst range, thus no conclusions can be drawn about the effect of this enrichment.

A parallel-consecutive reaction pathway was proposed for the oxidation of ethanol over $V_xFe_{1-x}SbO_4$, $0 < x < 1$ catalysts. From the acetaldehyde, this study proposes that acetic acid and ethyl acetate form parallel. The shapes of the selectivity curves for partial oxidation products relative to carbon oxides show a definite change in the mechanism for the oxidation of ethanol as the temperature is increased over all the metal oxide systems investigated. This is attributed to a change in the population of nucleophillic and electrophillic oxygen species on the catalyst surface, a proposition that has been largely covered in literature pertaining to oxidation catalysis by molecular oxygen (Libre *et al.*, 1983).

Another important conclusion from this work must be the effect of inlet water partial pressure on the selectivity to different ethanol oxidation products. Coupling this study to the space time study brought about the understanding of many conflicting findings in literature concerning the effect of water partial pressure on oxidation reactions. This systematic study brought about the understanding that the effect of co-feeding water is largely dependent on the reaction conditions (i.e. the position in the oxidation reaction sequence). For example, the effect of inlet water partial pressure at low space-time and low reaction temperature is an increase in the selectivity to acetaldehyde, and a decrease in all other parallel and consecutive products. At high space-time and high reaction temperature, however, acetaldehyde and carbon oxides selectivity decreases, while acetic acid plus ethyl acetate selectivity increases.

Although this work has shown that the selectivity to acetic acid can be drastically improved by co-feeding water with ethanol, two staged industrial processes would still appear as a more attractive approach. There is a high possibility of formation of complete oxidation products at the reaction conditions where acetic acid yield is at maximum.

REFERENCES

6 REFERENCES

Ai, M., *J. Catal.* **83** (1983) 141

Albonetti, S., Blanchard, G., Burattin, P., Cavani, F., Masetti, S., Trifiro, F., *Catal. Today*, **42** (1998) 283

Allen, M., Betteley, R., Bowker, M. and Hutchings, G.J., *Catal. Today*, **9** (1991) 97

Anderson, J. S. *In Problems in Nonstoichiometry*; Rabenau, A. Ed.; North Holland: Amsterdam (1970) 1

Andersson A., Andersson S.L.T., Centi G., Grasselli R.K., Sanati M., and Trifiró F., *Appl. Catal.*, **113** (1994), 43

Andrushkevich, T. V., *Kinetics and Catalysis*, **38** (1997) 266

Aso, I., Furukawa, S., Yamazoe, N,. Seiyama, T., *J. Catal*, **64** (1980), 29

Ballarini, N., Cavani, F., Cavani, F., Millini, R., Stocchio, B., Trifiro, F., Ghisletti, D., Cornaro, R., *Stud. Surf. Sci. Catal.*, **136** (2001a) 135

Ballarini, N., Cavani, F., Ghisletti, D., Catani, R. and Cornaro, U., *Catal. Today.*, **2831** (2002), 1-9

Ballarini, N., Cavani, F., Guinchi, C., Masetti, S., Trifiro, F., Ghisletti, D., Cornaro, R., Catani, R., *Topics Catal.*, **15** (2001b) 111

Barbaux, Y., Elamrani, A., Bonnelle, J.-P., *Catal. Today.*, **1** (1987), 147

Barteau, M. A., *Chem. Rev.*, **96** (1996) 1413

Bauer, W.H., *Z. Kristallogr.*, **209** (1994) 143

Benziger, J. B., in: *Metal-Surface Reaction Energetics,* Shustarovich, E. (Ed.) VCH, New York, 1991

Berry, F. J., Brett, M. E., and Patterson, W. R., *J. Chem. Soc. Dalton Trans.*, **9** (1983)

Berry, F. J., Smart, L. E., and Duhalde, S., *Polyhedron,* **15(4)** (1996) 651

Berry, F.J., Holden, J.G. and Loretto, M.H., J. Chem Soc., Faraday Trans., **7** (1987) 1727

Bielanski, A.., Haber, J., *Oxygen in Catalysis,* Marcel Dekker Inc., New York, (1991), 44

Birchall, T., and Sleight, A. W., *Inorg. Chem.* **15** (1976) 868

Blanchard, G., Burattin, P., Cavani, F., Masetti, S., Trifiro, F., *WO Patent* 97/23,287 A1 (1997), assigned to Rhodia

Boaventura, J., Ph.D. dissertation, University of Delaware, 1989

Boehm, H.P., Knözinger, H., in Catalysis Science and Technology, Anderson, J.R., and Boudart, M. (eds), Springer-Verlag: West Berlin, **4** (1983) 39

Bol, C. W. J. and Friend, C. M., *J. Phys. Chem.,* **99** (1995), 11930

Boreskov, G.K, Popov, B.I., Bibin, V.N., and E.S. Kozishnikova, *Kinetika I Kataliz.,* **9** (1968) 768

Bowker, M., Bicknell, C. R., and Kerwin, P. *Appl. Catal., A. General,* **136** (1996) 205

Bruckman, K., Grabowski, R., Haber, J., Mazurkeiwicz, A., Sloczynski, I., and Wiltowski, I., *J. Catal.,* **104** (1987), 71

Burch, R., Squire, S.C. and Tsang, S.C., *Appl. Catal* A, **46** (1989) 69

Burriesci, N., Garbassi, F., Petrera, M., Petrini, G., *J. Chem. Soc.*, Faraday Trans. 1, **78**, (1982), 817.

Busca, G., and Lorenzelli, V., *Mater. Chem.* **89** (1982)

Busca, G., *J. Phys. Chem.*, **91** (1987) 5263

Busca, G., *Langmuir*, **2** (1986) 577

Callahan, J. L., Grasselli, R. K., *AIChE J.,* **9**, (1963), 755

Carbucicchio, M., Centi, G., Trifiro, F., *J. Catal.*, **91** (1985), 85

Castillo, R., Awasarkar P. A., Papadopoulou C., Acosta D. and Ruiz P., "New Developments in Selective Oxidation II" in *Stud. in Surf. Sci. and Catal.*, Cortes Corberan V. and Vic Bellon S. (eds) (Elsevier Amsterdam), **82** (1994) 293

Cavani, F. and Trifiro, F., in *3rd World Congress on Oxidation Catalysis*, Grasselli, R. K. Oyama, S. T. Gaffney, A. M., Lyons, J. E. (Eds.) Elsevier Science, Amsterdam (1997) 19

Cavani, F. and Trifiro, F., in *Catalysis, Specialist Periodical Report;* Chp. 7, Royal Society of Chemistry: London (1995) 246

Cavani, F., Ligi, S., Monti, T., Pierelli, F., Trifiro, F., Albonetti, S., and Mazzoni, G., *Catal. Today* **61** (2000) 203

Centi G;, Perathoner S., *Appl. Catal*, **124** (1995) 317.

Centi, G. *Appl. Catal. A: General* **147,** (1996) 267

Centi, G., Grasselli, R.K. and Trifiró, F., *Catal. Today,* **13** (1992) 661

Centi, G., Perathoner, S. and Trifirò, F., *Appl. Catal., A: General*, **157** (1997) 143

Centi, G., Perathoner, S., Stella, G., in: Delmon, B., Fromant, G. F., (Eds.). Catalyst Deactivation, vol. **88**. Elsevier, Amsterdam (1994) 393

Centi, G., Pesheva, D. and Trifiro, F., *Appl. Catal.,* **33** (1987) 343

Cong, Y., van Spaendonk, V., and Masel, R. I., *Surf. Sci.,* **385** (1997) 246

Davy, E., *Schweiggers J.* **34** (1923) 91

Davy, H., *Phil. Trans*, **97** (1817) 45

De Rossi, S., jacono, M. W., Pepe, R., Schiavello, M., Tilley, R. J. D. *Phys.Chem.* **130** (1982) 109

De Wolf, P. M., *J. Appl. Crystallogr.* **1** (1968) 108

Delmon, B. and Ruiz, P., *Catal. Today*, **1** (1987) 1

Desikan, A. N., Compiled from C&EN, June (1991); Chemical week, June (1991), Current Industrial Reports, (1990); U.S. International Trade Commission Report 2470, (1990)

Desikan, A. N., Zhang, W. M. and Oyama, S.T., *J. Catal.,* **157(2)** (1995) 740

Diagne, C., Idriss, H., Pepin, I., Hindermann, J. P., and Kiennemann, A., *Appl. Catal.* **50** (1989) 43

Doca, N., and Segal, E., *Rev. Roumaine Chim.*, **30** (1985) 948

Doca, N., and Segal, E., *Rev. Roumaine Chim.*, **31** (1986) 567

Fattore, V., Fuhraman, Z. A., Manara. G., Notari, B., *J. Catal.*, **37**, (1975), 215

Fogler, H.S., Elements of Chemical Reaction Engineering, 3rd Ed., Prentice Hall PTR, (1999) 758

Forzatti, P., Elmi, A. S., Tronconi, E., Cristiani, C., Martin, J. P. G., *Ind. Eng. Chem. Res.*, **28** (1989) 387

Forzatti, P., Elmi, A. S., Tronconi, E., Ferlazzo, N., *Ind. Eng. Chem. Res.*, **26** (1987) 1269

Fraser J., Business Report, 22 July (1999).

Gai, P. L., Boyes, E. D., Bart, J. C. J. *Philos. Mag. A* **45** (1987) 531

Glaesser, L. C., Brazdil, J. F., and Toft, M. A., *US Patent,* 4,767,739 , 4,769,355 , 4,783,545, 4,843,655 , 4,835,125 and 4,837,191 (1988); assigned to Standard oil Co. (Ohio).

Glaesser, L. C., Brazdil, J. F., Toft, M. A., *US Patent,* 4,871,706 (1989)

Gleaves, J. T., Ebner, J. R. and Kuechler, T. C., *Catal. Rev. Sci. Eng.*, **30(1)** (1989) 43

Golodets, G. I., *Dokl. AN SSSR,* **184** (1969) 1334

Golodets, G.I., *Stud. Surf. Sci. Catal*, **15** (1983)

Golodets, G.I., *Stud. Surf. Sci. Catal*, **55** (1990), 121.

Gonzalves, F. M., Medeiros, P. R., Eon, J. G., Appel, L. G., *Appl. Catal.* **193** (2000) 195

Grasselli, R. K., Bradzil, J. F., Burrington, J. D., *Appl. Catal.* **25** (1986) 335

Grasselli, R. K., Featured Lectures for the 4th World Congress on Oxidation Catalysis, September (2001)

Grasselli, R. K., Handbook of Heterogenous Catalysis, Ertl, G., Knoezinger, H. and Wietkamp, J. (eds), B (1997) 4.6.7

Grimaux, R.S., *Bull. Soc. Chim. (II)*, **45** (1886) 481

Grootedorst, E. J., Pestman, R., Koster, R. M., and Ponec, V., *J. Catal.*, **148** (1994) 261

Grzybowska-Swierkosz B., *Appl. Catal. A*, **157** (1997) 409

Gursahami, K. I., Alcala, R., Cortright, R. D., Dumesic, J. A., *Appl. Catal.A: General* **222** (2001) 369

Guttmann, A. T., Grasselli, R. K., and Brazdil, J. F., *US Patent,* 4,746,641, 4,788,173 and 4,837,233 (1988)

Haber, J., *ACS Symposium Series 638*, (1996), 20

Haber, J., In: *Proceedings of the 4th International Conference of Chemistry and uses of Molybdenum, Golden Colorado, 1982,* (Barry, H. F., Mitchell, P. C. H., Eds.), Climax Molybdenum, (1982), 395

Haber, J., Materials Sci. Forum 25 (1988) 17

Haber, J., *Stud. Surf. Sci. Catal*, **72** (1992) 279

Haddeland, G. in Chemical production by Fischer-Tropsch and related syntheses, **100** (1976) 95

Halasz, I., Vinek, H., Thomke, K., Noller, Z., *Phys. Chem.* **163** (1985) 157

Handbook of X-ray Photoelectron Spectroscopy, Chastain, J. and King Jr, R.C. (eds), Physical Electronics Inc., Eden Prairie, 1995

Hansen, S., Stahl, K. Nilsson, R., Andersson, A., *J. Solid State Chem.,* **102**(1993) 340

Hayes, E.R. in Kirk-Orthmer encyclopedia, 4th ed, John Wiley & Sons Inc. (1970) 446

Herrmann, J. M. in: Catalyst Characterization, Physical Techniques for Solid Materials, eds. Imelik, B. and Védrine; J. C., Plenum Press (New-York), (1994) 559

Hewlett Packard, Workbook, Publication No. G1030-90004, (1989)

Holstein W.L. and Machiels C.J., *J. Catal.*, **162** (1996) 118

Houben-Weyl, in German patent DRP 579566, 1933

Hussak, E., Prior, G.T., *Mineral. Mag. J. Mineral. Soc.*, **11** (1897) 302

Idriss, H. and Seebauaer, E. G., *J. Vac. Sci. Technology* A, **14** (1996) 1647

Idriss, H., and Madhavaram, H., *J. Catal.* **184** (1999) 553

Idriss, H., Barteau, M. A., and Kim, K. S., *J. Catal.* **139** (1993) 119

Idriss, H., Diagne, C., Hindermann, J. P., Keinnemann, A., and Bartaeau, M. A., *J. Catal.,* **155** (1955) 219

Idriss, H., Kim. K. S., Barteau, M. A., *Stud. Surf. Sci. Catal.* **64** (1991) 327

Idriss, H., Libby, H., and Barteau, M. A., *Catal. Lett.,* **15** (1992) 13

Idriss, H., Pierce, K. G., Barteau, M. A., *J. Am. Chem. Soc.* **113** (1991) 715

Idriss, H., Seebauer, E. G., *Catal. Lett.* **66** (2000a), 139

Idriss, H., Seebauer, E. G., *J. Mol. Catal.* A **152** (2000b), 201

Irigoyen, B., Juan, A., Larrondo, S. and Amadeo, N. *J. Catal.* **201** (2001) 169

Iwasawa, Y., Nakano, Y., and Ogaswara, S., *J. Chem. Soc. Faraday Trans.*1, **74** (1978) 2986

Kaiser, R., Chromatograhie in der Gasphase, Vol. 3, 2nd Edition, Bibliographisches Institut, Mannheim, 1969

Kannan, S., Sen, T. and Sivasanker S., *J. Catal.*, **170** (1997) 304

Kanoun, N., Astier, M.P. and Pajonk, G.M., *Appl. Catal* , **70(1)** (1991) 225

Kiennemann, A., Idriss, H., Keiffer, R., Chaumette, P. and Durand, D., *Ind. Eng. Chem. Res.*, **30** (1991) 1130

Kim, K. S. and Barteau, M. A., *J. Catal.* **125** (1990) 153

Kim, K. S. and Barteau, M. A., *Surf. Sci.* **223** (1989), 13

Konishi, Y. Sakara, K., Misono, M. and Yoneda, Y., *J. Catal.*, **77** (1982) 169

Kriegsmann H., Öhlmann G., Scheve J. and Ulrich F.J., *in Proceedings, 6th International Congress on Catalysis*. (Bond G.C., Wells P.B., Tompkins F.C., Eds), The Chemical Society London, Vol. **2** (1977).836

Kuhlmann, F., *Ann.*, **29** (1839) 286

Kurina, L. M. and Morozov, V. P., *Russ. J. Phys. Chem.*, **50** (1976) 538

Lamotte, J., Moravec, V., Bensitel, M., Lavalley, J. C., *React. Kinet. Catal. Lett.*, **36** (1988) 113

Landa-Canovas, A. Nilsson, J., Hansen, S., Stahl, K., Andersson, A., *J. Solid Stae Chem.*, **116** (1995) 369

Libre, J.0 M., Parbaux, Y., Grzybowska, P., Conflant, P., Bonnelle, J. P., *Appl. Catal.*, **6**, (1983), 315

Lorenzetti, M., *Oil and Gas J.*, March (2002) 30

Lynch M. W., Winslow, L. N., Klendworth D. D., Fields, G. L and Cincinnati, O., US *Patent* 553,447,2 (1997), assigned to Quantum Chemical Corporation

Madhavaram, H., and Idriss, H., *Stud. Surf. Sci. Catal.*, **110** (1997) 265

Madix, R. J., Roberts, J. T., In *Surface reactions* (Madix, R. J., Ed.) Springer-Verlag: Berlin, (1994) 5

Marek, L. F. and Hahn, D. A., *The catalytic oxidation of organic compounds in the vapor phase* The Catalog Company Inc, (1932)

Mars, P. and van Krevelen, D. W., *Chem. Eng. Sci. Suppl.*, **3** (1954) 41

Mason, B., Vitaliano, J., *Mineral. Mag. J. Mineral. Soc.*, **30**, (1955) 100

Matsumura, Y., Hashimoto, K., and Yoshida, S., *J. Chem. Soc., Chem. Commun.*, (1987) 1599

McKenze, A., Fishel, C., and Davis, R., *J. Catal.*, **138** (1992) 547

Mckie, D. and Mckie, C., *Crystalline Solids*, A. Wheaton and Co. Ltd., (1980) 32

Mears, D. E., *Ind. Chem. Process Des. Dev.*, **10**, (1971) 541

Medeiros, P. R., Eon, J. G., and Appel, L. G., *Catal. Lett.*, **69** (2000) 79

Meharg, V.E. and Adkins, A., U.S. patent 1,913,405 (1933)

Miller, J. B., *Chemical and Process Engineering*, (1968) 75

Millet, J. M. M., Rouzies, D. and Védrine, J.C., *Appl. Catal. A: General*, **124** (1995) 205

Mimura, Y., Ohyachi, K., Matruura, in *Sci. Tech. Cata. 1998.* Hattori, H., Otsuka, K. (Eds.) Kodansha, Tokyo (1999) 69

Muggli, D. S., Falconer, J. L., *J. Catal.* **175**, (1998) 213

Nilsson J., Landa-Canovas A.R., Hansen S., and Andersson A., *J. Catal.*, **160** (1996) 244

Nilsson, R., Linblad, T., Andersson, A., Song, C. and Hansen, S., "New Developments in Selective Oxidation" in *Stud. in Surf. Sci. and Catal.*, Cortes Corberan V. and Vic Bellon S. (eds) (Elsevier Amsterdam), **82** (1994) 293

O'Keefe, M. *Fast Ion Transport in solids:* North Holland: Amsterdam (1973) 233

Okuhara, T. and Mosono, M. *Catal. Today* **16** (1993) 61

Ono, T., Kamisuki, H., Hisashi, H., and Miyata, H., *J. Catal.,* **116** (1989) 303

Orloff, E., in *The catalytic oxidation of organic compounds in the vapor phase* The Catalog Company Inc, (1932)

Orloff, M. *Oxidation of hydrocarbons.* Academic Press, New York (1909) 59

Oyama, S. T., *Bull. Chem. Soc. Japan,* **61** (1988) 2585

Oyama, S. T., In: *Heterogeneous Hydrocarbon Oxidation,* (Warren, B. K., Oyam S. T., Eds.), ACS Symposium Series 638, Chapter 1, American Chemical Society, Washington, (1996) 2

Pal, B. B. and Sen Gupta, K. K., *Inorg. Chem.* **14** (1975) 2268

Raje, A.P. and Davis, B.H., *Energy Fuels,* **10** (1996) 522

Rajesh, H. and Ozkan, U. S., *Ind. Eng. Chem. Res.* **32** (1993) 1622

Rajumon, M.K., Roberts, R.S., Wang, F. and Wells, P.B., *J. Chem. Sc., Faraday Trans.*, **94** (1998) 3699

Rethwisch, D. G., and Dumesic, J. A., *Appl. Catal.,* **21** (1986) 97

Roth, R. S. and Waring, J. L., *Am. Mineral.,* **48** (1963) 1348

Roussel, H., Mehlomakulu, B. Belhadj, F., van Steen E. and Millet, J.M.M., *J. Catal.*, **205** (2002) 97

Rudd J., Chemical Economics Handbook, SRI International, (1981) 65.

Sachtler, W. H. M. and De Boer, N. D., *Proc. Int. Cong. Catal. 3rd. 1964; (*Grasselli, R.K.) eds., Kodansha-Elsevier, Amsterdam, (1965) 25

Sala, F. and Trifirò, F., *J. Catal.,* **41** (1976) 1

Saleh-Alhamed, Y. A., Hudgins, T. T. and Silveston, P. L., *Appl. Catal.* A: General, **127** (1995), 177

Sanderson, R. T., "Chemical Bonds and Bond Energy"., 2nd ed., Academic Press, New York, (1976)

Scheele, P.M., in *The catalytic oxidation of organic compounds in the vapor phase* The Catalog Company Inc, (1932)

Schnobel, M., *PhD Thesis*, University of Cape Town (1997)

Schuer, H., and Klemm, W., Anorg, Z., *Allg. Chem.*, **395** (1973) 287

Schuit, G.C.A and Gates, B.C., The winning catalysts are multifunctional in *Chemtech,* (1983) 556

Schulz, H., Bohringer, W., Kohl, C.P., Rahmano N.P. and Will, A., *D6NK-FORSCHUNGSBERICHT 320*, D6NK, Humburg (1984)

Schulze, J., *Chem. Ing. Tech.*, **46 (22)** (1974) 925

Shannon R.D. and Prewitt C.T., *Acta Crystallogr.*, B25 (1969) 925

Shchukin, B. P., Boreskov, G. K., Bent'yaminov, S. A., Tarasova, D. V., *Kinet. Katal.*, **11**(1970) 153

Shishido, T., Konishi, T., Matsuura, I., Wang, Y., Takaki, K., and Takehira, K., *Catalysis Today,* **71** (2001) 77

Sokolovskii, V. D., *Catal. Rev.-Sci. Eng.,* **32** (1990) 1

Sokolovskii, V.D., A.A. Davydov and O.Yu. Ovsitser, Catal. Rev.-Sci. Eng., 37(3) (1995) 425

Sperber, H., *Chem. –Ing. –Techn.*, **41** (1969) 962

Straguzzi, G. I., Bischoff, K. B., Koch, T. A., Schuit, G. C. A., *J. Catal.,* **104**, (1987), 47

Strecker, B., *Ann.,* **93** (1855) 370

Sureh, D. D., Ornoff, D. A., Bradzil, D. F., Glaeser, L. C., Friedrich, M. S., *US Patent,* 4,760,159 (1988)

Tanabe, K., *Solid acids and bases,* Academic Press, New York (1970) 59

Toft, M. A., Bradzil, L. F., Glaeser, L. C., US. *Patent* 4,784,979 (1988)

Trifiro, F., Centola, P., Pasquon, I., *J. Catal.,* **10** (1968), 68

Trifiro, F., Centola, P., Pasquon, I., Jiru, P., In: *Proceedings of the 4th International Congress on Catalysis, Moscow, 1968,* (Kazanskii, V. B., Ed.), Akademiai Kiado, Budapest, Vol. 1 (1971), 252

Trifiro, F., Kubelkova, L., Pasquo, I., *J. Catal.*, **19** (1970), 121

Trillat, A., *Bull. Soc. Chim.* Fr., **27** (1902) 797

Trillat, A., *Bull. Soc. Chim.* Fr., **29** (1903) 35

Tu, Y. J., Chen, Y. W., Li, C., *J. Chem. Technol. Biotechnol.* **59** (1994b) 141

Tu, Y. J., Chen, Y. W., Li, C., *J. Mol. Catal.* **89** (1994a) 179

Uhl, H. B. and Cooper, I. H., *U.S. Patent* 2,465,498 (1949)

Valitov, L. K. and Lakiza, S. M., Russ. J. Phys. Chem., 49 (1975) 1853

Van Steen, E., Schnobel, M., Walsh, R., Riedel, T., *Appl. Catal. A*, **165** (1997) 349

Vedrine, J. C., Coudurier, G., Millet, J. M. M., Catal. Today, **33** (1997), 3

Vernon, L. W., and Milligan, W. O., *Tex. J. Sci.*, **82** (1951)

Volta, J. C. and Portefaix, J. L., *Appl. Catal.* **18** (1985) 1

Volta, J. C. Desquesnes, W., Moraweck, B., Coudurier, G., React. *Kin. Catal.Lett.* **12** (1979) 241

Volta, J. C., Bere, K., Zhang, Y. J., Olier, R. In *Catalytic Selective Oxidation*, Oyama, S. T., Hightower, J. W., Eds., American Chemical Society: Washington D.C. (1993) 217

Volta, J. C., Desquesnes, W., Moraweck, B., and Tatibouet, J. M. *Proc. 7th Int. Cong. Catal. Tokyo, 1980.* (Seiyama, Y., Tanabe, K., Eds.) Elsevier, Amsterdam, (1981), Part B,1398

Volta, J. C., Moraweck, B., *J. Chem Soc. Chem. Commun.*, (1980) 330

Volta, J. C., Phichitkul, C., Germain, J, E., Tatibouet, J. M. *Proc. 8th Int. Cong. Catal. Berlin, 1984,* Vol. 4; Verlag Chemie: Berlin, (1984).451

Walter, M., Ger Pat. 168,291 (1904); Brit Pat. 21,941 (1905); French Pat. 360,785 (1905)

Wells, A. F., *Structural inorganic chemistry,* Claredon Press, Oxford (1975) 203

Weng, L. T., Delmon, B., *Appl. Catal* A: General, **81** (1992), 141

Wyckhoff, R. W. G., *Crystal Structures,* Vol. 1, Second edition, John Wiley and Sons, New York, 1963

Yamazoe, N., Aso, I., Amamoto, T., Seiyama, T., In: *"New Horizons in Catalysis", Proceedings of the 7th International Congress on Catalysis, Tokyo, 1980,* Studies in Surface Science and Catalysis 7B, (Seiyama T., Tanabe, K., Eds.), Kodansha-Elsevier, Tokyo-Amsterdam (1980) 1239

Yee, A., Morrison, S. J., and Idriss, H. *Catalysis Today,* **63** (2000b), 327

Yee, A., Morrison, S. J., and Idriss, H., *J. Catal.,* **186** (1999) 279

Yee, A., Morrison, S. J., and Idriss, H., *J. Catal.,* **191** (2000a) 30

Yokoyama, T., Fujita, N., Make, T., *Appl. Catal* A: General, **125** (1995), 159

Young, R. A., *"The Rietveld Method",* IUCr, Oxford University Press, 1993

Zanthoff, H. W., Buchholz, S., Ovsitser, O. V., *Catal. Today* **32** (1996) 291

Zhang, W., Desikan, A., and Oyama, T., *J. Phys. Chem.,* **99** (1995) 14468

Zhou, E, Sham, E., Machel, T., Bertrand, P., Ruiz, P. and Delmon, B., *J. Catal.*, **132** (1991) 157

APPENDICES

7 APPENDICES

7.1 GAS CHROMATOGRAPHY OUTPUTS

An overview of the Gas Chromatography (GC) setup conditions and the temperature program of the GC oven are given in section 2.4.2.2.

Ethanol oxidation over $V_xFe_{1-x}SbO_4$ catalysts:

Reaction temperature: 150°C

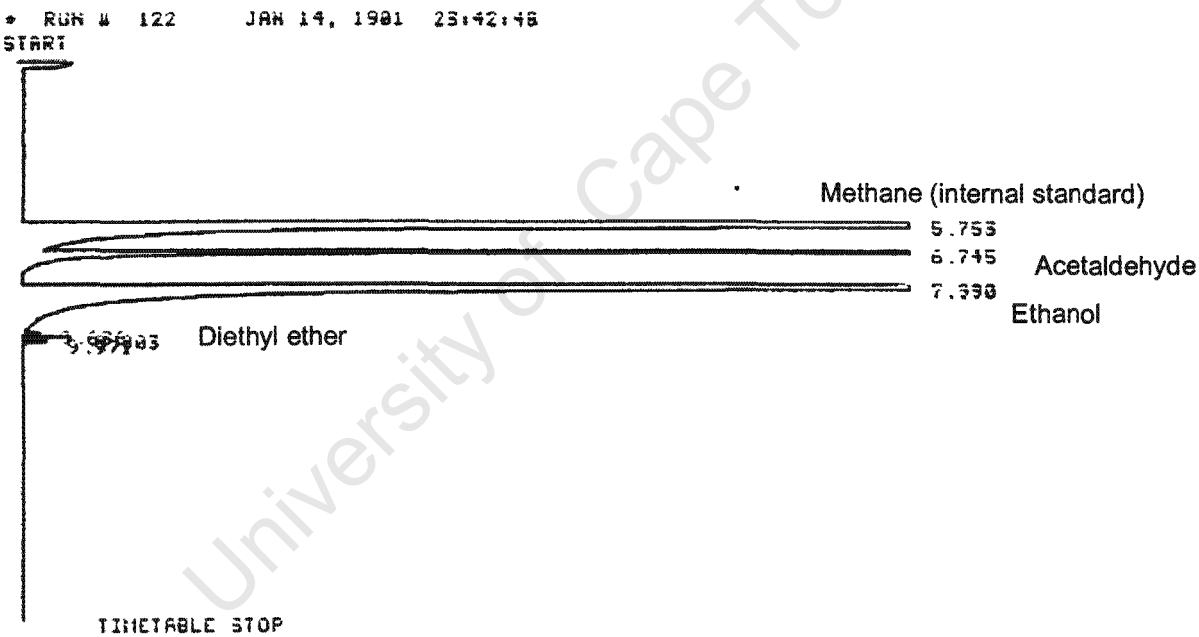

RUN# 122 JAN 14, 1901 23:42:46

AREA%

RT	AREA	TYPE	WIDTH	AREA%
5.753	6536352	SB8	.060	63.21173
6.745	391840	TB8	.066	3.78941
7.990	3396680	PB	.060	32.84861
9.636	2780	BV	.064	.02688
9.805	7947	VV	.066	.07685
9.971	4011	VB	.070	.04653

TOTAL AREA=1.0340E+07
MUL FACTOR=1.0000E+00

Ethanol oxidation over $V_xFe_{1-x}SbO_4$ catalysts:

Reaction temperature: 200°C

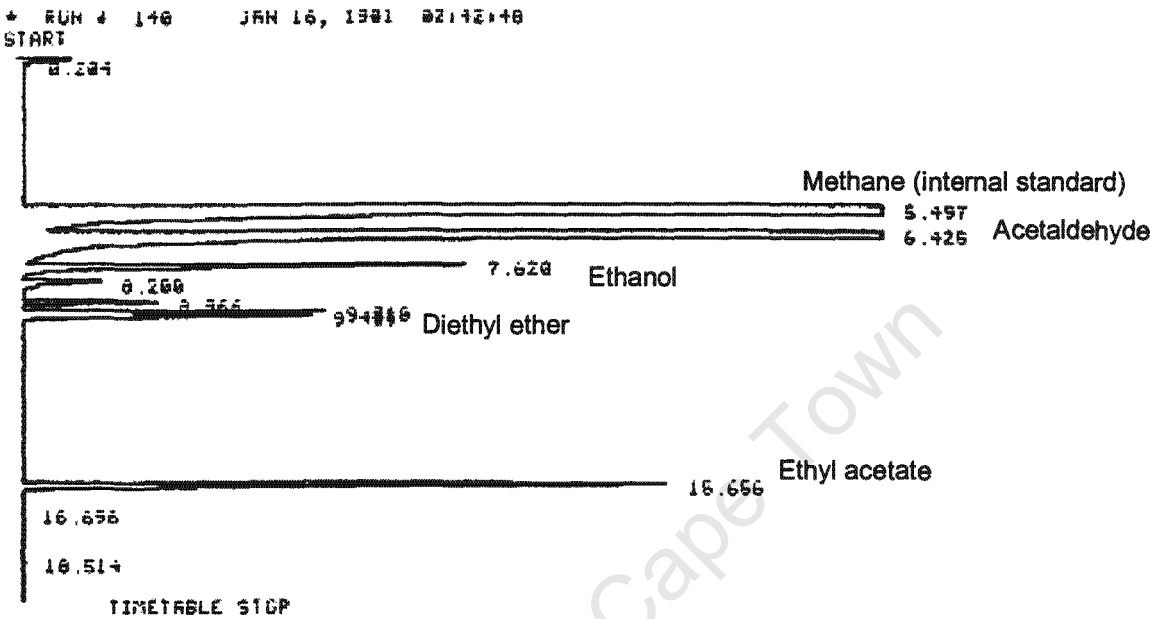

RUN# 140 JAN 16, 1981 02:42:48

AREAX

RT	AREA	TYPE	WIDTH	AREAX
.284	6876	BB	.124	.03892
5.497	12766104	SBB	.122	72.36887
6.425	4178954	TBV	.124	23.65189
7.620	142596	TVV	.136	.80783
8.280	25894	TVV	.125	.14665
8.966	41942	BV	.119	.23669
9.310	78707	VV	.105	.44545
9.453	96872	VB	.131	.54825
15.656	232954	BB	.144	1.31842
16.676	52884	PB	1.107	.29452
16.514	24257	BB	.271	.13731

Ethanol oxidation over $V_xFe_{1-x}SbO_4$ catalysts:

Reaction temperature: 250°C

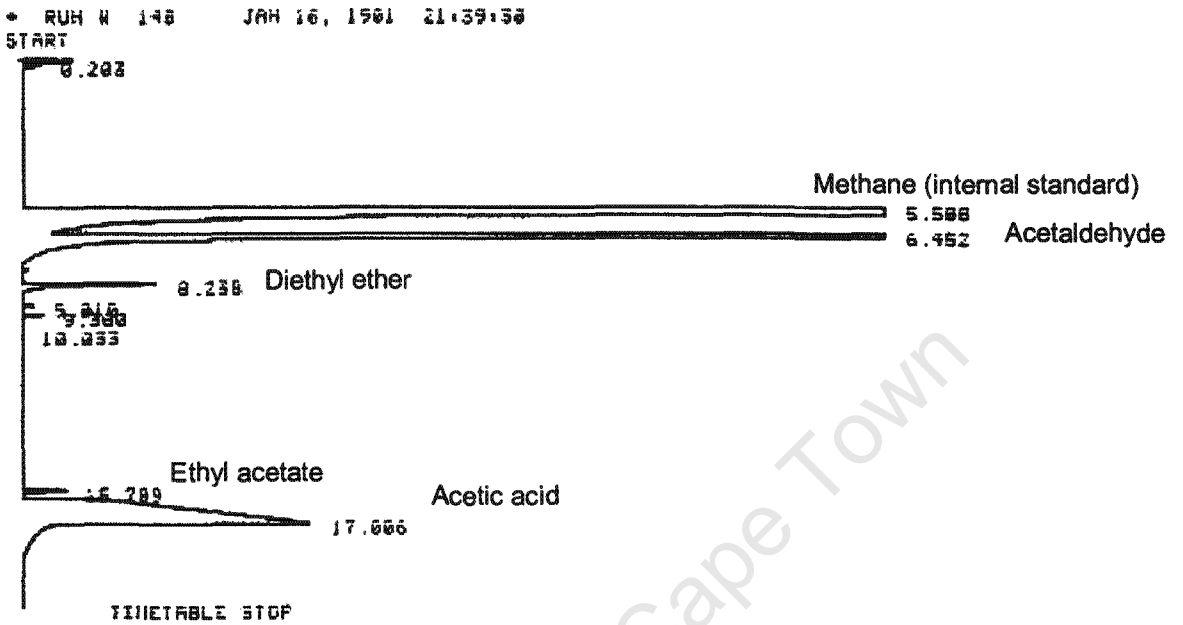

RUN# 148 JAN 16, 1981 21:39:38

AREA%

RT	AREA	TYPE	WIDTH	AREA%
.203	7076	BB	.144	.86849
5.588	9721171	BBB	.897	83.89561
6.452	1307127	TBV	.896	11.17332
8.238	44084	PB	.128	.37614
9.010	6305	PP	.036	.05369
9.360	8596	PV	.091	.07348
10.033	5076	PB	.116	.04339
15.789	23011	BV	.136	.19670
17.006	676390	VV	.765	5.82694

TOTAL AREA=1.1639E+07
MUL FACTOR=1.0000E+00

Ethanol oxidation over $V_xFe_{1-x}SbO_4$ catalysts: Product identification using GS-MS

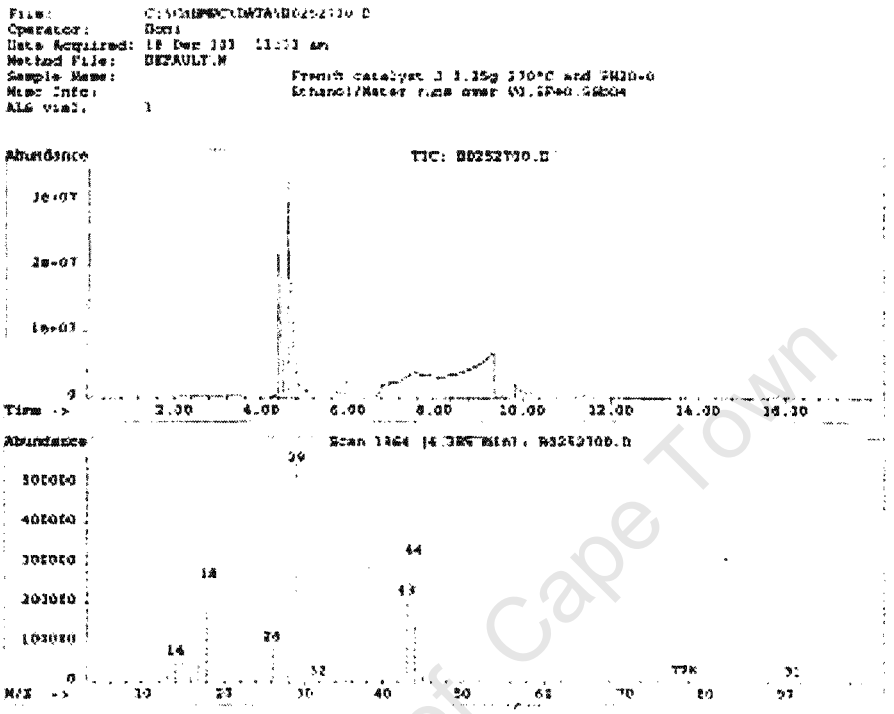

7.2 DATA PROCESSING AND ANALYSIS

7.2.1 Mass balance calculation

An example from the experimental data derived from the oxidation of ethanol over $VSbO_4$ at 250°C has been taken to illustrate the mass balance calculation. From a GC trace example shown on section 7.1, page 188; the area associated with each product (as identified by GC-MS) is obtained as shown below:

Table 7-1: Calculation of carbon balance from GC output of the experimental data

Product	Area	Yield	Selectivity
Methane	1369271		
Acetaldehyde	581219	78.81	92.40
Ethyl acetate	10980	2.53	2.97
Acetic acid	4493	0.61	0.71
Diethyl ether	0	0	0
Others	12626	1.71	2.00
CO	0.08 @ 75.8ml/min	0.39	0.56
CO_2	0.25 @ 75.8ml/min	1.23	1.75
Ethanol (feed unreacted)	177995	15.57	
Carbon Balance		**100.85**	

The carbon balance was then calculated by adding yields of different products at the outlet of the reactor:

7.2.2 Reaction order determination

The ethanol oxidation reactions were performed over a range of temperatures. For 1st order reactions, it can be derived that:

$$\ln\ln(\frac{1}{1-x_{Ethanol}}) = \ln k_o - \frac{E_a}{T} - \frac{1}{t}$$

Hence, for 1st order reactions, a plot of

$$\ln\ln(\frac{1}{1-x_{Ethanol}}) \; vs. \; \frac{1}{T}$$

should give a straight line. An Arrhenius in Figure 7-1 below a demonstration of a first order kinetics of the ethanol oxidation over selected $V_xFe_{1-x}SbO_4$ catalysts.

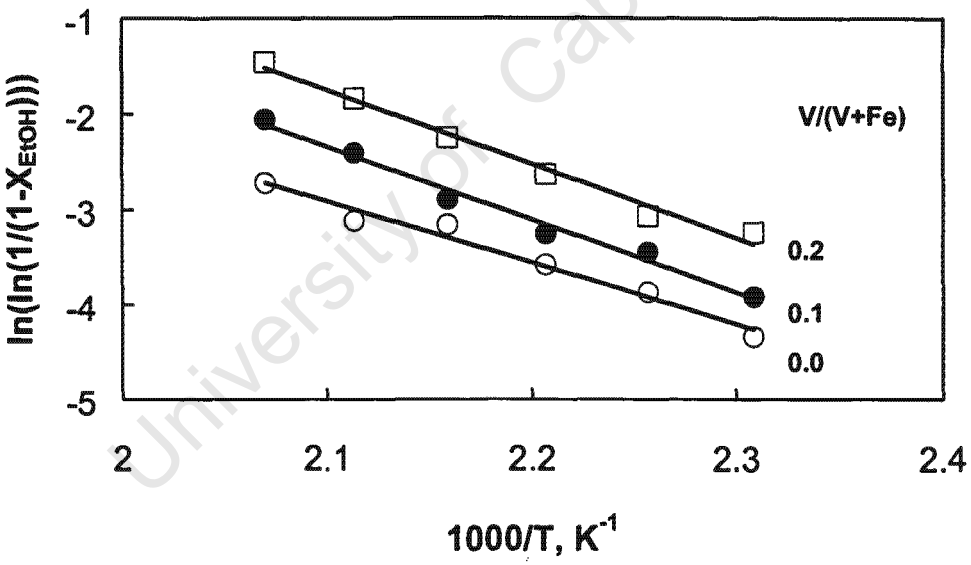

Figure 7-1: Arrhenius plot showing the experimental data for ethanol oxidation over $V_xFe_{1-x}SbO_4$ catalysts can be described by a first order rate equation

This shows that at low ethanol conversion the ethanol oxidation reaction can be reasonable described by the first order rate equation.

7.2.3 Estimation of Diffusion and Reaction-Limited Regimes

Weisz-Prater criterion for internal diffusion

The Weisz-Prater criterion was used to determine if internal diffusion is limiting the reaction (Fogler, 1999). The criterion uses measured values of the rate of reaction - $r'_A(obs)$ to estimate the Weisz-Prater parameter (C_{WP}).

$$C_{WP} = \frac{-r'_A(obs)\rho_c R^2}{D_e C_A}$$

where

$-r'_A$ (obs) = observed reaction rate. The maximum rate of reaction which would have been achieved was 2.5 $g_{Ethanol}/ g_{cat}.hr$

C_A – Concentration of ethanol in reactor inlet= 6.58×10^{-6} mol/cm^3

R = Radius of the catalyst particle = 1.06×10^{-2} cm

ρ_c = estimated density of the catalyst particle = 3.6 g/cm^3

D_e = Knudsen diffusivity = $9.7 \times 10^3 a (T/M)^{1/2}$

Where

a = average pore diametr in catalyst particle (giving smallest possible diffusivity) = 50×10^{-8} cm

T = reaction temperature = 500-600 K,

M = molar mass of ethanol = 46 g/mol

If C_{WP} <1, then there are no diffusion limitations and consequently no concentration gradient exists within the pellet.

If C_{WP} >1, then internal diffusion limits the reaction.

The evaluation of the Weisz-Prater constant was estimated for high conversion at moderate temperature (500 K) to be:

$$\mathbf{C_{WP} = 0.015 <<< 1}$$

Hence it can be concluded that the internal diffusive limitations did not affect the ethanol oxidation over these metal oxides.

External diffusion limitation was estimated using Mears' criterion for external diffusion

The Mears criterion, like the Weisz-Prater criterion uses measured values of the rate of reaction ($-r'_A$, in $kmol/kg_{cat}.s$) to estimate the existence of external mass transfer limitations (Mears, 1971).

Mears proposes that when $\frac{-r'_A \rho_b R^n}{k_c C_A} < 0.15$, external mass transfer effect can be neglected.

Where

n = reaction order = 1

R = catalyst particle radius, m

ρ_b = bulk density of catalyst bed, kg/m^3

C_A = bulk concentration $kmol/m^3$

k_c = mass transfer coefficient, m/s = Sh x $D_{EtOH\ in\ air}/d_p$ = 0.2 m/s

The calculated value = 1.63×10^{-4} << 0.15

Hence, the mass transfer from the bulk gas phase to the catalyst surface can be neglected.

7.3 INFRARED (IR) SPECTROSCOPY (PYRIDINE ADSORPTION ACIDITY ANALYSIS)

The following catalysts were characterised for the acidity using the IR pyridine adsorption technique as described in section 3.1.7.

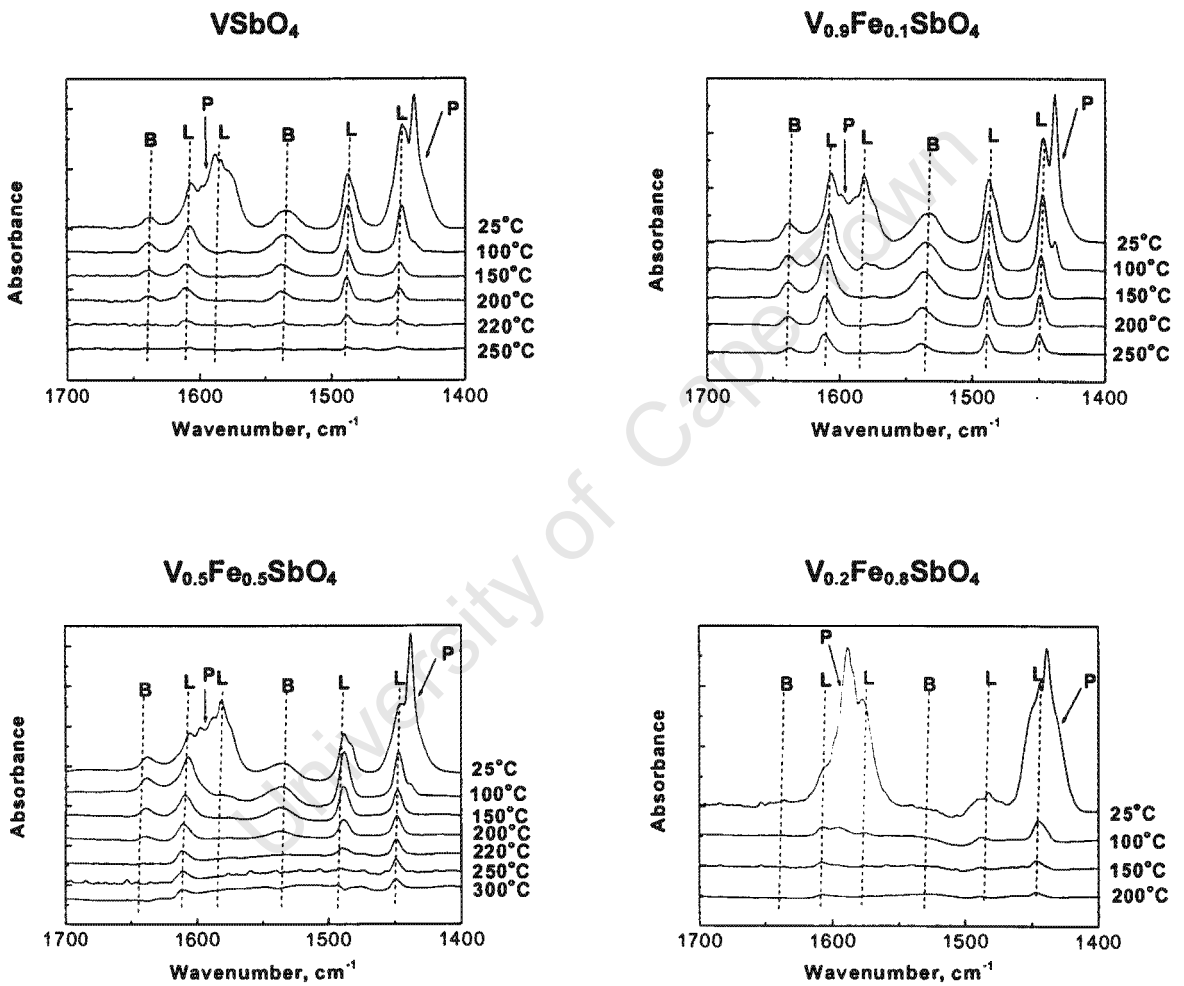

Figure 7-2: Pyridine desorption pattern for vanadium iron antimonate catalysts ($V_xFe_{1-x}SbO_4$). $T_{pretreatment}$ = 220℃ for 2 hours under vacuum, $T_{adsorption}$ = 25℃, $T_{evacuation}$ = 25℃, 100℃, 150℃, 200℃, 220℃, 250℃ and 300℃ for 1 hour, spectra recorded at 25℃. L stands for Lewis, B for Brønsted acid sites, while P stands for physisorbed pyridium ions.

The catalysts were then compared at different temperature as shown in Figure 7-3

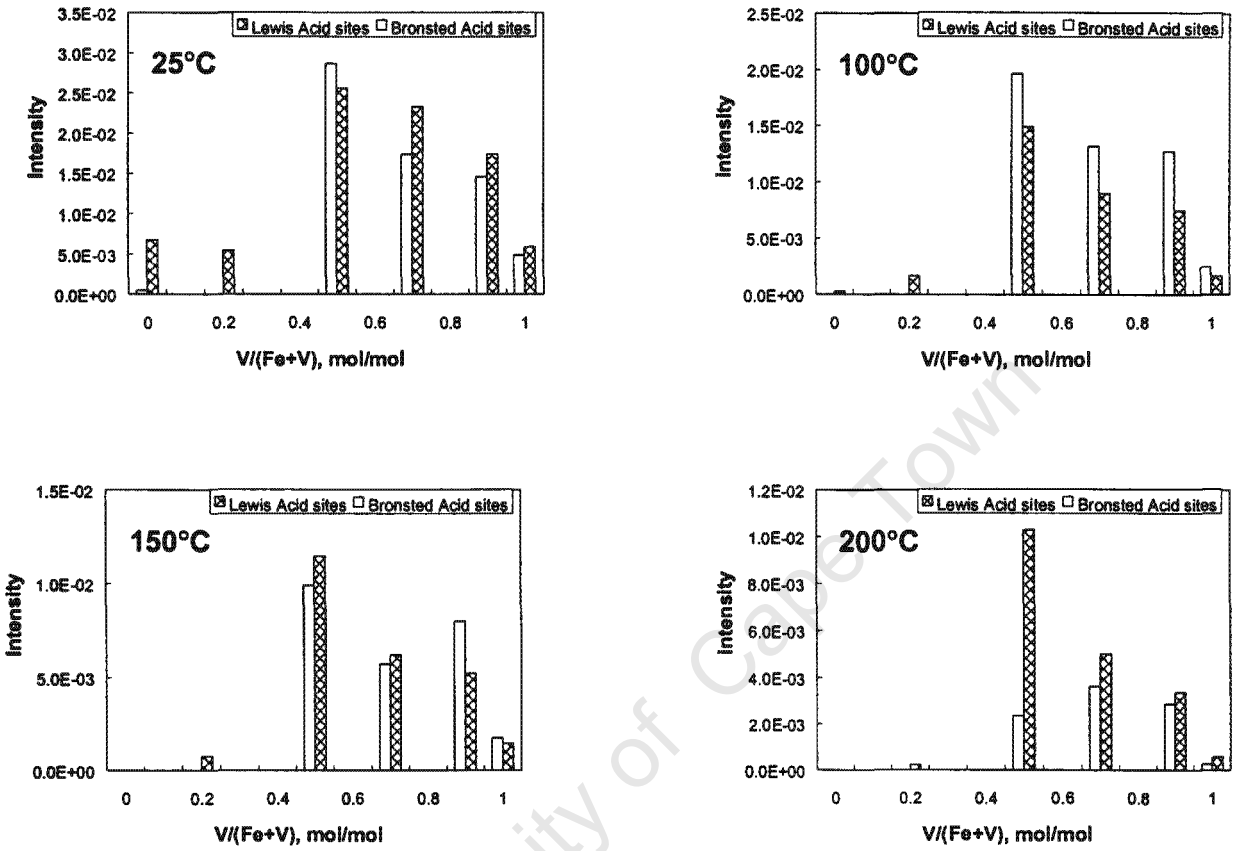

Figure 7-3: Comparison of Brønsted and Lewis acidity for vanadium iron antimonate catalysts ($V_xFe_{1-x}SbO_4$) determined at different evacuation temperatures as a function of V/(Fe+V).

7.4 PARTIAL OXIDATION OF ETHANOL OVER SINGLE METAL OXIDES

To establish some basic understanding of the oxidation of alcohols over metal oxide systems, the study of ethanol oxidation over simple metal oxides was undertaken. The basis for studying a wide range of simple metal oxides was to establish trends for activity in ethanol oxidation and selectivity towards desired products.

Similar comparative studies over an analogous range of metal oxides have been reported in literature, but these studies were on methanol oxidation (Boreskov, 1968 and Golodets, 1983). Studying ethanol oxidation over the similar range of metal oxides should bring some general understanding of mechanisms of these alcohols oxidation over metal oxides. It has been proposed by Forzatti *et al.* (1987) that methanol oxidation will follow different reaction pathway to other higher alcohols because of the uniqueness of the reactivity of C-1 molecules of any homologous series

The study of these single metal oxides should impact on the understanding of the complex metal oxides which form the main body of this thesis. Furthermore, such a study should serve to corroborate isolated studies reported in literature on ethanol oxidation over these simple metal oxides.

Figure 3-35 shows the conversion of ethanol over a range of metal oxides under the same set of reaction conditions.

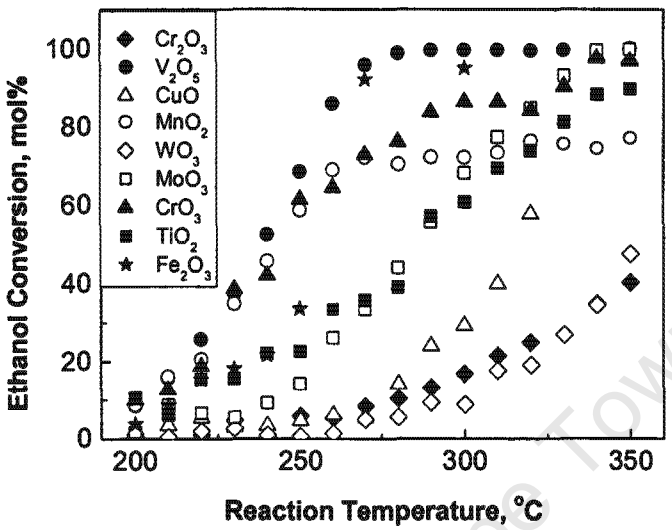

Figure 7-4: Conversion of ethanol over different single metal oxides (CrO_3, WO_3, MoO_3, TiO_2, V_2O_5, Cr_2O_3, MnO_2, Fe_2O_3 and CuO) as a function of reaction temperature. $T_{reaction}$ = 200-350°C, WHSV = 2.436 $g_{ethanol}/(g_{catalyst}\ h)$; $P_{ethanol}$ = 0.27 bar, P_{O2} = 0.3 bar, balanced by N_2 to a total pressure of 1.7ba

Generally, conversion increases with increasing temperature, from left to right of Period IV of transition metals, and decreases from top to the bottom of Group VI. V_2O_5 exhibits superior activity compared to other metal oxides under the stipulated reaction conditions, while WO_3 exhibits lowest activity. Most of the metal oxides show a break point, where the conversion suddenly increases sharply. This effect is observed for CuO, Fe_2O_3 and MoO_3. These metal oxides exhibit low activity at moderate temperatures and the activity suddenly increases sharply at a characteristic temperature. Another notable effect of increasing temperature on the oxidation of ethanol over these metal oxides is that over CrO_3 and MnO_2 the conversion flattens at high temperatures. The temperature from which the flattening starts to occur varies for different metal oxides and could also be a characteristic of the metal oxide.

On the whole, the observed trend in catalytic activity in the investigation of ethanol oxidation over simple metal oxides at 300°C is as follows: V_2O_5 > Fe_2O_3 > CrO_3 > MnO_2 > MoO_3 >TiO_2 > CuO > Cr_2O_3 > WO_3.

Table 7-1 presents the kinetic parameters obtained from the oxidation of ethanol over single metal oxides.

Table 7-1: Activation energies Ea and pre-exponential factors obtained from the oxidation of ethanol over a range of metal oxides

Metal Oxide	**Activation energy, Ea (kJ mol^{-1})**	**Pre-exponential factor, A (mmol g^{-1} sec^{-1})**
CuO	41.21	$1.03 \times 10^{+3}$
CrO_3	44.66	$2.41 \times 10^{+4}$
TiO_2	64.58	$8.86 \times 10^{+5}$
MnO_2	91.13	$3.71 \times 10^{+8}$
V_2O_5	116.71	$6.94 \times 10^{+11}$
MoO_3	131.75	$7.86 \times 10^{+11}$
Cr_2O_3	142.59	$1.24 \times 10^{+14}$
Fe_2O_3	117.11	$1.12 \times 10^{+18}$
WO_3	186.06	$5.59 \times 10^{+15}$

The main reaction product from the oxidation of ethanol over single metal oxides is acetaldehyde. Minor products include diethyl ether, ethyl acetate, acetic acid, acetone and carbon oxides. Figure 3-36 presents typical selectivity of products over one of the single metal oxides (V_2O_5). Similar plots for the rest of the metal oxides are presented in Appendix VI.

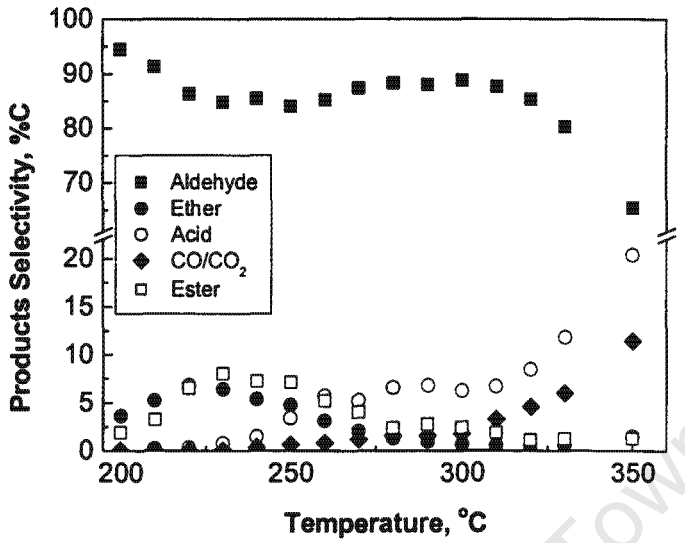

Figure 7-5: Typical selectivity pattern for ethanol oxidation over single metal oxides (example from V_2O_5 reaction). $T_{reaction}$ = 200-350°C, WHSV = 2.436 $g_{ethanol}/(g_{catalyst}\ h)$; $P_{ethanol}$ = 0.27 bar, P_{O2} = 0.3 bar, balanced by N_2 to a total pressure of 1.7bar

A typical consecutive parallel reaction pathway is observed. Acetaldehyde selectivity is high at low temperature and decreases steadily with increasing temperature, due to consecutive reactions. The main competing reaction pathway at low reaction temperatures is that leading to the formation of diethyl ether. Selectivity to diethyl ether increases with increasing temperature and reaches a maximum at about 220°C, and then decreases and remains below 2% with further increase in temperature. Ethyl acetate selectivity also increases in the same manner as diethyl ether reaching the maximum at 230°C then decreases. At the temperature range where both diethyl ether and ethyl acetate selectivity is high, acetaldehyde selectivity forms a local minimum and then somewhat increases as the two products selectivity decrease simultaneously.

Notable though is that as the diethyl ether and ethyl ether selectivity starts to decrease, the selectivity to acetic acid and carbon oxides starts to increase. In some of the oxides the selectivity to acetic acid reaches a maximum at about 340°C while at the same time the selectivity to acetaldehyde continues to decrease, giving way to complete oxidation

products (carbon oxides and water). The formation of diethyl ether is observed on WO_3, V_2O_5, MoO_3 and CuO_3. The formation of ethyl acetate and acetic acid is observed only on V_2O_5, MoO_3, TiO_2. For other metal oxides acetaldehyde and carbon oxides are the main products throughout the temperature range.

For the metal oxides that show a break effect (i.e. sharp increase in ethanol conversion at a certain temperature), e.g. CuO, Fe_2O_3 and MoO_3, the break is associated with a sudden change in selectivity pattern, and always results in a sudden increase in the selectivity to carbon oxides.

For CrO_3 and MnO_2 for which the conversion flattening effect was observed at high temperatures, the selectivity to acetaldehyde decrease further and sharply at the flattening region and carbon oxides selectivity increases Figure 7-6.

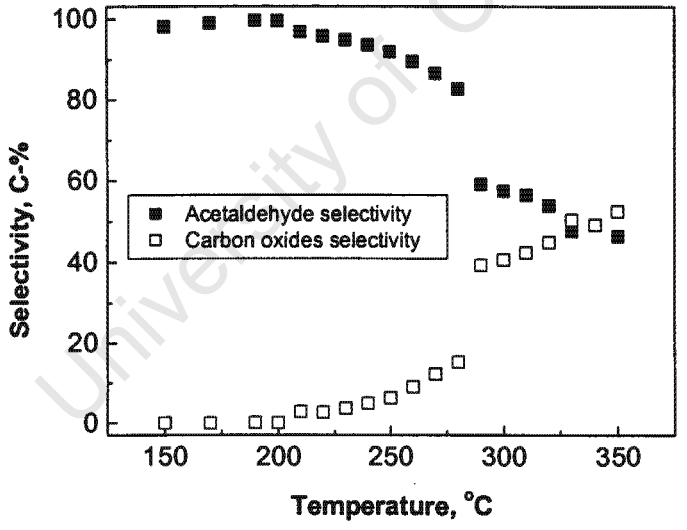

Figure 7-6: Selectivity of acetaldehyde and carbon oxides over MnO_2. $T_{reaction}$ =200-350°C, WHSV = 2.436 $g_{ethanol}/(g_{catalyst}\ h)$; $P_{ethanol}$ = 0.27 bar, P_{O2} = 0.3 bar, balanced by N_2 to a total pressure of 1.7bar